Genetic and Cytological Analysis of Host Root Responses to Cyst Nematode Infection in Wheat

Kara A. Levin

Thesis submitted in fulfilment of the requirements for the degree of Doctor of Philosophy

School of Agriculture, Food and Wine

Faculty of Sciences

The University of Adelaide

March 2020

Table of Contents

Abstract

Cereal cyst nematodes (CCN, *Heterodera avenae*) are soil-dwelling parasites that substantially reduce yields of cereal crops including wheat (*Triticum aestivum*). They establish feeding sites within the root vascular tissue and divert nutrients from the host plant to serve their life cycle. Female nematodes continue to feed and mature into cysts which contain hundreds of eggs. These eggs remain in the soil and release infective juvenile nematodes the following crop season.

To better understand this host-parasite relationship, it was first necessary to establish protocols for nematode-infected plant materials. Methods for growing and maintaining infected plants, sample preparation, and staining for microscopic observation were evaluated. Once appropriate methods, including methods for hydroponic growth and confocal microscopy, were established, it was possible to maintain nematode infected tissue for long periods (up to 40 d after inoculation (DAI)) and observe syncytia within the vascular tissue.

Methods were then developed to obtain high-quality three-dimensional images of thick (up to 150 μm) sections of root tissue. Specialised clearing provided unprecedented views of the feeding sites and surrounding tissues. Surprisingly, segments of the central metaxylem (cMX) vessels near the feeding sites looked very different from the expected narrow hollow tubes. In the atypical cMX segments, individual elements were short and plump rather than long, narrow and cylindrical. It was determined that during a period of 15 d in which cMX vessel elements would normally elongate and then mature to form a hollow tube, cMX vessel elements near CCN infection sites do not elongate. Instead, they expand radially, becoming plump. Their outer walls undergo secondary thickening and not all walls between elements degrade.

Similar to other parasites, CCN must secure nutrients from its host – without killing the host. The results presented here lead to new hypotheses about how CCN diverts water and nutrients

for its own use and how wheat plants survive this attack. Mobile tracer dyes were used to trace water flow in CCN-infected roots. Results indicated that transport is hindered in infected regions.

Although CCN can cause significant yield loss in wheat, much of this can be prevented through the use of resistant varieties, which limit the build-up of CCN populations in soils. In Australia, breeding for CCN resistance has been very successful, but little is known about the mechanisms of resistance. One of the resistance genes used in wheat breeding is *Cre8*, which maps on chromosome 6B. Previous reports on *Cre8* have associated it with plant vigour and resistance. To further investigate this, differences in root and shoot development were quantified between +*Cre8* and -*Cre8* materials. Sister lines were genetically selected to diminish background differences observed between parental lines TMDH6 and TMDH82. Analysis of these experiments indicated no evidence of *Cre8* affecting plant vigour but established that differences in CCN resistance can be detected within 21 DAI.

To evaluate differences in feeding site structure between CCN-infected -*Cre8* and +*Cre8* plants, protocols established in this research were used to compare transverse and longitudinal sections of feeding sites. This revealed that feeding sites in -*Cre8* plants developed closer to the cMX and contained more intricate cell walls within the feeding site than those in roots of +*Cre8* plants. It was also observed that the structural modification of the cMX was more extreme in roots of -*Cre8* plants than in +*Cre8* plants. Differences in cell wall composition were also investigated. Microscopy images revealed that the roots of +*Cre8* plants contained more lignified xylem vessels and more (1,3;1,4)-β-glucan deposition surrounding feeding sites than in roots of -*Cre8* plants.

Finally, this thesis reports a detailed genetic map of the *Cre8* region of chromosome 6B. Through a repetitive process of marker development, recombinant identification and resistance testing, *Cre8* was mapped to a region of 0.22 cM, corresponding to a physical region of 334 kbp on the IWGSC RefSeq 2.0 reference genome assembly. Within that region

there are ten high-confidence gene models, of which only two were previously shown to be expressed in roots. One of these genes, TraesCS6B02G466600, encodes a SUS III class sucrose synthase. It was found to contain non-synonymous polymorphisms between resistant and susceptible lines resulting in five amino acid residue substitutions within the protein sequence.

As sucrose synthase provides substrates for polysaccharide synthesis, it is hypothesised that differences in the enzymes localisation or activity could indirectly affect nematode development. These differences may change the synthesis of starch and/or cell wall polysaccharides and explain possible resistance mechanisms. Therefore, TraesCS6B02G466600 is a plausible candidate gene for *Cre8* resistance against CCN in wheat.

The research outcomes reported in this thesis have provided new insights into CCN parasitism and plant defence, and have improved the understanding of how the *Cre8* locus affects the resistance of wheat against CCN.

Thesis declaration

I certify that this work contains no material which has been accepted for the award of any other degree or diploma in my name, in any university or other tertiary institution and, to the best of my knowledge and belief, contains no material previously published or written by another person, except where due reference has been made in the text. In addition, I certify that no part of this work will, in the future, be used in a submission in my name, for any other degree or diploma in any university or other tertiary institution without the prior approval of the University of Adelaide and where applicable, any partner institution responsible for the joint-award of this degree.

I acknowledge that copyright of published works contained within this thesis resides with the copyright holder(s) of those works.

I also give permission for the digital version of my thesis to be made available on the web, via the University's digital research repository, the Library Search and also through web search engines, unless permission has been granted by the University to restrict access for a period of time.

I acknowledge the support I have received for my research through the provision of a Beacon Enlightenment Scholarship by the University of Adelaide.

Kara Ann Levin 20/03/2020

Acknowledgments

I would first like to thank The University of Adelaide for awarding me the Beacon of Enlightenment PhD Scholarship and the Grains Research and Development Corporation for funding this research. This PhD experience has been an incredible adventure. I am honoured to express my appreciation to all of the extraordinary people that made this journey possible.

Firstly, I would like to thank my amazing supervisory team. To my principal supervisor, Professor Diane Mather, thank you for putting your faith in me and giving me this research opportunity. Your passion for science and constant encouragement was a great motivator. Thank you for your unconditional support, your open-door policy and your incredible speediness in editing drafts. This thesis would not have been possible without you. To my co-supervisor, Associate Professor Matthew Tucker, thank you for always giving me your genuine time and advice. You really grounded this project and provided a voice of reason. Thank you for always making me feel welcome in your lab.

To my external supervisor, Professor David Bird, thank you for your intellectual conversations and your physical presence in Adelaide for meetings. Your stimulating ideas and encouragement really added another dimension to this project. To my independent advisor, Dr. Kerrie Davies, thank you for your compassionate support and expertise in nematology. I especially thank you for your encouragement and including me in your nematology class and discussions with colleagues. To my postgraduate coordinator, Associate Professor Chris Ford, thank you for your warm welcome to the PhD journey and your continued support.

This journey would not have been possible without the help and guidance of the very patient postdoc, Dr. Kelvin Khoo. Thank you for taking me under your wing to teach me everything about plant genetics, of which no amount of Friday coffees could have possibly repaid you. Your vast knowledge, unrelenting support and incredible friendship made this adventure unforgettable.

My appreciation also goes to Mr. John Lewis for his careful nematode resistance testing and constant smiles. I thank Dr. Gwenda Mayo of Adelaide Microscopy for her microscopy training and expert advice. I also thank Dr. Neil Shirley for running the qPCR analysis for my candidate genes and analysing the data. I would like to thank Chao Ma for running countless *in situ* hybridisation experiments and keeping a positive attitude. I especially thank Professor Steve Tyerman for making me feel welcome at The University of Adelaide so much that I came back for a PhD, his unrelenting support for the PhD scholarship and further for his advice on this project about water transport.

I would also like to thank past and present members of the Molecular Marker Lab for their constant support in the laboratory and for wonderful lunch conversations. To all the beautiful people I met at the Waite Campus, especially those who I worked with on the PAWS committee, thank you for creating a welcoming and warm environment on campus. I am also thankful to all my Australian friends (especially the Hewie crew) for the weekend adventures and much needed banter.

Finally, I am so grateful for the unconditional love and encouragement from my family. Dad, thank you for your loving support in all that I do and being a constant rock in my life. Mom, thank you for your endless love, your science genes and care packages for every occasion sent across the world. You both have given me the world and always believed in me. Erik and Jessica, thank you for always checking in with me and the loving support. I am especially grateful to my Australian family, especially Gabi and Craig, for hosting me in your home for the first two years and loving me as another daughter. You made me feel at home in the land down under. Last but not least, a very endearing thanks goes to my fiancé, Kym. This adventure was infinity times better with you by my side. Thank you for your loving attitude, emotional support and always being there for me.

List of abbreviations

ABA	abscisic acid
AF	acid fuchsin
BF	basic fuchsin
BG1	(1,3;1,4)-β-glucan
BH	berberine hemisulphate
BR	brassinosteroids
CBP	cellulose binding protein
CCN	cereal cyst nematode
CK	cytokinin
cM	centiMorgan
cMX	central metaxylem
CR	congo red
CW	calcofluor white
DAI	d after inoculation
ER	endoplasmic reticulum
ET	ethylene
ETI	effector triggered immunity
ETS	effector triggered susceptibility
FDA	fluorescein diacetate
GB	gibberellins
HR	hypersensitive response
JA	jasmonic acid
MAPKs	mitogen-activated protein kinases
MLG	mixed-linkage glucan
NBS-LRR	nucleotide-binding site- leucine-rich repeat
NLR	nucleotide-binding/leucine-rich repeat receptor
PAMP	pathogen associated molecular pattern
PCN	potato cyst nematode
PI	propidium iodide
pMX	peripheral metaxylem
PPN	plant parasitic nematode
PTI	PAMP triggered immunity
RKN	root-knot nematode
RLP	receptor-like protein
ROS	reactive oxygen species
SA	salicylic acid
SCN	soybean cyst nematode
SEM	scanning electron microscopy
TB	toluidine blue
TEM	transmission electron microscopy

List of figures

List of tables

List of appendices

Chapter 1: Introduction

Nematodes are among the most ancient animals on earth, evolving over time to cover a diverse range of roles in nature (Wang *et al.*, 1999). Some species parasitise plants by feeding through stylets. Many of these plant parasitic nematodes use their stylet to kill plant cells from which they feed. However, cyst nematodes, which are among the most economically damaging plant parasites, keep plant cells alive and establish lasting feeding sites.

Cyst nematodes (including *Heterodera* and *Globodera spp.*) establish syncytial feeding sites to divert vital nutrients from the plant to support their growth and development (Heinrich *et al.*, 1998). The effects on plants include symptoms similar to nutrient deficiency (chlorosis and stunted growth) leading to significant yield loss. One of the most economically concerning species is the cereal cyst nematode (CCN, *Heterodera avenae*) which causes damage to a range of cereal crops, including wheat and barley.

In Australia, CCN was previously a major threat to the most important crop in agriculture, wheat (*Triticum aestivum* L.). With the development and adoption of resistant cultivars as well as changes in crop management practices, nematode populations in soils dramatically decreased and yield loss was reduced (Murray & Brennan, 2009). In wheat, several resistance loci have been found but no causal genes have been identified and the resistance mechanism is not well understood. One of the resistance loci, *Cre8*, is favoured in breeding programs due to its reported contributions to both resistance and tolerance against CCN (Williams *et al.*, 2003).

Although the use of resistant cereal cultivars has diminished the immediate concern about CCN in Australia, the threat to agriculture remains. The use of susceptible cultivars or improper crop management could cause an increase in CCN populations. Further, to foresee potential failures in current resistant cultivars, it is necessary to understand the current resistance mechanisms. Therefore, the overall objectives of the research reported in this thesis were to (**1**) identify differences between *Cre8*-containing resistant and susceptible wheat to

decipher possible resistance mechanisms and (**2**) fine-map *Cre8* and identify potential candidate genes.

Preceding the research reported in this thesis, the *Cre8* locus had been mapped to the long arm of chromosome 6B (Williams *et al.*, 2003; Williams *et al.*, 2006) and subsequently mapped between the markers *wri16* and *BS0002244* (Jayatilake *et al.*, 2015). Further, fine-mapping had commenced and *Cre8* was positioned to a relatively small region of the wheat genome assembly (Hendrikse, 2016; Kumsa, 2015). Little was known about the mechanism by which *Cre8* confers resistance. Jayatilake (2014) made some observations of syncytial development but did not report any differences between lines with and without *Cre8*.

To address the research objectives, the specific goals of this research were: (**1**) to develop methods to visualise feeding sites in three dimensions to understand their development within wheat root tissue; (**2**) to identify phenotypic differences between *Cre8*-containing resistant and susceptible wheat; (**3**) to fine map the CCN resistance locus *Cre8* and (**4**) to identify possible candidate genes for *Cre8*.

The thesis consists of nine chapters as follows:

Chapter 1 (Introduction): A brief background to introduce the research topic and identify objectives of the thesis research.

Chapter 2 (Literature review): A review of the relevant literature to further develop background on the research topic and identify research gaps as well as introduce methods used in the research.

Chapter 3 (Methods for microscopic observation of cereal cyst nematodes and their feeding sites in wheat roots): A report on methodology developed for production of infected tissue and analysis of CCN feeding sites using microscopy.

Chapter 4 (Infection by cyst nematodes induces rapid remodelling of developing xylem vessels in wheat roots): A report on the response of xylem vessels to nematode infection discovered using 3D microscopy techniques. This chapter was accepted for publication in Scientific Reports on 18/03/2020.

Chapter 5 (A first look: methods for water transport observation in CCN-infected wheat roots): A report on preliminary water transport experiments in nematode infected roots.

Chapter 6 (Responses of *+Cre8* and *-Cre8* wheat lines to CCN inoculation): A report on phenotypic differences between resistant and susceptible wheat.

Chapter 7 (Cytological analysis of CCN feeding site development in *+Cre8* and *-Cre8* wheat lines): A report on cytological differences between syncytia induced in resistant and susceptible wheat.

Chapter 8 (Genetic analysis of the wheat *Cre8* locus): A report on fine-mapping that narrows the *Cre8* region and identifies possible candidate genes.

Chapter 9 (General discussion): A discussion on the overall accomplishments of this research including suggested resistance mechanisms for *Cre8* and future work.

Chapter 2 : Literature review

2.1 Wheat

As one of the most widely grown crops in the world, wheat is important for food security. With the human population continuously growing, the importance of wheat research is considerable. To make advancements in wheat breeding, knowledge of its genome is valuable. Wheat belongs to the genus Triticum, which includes common bread wheat (*Triticum aestivum* L.), an allohexaploid with its three subgenomes (A, B and D), each consisting of seven pairs of chromosomes. Chinese Spring was chosen as the reference cultivar for wheat genome sequencing (Sears & Miller, 1985). It had previously been found to easily cross with rye (Sears, 1939) and had been used to produce hundreds of aneuploids (Sears, 1976). Despite the complexity of sequencing, assembling and annotating such a large (17 Gb) and complex genome, the current reference assembly is a fully annotated and ordered genome (Alaux *et al*., 2018). One of the benefits of a hexaploid genome is its ability to cope with introgressions from alien species. This ability has allowed for the addition of disease-resistance traits from wild relatives and has advanced the modern wheat cultivars we use today (Friebe *et al*., 1996; Mason, 2017; Sears, 1981).

The life cycle of wheat can be broken down into developmental stages, as was comprehensively outlined by Bowden *et al*. (2007). The first stage, germination, begins with a dry caryopsis, consisting of an embryo and a starchy endosperm surrounded by the seed coat (testa) and pericarp. The endosperm tissue provides energy for germination while the embryo contains the plant structures which will become the growing plant. Germination begins with the emergence of a single primary root, called the radicle, and the start of the shoot, called the coleoptile. Roots function by absorbing nutrients and water for the plant. Initially, three primary roots (also called seminal roots) emerge. These later develop lateral roots that branch outwards from the primary roots which help anchor the plant and facilitate uptake. The root anatomy of primary roots is arranged in a circular pattern. The outermost layer of cells (the epidermis) helps protect the root from water loss. The next tissue is the cortex. In the centre is

the vascular cylinder, which is bordered by endodermis cells that help restrict water flow. The vascular cylinder contains phloem tissue, between six and eight peripheral xylem vessels and one large central metaxylem vessel. The phloem transports sugars and other metabolic products. The xylem transports water and mineral solutes, mainly through the large central metaxylem vessel. The primary roots support the plant until secondary roots (also called adventitious roots) develop, which occurs at approximately two to three weeks. Secondary roots are thicker than primary roots and initiate just below ground level. They develop when the crop begins to tiller and generally grow horizontally without branching.

Above ground, the plant continues to grow through leaf emergence stages and produces additional shoots called tillers. Primary tillers arise from a bud at the base of the main stem and can produce their own secondary tillers. Some of these tillers will produce heads. Factors that affect plant development include vernalisation and photoperiod. Vernalisation is the requirement of exposure to prolonged cold while photoperiod refers to the hours of daylight. Different varieties of wheat have different dependencies on these factors. Winter wheats depend on vernalisation to cue reproductive development while spring wheats rely solely on an increase in photoperiod to start their reproductive development.

The reproductive phase begins once the plant stops producing leaves and begins to produce the head of the plant. The head will develop internally until the flag leaf has fully extended and the awns are visible. Booting occurs when the head swells within the sheath of the flag leaf and is followed by the emergence of the head. Shortly after, the stamens and carpel fully mature and anthesis occurs. Anthesis is when pollen sacs burst and fertilisation of the carpel occurs. In most cases (96%), each floret will self-pollinate. Finally, the plant will go through a grain filling stage until it reaches physiological maturity. After, the grain loses moisture and is ready to harvest and store.

2.2 Cereal cyst nematode

2.2.1 Symptoms and impact

Cereal cyst nematodes (CCN, *Heterodera avenae*) are sedentary endoparasites affecting wheat (*Triticum aestivum* L.), barley (*Hordeum vulgare* L.), oat (*Avena sativa* L.) and rye (*Secale cereale* L.). Symptoms on host roots include distinct white cysts. Above-ground symptoms include chlorosis, stunted growth, and yield loss. Several species of *Heterodera* species, including *H. filipjevi*, *H. latipons*, and *H. avenae*, are known to infect cereal crops and have been reported in many parts of the world including North Africa, West Asia, China, India, Australia, America and Europe (Nicol *et al.*, 2011). In Australia, the CCN population consists of a single pathotype known as Ha13, classified as *H. avenae* (Andersen & Andersen, 1982) or *H. australis* (Subbotin *et al.*, 2002, 2003). CCN has been identified in most wheat growing regions of Australia. It has been estimated to affect up to 35% of wheat crops and to cause annual losses of 58 million AUD (Murray & Brennan, 2009).

2.2.2 Life cycle

The life cycle of cyst nematodes is distinct from those of other plant parasitic nematodes such as root-knot nematodes (Heinrich *et al.*, 1998; Jones, 1981; Lilley *et al.*, 2005). Nematode eggs, encased in a protective cyst, stay dormant in the soil until environmental conditions are favourable (Ellenby & Perry, 1976). In Australia, these conditions include decreased temperatures and increased moisture. Juvenile larvae (J1) moult within the eggs, and once hatched, begin their journey as mobile infective juveniles (J2). A stylet is developed from secreted proteins which is used for several roles. The stylet is first used to penetrate the root and enter the root at the zone of elongation (Heinrich *et al.*, 1998). After the nematode has travelled intracellularly to the vascular tissue, a cell is chosen as a permanent feeding site (Dropkin, 1969). The stylet is used to inject the host with effectors produced from specialized oesophageal glands including two subventral cells and one dorsal cell (Davis *et al.*, 2008; Hussey, 1989). Secretions include specialised effector proteins and hormones that aid in

successful penetration and control of a plant cell within the vascular tissue. Formation of the multinucleate syncytia is induced by these secretions which involves partial breakdown of neighbouring cell walls and protoplast fusion (Dropkin, 1969). The syncytium works as a transfer cell, drawing in solutes from which the nematode feeds intermittently (Jones & Northcote, 1972). The syncytium extends longitudinally, expanding into many cells, and fills with cytoplasm, organelles, and nuclei (Heinrich *et al.*, 1998). During this expansion, the nematode matures into an adult as either male or female. Larvae will become females if their syncytia are of sufficient size and nutrient content; otherwise they become males and leave the root (Trudgill, 1967). The females' bodies continue to enlarge until they extend outside of the root as visible white cysts, allowing mating with males (Lilley *et al.*, 2005). CCN females moult once more before they die and become hard brown barriers that protect the eggs (Heinrich et al. 1998).

2.3 Host resistance

Resistance is the ability of a plant to hinder nematode reproduction. Plant pathogen resistance has been studied for many plant diseases and much is understood about how plants combat fungal, bacterial and viral pathogens. Although interactions with parasitic nematodes may be more complex, the defence systems that plants use share common elements. Therefore, it is important to look at plant defence in general.

2.3.1 Plant defence system

The plant's first lines of defence are the plant cuticle and cell walls (Martin, 1964). Plants have the capability to reinforce their cell walls in response to damage by inducing accumulation of protective polysaccharides such as callose. The plant's immune system is structured to alarm the plant if a pathogen is present by inducing plant defences (Dangl *et al.*, 2013). One type of response is triggered by pathogen—associated molecular patterns

(PAMPs). Pattern recognition receptors (PRR) identify the PAMPs creating intracellular signals. These signals trigger PAMP-triggered immunity (PTI), which can stop further establishment of the pathogen (Jones & Dangl, 2006). Another type of response is called effector-triggered immunity (ETI). This is activated by the presence of a pathogen "effector" which causes the activation of "resistance genes" or R genes, and will stop pathogen growth (Jacob *et al.*, 2013, Jones & Dangl, 2006). Both PTI and ETI activate responses that impact plant hormonal homeostasis and the expression of development genes (Denancé *et al.*, 2013; Pieterse *et al*., 2012).

2.3.2 Hormone signalling pathway

The main hormones involved in plant defence signalling pathways include salicylic acid (SA), ethylene (ET), and jasmonic acid (JA). Bari and Jones (2009) discovered that these signal pathways interact. Regulator proteins from the SA pathway suppress the JA pathway while ET regulator proteins enhance the JA pathway. Other hormones including auxin, abscisic acid (ABA), cytokinins (CK), gibberellins (GB), and brassinosteroids (BR) may also play roles in defence signalling. By modulating these phytohormones, plants change the expression of defence genes and therefore trigger a defence response. Plants are able to modify the amount of phytohormone levels in order to coordinate the correct expression of defence genes depending on what stress is present.

Once hormones have been activated, secondary responses often include signal transduction components. These include reactive oxygen and nitric oxide species production, calcium fluxes, and mitogen-activated protein kinases (MAPKs) activation (Nurnberger *et al.*, 2004). Oxidative bursts involve the rapid release of reactive oxygen species (ROS) in response to increased calcium in the cytoplasm. The location and duration of the ROS determines the specificity of the response (Bailey-Serres & Mittler, 2006). ROS produced are part of the plant's hypersensitive response (HR) which causes cell death to prevent further pathogen advances (Heath, 2000).

2.4 Nematode resistance

Plant parasitic nematodes (PPN) are resilient parasites. Their bodies are coated with a protective cuticle made up of collagen (Perry & Moens, 2011). They can survive for long periods by entering into an inactive metabolic state. Two chemosensory organs located on the head, called the amphids, help the nematode perceive chemotactic stimuli in their surroundings (Perry, 1996). By responding to gradients of CO2, amino acids, pH and sugars that surround a root, J2s are able to migrate to compatible roots (Lilley *et al.*, 2005).

Sedentary endoparasitic nematodes have evolved to impede host defences. Once feeding sites are initiated, nematodes secrete effectors, including proteins that target plant transcription factors as and proteins involved in cell-wall modification (summary of genes listed in Vanholme *et al.* (2004); reviewed in Ali *et al.* (2018)). These secretions help nematodes suppress host defences and/or increase host susceptibility. Nematode effectors trigger the PTI and ETI response in plants (Cui *et al.*, 2015). In parallel, host effectors can cause an 'effector triggered immunity' in nematodes that reduces nematode parasitism (Hewezi & Baum, 2013).

2.4.1 Zig-zag evolutionary change

Evolution has resulted in a complicated relationship, reflecting the struggle for survival between parasite and host. This relationship was first described as a 'zig-zag' model by Jones and Dangl (2006), then further elaborated in the context of cyst and root-knot nematodes by Hewezi and Baum (2013). Hewezi and Baum (2017) comprehensively outlined how nematodes have evolved to manipulate their hosts.

To survive, nematodes have evolved to defeat plant defence systems. To avoid defeat, plants have evolved to overcome nematode effector proteins. The 'zig-zag' can be broken up into the following:

1. PAMPs are detected from the nematode, and the plant's **PTI** is triggered. PTI can include ROS, cell wall thickening, or callose deposition.

2. Nematode evolution has allowed them to overcome PTI with **ETS** (effector triggered susceptibility). ETS can include effector proteins that suppress genes or affect auxin levels.
3. Plant evolution has allowed plants to recognize further attacks whether it be direct or indirect and activate **ETI** (effector triggered immunity) with the use of **R genes (Resistance Genes)**
4. Further nematode evolution has allowed nematodes to **suppress ETI** by altering the effector or targeting another weakness.
5. Further plant evolution enables plants to fight back

2.4.2 Nematode ETS: Suppressing host defence

Knowledge on how nematodes suppress host defences is incomplete. There is strong evidence that nematode effectors target the plant immune system. In *Heterodera*, it has been shown that effector 10A06 inhibits the SA signalling pathway (Hewezi *et al.*, 2010). Another *Heterodera* effector, 30C02, was found to associate with and suppress β-1,3-endoglucanase, a pathogenesis-related protein known in plants for defence against fungal systems (Hamamouch *et al.*, 2012). *Heterodera* effector 4FO1 was found to mimic plant annexin, which interacts with oxidoreductases and prevents the activation of defence genes (Patel *et al.*, 2010). In soybean cyst nematode (SCN, *H. glycines*), the effector HgGLAND18 was shown to inhibit the host basal immune response and inhibit hypersensitive cell death (Noon et al. 2016). It has also been shown that cyst and root-knot nematodes have been able to suppress cell death by targeting nucleotide-binding site leucine-rich repeat (NBS-LRR) resistance proteins (Hewezi & Baum, 2017), products of many R genes.

2.4.3 Nematode ETS: Increasing host susceptibility

Research has also revealed examples of nematode effectors that increase host susceptibility. Some effectors of *Heterodera* spp. specifically target cell wall modification. These have included cellulases, pectate lyases (Popeijus *et al.*, 2000) and β-1,4-endoglucanases (Smant *et al.*, 1998). Other effectors have been identified that indirectly target cell wall modification including cellulose binding protein (CBP). A CBP effector identified in *H. schachtii* was found to increase the activity of a pectin-weakening protein PME3, allowing better access for the nematode's cell wall modifying effectors (Hewezi *et al.*, 2008).

It has also been shown that several nematode effector proteins target the auxin signalling pathway. In *H. schachtii*, the effector 19C07 increases auxin influx (Lee *et al.*, 2011a) while another effector, 10A07 was found to target an auxin-suppressing transcription factor IAA16, resulting in increased auxin levels (Hewezi *et al.*, 2015). The relationship between auxin and successful parasitism is not well understood, but it is known that increased auxin levels can promote lateral root emergence and upregulate cell wall modifying genes (Majda & Robert, 2018). These changes could facilitate syncytium development.

2.5 Characterising resistance genes

Isolation of resistance genes is useful, both for enhancing scientific understanding of host plant resistance and for enabling accurate selection in plant breeding. However, it can be difficult, especially in plants such as cereal crops, which have large and complex genomes.

2.5.1 Known nematode resistance genes

A shared characteristic of successfully resistant hosts (against pathogens and parasites) is a family of intracellular nucleotide-binding/leucine-rich repeat (NLR) receptors (Cui *et al.*, 2015; Nurnberger *et al.*, 2004). These receptors initiate ETI within the plant, stopping pathogen growth (Jacob *et al.*, 2013) and often initiating the HR. Due to pathogen pressure,

there is a vast amount of sequence diversity within different species, each containing up to several hundred NLR genes within a plant genome (Guo *et al.*, 2011; Karasov *et al.*, 2014; Yue *et al.*, 2012). Therefore, identified R genes have been further classified by structure and function, as outlined by Sekhwal *et al.* (2015).

The sugar beet (*Beta vulgaris* L.) gene *HS1^{pro-1}* which confers resistance against *H. schachtii* (Cai *et al.*, 1997) is classified as a receptor-like protein (RLP) and is expressed in response to nematode contact (Thurau et al. 2003). The tomato (*S. lycopersicum*) gene, *Mi* which confers resistance against *Meloidogyne* spp is classified as a NBS-LRR (Milligan *et al.*, 1998). This resistance involves activation of the HR, showing necrosis of cells near the feeding site 12 h after inoculation (Paulson and Webster 1972). Another tomato gene, *Hero*, is also classified as a NBS-LRR, however only confers resistance against *G. rostochiensis* (Ernst *et al.*, 2002). Two potato genes, *Gro1-4* and *Gpa2,* which confer resistance against *G. pallida* are both classified as NBS-LRR and have been shown to elicit the HR response (Paal *et al.*, 2004; van der Vossen *et al.*, 2000).

In barley, four loci for resistance against *H. avenae* have been mapped: *Rha1*, *Rha2*, *Rha3,* and *Rha4* (Andersen & Andersen, 1968; Andersen & Andersen, 1973; Barr *et al.*, 1998; Cotten & Hayes, 1969; Kretschmer *et al.*, 1997), but no causal genes have been isolated. Van Gansbeke *et al.* (2019) fine-mapped the resistance locus *Rha2* and discussed three candidate genes, including one that encodes a zinc-binding protein RAR1 which is known to activate the HR response against powdery mildew (Shirasu *et al.*, 1999).

2.5.2 Resistance against *Heterodera avenae* in wheat

Despite the genomic complexity of wheat, several loci that affect resistance against CCN have been mapped. At some of these, the resistance alleles are known to have been introgressed from related species, including *Ae. ventricosa* (*Cre2*, *Cre5*, and *Cre6* ; (Jahier *et al.*, 2001; Ogbonnaya *et al.*, 2000)), *Ae. tauschii (Cre3* and *Cre4* (de Majnik *et al.*, 2003; Jahier *et al.*, 2001)), *Ae. triuncialis* (*Cre7*; (Jahier *et al.*, 1998; Romero *et al.*, 1998)), *Secale cereal (CreR*;

(Taylor *et al.*, 1998)) and *Ae. variabilis* (*CreX* and *CreY;* (Barloy *et al.*, 2007)). At two other loci, *Cre1* and *Cre8*, the resistance alleles are thought to originate from bread wheat itself (de Majnik *et al.*, 2003; Paull *et al.*, 1998; Safari *et al.*, 2005).

Resistance can be assessed by counting the number of cysts that develop on plant roots. Cyst counts have been used to rank the effectiveness of various *Cre* genes. Safari *et al.* (2005) compared cyst counts (likely pathotype Ha13, collected in Victoria, AUS) of wheat materials though to carry resistance alleles at the *Cre1, Cre3* and *Cre8* loci and ranked the effectiveness of these loci as *Cre3* > *Cre1* > *Cre8*. Similarly, Cui *et al.* (2017) compared eight *Cre* loci (using pathotype Ha91, collected in Beijing, China) and concluded that *Cre3* was the most effective and *Cre1* and *CreR* were the least effective.

No causal genes for nematode resistance have been isolated in wheat. However, research on both *Cre1* and *Cre3* (located at homoeologous loci 2B and 2D, respectively) have identified a NBS-LRR on both loci as likely candidates (de Majnik *et al.*, 2003).

2.6 Microscopy techniques

There are many types of microscopy, including electron, optical, confocal, and tomography which all serve different purposes. Due to the short wavelengths of electron microscopy, high resolution (less than 0.2 nm) can be obtained to image cell ultrastructure of very small specimens. Optical microscopy, also known as light microscopy, uses visible light that shines through the sample. Confocal microscopy uses lasers to excite fluorophores. Histochemical optical microscopy allows for specific labelling of biological structures with coloured or fluorescent stains. Tomography uses X-rays and can be used for imaging whole tissue without the need for tissue sectioning.

2.6.1 Microscopy as a tool for understanding feeding site development

Different microscopy tools have been used to study the development of *Heterodera* spp. feeding sites within host tissue. Application of scanning and transmission electron microscopy (SEM and TEM) revealed how syncytia are formed, with images showing large multinuclear cells full of cytoplasm, mitochondria, Golgi bodies, and enlarged nuclei (Jones, 1981; Jones & Dropkin, 1975; Jones & Northcote, 1972; Sobczak & Golinowski, 2009). Optical microscopy has revealed anatomical relationships with surrounding cells (Golinowski *et al.*, 1997; Grymaszewska & Golinowski, 1991) and the timing of syncytial development (Golinowski *et al.*, 1996; Williams & Fisher, 1993). These microscopy techniques have relied on very thin (< 3 µm) sections to ensure clarity under the microscope.

More recently, microscopy techniques have been used for analysing three-dimensional structure of feeding sites. Confocal microscopy has been used to study feeding sites of *H. glycines* using z-plane stacks, revealing pillar structures within SCN feeding sites (Ohtsu *et al.*, 2017). Laser-ablation tomography has been used to reveal three-dimensional structures of *H. avenae* feeding sites in barley roots (Strock *et al.*, 2019). More investigations using three-dimensional imaging are needed.

2.6.2 Differences of feeding sites induced in resistant plants

As reviewed by Sobczak and Golinowski (2009), feeding site development can differ between resistant and susceptible plants. Some differences are subtle, such as a difference in the endoplasmic reticulum (ER) in the feeding sites of *H. schachtii* between susceptible host plants (smooth ER) and resistant plants (rough ER with large vacuoles) (Wyss *et al.*, 1984). Others are more obvious such as a necrotic layer around feeding sites of *H. glycines* that was observed in resistant plants but not in susceptible plants (Kim *et al.*, 1987).

Although the development of cyst nematode feeding sites is generally conserved throughout different hosts, each host-parasite relationship should be considered due to differences in anatomy and physiology of the host. For example, many studies have focused on feeding site

development within the model plant *Arabidopsis thaliana* (e.g. Golinowski *et al.*, 1996; Grundler *et al*., 1994; Grundler *et al.*, 1998), which differs in root size and anatomy from other hosts. The roots of wheat are approximately four times larger than those of Arabidopsis and contain a central xylem vessel that Arabidopsis lacks.

The development of *H. avenae* syncytia has been studied in wheat plants with some *Cre* genes. Grymaszewska and Golinowski (1991) found that syncytia in resistant *Cre1* wheat roots were delayed in development and lacked contact with xylem elements. Williams and Fisher (1993) found plants containing *Cre1* showed similar syncytia development to a susceptible cultivar up until 15 d after inoculation (DAI). At this stage, syncytia appeared more active with more cytoplasm and organelles in susceptible plants than in resistant plants. Seah *et al.* (2000) confirmed this observation for *Cre1* and found a similar pattern in syncytia of plants containing *Cre3*. Similarly, Cui *et al.* (2017) reported non-active syncytia with dense cytoplasm in *Cre3* plants but large and highly active feeding sites in susceptible plants.

2.7 Resistance locus *Cre8*

The *H. avenae* resistance associated with *Cre8* was first reported in the cultivar Festiguay and its derived cultivars including Molineux, Barunga and Frame (Paull *et al.*, 1998). The *Cre8* locus was assigned to the long arm of chromosome 6B (Williams *et al.*, 2003) and later mapped relative to molecular markers on that chromosome arm (Williams *et al.*, 2006). Further mapping placed *Cre8* in an interval of 8.1 cM between the markers *wri16* and *BS00022444* (Jayatilake *et al.*, 2015). Kumsa (2015) added two additional co-dominant markers to this region, determined the locus order to be *wri16-wri13-BS00109879-Cre8-BS00022444* and anchored BS00109879 and BS00022444 to the '6B 139.160 cM' genetic bin on the TGACv1 draft wheat genome assembly (ftp://ftp.ensemblgenomes.org/pub/plants/pre/fasta/triticum_aestivum/dna/). Both markers

were assigned to the same genetic bin '6B 139.160 cM' containing 41 predicted genes. Subsequently, Hendrikse (2016) mapped 12 out of 41 predicted genes in that bin and excluded 9 genes as being outside of the candidate interval. At the time of that work, there was still no reference assembly of the wheat genome. This made it difficult to know whether there might be other predicted genes in the region. During the period in which research was conducted for this thesis, the International Wheat Genome Sequencing Consortium released two versions (IWGSC RefSeq v1.0 assembly and IWGCS RefSeq v2.0 assembly, https://wheat-urgi.versailles.inra.fr) (Alaux *et al.*, 2018), of an annotated reference genome for Chinese Spring wheat and the 10+ Wheat Genomes Project (http://www.10wheatgenomes.com) assembled genome assemblies for other wheat cultivars.

2.8 Tolerance

Tolerance to PPNs is the ability of a plant variety to maintain yield despite infection by nematodes. Both tolerance and resistance are important traits. Varieties that are resistant but not tolerant may fail in a heavily infested soil (Rathjen *et al.*, 1998) while varieties that are tolerant but not resistant can allow nematode populations to reach damaging levels (Fisher *et al.*, 1981). One challenge associated with tolerance is that its measurement requires assessment of crop yield at varying nematode population densities (Trudgill, 1991). Due to the difficulties associated with obtaining this information, plant vigour and/or yield under high nematode pressure are sometimes used as indicators of tolerance. In addition to evaluating resistance in the Trident/Molineux mapping population, Williams et al. (2003) rated plant vigour at 12 weeks after sowing as an indicator of tolerance. These traits mapped to the same region, the *Cre8* locus, but the relationship between these traits remains unknown.

2.9 Research Gaps

The overall aim of this study was to improve understanding of how the *Cre8* locus affects the resistance of wheat against cereal cyst nematode. Based on the literature reviewed here, the following research gaps and opportunities were identified:

- There is a limited knowledge of cyst nematode feeding site development in cereal roots and therefore more investigations need to be conducted.
- Most microscopy studies so far on nematode feeding sites have used thin sections and 2-dimensional images which provide limited information on spatial relationships and 3-dimensional structures. Alternate methods are needed for better understanding of nematode feeding sites.
- Little is known about the resistance mechanisms of any CCN resistance gene, and almost nothing is known about the resistance mechanism of *Cre8*.
- A few nematode resistance genes have been identified, however no causal genes against CCN have been isolated.
- Although *Cre8* has been genetically mapped at quite high resolution, the region was still too large to identify candidate genes and lacked reliable reference genome information to help delineate the *Cre8* region.

Chapter 3 : Methods for microscopic observation of cereal cyst nematodes and their feeding sites in wheat roots

3.1 Summary

This chapter reports on the evaluation of methods for observing nematodes and their feeding sites within roots. Several methods for soil-free plant growth were compared. A single embedding and sectioning method was used for all tissues, involving embedding in agarose and use of a vibratome to prepare thick sections. Various combinations of methods for sample preparation and staining were compared. Both light and confocal microscopes were used. The results made it possible to select appropriate methods for use in research that will be reported in subsequent chapters.

3.2 Introduction

Observation of nematode feeding sites within plant roots requires robust and reproducible techniques for preparing and imaging root tissue. The main challenges associated with imaging roots are maintaining soil-free growth conditions, handling tissue with care as to not disturb cell morphology and using methods that can penetrate the multi-layered root tissue.

Microscopic analysis has previously been conducted on CCN-infected tissue from plants that were inoculated and grown in soil, e.g. Grymaszewska and Golinowski (1991), or inoculated in soil and transferred to perlite, e.g. Seah *et al.* (2000), but this can be problematic. If soil particles remain attached, they can damage blades during sectioning and/or lead to poor quality images. While there has been some use of soil-free methods involving agar (Bohlmann & Wieczorek, 2015) or hydroponics (Hasegawa *et al.*, 2016; Zhang *et al.*, 2017), no comparisons of these methods have been reported.

Most previous microscopy of nematode-infected roots has used thin sections (< 3 µm) compatible with light microscopy (Aditya *et al.*, 2015; Cui *et al.*, 2017; Grymaszewska & Golinowski, 1991; Kim *et al.*, 1987; Seah *et al.*, 2000; Sobczak & Golinowski, 2009; Williams & Fisher, 1993; Zhang *et al.*, 2017). Prior to sectioning, tissue is typically fixed and then embedded in resin or paraffin. Although tissue fixation helps preserve cell content, the

chemicals used can unintentionally alter morphology or affect permeability of some dyes. Additionally, resin and paraffin embedding are long laborious procedures that can also unintentionally alter morphology. Better structural preservation can be achieved by using whole mount or thicker sections in combination with the use of clearing agents such as ClearSee and TOMEI (Hasegawa *et al.*, 2016; Ohtsu *et al.*, 2017; Ursache *et al.*, 2018). While ClearSee has been successful in clearing tissue, the published techniques for its use involve harsh fixatives and some laborious embedding methods.

The aim of the research reported in this chapter was to establish appropriate microscopy preparation techniques and staining protocols for imaging nematode feeding sites in wheat roots (Fig. 3-1). To accomplish this, different sample preparations and tissue stains were tested and compared. Sample preparations included fresh tissue (no fixation) versus fixation, with and without the addition of ClearSee as a clearing reagent. Finally, although acid fuchsin has long been used for nematode detection in roots (McBeth *et al.*, 1941), especially since the technique was improved by Bybd *et al.* (1983), there are no published reports that combine acid fuchsin-stained tissue with confocal microscopy. For staining comparisons, the use of optical microscopy stains and several combinations of fluorescent dyes for confocal microscopy were analysed. The organisation of this chapter follows the workflow outlined in Figure 3-1. First, methods and results of nematode inoculation and plant growth are reported. Next, sampling protocols and tissue preparation are presented followed by staining protocols. Further, results of these protocols are discussed in the context of light and confocal microscopy. To conclude, an overall discussion of microscopy for use in nematode-infected roots is presented.

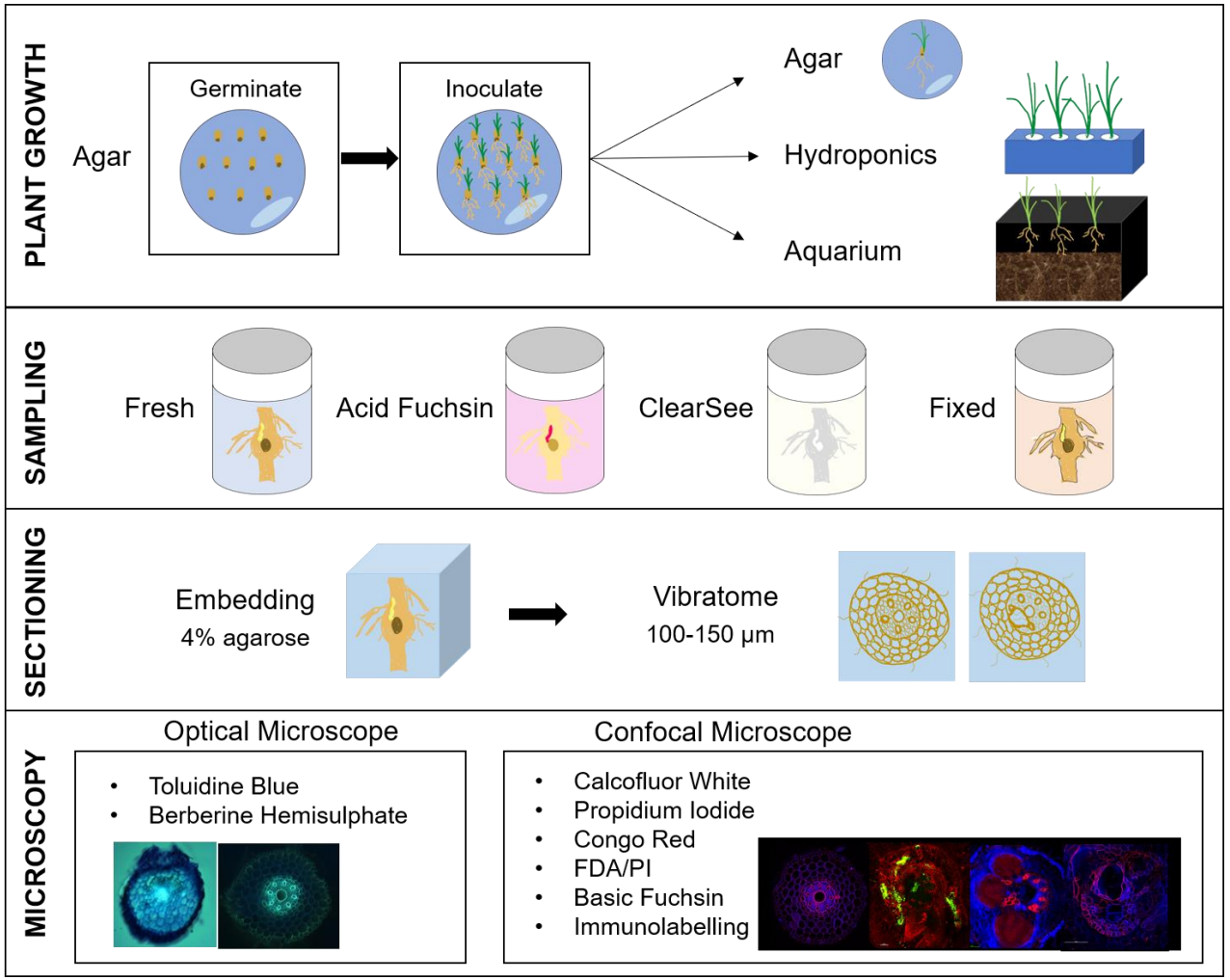

Figure 3-1: Outline of methods to investigate nematode-infected wheat roots. Methods investigated included different plant growth media, sampling treatments, and staining for observation using optical and confocal microscopy. A central and unified method was used for tissue sectioning.

3.3 Inoculation and plant growth

3.3.1 Materials and methods

3.3.1.1 Plant materials

The susceptible wheat (*Triticum aestivum*) line TMDH82 was used. It is a doubled haploid line derived from the F_1 generation of a cross between the Australian wheat cultivars Trident and Molineux.

3.3.1.2 Nematode inoculum

In order to obtain J2 nematodes for plant inoculation, CCN (*Heterodera avenae* Woll., pathotype Ha13) cysts were obtained (originating from infested soil sampled from the Yorke Peninsula, South Australia). Cysts were mixed with organic material and put into synthetic silk cloth bags (100 µm) to create nematode 'farms' which were kept immersed in water at 4°C in darkness. Prior to inoculation, nematode farms were washed 24 h before nematode collection to ensure freshly hatched J2 nematodes. To harvest, water from the farms was poured through a 38 µm sieve. The sieve was rinsed, and the water collected with nematodes as inoculum. 20 µL aliquots were sampled and the numbers of nematodes in these aliquots were counted. Water was added to the inoculum to adjust the concentration to approximately 2,000 nematodes/mL.

3.3.1.3 Preparation of agar plates, seed germination, and inoculation

Sterile 2% agar was prepared in sterile petri dishes (140 mm diameter). Seeds were surface sterilised in 3% sodium hypochlorite (NaOCl) for 10 min on a shaker, then rinsed three times with sterile water for 5 min. Between 10 and 12 sterilised seeds were placed on a 2% agar plate in three rows (Fig. 3-2a) with all embryos facing downward, so that all roots emerged the same direction (Fig. 3-2b). Agar plates were sealed with parafilm, placed in a growth chamber and kept at 15°C in darkness until the seeds had germinated and roots were between

4 and 6 cm long (approximately 3 d). In a laminar flow cabinet, 20 µL of inoculum was pipetted directly at each root tip (Fig 3-2b). During inoculation, inoculum was constantly stirred to ensure an even distribution of nematodes. For mock-inoculated material, 20 µL of water was pipetted at the root tip. Plates were returned to 15°C and maintained in a 12 h light: 12 h dark cycle for 24 h.

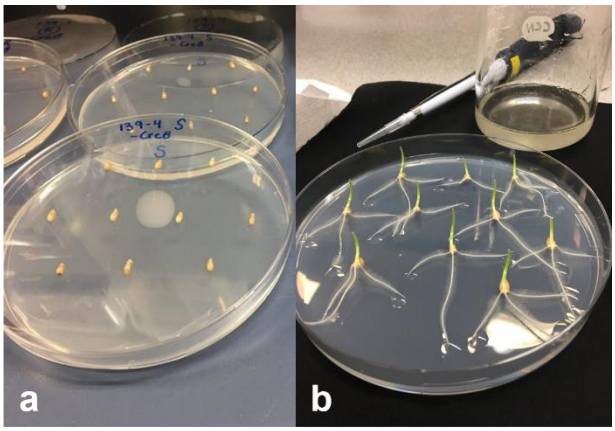

Figure 3-2: Seed germination and inoculation on agar plates. (a) Placement of seeds on agar plates for germination and (b) Seedlings inoculated with *H. avenae* inoculum at root tips.

3.3.1.4 Plant growth

After the 24 h inoculation period, roots were washed to remove any external nematodes. To wash, each seedling was first removed from the agar by holding the shoot and gently lifting the roots (to avoid root breakage). Roots were then gently submerged several times into a beaker of sterile water. Each seeding was then transferred to one of the following growth media:

3.3.1.4.1 Agar

Washed inoculated plants were placed on new 2% agar plates. For experiments lasting up to 5 DAI, three to five plants were placed on a plate (Fig. 3-3a). For experiments lasting longer than this, only one or two plants were placed on a single plate (Fig. 3-3b). Plates were kept at 15°C on a 12 h light: 12 h dark cycle.

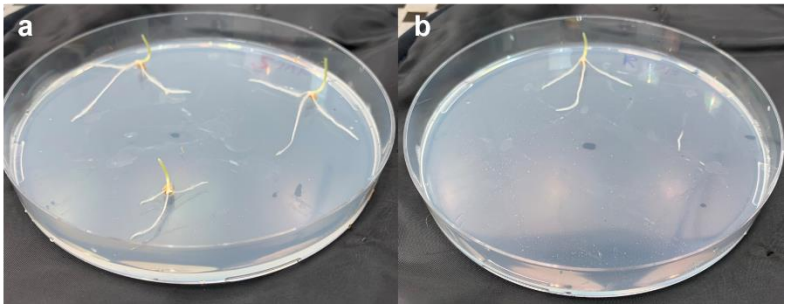

Figure 3-3: Agar growth method. (a) Three plants were placed on agar for experiments under five days (b) One plant was placed on agar for experiments longer than five days.

3.3.1.4.2 Hydroponics

The nutrient solution used for hydroponics was a modified Johnson's solution (Johnson *et al.*, 1957) as described by Melino *et al.* (2015) containing a final concentration of 0.5 mM MgSO4, 0.5 mM KH_2PO_4, 0.25 mM $Ca(NO_3)_2$, 0.5 mM KNO_3; and the micronutrients, 50 µM KCl, 25 µM H_3BO_3, 2 µM $MnSO_4$, 2 µM $ZnSO_4$, 0.5 µM $CuSO_4$, 0.5 µM Na_2MoO_4, and 50 µM Fe-EDTA. On the day of transferring plants to the hydroponic tank, solutions were diluted to the final concentration in each hydroponic bin (up to 10 L) (See Appendix 1 for stock solution preparation). Nutrient solution was replaced twice a week. To transfer each plant, the end of a 1.5 mL Eppendorf tube was cut off just above the tip. The shoot was gently pushed up through the cut end of the tube. Forceps were then used to pull the plant further into the tube, such that the seed was about 1 cm above the cut edge (Fig 3-4a) and the roots were protruding through the cut end of the tube. Each 1.5 mL tube was then placed into a 50 mL tube with the end cut off (Fig 3-4b). That tube was placed within the hydroponic tank (Fig 3-4c), taking care to not damage the roots. Tanks were kept at 15°C on a 12 h light: 12 h dark cycle with constant aeration from an air pump connected to an air stone (Aqua One 2500 precision air pump, HI setting).

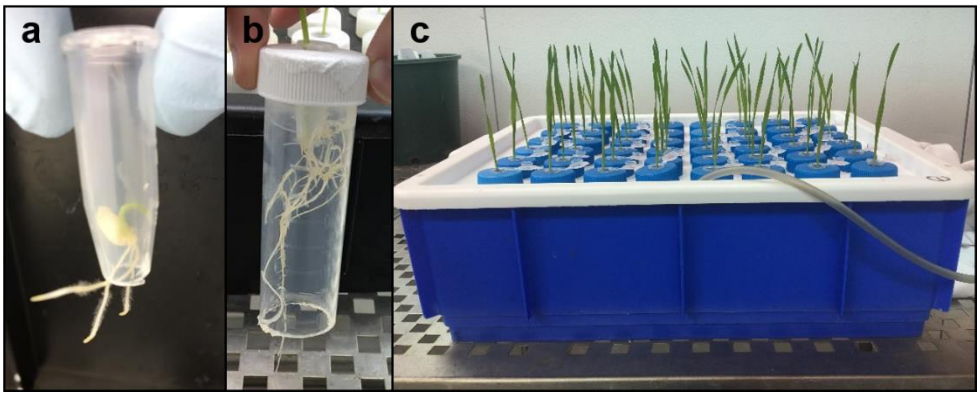

Figure 3-4: Hydroponic growth method. (a) Seedling placed into 1.5 mL Eppendorf tube. (b) Plant within a 50 mL tube. (c) Hydroponic tank with plants and aerator tube. (*This figure also appears as Figure 4-5 in the published manuscript presented in Chapter 4*.)

3.3.1.4.3 Aquarium soil tank

A 75 L glass fish tank (62 × 32 × 43 cm) was filled to two thirds with cocopeat. A cloth was used to line the inner surface of the upper third of the tank. Sandy loam was added on top of the cocopeat to keep the cloth lining in place, and an aluminium foil covered box was placed on top of sandy loam (Fig. 3-5a). Inoculated and washed plants were placed against the inner surface of the tank wall, between the cloth and glass. Once plants were in place, cardboard panels were placed on the outer surface of the tank to exclude light (Fig. 3-5b). Soil was watered every other day as needed. Tanks were kept at 15°C on a 12 h light: 12 h dark cycle.

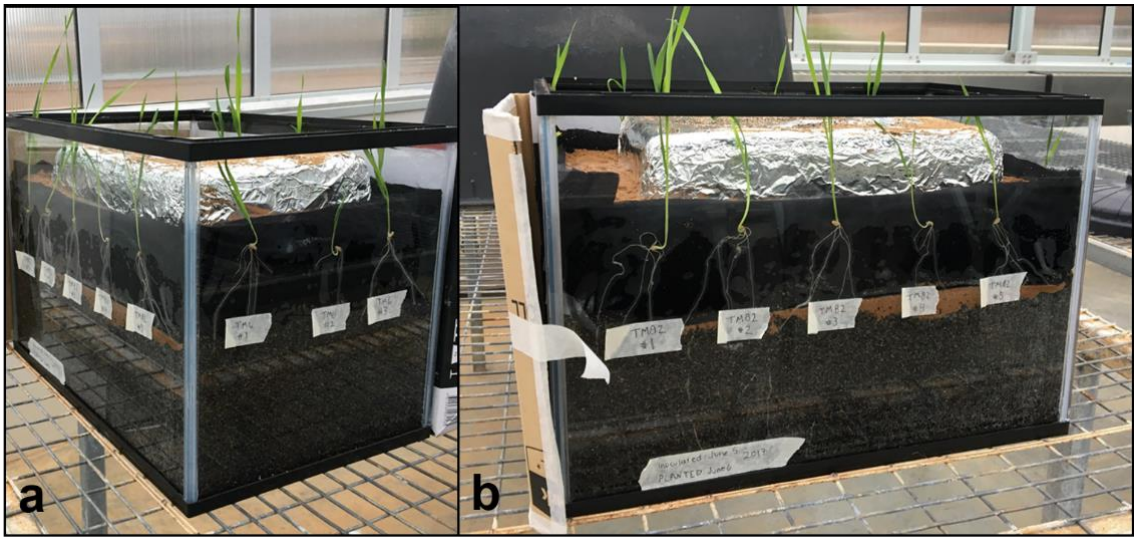

Figure 3-5: Aquarium tank method. (a) Seedlings arranged on all sides of the tank between soil and cloth for observation. (b) Cardboard was taped around the outside of the tank to keep roots in darkness.

3.3.2 Results

Inoculated plants grown on agar had visibly infected regions as early as 1 DAI (Fig. 3-6). Infection was indicated by dense root hairs, swelling and slight bending. By 7 DAI, the plants had numerous lateral roots in infected regions. The length of roots increased steadily until approximately 14 DAI, reaching about 8 cm, but did not continue to increase after this. It was difficult to maintain the sterility of agar plates over time due to the addition of inoculum. Nevertheless, infected tissue samples with plump roots without obvious contamination could still be obtained from some inoculated plants up to 17 DAI.

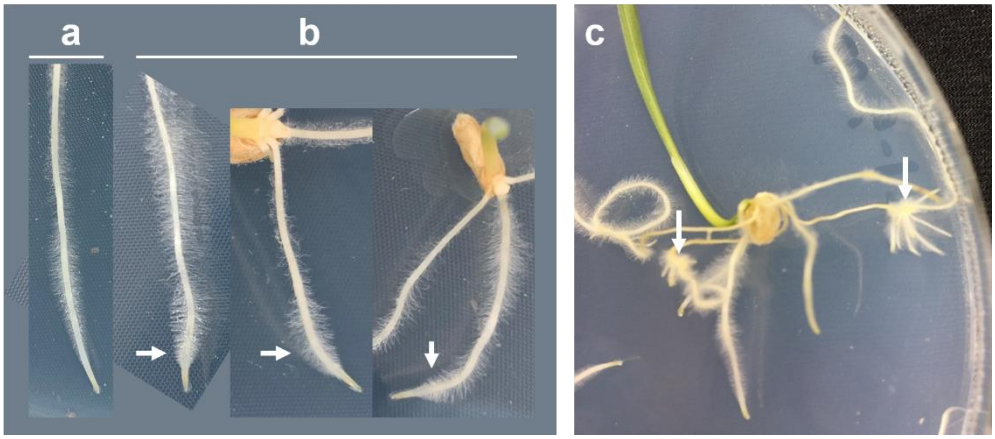

Figure 3-6: Identifying CCN-infected regions. On agar plates, wheat roots infected with *H. avenae* showed distinct swollen regions. (a) Mock-inoculated roots at 1 DAI with no swollen region. (b) CCN-infected roots at 1 DAI with arrows indicating swollen infected regions with dense root hairs. (c) CCN-infected roots at 7 DAI with arrows indicating infected regions seen as swollen roots with proliferation of lateral roots.

Inoculated plants grown in hydroponics had infected regions that were less visible compared to plants grown in agar. When plants were removed from the hydroponic tank, root hairs were slick against the root, making it difficult to distinguish dense root hairs, however, swollen root regions were still visible. By 7 DAI, infection sites were clearly visible, based on lateral root formation at the site of infection (Fig. 3-7). Root length, number of lateral roots, and length of lateral roots increased between 10 and 15 DAI (Fig. 3-7). Infected sites continued to be visible for as long as plants were maintained in hydroponics. The capacity of the hydroponic tanks was sufficient to support root growth up to 40 DAI. By that time, white cysts could be seen on roots (Fig. 3-8).

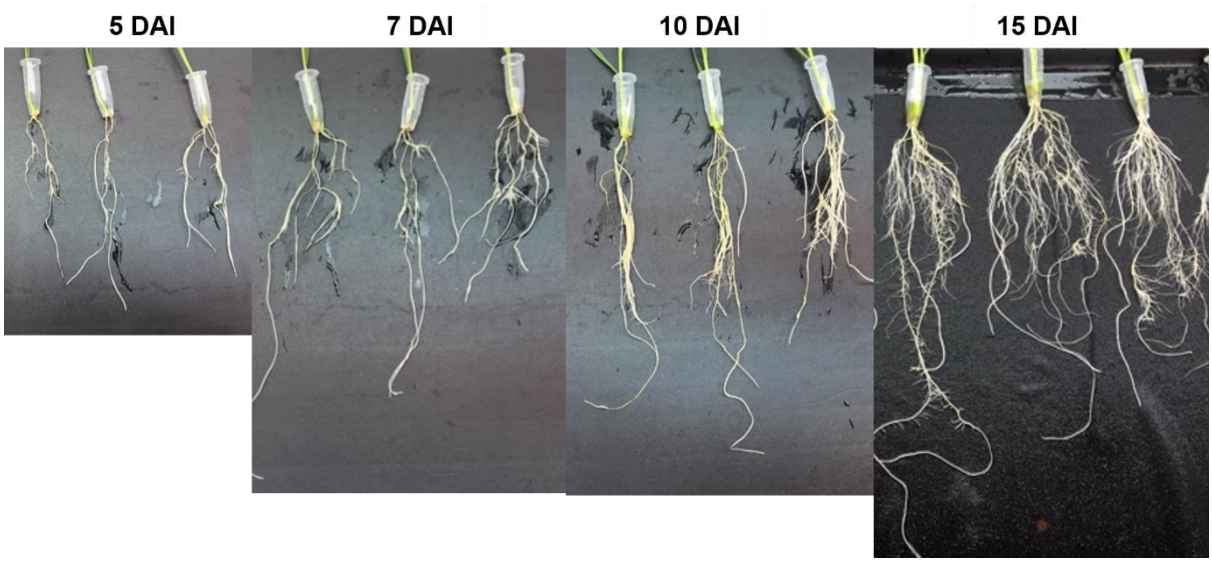

Figure 3-7: Root growth of CCN-infected plants grown in hydroponics. Observation of infected root systems at 5, 7, 10 and 15 DAI with *H. avenae*.

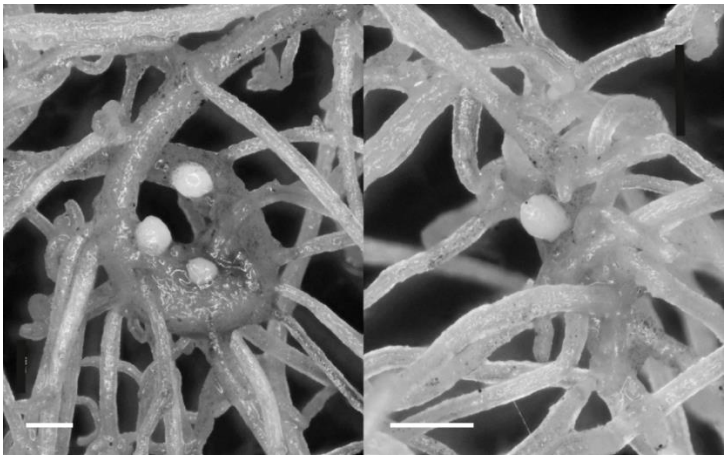

Figure 3-8: CCN cysts observed on roots grown in hydroponics. Observation of root systems at 40 DAI with *H. avenae*. Scale bar 500 µm.

Until 7 DAI, infected regions developed similarly regardless of whether plants were grown on agar or in hydroponics. By 9 DAI, plants grown hydroponically had slightly longer roots and shoots than those grown on agar (Fig 3-9). At 14 and 17 DAI, plants grown hydroponically had much longer roots and shoots than those grown on agar (Fig 3-9).

Figure 3-9: Comparison of CCN-infected plants grown in agar and hydroponics. Observation of *H. avenae* infected plants (a) grown on agar and (b) grown in hydroponics at 9, 14, and 17 DAI.

The aquarium tank method was useful for observation of infected roots over time since roots could easily be viewed through the glass. The development of infected sites was similar to that observed for plants grown on agar. By 9 DAI, swollen regions were visible with some lateral root development. By 14 and 17 DAI, swollen regions were still visible however, lateral root growth was very minimal (Fig. 3-10). Inoculated plant tissue grown in the aquarium tank could be collected up to 17 DAI. After this time point, plants continued to grow, however, existing infected sites began deteriorating. Plants were grown until maturity, but cysts were never observed. Overall, plants were more robust than agar grown plants but less robust than hydroponically grown plants.

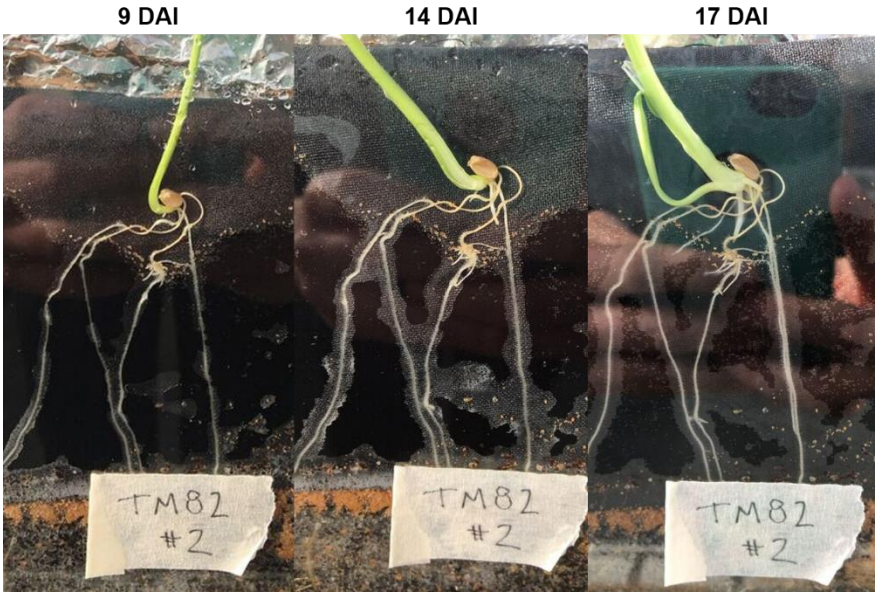

Figure 3-10: Root growth of CCN-infected plants grown using the aquarium tank method. Observation of *H. avenae* infected roots at 9, 14, and 17 DAI.

3.3.3 Growth media conclusions

In order to produce soil-free tissue for microscopy, three growth methods were tested: agar, hydroponics, and an aquarium tank method. All three methods could successfully produce infected tissue up to 17 DAI. After this, root vigour declined in both the agar and aquarium methods. In contrast, it was possible to obtain infected tissue from plants in up to 40 DAI in a hydroponic system. The hydroponic conditions were also favourable for CCN development showing cyst formation by 40 DAI. Neither agar nor aquarium methods supported maturation of nematodes. The hydroponic method was therefore selected for further microscopy research due to its robust plant growth, lack of contamination issues, and ability to support nematode development.

3.4 Sampling, preparation and staining protocols of root tissue

This section reports on methods used for sampling, preparation and staining of root tissue for microscopy. Results are reported in section 3.5.

3.4.1 Acid fuchsin staining of whole roots

Whole plants were collected and the shoots were cut off so that only a small portion of shoot remained to hold the root system together. To stain with acid fuchsin, roots were treated according to the protocol from Bybd *et al.* (1983). In short, root tissue was cleared in 2% NaOCl for 1 min, then stained and heated with an acid fuchsin solution (33% glycerol v/v, 33% lactic acid v/v, and 0.5 g/L acid fuchsin). Roots were cooled at room temperature for 5 min. Infected tissue was collected and embedded the same way as fresh tissue described below.

3.4.2 Tissue collection

Infected regions were identified (see Fig. 3-6) as swollen regions of roots with proliferation of lateral roots. Root segments between 1 and 2 cm long were excised by cutting above and below the swollen tissue. For control tissue, corresponding root regions were excised from mock-inoculated tissue.

3.4.3 Preparation of tissue for embedding

3.4.3.1 Fresh tissue

Fresh tissue collected from hydroponics was gently dabbed with a cotton bud to remove excess water before embedding.

3.4.3.2 Fixation

To fix tissue for microscopy, up to four root segments were placed into a 1.5 mL tube and covered with 4% paraformaldehyde (PFA) for 1 h. PFA was prepared according to Ursache *et al.* (2018). Samples were then washed with 0.1 M phosphate-buffered saline (PBS) three times by pipetting, then washed with sterile water. Tissue was dabbed dry using a cotton bud before embedding.

3.4.3.3 ClearSee

ClearSee, an optical clearing agent, was made by mixing 10% (w/v) xylitol powder, 15% (w/v) Na-deoxycholate, and 25% (w/v) urea as described by Kurihara *et al.* (2015). To clear roots, up to four root segments were placed in a 1.5 mL tube, covered in ClearSee and kept at room temperature for 30 d. ClearSee solution was changed every 4 to 7 d, or when discolouration of the solution was observed. Samples were then removed from the ClearSee using a paintbrush, placed into a new 1.5 mL tube and washed with 0.1 M PBS three times by pipetting. A final wash was done using sterile water. Tissue was dabbed dry using a cotton bud before embedding.

3.4.4 Embedding, sectioning and screening for microscopy

3.4.4.1 Embedding

A thick gel was used for all embedding by making a 4% agarose (w/v) solution in a large flask and heated in a microwave to dissolve. The flask was placed in a large container of water to prevent the agarose from boiling over and was removed from the microwave occasionally, stirred, then returned to heating in the microwave. Once the agarose was completely dissolved, it was cooled (e.g. for 200 mL agarose, 2 min at room temperature while stirring). Agarose was poured into petri dishes (50 mm diameter). Tissue samples were added gently and aligned using a paintbrush, maintaining approximately 0.5 cm between samples (Fig. 3-11). Agarose was then cooled for at least 10 min at room temperature.

Figure 3-11: Embedding wheat root tissue. Tissue was added to 4% agarose (w/v) and arranged with about 0.5 cm between samples.

3.4.4.2 Vibratome

Agarose pieces were cut into blocks for vibratome sectioning. This was done using a razor blade to cut the agarose into a rectangle or square, leaving at least 4 mm of agarose on all sides of the tissue. For each block, it was decided whether the tissue would be sectioned transversely or longitudinally. The block was then glued onto the vibratome plate using Selly's quick drying glue. For transverse sections, one end of the block was glued to the plate (tissue sample sitting upright, Fig. 3-12a). For longitudinal sections, one side of the block was glued to the plate (tissue sitting on its side, Fig. 3-12b). Vibratome step sizes ranging from 100 to 200 µm were used. A flat-headed paintbrush was used to catch each section from the vibratome (Fig 3-12c). Sections were placed on a labelled microscope slide for screening.

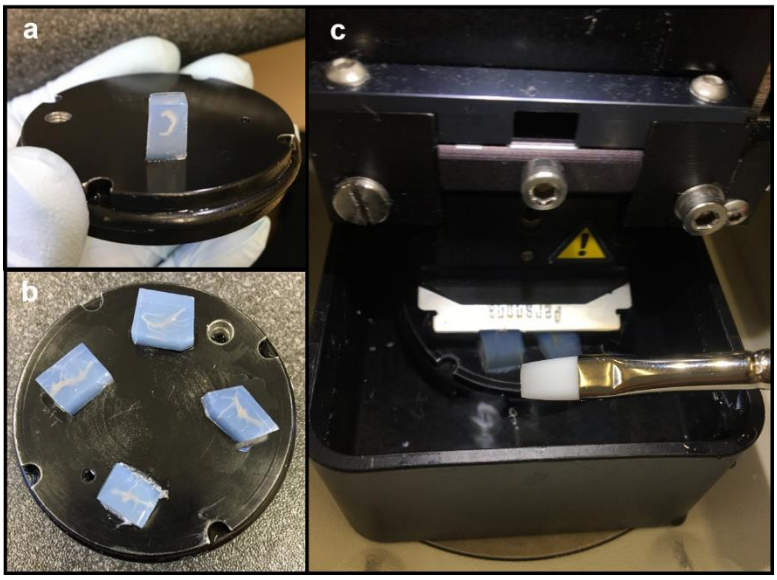

Figure 3-12: Vibratome sectioning of wheat roots. Orientation of tissue for cutting (a) transverse sections with tissue positioned upright or (b) longitudinal sections with tissue positioned on its side. Multiple sections could be glued to the vibratome plate. (c) Vibratome plate in place, covered in water, and vibratome cutting sections. A flat headed paintbrush was used to catch sections as they were cut.

3.4.4.3 Screening sections

Sections were examined under a light microscope at 10X magnification to determine which sections contained nematodes and/or feeding sites in order to select sections for further preparation and microscopy.

3.4.5 Staining protocols

Selected sections were mounted onto Teflon 3-well (12 mm diameter) slides. For all staining procedures, a pipette was used to add sufficient stain to cover each section. After staining and mounting, a glass coverslip (22 mm × 50 mm) was placed on the sections. More information for each stain can be found in Table 3-1.

3.4.5.1 Toluidine blue

For toluidine blue (TB) staining, 0.01% (w/v) TB was prepared in 0.1% (w/v) sodium tetraborate and sections were stained for 1 min. Tissue was washed with water three times then mounted in 50% glycerol (v/v).

3.4.5.2 Berberine hemisulphate

Berberine hemisulphate staining was used as described by Brundrett *et al.* (1988) . First, 0.25% (w/v) toluidine blue was prepared in water and tissue was stained for 90 s. Tissue was washed with water three times. Next, sections were stained in freshly made 0.1% (w/v) berberine hemisulphate for 60 min, changing solutions halfway, then washed with water three times. Lastly, freshly made 0.1% (w/v) $FeCl_3$ in 50% (v/v) glycerol was used to mount sections. Berberine hemisulphate and $FeCl_3$ must be made fresh.

3.4.5.3 Calcofluor white and propidium iodide

For calcofluor white and propidium iodide (CW/PI) staining, a 1:1 solution of 0.1% (w/v) CW and 10 ug/µL PI was prepared. Tissue was stained for 15 min then washed with water three times. Sections were mounted in 50% (v/v) glycerol.

3.4.5.4 Calcofluor white and Congo red

For calcofluor white and Congo red (CW/CR) staining, tissue was first stained with 0.1% (w/v) CW for 15 min, then washed with water three times. Next, tissue was stained with 0.1% (w/v) CR for 10 min, then washed with water three times. Sections were mounted in 50% (v/v) glycerol.

3.4.5.5 Fluorescein diacetate and propidium iodide

For fluorescein diacetate and propidium iodide (FDA/PI) staining, all tissue was fixed for 1 h before sectioning or embedding. The staining protocol used on sections was described by Jones and Senft (1985). A stock solution of FDA was prepared by adding

5 mg FDA to a final volume of 1 mL acetone (stored at -20°C). Stock solution of PI was prepared by adding 2 mg PI to a final volume of 1 mL 0.01M PBS (stored at 4°C). A fresh working solution of FDA/PI was prepared by adding 8 µL FDA stock and 50 µL PI stock to a final volume of 5 mL of water. The working solution was used to stain sections for 20 min. Sections were washed with water three times then mounted in 50% glycerol.

3.4.5.6 Basic fuchsin

For basic fuchsin (BF) staining, a modified protocol described by Ursache *et al.* (2018) was used. To stain, 0.2% (w/v) BF was prepared in ClearSee and sections were stained for 20 min then washed with water three times. After, sections were stained with 0.1% CW for 10 min, washed with water three times, then mounted in 50% glycerol.

3.4.5.7 Immunolabelling

For immunolabelling, all tissue was fixed for at least 1 h or overnight. Once sectioned, protocols for each antibody were followed according to Aditya *et al.* (2015). The antibodies, (1,4)-β-xylan/arabinoxylan (LM11) specific rat monoclonal antibody (PlantProbes, Leeds, UK) and (1,3;1,4)-β-glucan (BG1) specific mouse primary antibody were used (Meikle *et al.*, 1991; Meikle *et al.*, 1994). Secondary antibodies were conjugated to Alexafluor 555 (Life Technologies, Carlsbad, CA, USA). For both antibodies, 0.1% CW was used for a counterstain by staining for 5 min. Sections were then washed with water three times and mounted in 50% glycerol.

Table 3-1: Stains used in this study. Outline of the microscopy type each stain was used for (light or confocal); what each stain was used to target (substrate); whether the stain was compatible with ClearSee-treated tissue; the working solution concentration for staining; the amount of time samples were incubated in stain; and additional notes about staining procedures.

Name of stain	**Microscopy type**	**Substrate**	**ClearSee compatible?**	**Working solution %(w/v)**	**Time**	**Notes**
Toluidine blue	light microscopy	acidic tissue	No	0.01% in 0.1% sodium tetraborate	1 min	Used for most counterstains in light microscopy
Berberine hemisulphate	light microscopy	lignin, suberin, callose	No	0.1% in H20	1 h	Must be made fresh. Requires pre-treatment with toluidine blue and requires fresh $FeCl_3$ after staining
Calcofluor white	confocal	cellulose, chitin	Yes	0.1% in 70% EtOH	15-20 min	Used for most counterstains in fluorescence microscopy
Propidium iodide	confocal	nuclei/dead cells	Yes	10 µg/ µL in H_20	15-20 min	
Congo red	confocal	polysaccharides	Yes	0.5% in 50% EtOH	5 min	
FDA (fluorescein diacetate)/PI (propidium iodide)	confocal	live cells	No	see FDA/PI	20 min	
Basic fuchsin	confocal	lignin	Yes	0.2% in ClearSee	20 min	

3.5 Examination of root tissue with light and confocal microscopy

3.5.1 Light microscopy

3.5.1.1 Methods

Roots stained with acid fuchsin were examined using a Nikon SMZ25 stereo microscope with a 0.5 × objective lens. Unstained, TB stained and BH stained sections were examined using a Nikon Ni-E optical microscope at 10× and 20×. Unstained and TB stained sections were imaged using the bright-field setting. BH stained sections were imaged using the DAPI (340-380) filter and the use of a UV light source (solid state Lumencor Sola).

3.5.1.2 Results and Discussion

3.5.1.2.1 Acid fuchsin stained whole roots

Acid fuchsin staining made it possible to pinpoint the locations of nematodes relative to the swollen region (Fig 3-13). Although some drawings of cyst nematode life cycles have depicted nematodes below their feeding sites (e.g. Heinrich *et al.* (1998), Vanholme *et al.* (2004), Lilley *et al.* (2005)), nematodes were consistently oriented 'facing' downward, with their tails positioned above their heads.

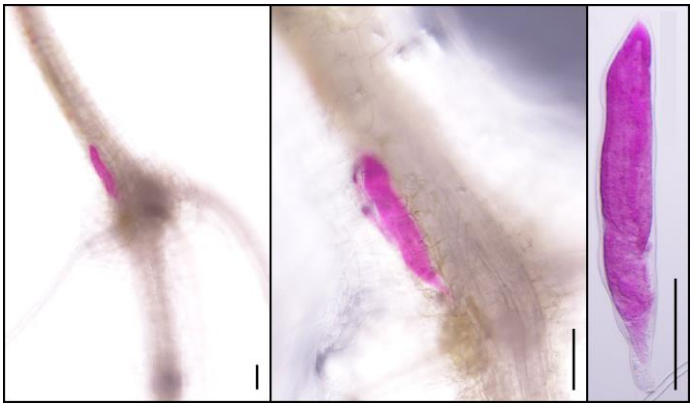

Figure 3-13: Nematode within a root. Acid fuchsin stained samples at increasing magnification of *H. avenae* within a wheat root sampled at 14 DAI. Scale bar: 100 µm.

3.5.1.2.2 Unstained sections

When unstained sections were examined by light microscopy with a 10× objective lens, key features were easily identified. Nematodes differed in colour from the surrounding plant tissue (Fig. 3-14a) while feeding sites looked like 'holes' within the tissue (Fig. 3-14b, c). In longitudinal sections, the most obvious sign of nematode infection was the presence of series of wide (bulging) central metaxylem cells (Fig. 3-14b,c).

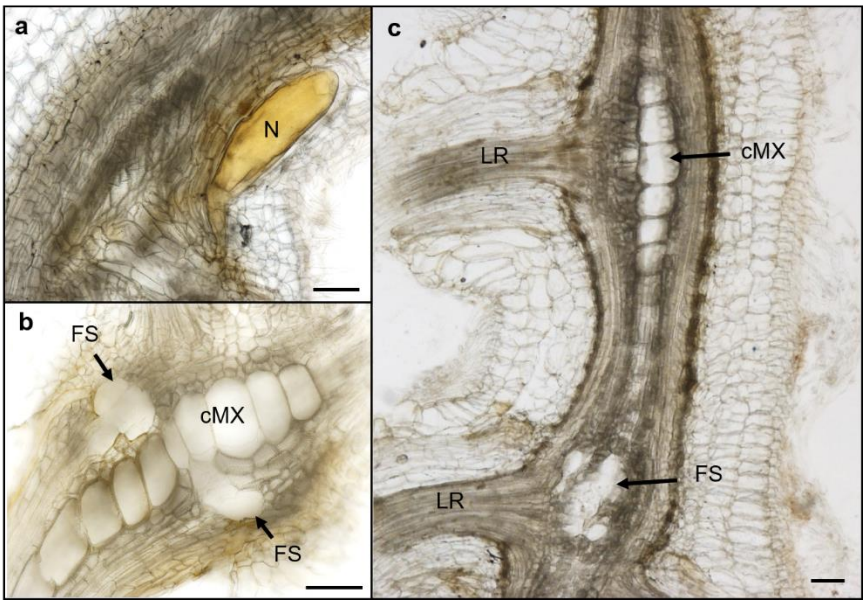

Figure 3-14: Unstained root vibratome sections. Optical microscope images of 150 µm sections of wheat roots sampled at 21 DAI with *H. avenae*. (a) A longitudinal section showing a nematode (N). (b) A longitudinal section showing two feeding sites (FS) adjacent to the central metaxylem (cMX). (c) A longitudinal section showing cMX, FS, and two lateral roots (LR). Scale bars: 100 µm.

3.5.1.2.3 Stained sections

Toluidine blue stained all cell walls blue. This staining was especially dense around the exodermis (Fig 3-15). Additionally, TB stained the agarose embedding material blue, causing the image background to have a blue tint.

When the combination of BH and $FeCl_3$ was used as a fluorescent stain with TB as a quencher, staining was visible within the vascular cylinder, endodermis and exodermis (Fig 3-

16). The strongest stained feature was cell walls of xylem vessels including central metaxylem and peripheral metaxylem (pMX) (Fig. 3-16a, b). In longitudinal sections of infected tissue, enlarged and thickened cMX cells were observed (Fig. 3-16d).

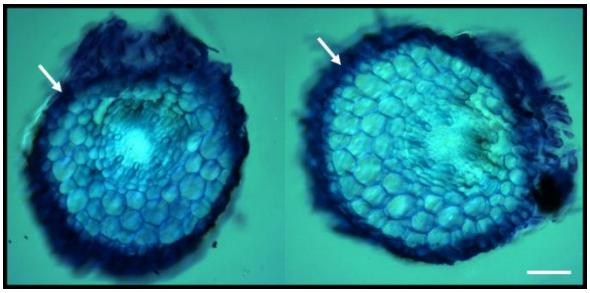

Figure 3-15: Root sections stained with toluidine blue. Optical microscope images of wheat root samples. Arrows indicate exodermis. Scale bar: 100 µm.

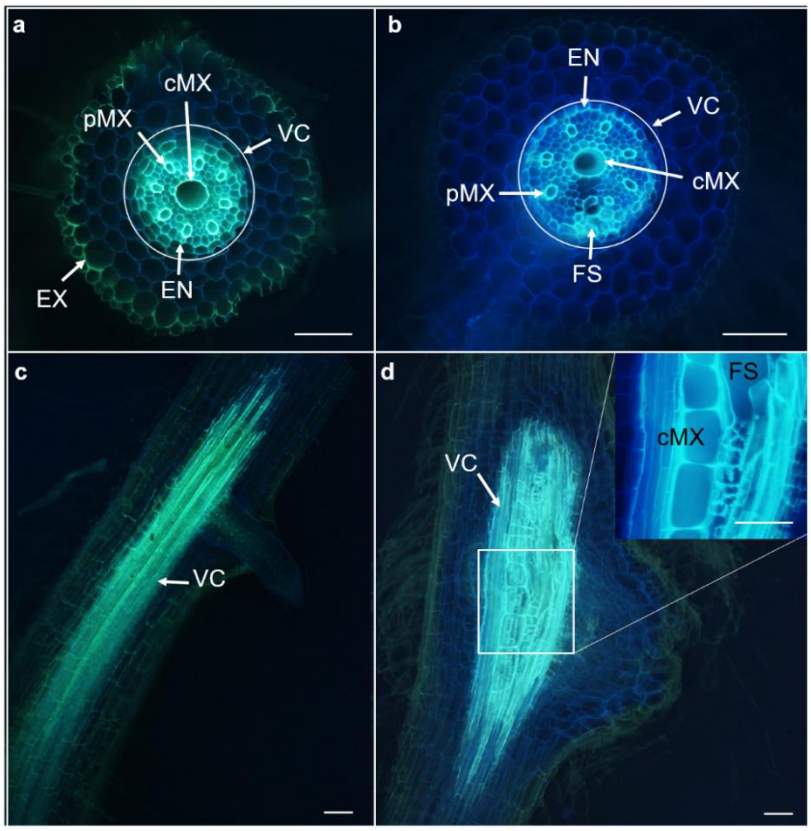

Figure 3-16: Root sections stained with berberine hemisulphate. (a) Transverse section of control root showing BH staining in exodermis (EX), vascular cylinder (VC), endodermis (EN), central metaxylem (cMX) and peripheral metaxylem (pMX). (b) Transverse section of CCN-infected root showing BH staining in VC, EN, cMX, pMX, and around nematode feeding site (FS). (c) Longitudinal section of control root showing BH staining throughout the VC. (d) Longitudinal section of CCN-infected root showing BH staining throughout VC, particularly in cell walls of cMX and FS. Scale bars: 100 µm.

3.5.2 Confocal microscopy

3.5.2.1 Methods

A Nikon A1R Laser Scanning Confocal microscope was used with two laser channels, DAPI (405 nm, blue) and TRITC (561 nm, red). Laser power and gain settings were adjusted for each section to avoid pixel saturation and minimise background luminescence.

3.5.2.2 Results

3.5.2.2.1 Transverse and longitudinal sectioning

Using acid fuchsin treated samples, it was relatively simple to pinpoint the location of the nematode and subsequent sectioning/imaging of the sample made it possible to identify the location of the syncytium (Fig. 3-17a). Most transverse sections of feeding sites did not contain the nematode. In some cases, a careful longitudinal section would capture both the nematode and feeding site (Fig. 3-17b) showing the nematode's body within cortex cells and only the tip of the head and stylet crossing over the endodermis

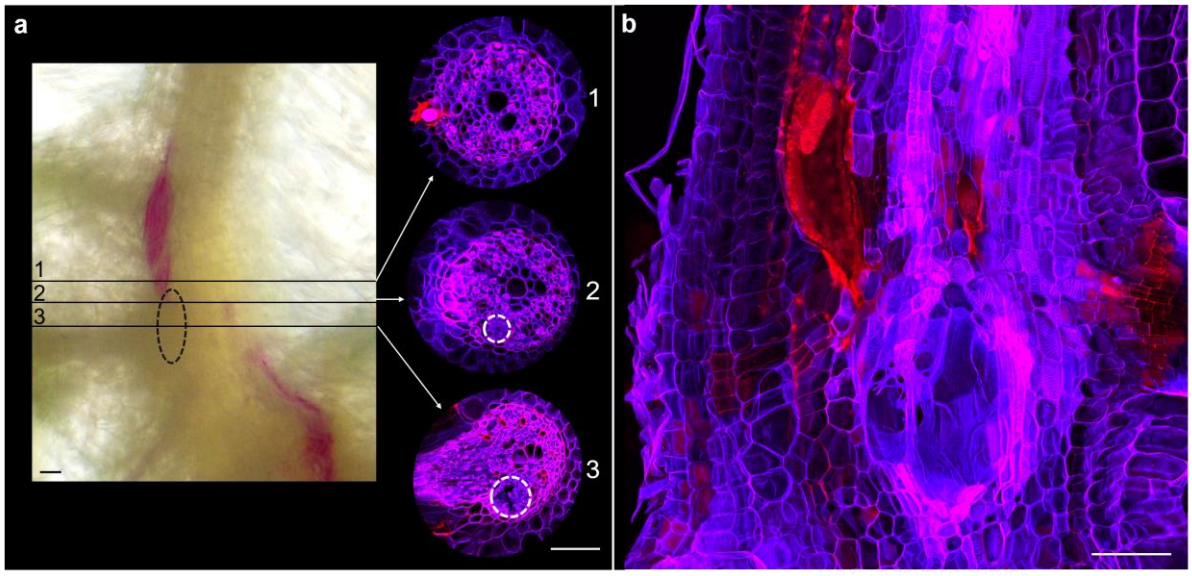

Figure 3-17: Nematode position in transverse and longitudinal sections. Root sections of *H. avenae* infected wheat roots. (a) Acid fuchsin staining revealed the location of the nematode within the root compared to the feeding site (dotted circle) followed by three consecutive transverse sections of the root: (1) nematode head just on the edge of the endodermis (2) no nematode and small width of feeding site (white dotted circle) (3) no nematode, largest portion of the feeding site and a lateral root initial. (b) Longitudinal image showing both nematode body, head, and feeding site. Scale bars: 100 µm.

3.5.2.2.2 Effects of sample preparation

Depending on how samples were prepared before embedding, staining results appeared differently under the confocal microscope. As a baseline, fresh tissue was stained with CW and PI on mock-inoculated (Fig. 3-18a) and infected (Fig. 3-18b) tissue. This showed CW staining on all cell walls and distinct PI staining on xylem vessels, endodermis, and nuclei within lateral roots initials (Fig 3-18a). In acid fuchsin treated roots, CW and PI stained sections showed shrivelled cortex cells (Fig. 3-19a) and showed inconsistent staining (Fig. 3-19b, c). When fresh tissue sections were stained with CW and BF, BF distinctly stained lignified pMX vessels (Fig 3-20a). Similar staining of pMX cells was obtained when fixed tissue sections were stained with CW and BF with additionally BF staining appearing in the nuclei of lateral root initials (Fig 3-20b). In ClearSee treated sections, CW and PI stained cell

walls evenly, appearing monotone (Fig. 3-21). The distinct CW/PI staining seen in fresh tissue was not apparent in acid fuchsin or ClearSee treated sections. Additionally, tissue treated with ClearSee over 30 d made tissue sections more translucent, increasing confocal laser depth from approximately 20 µm in non-treated samples (Fig 3-21a) to approximately 70 µm in treated samples (Fig 3-21b). The additional laser depth revealed more cell wall structures within feeding sites and revealed greater detail in the texture of cell walls.

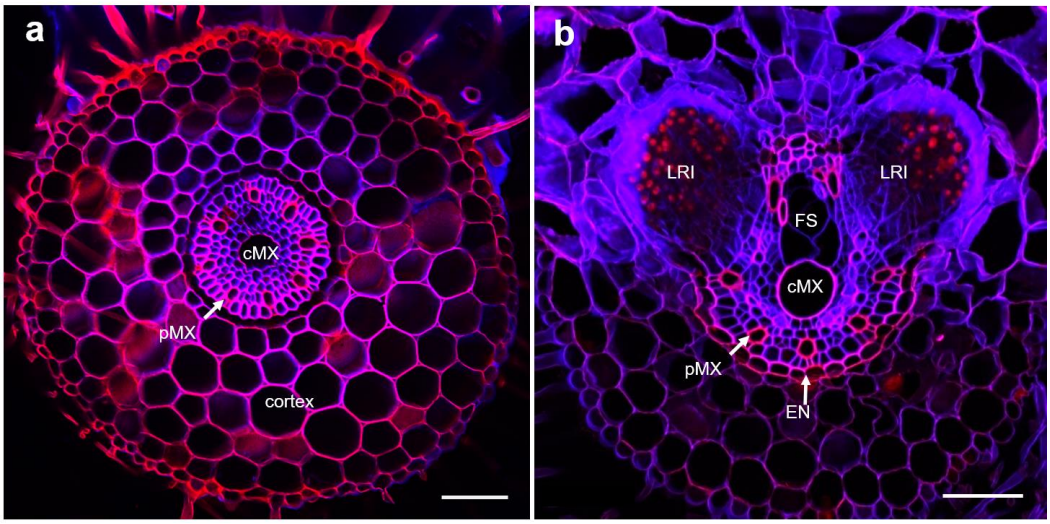

Figure 3-18: Confocal microscopy images of fresh root tissue. (a) Mock-inoculated (control) wheat root and (b) infected wheat root 10 DAI with *H. avenae* stained with calcofluor white (CW, blue) and propidium iodide (PI, red). PI staining visible in peripheral metaxylem (pMX), central metaxylem (cMX), endodermis (EN), and nuclei within lateral root initials (LRI). Feeding site (FS). Scale bar: 100 µm.

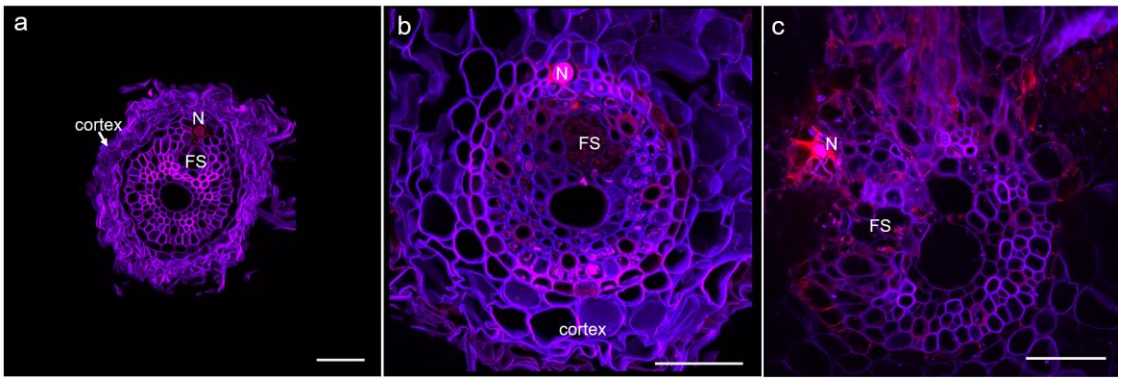

Figure 3-19: Confocal microscopy images of acid fuchsin treated roots. Transverse sections of infected wheat roots at 10 DAI with *H. avenae* and stained with calcofluor white (blue) and propidium iodide (red). Effects of acid fuchsin caused (a) damaged cortex cells and (b-c) irregular staining. Nematode (N); feeding site (FS). Scale bar 100 µm.

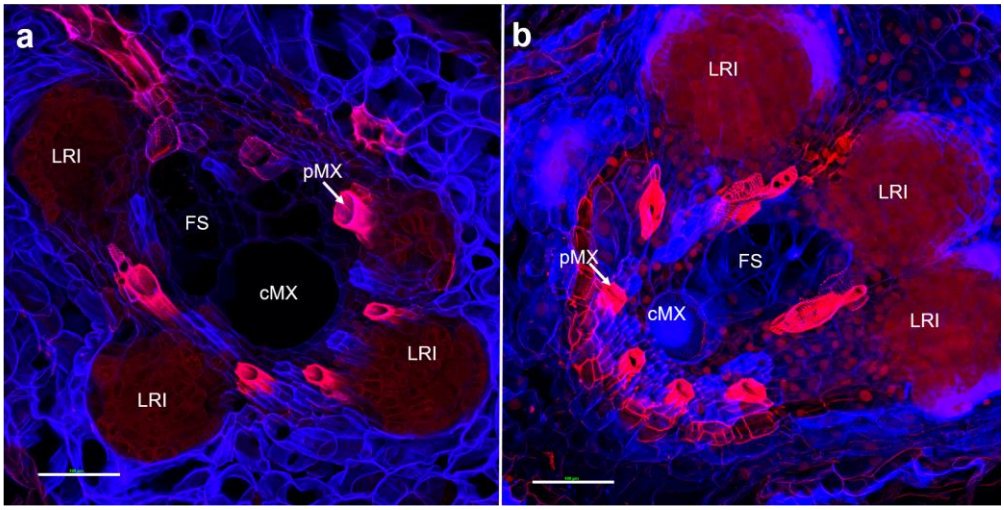

Figure 3-20: Effect of fresh and fixed tissue preparation on confocal microscopy images. Transverse sections of (a) fresh and (b) fixed wheat roots 10 DAI with *H. avenae* and stained with calcofluor white (blue) and basic fuchsin (red). Lateral root initial (LRI), feeding site (FS), central metaxylem (cMX), peripheral metaxylem (pMX), endodermis (EN). Scale bars: 100 µm.

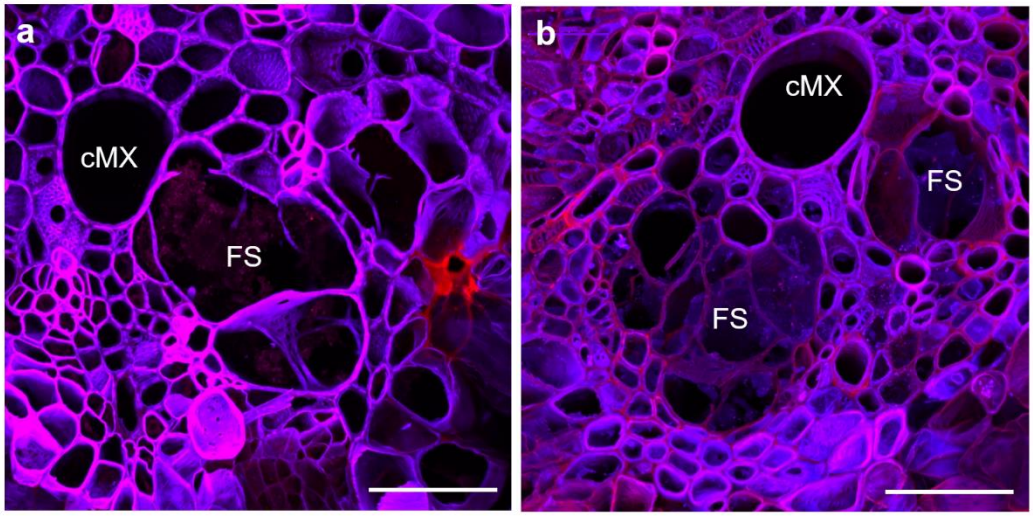

Figure 3-21: Effect of ClearSee treatment of root tissue on confocal microscopy images. *H. avenae* infected transverse sectioned wheat roots at 40× magnification. (a) Control sample (no ClearSee treatment) showing laser depth of 20 µm. (b) ClearSee treated sample showing laser depth of 70 µm. Central metaxylem (cMX); feeding site (FS). Scale bar 100 µm.

3.5.2.2.3 Observations of stained sections

Calcofluor white (CW) stained all cell walls evenly in control and infected wheat roots and therefore was used in combination with other fluorescent dyes (Fig. 3-22). Propidium iodide (PI) stained peripheral and central metaxylem cells within the vascular cylinder (Fig. 3-22b). In infected roots, PI stained cMX cells and pMX cells including cells around the feeding site, but not the cell walls of the feeding site (Fig 3-22b, c). Congo red (CR) stained similarly to CW, staining all cell walls in control roots (Fig. 3-22d). In nematode infected roots, CR staining was not consistent, appearing heavily stained in some areas (Fig 3-22e, f). Basic fuchsin (BF) stained the pMX very brightly and distinctly in control roots (Fig 3-22g). In nematode infection roots, BF also stained pMX brightly, however appeared to stain extra cells near the feeding site (Fig. 3-22h). Longitudinal sections of BF clearly showed the staining of each pMX tube (Fig. 3-22i). Fluorescein diacetate (FDA) was detected in portions of lateral roots of control roots, but never within the vascular cylinder (Fig. 3-22j). In nematode-infected roots, FDA was detected more frequently in various tissue including cortex cells, vascular cylinder, lateral roots, and within feeding sites (Fig. 3-22k, l). Immunolabeling of BG1 in control roots showed staining within the vascular cylinder (Fig. 3-22m). In nematode infected tissue, BG1 was detected in cell walls outlining the feeding site (Fig 3-22n). Longitudinal sections further showed the stain detected in cell walls of xylem vessels, feeding sites, and nuclei (Fig. 3-22o).

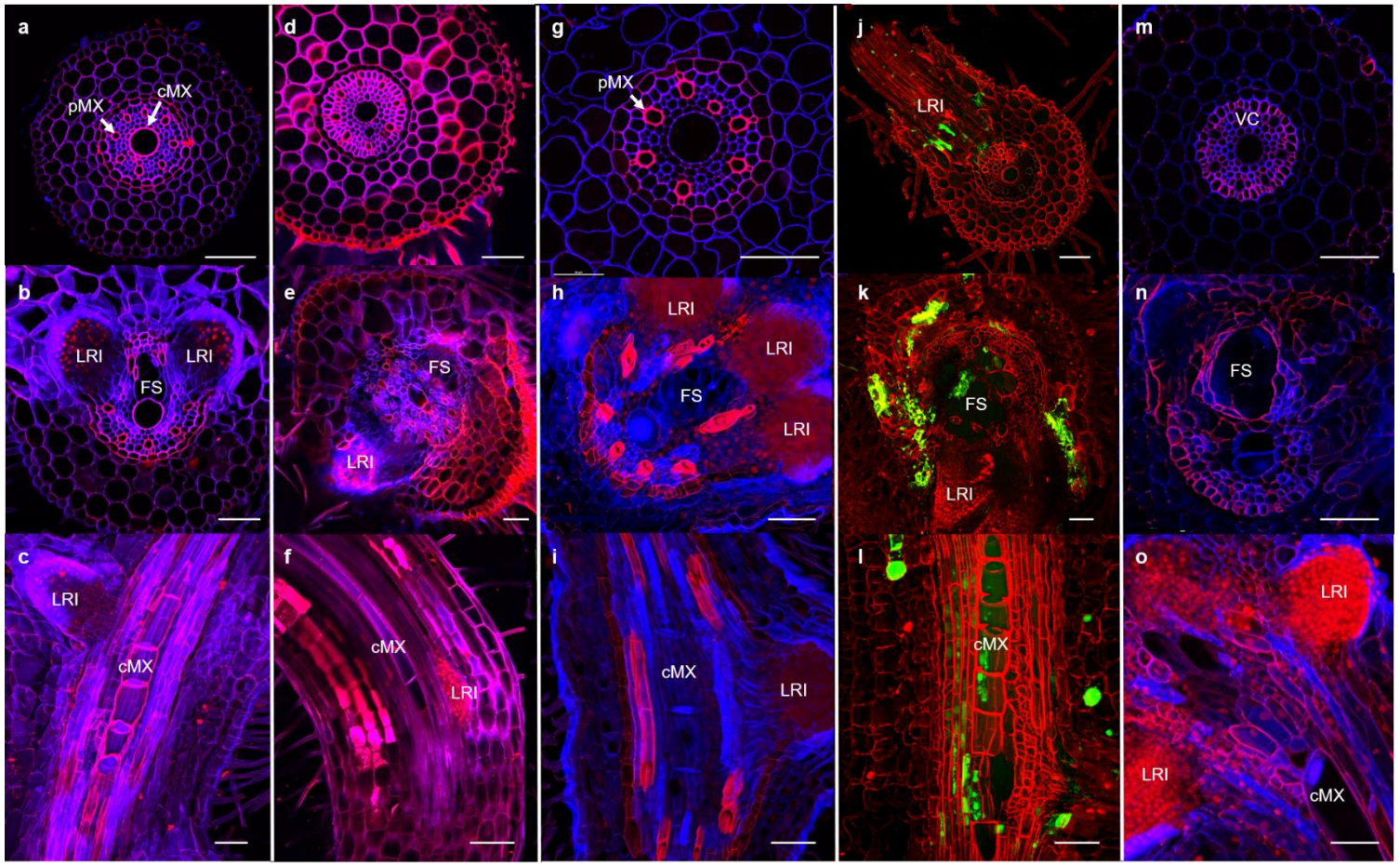

Figure 3-22: Confocal microscopy images of tested fluorescent dyes on control and CCN-infected wheat roots. (a-c) Calcofluor white (blue) and propidium iodide (red); (d-f) Calcofluor white (blue) and Congo red (red) (g-i); Calcofluor white (blue) and basic fuchsin (red); (j-l) Fluorescein diacetate (FDA, green) and propidium iodide (red); (m-o) Calcofluor white (blue) and immunolabelling with BG1 (red). (Top row) Control transverse section, (Middle row) CCN- infected transverse section, (Bottom row) CCN-infected longitudinal section. Peripheral metaxylem (pMX), central metaxylem (cMX), lateral root initial (LRI), feeding site (FS), vascular cylinder (VC). Scale bars: 100 µm.

3.6 Discussion

This research was undertaken to determine how much structural detail of nematode feeding sites in thick wheat roots could be observed using different microscopy techniques. One of the outcomes from this research was a better understanding of the nematode's location within the root relative to its feeding site, generally located above the structure. These results also agree with three-dimensional reconstructions of CCN feeding sites in barley (Strock *et al.*, 2019).

In this study several sample preparation treatments were tested, and based on the outcomes, specific methods were chosen depending on the needs of each experiment (Table 3-1). For rapid and efficient staining, fresh tissue was preferred. However, if cell preservation was required, tissue was fixed. For structural investigations, ClearSee treated samples were preferred as the treatment increased laser depth. However, ClearSee was the most time-consuming method, taking 30 d. Acid fuchsin treatment of roots made it easy to pinpoint infected regions and the locations of nematodes, but often damaged cortex cells and reduced the consistency of staining.

Table 3-2: Key points highlighting pros/cons of each sample treatment method.

Preparation method	Pros	Cons
Fresh	• Clear staining • Least time	• Cell contents not preserved (must use immediately)
Fixed	• Clear staining • Cell contents preserved	• Alters dye permeability
ClearSee	• Additional depth	• Time consuming • Inconsistent staining
Acid fuchsin	• Aids in identifying infected region	• Inconsistent staining • Disrupted root morphology

Several dyes were tested for use with light and confocal microscopy. Light microscopy was ideally suited to the observation of unstained sections of feeding sites. This was particularly useful for selecting sections that contained feeding sites for further processing with staining and confocal microscopy imaging. For confocal microscopy, several fluorescent dyes were tested. Calcofluor white has previously been shown to bind to chitin, cellulose and other cell-wall polysaccharides (Albani & Plancke, 1998; Maeda & Ishida, 1967). In wheat roots, CW stained all cell walls. The even and consistent staining of CW made it suitable for use as a counterstain with more specific stains including propidium iodide, basic fuchsin, FDA, and cell wall-specific antibodies such as BG1.

Propidium iodide is known to bind to cell walls and nucleic acids but is not able to penetrate viable cells, therefore has been used to distinguish necrotic cells (Riccardi & Nicoletti, 2006). In wheat root tissue, propidium iodide stained peripheral and central xylem cells as well as nuclei in lateral roots. This is expected since xylem cells undergo cell death during maturation and therefore the cell walls of both pMX and cMX were stained. The staining of nuclei in lateral root initials is likely due to the cut made from sectioning. Although these young cells are viable, the cut surface allows the dye to penetrate the new cells which are abundant in nuclei. Basic fuchsin been shown to stain the lignified cell walls of xylem (Carlsbecker *et al.*, 2010; Ursache *et al.*, 2014). This was consistent with the results observed. In nematode infected roots, however, there was extra lignification of cells near the feeding site, but not within the feeding site itself. Lignification around nematode feeding sites has been previously observed and suggested as structural support since the syncytium builds a large turgor pressure (Grundler *et al.*, 1998).

FDA is a molecule that is hydrolysed in living cells to cause a fluorescent signal. As previously mentioned, PI detects non-viable cells. In order to determine the viability of syncytial cells and associated xylem vessels, the combination of FDA and PI has been used to differentiate living and non-living cells (Jones & Senft, 1985). However, this method is

difficult for plant root sections since cells are extremely long and difficult to keep alive for extended periods once cut (Escamez *et al.*, 2017). In the thick root sections used in this method, it was difficult to distinguish living cells. Although some cells fluoresced green with FDA, this was not consistent between sections. In nematode infected roots, there was FDA detected within the feeding site. The presence of FDA and lack of PI within feeding sites indicates these are active living cells. This is not surprising, as the feeding site is a functioning source of cells used to feed the nematode. However, most cells did not fluoresce, despite the fact they are unlikely to be dead.

The method for immunolabelling was adapted from Aditya *et al.* (2015), however instead of resin embedded sections (0.8-1.0 µm thick), thick agar sections were tested. This technique worked especially well with BG1, which showed staining within the vascular cylinder. In nematode infected tissue, BG1 was detected around the feeding site. This was also reported in nematode infected barley by Aditya *et al.* (2015), confirming that 1,3;1,4-β-glucan is an abundant component of the outer feeding site wall.

The embedding and sectioning technique used in this study was critical to the ease of the method and the high quality of images obtained. Agarose embedding was less laborious and safer than the more conventional paraffin and resin embedding. Further, it allowed for much thicker sectioning (up to 200 µm) than paraffin or resin, for which the standard thicknesses are only up to 10 µm and 1 µm, respectively. For light microscopy, the limitations of agarose embedded material included the types of stains that could be used and the size of sections. For confocal microscopy, agarose had no specific limitations and the thick size of sections was an important aspect of developing image depth. Vibratome sectioning was a straightforward approach that provided uniform thick sections. Verhertbruggen *et al.* (2017) has stated that vibratome sectioning was the “easiest to master” compared to microtome or ultramicrotome sectioning.

Plant root cells are organised radially along the transverse plane; but grow and elongate axially along the longitudinal plane. To determine the best way to image feeding sites, both transverse and longitudinal sections were prepared and analysed. Transverse sections showed all cell types and revealed their symmetrical arrangement in non-infected roots. In transverse sections of nematode-infected roots, feeding sites could be readily identified based on disruption of this symmetry. In longitudinal sections, feeding sites were observed less frequently. However, in longitudinal sections in which feeding sites were visible, their shapes and positions could be observed throughout much of their length. Overall, transverse sections were best for identifying feeding sites and longitudinal sections were best for observing the position of feeding sites relative to other plant vascular tissue. Since root segments are longer than they are wide, transverse sectioning took longer than longitudinal sectioning. However, longitudinal sections required more precision when positioning the agarose block to ensure sections would be parallel to the vascular tissue.

3.7 Conclusion

One of the overall objectives of the research reported in this thesis was to identify differences between CCN-resistant (*Cre8*) and susceptible wheat lines. To address this objective, it was necessary to establish protocols for observation of nematodes and their feeding sites. The research reported in this chapter identified effective methods for growing nematode infected wheat roots and for observing nematodes and plant tissues within those roots. Although none of the individual protocols used are entirely novel, the combinations of protocols provided clear views of nematodes and nematode feeding sites within wheat roots giving new insights about their development.

It was determined that the best growth method for robust root growth was hydroponics. Fresh, fixed and ClearSee treated tissue samples were all useful. Fresh and fixed samples provided the best image clarity, with clean and distinct staining results. Samples treated with ClearSee had the best structural images, showing an additional 50 µm depth.

The use of agarose embedding and vibratome sectioning provided a compromise between whole-mount microscopy and thin sectioning, delivering both clarity and depth. The use of optical and confocal microscopy allowed for a variety of stains to be applied for the examination of root structure, and cell wall components of root tissue and feeding sites. Optical microscopy provided rapid screening of unstained sections. Overall, confocal microscopy stains outperformed optical microscopy stains in terms of clarity. For overall cell wall structure of the root and feeding site, the combination of CW and PI provided consistent results. For secondary cell-wall components, the lignin-specific dye BF was best and worked well with fresh or fixed tissue. Further, a protocol for immunolabelling was successful on thick agarose embedded sections, especially for the BG1 probe.

Evaluation of these methods made it possible to streamline technical workflow by establishing a single tissue preparation method that can be used with various sample preparations and microscopy stains. These techniques made it possible to undertake further scientific studies regarding the dynamics of nematode infection in wheat lines showing differential susceptibility to CCN.

Chapter 4 :
Infection by cyst nematodes induces rapid remodelling of developing xylem vessels in wheat roots

Statement of authorship

Statement of Authorship

Title of Paper	Infection by cyst nematodes induces rapid remodelling of developing xylem vessels in wheat roots
Publication Status	☐ Published ☒ Accepted for Publication ☐ Submitted for Publication ☐ Unpublished and Unsubmitted work written in manuscript style
Publication Details	Levin, K. A., Tucker, M. R., Bird, D. M., Mather, D. E. (2020). Infection by cyst nematodes induces remodelling of developing xylem vessels in wheat roots. Scientific Reports.

Principal Author

Name of Principal Author (Candidate)	Kara A. Levin		
Contribution to the Paper	Planned and designed the research. Conducted all experiments and carried out all microscopy and modelling. Interpreted results and wrote manuscript.		
Overall percentage (%)	70%		
Certification:	This paper reports on original research I conducted during the period of my Higher Degree by Research candidature and is not subject to any obligations or contractual agreements with a third party that would constrain its inclusion in this thesis. I am the primary author of this paper.		
Signature		Date	15/03/2020

Co-Author Contributions

By signing the Statement of Authorship, each author certifies that:

i. the candidate's stated contribution to the publication is accurate (as detailed above);
ii. permission is granted for the candidate in include the publication in the thesis; and
iii. the sum of all co-author contributions is equal to 100% less the candidate's stated contribution.

Name of Co-Author	Matthew R. Tucker		
Contribution to the Paper	Planned and designed research. Interpreted results and contributed to the revision of the manuscript.		
Signature		Date	19/3/20

Name of Co-Author	David M. Bird		
Contribution to the Paper	Interpreted results and contributed to the revision of the manuscript.		
Signature		Date	18/3/20

Name of Co-Author	Diane E. Mather		
Contribution to the Paper	Planned and designed research. Interpreted results and contributed to the revision of the manuscript.		
Signature		Date	16/03/2020

Infection by cyst nematodes induces rapid remodelling of developing xylem vessels in wheat roots

Kara A. Levin[1], Matthew R. Tucker[1], David McK. Bird[2] and Diane E. Mather[1,*]

[1]School of Agriculture, Food and Wine, University of Adelaide, Waite Campus, Urrbrae, South Australia, Australia

[2]Department of Entomology and Plant Pathology, North Carolina State University, Raleigh, North Carolina, USA

[*]Author for correspondence

Diane Mather Phone: +61 420 959 955 E-mail: diane.mather@adelaide.edu.au

4.1 Abstract

Cyst nematodes induce host-plant root cells to form syncytia from which the nematodes feed. Comprehensive histological investigation of these feeding sites is complicated by their variable shape and their positions deep within root tissue. Using tissue clearing and confocal microscopy, we examined thick (up to 150 μm) sections of wheat roots infected by cereal cyst nematodes (*Heterodera avenae*). This approach provided clear views of feeding sites and surrounding tissues, with resolution sufficient to reveal spatial relationships among nematodes, syncytia and host vascular tissues at the cellular level. Regions of metaxylem vessels near syncytia were found to have deviated from classical developmental patterns. Xylem vessel elements in these regions had failed to elongate but had undergone radial expansion, becoming short and plump rather than long and cylindrical. Further investigation revealed that vessel elements cease to elongate shortly after infection and that they later experience delays in secondary thickening (lignification) of their outer cell walls. Some of these elements were eventually incorporated into syncytial feeding sites. By interfering with a developmental

program that normally leads to programmed cell death, *H. avenae* may permit xylem vessel elements to remain alive for later exploitation by the parasite.

4.2 Introduction

As the conduits through which water and mineral nutrients are transported from roots to shoots, the xylem vessels of roots are critically important for plant growth and development. As roots grow, xylem precursor cells differentiate from the root apical meristem and develop into protoxylem and metaxylem vessels (Esau, 1965). Metaxylem vessel elements elongate and begin to mature. They undergo secondary thickening (lignification) and programmed cell death and the end walls between adjacent elements erode to form hollow tubes (Růžička *et al.*, 2015). In the seminal roots of wheat (*Triticum aestivum* L.) and other cereal crops, there are multiple peripheral metaxylem (pMX) vessels arranged around one large central metaxylem (cMX) vessel. The pMX matures first and the cMX matures later (Caño-Delgado *et al.*, 2010). In these systems, the cMX can account for up to 80% of water transport (Weaver, 1926).

Many root pathogens and parasites take advantage of xylem tissue to sustain their own nutrient requirements. This can interfere with water transport and lead to symptoms resembling those induced by water stress (Dickson, 1956; Stirling & Stanton, 1997). Further, some sedentary parasitic nematodes are known to influence the development of plant vascular tissue. This has been thoroughly investigated for root knot nematodes (RKN, *Meloidogyne* spp.), which induce the development of new vascular tissue around their 'giant cell' feeding sites (Bartlem *et al.*, 2014). In contrast cyst nematode parasitism has not been reported to affect xylem development.

Like root knot nematodes, cyst nematodes (CN, including *Heterodera* spp. and *Globodera* spp.) are sedentary endoparasites of plants. Juvenile CNs emerge from soil-borne cysts and enter the elongation zones of host plant roots. After migrating intracellularly through the root cortex (Sijmons *et al.*, 1991), they select initial feeding cells, into which they inject complex mixtures of effectors. These effectors modify host cell metabolism, leading to partial breakdown of plant

cell walls and merging of cytoplasm between cells (Grundler *et al.*, 1994; Grundler *et al.*, 1998). The resulting syncytia 'recruit' adjacent cells and can eventually incorporate hundreds of cells. They act as transfer cells (Jones & Northcote, 1972), delivering nutrients to nematodes.

Cyst nematodes rely upon ongoing nutrient transfer from surrounding cells to feeding sites. Hofmann and Grundler (2007) proposed that developing syncytia are initially isolated and rely upon transport proteins to obtain nutrients, but later become symplasmically connected to the nutrient-dense phloem. Accumulated solutes are stored within syncytia (Hofmann *et al.*, 2007), allowing intermittent feeding by nematodes. As the syncytia expand, they may come into contact with metaxylem vessels (Grymaszewska & Golinowski, 1991) and incorporate those vessels as part of the syncytia (Golinowski *et al.*, 1996; Heinrich *et al.*, 1998; Williams & Fisher, 1993). Such expansion may enhance water uptake to support nematode development (Bohlmann & Sobczak, 2014) and/or help maintain high turgor pressure (Böckenhoff *et al.*, 1996) within the syncytia.

Much of what is known about CN feeding sites has been learned from microscopic analysis of thin sections of infected root tissue. Optical microscopy has provided detailed views of cells and tissues (Aditya *et al.*, 2015; Seah *et al.*, 2000), while electron microscopy has provided detailed views of ultrastructure within cells (Golinowski *et al.*, 1997; Jones & Northcote, 1972; Sobczak & Golinowski, 2009). While these approaches provide detailed cytological information regarding feeding site development, each thin section provides only a two-dimensional view of the feeding site and other features. Reconstitution of three-dimensional shapes is possible using such approaches, but to examine the relative positions of nematodes, feeding sites and surrounding tissues would require many serial sections.

Recently, alternative microscopic techniques have been used to generate three-dimensional (3D) models of infected root tissue. The use of tissue clearing reagents such as ClearSee (Kurihara *et al.*, 2015) and TOMEI (Hasegawa *et al.*, 2016), combined with confocal microscopy, have made it possible to capture and examine 3D structures within nematode-

infected roots without physical sectioning. This is has been achieved for *Arabidopsis thaliana* L. roots infected by the root-knot nematode *Meloidogyne incognita* (Antonino de Souza Junior *et al.*, 2017; Hasegawa *et al.*, 2016) and for Chinese milkvetch (*Astralagus sinicus* L.) roots infected by soybean cyst nematode (*Heterodera glycines*) (Ohtsu *et al.*, 2017). These host species have thin roots that are amenable to wholemount processing, but they may not be entirely realistic models for CN-susceptible host plants with thicker roots or different root anatomy.

Laser ablation tomography has been applied to segments of barley roots infected by the cereal cyst nematode (CCN) *Heterodera avenae* W.) (Strock *et al.*, 2019). This approach revealed the shapes and relative positions of nematodes, feeding sites and surrounding tissue, but with less detail than can be seen with microscopy.

Here, we report on the development of a systematic approach for preparation and confocal microscopy of thick sections of root tissue and present highly detailed images obtained from the application of this approach to CCN-infected roots of wheat (*Triticum aestivum* L.). Based on these images, we report on the discovery of a striking yet previously unreported modification of metaxylem vessels and present clear evidence of the 'invasion' of metaxylem vessels by feeding sites.

4.3 Results

A systematic approach for preparation and microscopic analysis of root tissue

An approach was developed to image the structure of vascular tissue in wheat roots. This was first established on mock-inoculated roots to determine the quality of image that could be rendered. Short segments from wheat seminal roots were embedded in agarose and sectioned at 150 µm intervals (Fig. 4-1a). Based on examination of the resulting sections by light microscopy, pairs of adjacent sections containing the features of interest were selected (Fig. 4-1b). The selected sections were stained and then examined using confocal microscopy. Z-stacks

of approximately 100 µm depth were obtained from the facing surfaces of each pair of sections. Within the resulting maximum projected confocal images, major cell and tissue types could be distinguished, including root hairs, epidermal and cortical cells and vascular tissue (Fig. 4-1c). In some samples, lateral roots or lateral root initials were visible. With IMARIS software, central metaxylem (cMX) vessel elements were manually selected (Fig. 4-1d) from images of longitudinal sections, and fluorescence signals from these elements were rendered into surfaces to generate 3D models (Fig. 4-1e). The cMX vessel elements were long, narrow and cylindrical, forming apparently hollow tubes, with 'scars' marking where the individual vessel elements had formerly been separated by end walls.

When this approach was applied to CCN-infected segments of wheat roots, feeding sites and/or nematodes were visible, often located near the cMX (Fig. 4-1f). In contrast to the long and cylindrical cMX vessel elements observed in non-infected roots, cMX vessel elements near feeding sites were short and plump. Some vessels appeared to be separated by intact or nearly intact end walls. Central metaxylem (cMX) vessels, feeding sites, and nematodes were selected (Fig. 4-1g) for the development of 3D models. These models helped clarify the relative positions of feeding sites and xylem vessels (Fig. 4-1h). Metaxylem vessel elements that were directly in contact with feeding sites had apparently porous cell walls (Fig. 4-1h, right panel) and appeared to have been 'invaded' by the feeding site (Fig. 4-1h, left panel). Feeding sites contained complex networks of remnant inner cell walls (Fig. 4-1h; Supplementary Video S1).

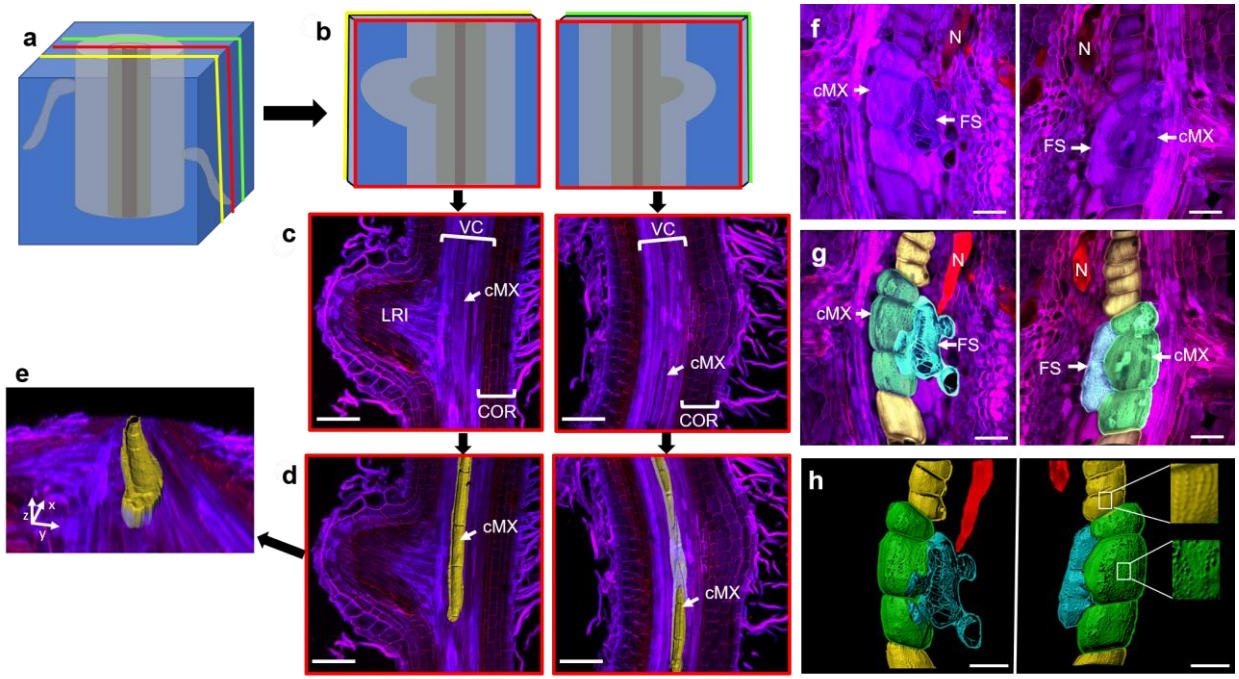

Figure 4-1: Method to image and model thick sections of control and infected wheat root tissue. (a) Root tissue was embedded and cut into 150 µm longitudinal sections.(b) Sections containing the central part of the vascular bundle were chosen. (c) Sections were stained with calcofluor white and propidium iodide and then imaged using a confocal microscope and processed with Nikon NIS-Elements to produce a maximum projected image. (d) Using IMARIS software, the central metaxylem vessel was manually selected and highlighted in order to render and (e) rotate a three-dimensional surface model of the central metaxylem. This same process was used to analyse wheat seminal root tissue at 15 d after inoculation with cereal cyst nematodes. (f) Maximum projected confocal images stained and showing facing surfaces of two consecutive sections containing a nematode (N), a central metaxylem (cMX) vessel and a feeding site (FS). (g) Features manually selected and coloured: the nematode in red, the feeding site in blue and the central metaxylem in green (three vessel elements that have been 'invaded' by the feeding site) and yellow. (h) Three-dimensional models of the selected features. A detailed rotation of the left-hand model is shown in Supplementary Video S1. (VC) vascular cylinder (cMX) central metaxylem, (LRI) lateral root initial, (COR) cortex. Scale bar (a-d) 200 µm (f-h) 100 µm.

Development of metaxylem vessels and feeding sites in nematode-infected roots

To investigate the effects of CCN infection on cMX development over time, infected roots were examined and compared to mock-inoculated (control) roots at 2, 7, 15, and 21 DAI. At 2 DAI, the cMX vessel elements in control and infected roots were similar in length (Fig. 4-2a) but those in infected roots were slightly plump. By 7 DAI, the cMX vessel elements in control roots were fully elongated while those in infected roots remained short and had expanded radially (Fig. 4-2b). Vessel element end walls were still present in both cases, but those in the infected roots appeared stretched and thin (Fig. 4-2b, lower panel). By 15 DAI, the end walls between vessel elements in control roots had broken down, leaving only thin remnants (Fig. 4-2c, upper panel). In infected roots, some end walls had broken down, leaving thick ridges (Fig. 4-2c, lower panel). Some other end walls in infected roots persisted. At 21 DAI, some fully intact end walls were still visible between very short and wide vessel elements (Fig. 4-2c, lower panel).

To investigate the relationship between feeding sites and metaxylem vessels, sections from infected regions sampled at 7, 15, and 21 DAI (at least four samples from each time point) were examined. All feeding sites examined (including feeding sites observed under light microscopy) were directly adjacent to or connected with metaxylem vessels. For example, a feeding site in tissue sampled at 7 DAI (Fig. 4-2e; Supplementary Video S2a) was directly adjacent to the cMX but separated from it by intact cell walls. A feeding site in tissue sampled at 15 DAI (Fig. 4-2f; Supplementary Video S2b) was located between two pMX vessels. In one of these vessels, two elements immediately adjacent to the feeding site were plump, had apparently porous cell walls and seemed to have been ‘invaded’ by the feeding site. A feeding site sampled at 21 DAI (Fig. 4-2g; Supplementary Video S2c) appeared to have entirely overtaken a section of a pMX vessel.

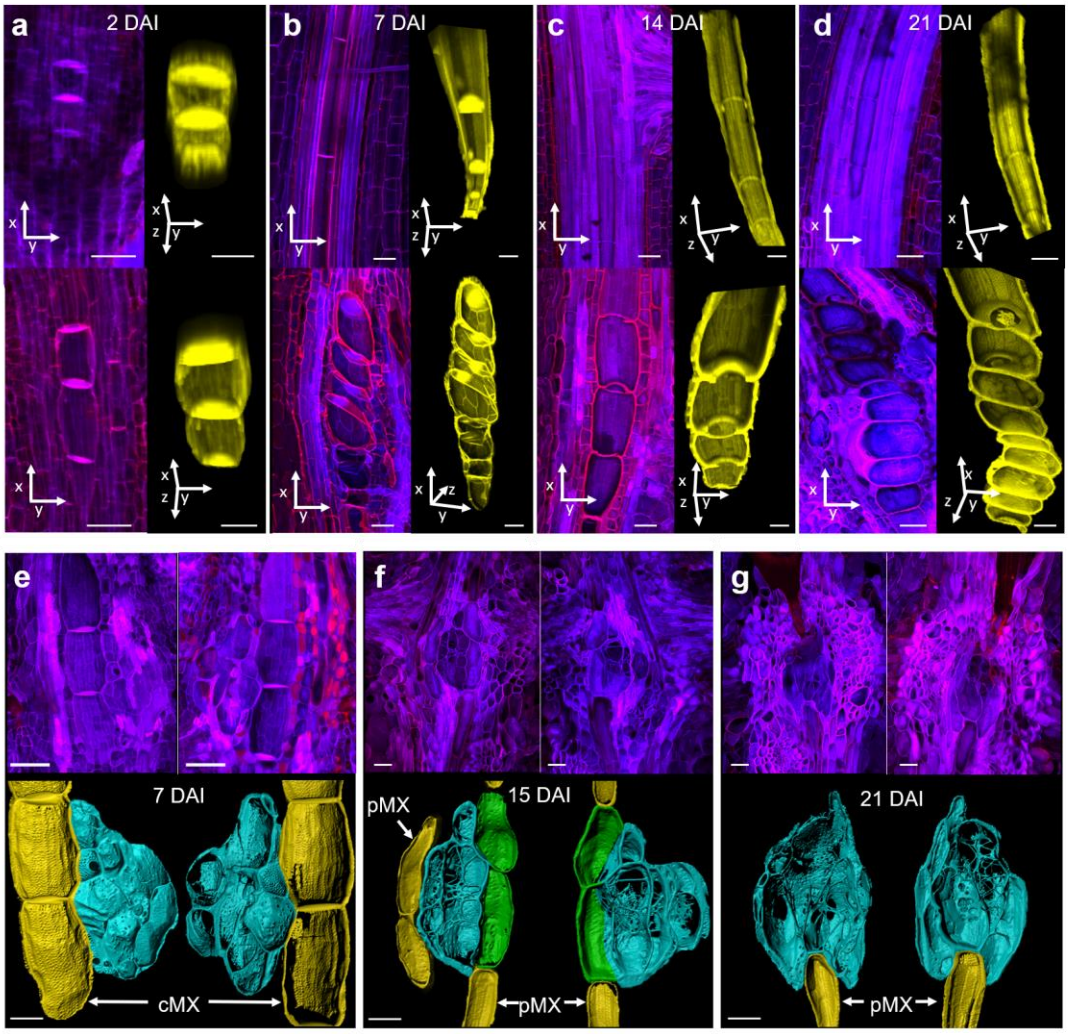

Figure 4-2: Central metaxylem development in wheat seminal roots with and without infection by cereal cyst nematodes. (a-d) The upper panel shows longitudinal sections from control (mock-inoculated) roots and the lower panel shows longitudinal sections of inoculated roots at (a) 2 d after inoculation (DAI), (b) 7 DAI, (c) 15 DAI, and (d) 21 DAI. Left-hand panels show maximum projection confocal images (processed with Nikon NIS-Elements) of tissue stained with calcofluor white (blue) and propidium iodide (red). Right-hand panels show the corresponding three-dimensional models (produced using IMARIS) of central metaxylem (cMX) vessels, coloured yellow and tilted to show vessel end walls. (e-f) Development of cereal cyst nematode feeding sites and xylem connectivity in wheat seminal roots. (e) A feeding site and a cMX vessel at 7 d after inoculation (DAI), (f) a feeding site and two peripheral metaxylem (pMX) vessels at 15 DAI and (g) a feeding site and a pMX vessel at 21 DAI. Each upper panel shows maximum projection confocal images (processed with Nikon NIS-Elements) of the facing surfaces of two consecutive sections of tissue stained with calcofluor white (blue) and propidium iodide (red). Each lower panel shows isolated 3-dimensional models (produced using IMARIS) of feeding sites in aqua and xylem vessels in green (vessel elements that have been 'invaded' by the feeding site) and yellow. Rotation of the models is shown in Supplementary Video S2. Scale bar 50 µm.

Secondary thickening of cell walls in nematode-infected roots

During xylem maturation, cells undergo lignification, a process of secondary thickening. To investigate secondary thickening of cell walls during nematode infection, transverse sections of infected and control roots were treated with the lignin-specific stain basic fuchsin. Lignin was never detected in the cell walls of feeding sites, but there were differences in the lignification of surrounding cells. At 2 DAI (Fig. 4-3a), lignin was detected in the cell walls of protoxylem, pMX and exodermis in both control and infected roots. In infected roots, lignin was also detected in the walls of some groups of endodermal and cortical cells. At 4 DAI and later (Fig. 4-3b-d), the 3D structure of some features (especially the pMX) was more obvious in infected roots than in control roots, probably due to the curvature of the roots in regions that have been infected. In infected roots, lignin was detected in the walls of some cells adjacent to the pMX. Over time, it became increasingly difficult to distinguish the pMX of infected roots from surrounding cells. At 6 DAI (Fig. 4-3c), control roots exhibited considerable lignification of the outer walls of the cMX and some lignification of endodermal cell walls. In infected roots, lignification of the outer walls of the cMX was not observed until 8 DAI (Fig. 4-3d). Intact end walls were sometimes visible within cMX vessels in infected roots (Fig. 4-3d), and only the outer rims of these walls were lignified.

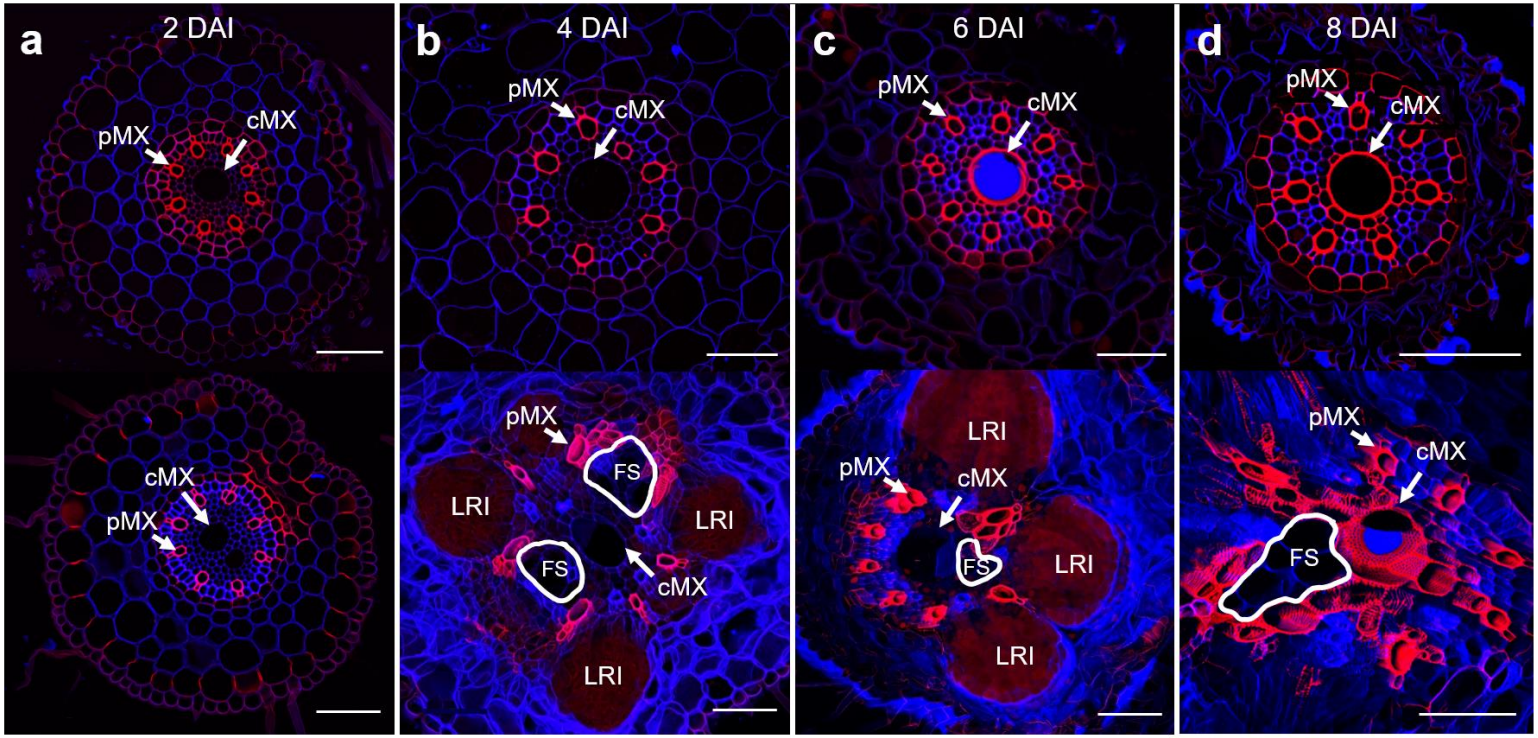

Figure 4-3: Transverse sections of wheat seminal roots treated with a lignin-specific stain. The upper panels show sections of control (mock-inoculated) roots. The lower panels show sections of roots inoculated with cereal cyst nematodes. All sections were stained with basic fuchsin (red) and calcofluor white (blue), imaged using a confocal microscope and processed with Nikon NIS-Elements to produce a maximum projected images. (a) 2 d after inoculation (DAI), (b) 4 DAI, (c) 6 DAI (d) 8 DAI. (LRI) lateral root, (FS, circled in white) feeding site, (pMX) peripheral metaxylem, (cMX) central metaxylem. Scale bars: 100 µm.

4.4 Discussion

Motivated by an interest in examining the structure and positions of cyst nematode feeding sites within thick roots of crop plants, we established a systematic approach to prepare and observe root tissue sampled from the seminal roots of wheat seedlings. Key elements of this approach included application of an optical clearing agent, tissue sectioning at 150 μm intervals, selection of adjacent sections containing features of interest, application of confocal microscopy and generation of 3D models. These combined methods enabled high-quality examination of feeding sites and provided new information on spatial relations of features within cereal roots. Use of a clearing agent (ClearSee) allowed deep penetration of confocal lasers into the thick sections. Imaging of facing surfaces of adjacent tissue sections provided an 'open-book' view of complex structures. Finally, 3D modelling made it possible to isolate specific structures and rotate them in space.

When applied to CCN-infected roots, this approach provided detailed 3D models of feeding sites and metaxylem vessels. These models confirmed the irregular shapes of feeding sites and provided detailed views of intricate cell wall networks within those sites. Surprisingly, some metaxylem vessel elements in infected roots were strikingly different from those in the roots of mock-inoculated control plants. Sections of cMX vessels near CCN feeding sites consisted of series of short, plump, bubble-like elements. The end walls between these elements did not erode as early or as completely as their counterparts in uninfected roots. End walls that did erode left thick ridges within xylem vessels, rather than the subtle 'scars' that marked the former positions of vessel element end walls in uninfected roots.

Examination of tissue samples taken at various times after inoculation revealed that structural modification of the cMX begins soon after infection, certainly by 7 DAI (when all feeding sites would have been initiated; Williams and Fisher 1993) and possibly as early as 2 DAI (when nematodes would be within the root, but not all would have selected an initial feeding cell). Instead of elongating to become cylindrical, cMX vessel elements near infection sites expanded

radially. Relative to their counterparts from uninfected roots, affected xylem vessel elements underwent secondary thickening (lignification) somewhat later and tended to retain their end walls longer. Further, the outer rims of their end walls underwent secondary thickening, leading to the thick ridges mentioned above. Overall, nematode infection appears to interfere with cell elongation (and/or favour radial growth) causing the formation of bubble-like vessel elements.

Considering that microscopy has been extensively used over many decades to examine CN feeding sites (as reviewed by Dropkin (1969); Jones (1981); Golinowski *et al.* (1997); and Kyndt *et al.* (2013)) it is surprising that nematode-induced bubble-like xylem elements have not previously been reported. One possible explanation is that much of the microscopy was applied to transverse sections, in which xylem modification would not be obvious. Even when longitudinal sections were used, research interest was focused on nematodes and/or their feeding sites, and structural modification of the xylem might have been missed. Consistent with this, some published micrographs (Fig. 2c and Fig. 4e in Seah *et al.* (2000); Fig. 2e in Aditya *et al.* (2015)) do include views of cells that resemble the bubble-like vessel elements reported here. Application of light or electron microscopy to sectioned tissue provides information only for a single plane through the tissue, making it difficult to appreciate the full complexity of 3D structures. Confocal microscopy has provided 3D views of whole-mount root tissue for Arabidopsis (Antonino de Souza Junior *et al.*, 2017; Hasegawa *et al.*, 2016) and Chinese milkvetch (Ohtsu *et al.*, 2017), but these plants have thinner roots (approximately 200 µm in infected regions) than the wheat plants used here (between 600 and 800 µm in infected regions). Further, the vascular anatomy of the seminal roots of wheat and other cereals is quite different from that of Arabidopsis roots, which lack a prominent cMX. The combination of optical clearing, confocal microscopy and 3D modelling made it possible to discover a previously unreported phenomenon within seminal roots of wheat.

Most of the bubble-like xylem elements examined here were in cMX vessels. Modification of pMX vessel elements was sometimes observed (e.g. Fig. 5b) but tended not to be as extreme.

This is consistent with the fact that pMX (also known as early-maturing metaxylem) matures much earlier than cMX (late-maturing metaxylem). This maturity difference was evident in samples stained with basic fuchsin. Even at 2 DAI, the pMX vessel walls were already highly lignified. Compared to the immature and not yet lignified cMX, pMX may be better able to resist the effects of nematode infection. This phenomenon is not specific to wheat; we have observed similar changes (results not presented) in barley (*Hordeum vulgare* L.). In the seminal roots of these cereals, cMX vessels are very large, making any modification of their structure quite obvious.

The success of developing CN feeding sites relies on access to water and nutrients from the plant's vascular tissue (Jones, 1981). Xylem connections enhance the surface area of the feeding sites through which nematodes can access water and solutes (Golinowski *et al.*, 1997). Based on analysis of CCN feeding site development, Grymaszewska and Golinowski (1991) concluded that syncytial efficiency is limited by the amount of solute flow from xylem vessels. Others have reported on the importance of xylem contact for successful development of syncytia (Heinrich *et al.*, 1998; Lilley *et al.*, 2005; Sobczak & Golinowski, 2009; Williams & Fisher, 1993). The results presented here demonstrate the structure and extent of the relationship between feeding sites and host plant xylem vessels.

Our 3D models confirmed that feeding sites are initiated near metaxylem vessels and maintain close contact with those vessels throughout development. Some feeding sites ultimately 'invade' vessel elements, making it difficult to distinguish vessel elements from feeding sites. The cell walls of metaxylem vessel elements that were (or may be destined to be) connected with feeding sites appeared porous, resembling the walls of phloem sieve cells, which serve as major conduits for transport of photosynthates.

Overall, it appears that infection of wheat roots by cereal cyst nematodes triggers a reprogramming of nearby xylem vessel elements, preparing them to be suitable for connection with, or integration into, feeding sites. Cell elongation is impeded (and/or radial expansion is

promoted) and cell maturation is delayed. Nematode-induced xylem modification may be an important element of the parasitic mechanism of sedentary nematodes. This is consistent with ideas discussed by Bird and Wilson (1994) and elaborated into a model by Bird (1996), who pointed out similarities between nematode feeding sites (CN syncytia and RKN giant cells) and developing xylem.

The phenomenon reported here differs from previously reported effects of parasitic nematodes on vascular tissue. As reviewed by Bartlem *et al.* (2014) networks of *de novo* xylem and phloem cells develop around RKN feeding sites (giant cells). In contrast, the response reported here for CCN involves cells that have already differentiated into cMX or pMX vessel elements but fail to elongate and are delayed in (or prevented from) undergoing programmed cell death. While vascular tissue proliferation in response to RKN infection could be a plant response that helps maintain nutrient and water transport for the host plant, remodelling of vascular tissue in response to CCN infection may benefit the parasite more than the host.

Given the importance of the cMX for water transport (Luxová, 1986; Weaver, 1926), delayed maturation of cMX vessel elements and retention of end walls between cMX vessel elements could significantly impede water transport within roots. This raises the question of how the host plant is able to survive. One possible explanation lies in the well-known proliferation of lateral roots near feeding sites (e.g., Fig. 4-4). These new roots may increase overall water uptake and ensure adequate water supply to xylem vessels above feeding sites and to the feeding sites themselves. Further, it is possible that new xylem vessels differentiate within the stele. This might explain the additional lignified cells that were observed near pMX and feeding sites as early as 4 DAI.

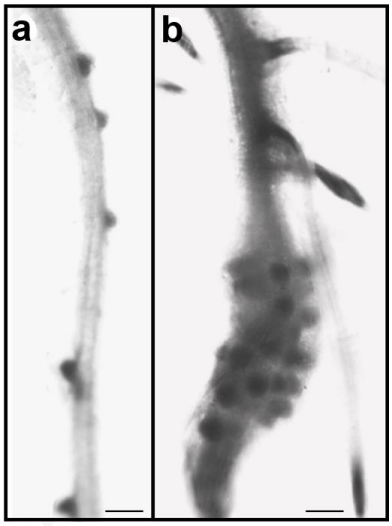

Figure 4-4: Proliferation of lateral root formation on wheat seminal roots infected with cereal cyst nematodes. (a) A control (mock-inoculated) root, with five emerging lateral roots. (b) A root at 7 d after inoculation with cereal cyst nematodes, with three advanced lateral roots above the infection site and many lateral roots emerging at the infection site. Scale Bar: 500 µm.

The systematic microscopy technique that was developed here for the examination of vascular tissue in wheat seminal roots infected by CCN could be applied to other plant species and other research questions. The 3D analysis of CCN feeding sites clearly revealed the structure of feeding sites and their connections with xylem vessels, while also enabling the discovery of previously unreported effects of nematode infection on xylem vessel anatomy. These observations lead to intriguing questions on how xylem remodelling is induced, on whether and how it benefits the parasite and/or affects the host plant.

4.5 Materials and methods

Nematodes, plant material, growth conditions, and inoculation

Cereal cyst nematode (*Heterodera avenae* Woll., pathotype Ha13) inoculum was prepared as described by Aditya et al. (2015). Cysts (originating from soil collected at Winulta and South Kilkerran on the Yorke Peninsula, South Australia) were mixed with organic material and placed in synthetic silk bags to be used as nematode 'farms'. These nematode farms were incubated in water at 5°C in darkness. One day prior to inoculum preparation, the farms were rinsed to remove nematodes that had already hatched. On the day of inoculum preparation, water from the nematode farms was washed through a 38 µm sieve to collect freshly hatched J2 nematodes. Nematode numbers were counted for 20 µL samples and the concentration of inoculum was adjusted to approximately 2000 nematodes per mL.

Seeds of the wheat (*T. aestivum*) line TMDH82 (a CCN-susceptible doubled haploid line derived from the F_1 generation of a cross between the Australian wheat cultivars Trident and Molineux) were surface sterilised in 3% sodium hypochlorite (NaOCl) for 10 min on a shaker, then rinsed three times with sterilised water for 5 min. Seeds were placed on sterile 2% agar plates and kept in darkness at 5°C for 24 h. The agar plates were then placed in a controlled environment chamber at 15 °C with a 12 h : 12h, light : dark cycle. After 3 d, when seeds had germinated and seedling seminal roots were 2-3 cm long, each seminal root tip was inoculated with 20 µL inoculum or (for control plants) sterile water. Once inoculated, seedlings were kept on agar for 24 h (Fig. 5a). Each seedling was then washed in water, then gently pushed into a 1.5 mL Eppendorf tube from which the tip had been cut off (Fig. 5b). That tube was then placed into a 50 mL tube from which the base had been cut off (Fig. 5c). The 50 mL tube was then placed into a hydroponic tank (Fig. 5d) containing modified Johnson's solution (Johnson *et al.*, 1957), as detailed by (Melino *et al.*, 2015), with constant aeration. The solution was changed twice a week.

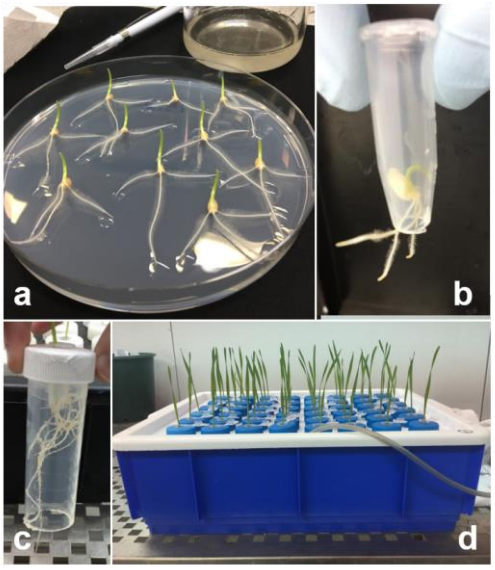

Figure 4-5: Experimental setup and growth hydroponics system. (a) seedlings germinated and inoculated on agar plates, (b) seedling transferred to Eppendorf tube with tip removed, (c) tube placed into a 50 mL tube with base removed (d) tubes arranged in an aerated hydroponic tank containing nutrient solution.

Clearing and sample preparation of root tissue for confocal microscopy

At various times after inoculation, wheat plants were collected and short segments (2-4 mm) were excised from the seminal roots. For inoculated plants, visibly swollen regions were excised. For mock-inoculated control plants, corresponding regions were excised from roots at the same distance from base of the root. Each piece of harvested tissue was placed into an Eppendorf tube, covered with ClearSee solution and incubated at room temperature for 30 d. The ClearSee solution, which had been prepared in advance as described by Kurihara *et al.* (2015) and kept at room temperature, was changed weekly. After 30 d, tissue samples were washed with 0.01 M phosphate-buffer saline (1X PBS) for 1 min, then washed in sterile water for 1 min. Tissue samples were embedded in 4% agarose and sectioned longitudinally at 150 µm intervals using a Leica VT1200 vibratome (Leica Biosystems, Nussloch, Germany). Resulting sections were screened by light microscopy (Nikon Eclipse Ci-L, Tokyo, Japan) and pairs of adjacent sections containing vascular tissue were selected. The selected sections were

incubated overnight in ClearSee solution at room temperature. Sections were rinsed twice with 1X PBS and once with sterile water, then stained with a 1:1 mix of 0.1% calcofluor white in 20% EtOH and 10 µg mL^{-1} propidium iodide in water for 20 min. Sections were washed three times with water and mounted in wells of three-well Teflon microscope slides. A drop of 50% glycerol was added to each section and a cover slip was applied.

Sample preparation for examination of feeding site development

Inoculated plants were collected at 7, 15, and 21 d after inoculation (DAI). Visibly swollen regions were excised from their roots. Tissue was cleared, embedded, and sectioned as described above. Resulting sections were screened by light microscopy and sections containing the feeding site were selected. For each sampling time, at least three pairs of adjacent sections were examined, each from a different root.

Sample preparation for examination of xylem development

Three inoculated plants and three control plants were collected at each of 2, 7, 15, and 21 DAI. For each inoculated plant, the distance from the base of the root was measured for each swollen region. Swollen regions, and the corresponding regions on control roots, were excised. Tissue samples were immediately embedded in 4% agarose without clearing. Longitudinal sections were cut at 150 µm intervals and screened by light microscopy. Sections containing central metaxylem were selected and immediately stained with 0.1% calcofluor white in 20% EtOH and 10 µg mL^{-1} propidium iodide in water for 20 min. Sections were washed three times with water and mounted in wells of three-well Teflon microscope slides. A drop of 50% glycerol was added to each section and a cover slip was applied.

Sample preparation for lignin analysis

Tissue samples were collected from inoculated and control plants at 2, 4, 6 and 8 DAI, excised, embedded, sectioned and mounted as described above. Sections were stained in a solution of 0.2% basic fuchsin dissolved in ClearSee, following a protocol described by Ursache *et al.*

(2018) except that the incubation time was reduced to 20 min, washed with water three times, stained with 0.1% calcofluor white in 20% EtOH for 10 min and washed with water three times. A drop of 50% glycerol was added to each section and a cover slip was applied.

Imaging

To capture a depth of approximately 100 µm, images were obtained using the z-capture function of a Nikon A1R Laser Scanning Confocal microscope (Nikon, Tokyo, Japan) using two laser channels, DAPI (405 nm) and TRITC (561 nm). For each section, the laser power and gain settings were adjusted to avoid pixel saturation and minimise background. Images were processed with Nikon imaging software (NIS-Elements, www.microscope.healthcare.nikon.com/products/software/nis-elements) to obtain maximum-intensity projection images. IMARIS (version 9.2, imaris.oxinst.com) was then used to render 3D models of features (metaxylem vessels, feeding sites and nematodes) by creating surfaces from the fluorescence signal. In some cases, models were rotated to facilitate observation of details.

4.6 Acknowledgements

The authors acknowledge the facilities, and the scientific and technical assistance of the Australian Microscopy & Microanalysis Research Facility at Adelaide Microscopy, the University of Adelaide, with special thanks to Gwen Mayo. We thank John Lewis for providing nematodes and advice and Steve Tyerman for helpful discussions. This work was financially supported by a Beacon of Enlightenment Scholarship awarded to KL by the University of Adelaide and by the Grains Research and Development Corporation (Project UA00143).

Chapter 5 :
A first look: methods for water transport observation in CCN-infected wheat roots

5.1 Summary

The discovery of xylem disruptions within CCN-infected wheat roots raised questions about water transport. This chapter reports on the water transport methods used and outcomes observed. To begin these investigations, a coloured dye and a fluorescent dye were used as tracers. Both dyes were successful used to visualise water transport in wheat roots and indicated that a hindrance was present in infected roots. This work will likely help shape future research to better understand water transport in CCN-infected roots.

5.2 Introduction

Due to the importance of the cMX in carrying approximately 93% of all water uptake when fully mature (Luxová, 1986), it seems likely that the CCN-induced xylem disruptions reported in Chapter 4 interrupt water transport. Consistent with this, reports of above-ground symptoms in CCN-infected plants resemble those of water stress (Dickson, 1956; Stirling & Stanton, 1997). Previous research on *G. rostochiensis* infection in potato showed that total water uptake is reduced by nematode infection (Fatemy & Evans, 1986). Additionally, work on RKN showed decreased water potential in infected plants (Meon, 1978). However, water disruptions have been attributed to the act of nematode feeding and syncytial requirements, not necessarily xylem cell wall obstructions.

The aim of the research reported in this chapter was to determine whether tracer dyes could be used to detect any interruption of water transport in CCN-infected roots.

5.3 Materials and methods

5.3.1 Plant materials, inoculation and growth conditions

The susceptible sister wheat line 139-S was used (see Chapter 6 for further genomic details). Plants were inoculated and grown in hydroponics as described in Chapter 3 (3.3.1.4.2).

5.3.2 Blue food dye to pinpoint water uptake

Plants were collected at 7 DAI and suspended above a petri plate (Fig. 5-1). Excess roots were cut to leave only seminal roots of similar length and containing swollen regions for infected samples. Blue dye (Queen brand, food colouring dye) was diluted to a 1:10 concentration. The blue dye was pipetted around the root, then the tip was cut off while submerged in dye. After 30 s, the root was removed from the dye and the swollen region piece (2-4 mm) was cut. Cut pieces were hand-sectioned using a razor blade into pieces above the feeding site, within the feeding site, and below the feeding site. Sections were placed onto a slide and immediately imaged under the stereo microscope. This was repeated for 3 control and 3 inoculated plants.

Figure 5-1: Experimental setup for blue dye. Roots from hydroponics were taped between two racks and suspended over a petri plate. The ends of roots were submerged in blue dye and cut to facilitate dye uptake.

5.3.3 Symplastic tracer dye for rate of water uptake

To trace water uptake in plants, the symplastic dye, HPTS-acetate (8-Hydroxypyrene-1,3,6-trisulfonic acid trisodium salt), was selected and used at a 0.4% concentration (Wright & Oparka, 1996). Plants were tested at 7 d after inoculation. The apparatus for testing was assembled as followed: in a controlled environment room set to 15°C, a plastic tray was placed at a 45° angle with a reservoir attached to the bottom of the tray (Fig. 5-2a). Plants were aligned on the tray so that all primary root tips were in the reservoir. HPTS-acetate was added to the reservoir so that the root tip of each plant was submerged. To cover the system and prevent roots from drying out, a petri plate was placed on top of the root system (Fig. 5-2a, b). Multiple trays were used during an experiment (Fig. 5-2b). Root length was measured from the base of the reservoir to the base of the plant. At 10 min intervals, the position of the dye within the root (seen as bright yellow) was measured (Fig. 5-2c). This continued for a 60 min period. The experiment was repeated three times using 8 uninfected (control) and 8 infected plants. At 60 min, selected root systems were imaged using UV detection to verify the position of dye.

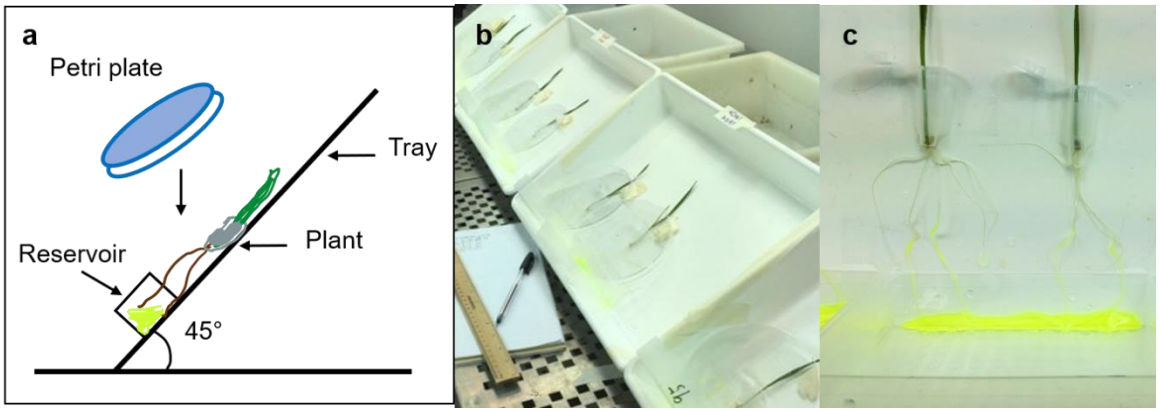

Figure 5-2: Experimental setup for HPTS-acetate tracer dye. (a) Diagram of assembly showing tray set in a 45° position with reservoir attached. Plants were positioned so that each root tip was within the reservoir. Plants were covered with a petri plate. (b) Multiple trays setup in growth chamber (c) Plants showing visible yellow dye uptake in roots.

5.4 Results

The blue dye could be tracked by eye from the outside of the root. After 10 s, the blue dye had travelled completely up the interior of the root, seen as a light blue hue (Fig. 4-3a). In the control root, the section showed blue staining heavily within pMX cells and light blue staining throughout the vascular cylinder (Fig. 5-3b). In the infected root, a slight change in root colour could be detected from the initial root immersion (Fig. 5-4a) to 10 s later (Fig. 5-4b). Sections were observed below, within, and above the swollen region. Below the swollen region, sections appeared similar to the control with most staining around pMX cells and throughout the vascular tissue (Fig. 5-4e). Within the swollen region, blue staining was found all around the feeding site and throughout the vascular cylinder (Fig. 5-4d). Above the swollen region, very little blue staining was seen, only lightly in some pMX cells (Fig. 5-4c).

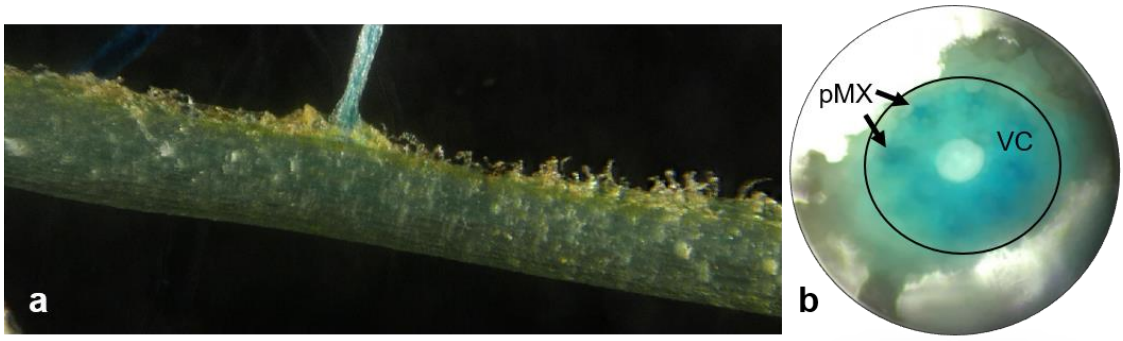

Figure 5-3: Blue dye within wheat root. (a) Visible blue hue from outside of root (b) Cross section of a control after 10 s of dye uptake showing a stained vascular cylinder (VC, circled) and heavily stained peripheral metaxylem (pMX) cells.

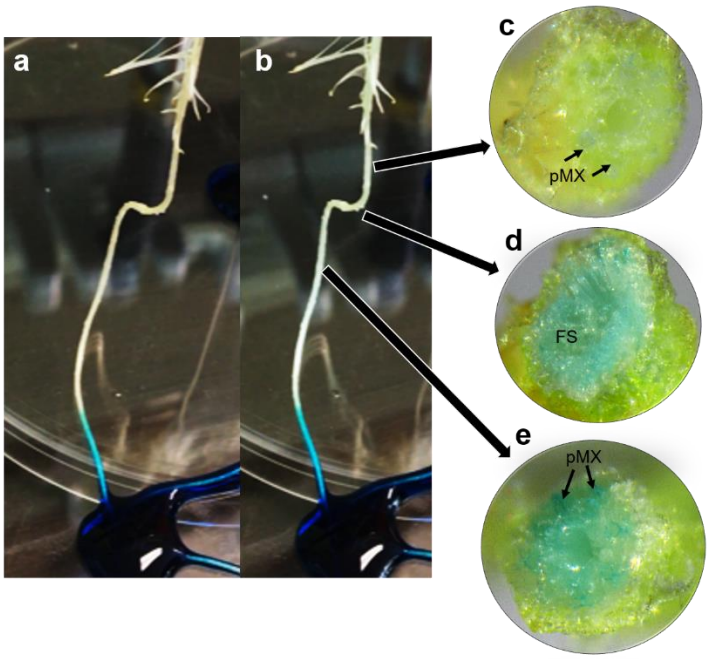

Figure 5-4: Blue dye within infected wheat root. *H. avenae* infected root in blue dye experiment. (a) Blue dye administered to root, time 0 s. (b) 10 s after blue dye administered. Stereomicroscope images of transverse sections taken from (c) above swollen region with little staining visible in some peripheral metaxylem cells (pMX), (d) within swollen region showing blue stain within the vascular cylinder and feeding site (FS), and (e) below swollen region showing blue stain within the vascular cylinder and heavily stained in pMX cells.

By using the fluorescent tracer dye HPTS, it was possible to track transport over a period of 60 min. Dye could be clearly seen as bright yellow roots. In control roots, dye was generally seen travelling all the way to the shoot (Fig. 5-5a) while infected roots showed dye that generally did not cross the swollen region (Fig. 5-5b). Further analysis under UV detection showed the brightest point (most concentrated dye) was positioned near the top of the swollen region (Fig. 5-5c).

Data analysis showed that dye uptake was slower in nematode infected roots, levelling off after 30 min (Fig. 5-6). After 60 min, the average dye position in control roots had reached 89% of the total root length and in infected roots had only reached an average of 39% of the

total root length. The average position of the swollen region in infected roots was located at 45% of the total root length.

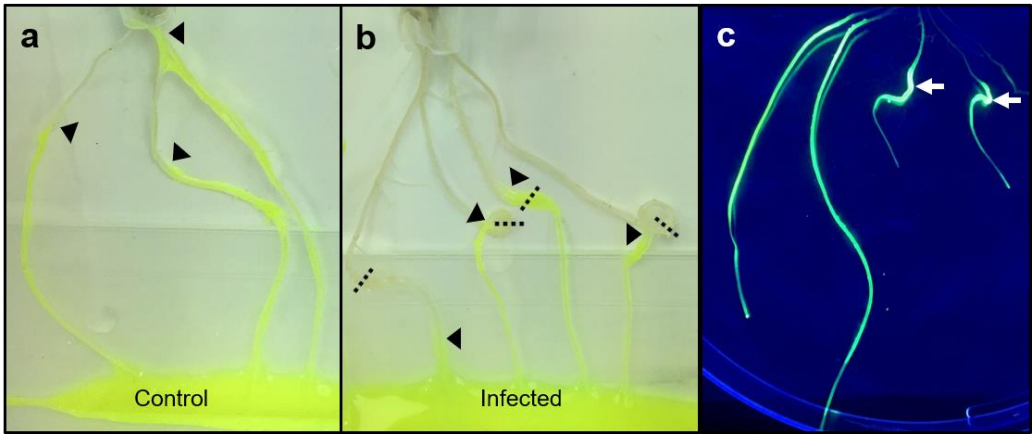

Figure 5-5: HPTS dye uptake in control and infected roots. Comparison of HPTS yellow dye movement after 60 min in wheat roots 7 d after (a) mock-inoculation with water (control) or (b) inoculation with *H. avenae* (infected). Triangles indicate the moving front of dye transport and dotted lines indicate the midpoint of the swollen region. (c) Root systems under UV light with arrows indicating the brightest point of dye within swollen regions of infected roots.

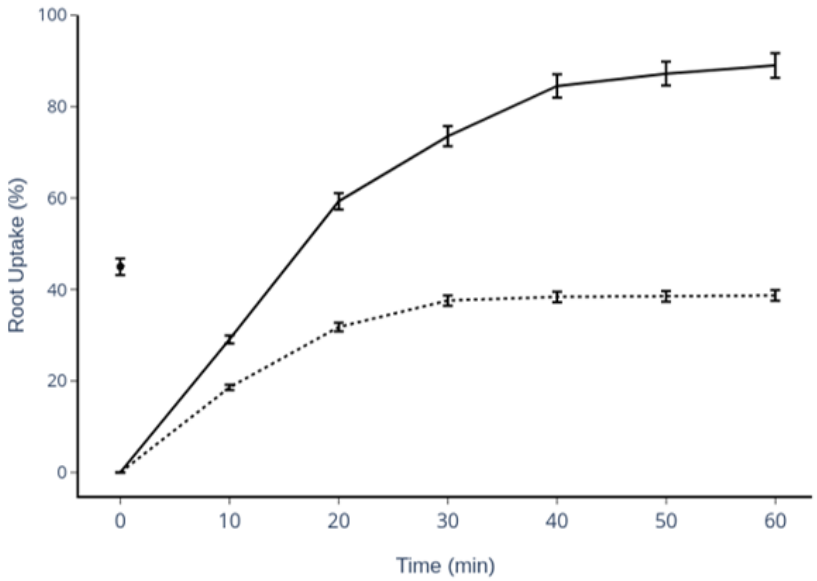

Figure 5-6: HPTS dye uptake over time. Averages and standard error of HPTS dye position over 60 min (measured every 10 min) in wheat roots 7 DAI with *H. avenae* (dotted line) or after mock-inoculation with water (solid line). Root uptake percentage on the Y-axis is calculated as the distance of dye travel/total length of root × 100. The average swollen region position is shown at time point 0 with standard error bars.

5.5 Discussion and conclusion

It was evident from the images presented in Chapter 4 that CCN-induced xylem morphology would likely disrupt water transport due to intact vessel walls and incorporation of xylem cells into syncytia. The experiments reported in this chapter tested the use of tracer dyes to observe water transport in CCN-infected roots.

The blue dye experiment was a quick test that showed water transport was impeded in infected roots. By cutting root tips, the blue dye was directly connected to the pMX/cMX channels and in just 10 s, control roots were able to transport the dye to the shoot through these channels. However, in infected roots, only some pMX faintly showed colour above the feeding site point, with no appearance of cMX transport above the infection point. This indicates that CCN-infection causes a major impediment of the plant's major water conduit by stopping/slowing flow through the cMX, however, limited flow is available through pMX. This is consistent with what was observed by microscopy (i.e. altered cMX but often intact pMX vessels located away from the feeding site).

The HPTS symplastic tracer dye experiment showed that within a 60 min period, water in a control root would likely reach the shoot while in an infected root would never reach the shoot, appearing to be stopped at the point of infection. Upon further analysis under UV light, it appeared that in the 60 min period, the dye could go beyond the point of infection, however, the dye was most concentrated at the top of the swollen region.

Both dyes were successful in tracing water transport in CCN infected roots. Further, they both identified that water transport is interrupted at infected sites. Water is transported either apoplastically (through cell walls) or symplastically (through cytoplasm). The blue dye likely travelled apoplastically as it was taken up quickly and stained pMX vessels more intensely than surrounding cells. The HPTS-acetate dye has been used as a symplastic tracer dye

(Wright & Oparka, 1996) but it can also be used as an apoplastic dye due to its pH-dependent properties (Wang & Fisher, 1994). Based on the slower rate at which HPTS rose through roots in this research, the dye seemed to travel symplastically. Therefore, an impediment was observed in both the apoplastic and symplastic pathways.

It remains unclear as to what advantages the cMX connection and subsequent impediment of major water flow may have for the nematode. However, as the impediment appeared regardless of the transport system tested, it is likely that it is not just physically due to the xylem morphology. More likely, it is due to the nematode and feeding site acquiring water from the water transport system as a whole, which would reduce transport in the apoplastic system and provide a large sink for the symplastic pathway. Consistent with this, previous research showed that syncytia exhibit high turgor pressure (Böckenhoff & Grundler, 1994), creating a sink for nutrient and water. Similarly, a constant flow of water may be important to maintain transport activity from surrounding phloem tissue to sustain nutrient influx. This leads to another question; what happens to all of the water that flows toward the syncytia? As previously mentioned, some water does appear to make its way above the feeding site, but a large portion is retained. Some studies on syncytial volume have mentioned that nematode defecation is mainly water (Müller *et al.*, 1981; Wyss & Grundler, 1992). This supports the theory that water is necessary for successful nutrient intake for the nematode, leaving behind water.

The research reported in this chapter indicates that the CCN-induced structural modification of cMX does have implications on water transport and that tracer dyes could be used to determine these impediments. Further work is needed to refine the methods used and apply them to understand the water transport mechanism and its relation to the xylem modifications seen in CCN-infected roots.

Chapter 6 : Responses of +*Cre8* and -*Cre8* wheat lines to CCN inoculation

6.1 Summary

To investigate a previously reported association of *Cre8* with plant vigour and potentially tolerance of CCN infection, experiments were conducted to examine differences in root and shoot development between materials that carry the *Cre8* resistance allele (*+Cre8)* and materials that lack the allele (*-Cre8*). No evidence was found for *Cre8* affecting plant vigour. In wheat plants grown in pots, the resistance of *+Cre8* plants was detectable by 21 d after inoculation, based on significantly higher numbers of nematodes in their roots, compared with the roots of *-Cre8* plants.

6.2 Introduction

In order to understand the mechanism by which a gene can confer resistance against a parasite or pathogen, it can be useful to compare plants that carry the resistance gene with those that do not. Differences observed between resistant and susceptible plants may give hints about mechanisms and/or consequences of resistance.

The terms non-preference, antibiosis and tolerance, which have been applied to insect resistance (Painter, 1951), may also be useful in the consideration of nematode resistance. Non-preference resistance, which can be tested by investigating attraction and penetration, is not known to occur in CCN-wheat interactions. Even CCN-immune host plants attract nematodes and allow penetration (Cui *et al.*, 2017). Antibiosis resistance, which can be investigated by analysing the development of nematodes and their feeding sites, has been reported for both the *Cre1* and *Cre3* resistance loci of wheat (Cui *et al.*, 2017; Seah *et al.*, 2000). Tolerance refers to plants thriving despite infection. In general, differences in tolerance to cyst nematodes have been considered to be independent of differences in resistance, however, relationships between resistance and tolerance have been reported (Fisher *et al.*, 1981; Smiley & Marshall, 2016; Trudgill, 1986). Based on mapping of early vigour to the same genomic region as CCN resistance, Williams *et al.* (2003) proposed that the *Cre8* locus

on chromosome 6B of wheat may confer both resistance and tolerance, but this has not been investigated further.

One of the aims of the research reported in this chapter was to investigate whether *Cre8* affects plant vigour. Another aim was to investigate the timing at which the antibiosis effect of *Cre8* could be detected.

6.3 Materials

6.3.1 Plant materials

The materials used in this study included the wheat lines TMDH6 (+*Cre8*) and TMDH82 (-*Cre8*) and progeny derived from crossing between these lines. Both TMDH6 and TMDH82 are doubled haploid (DH) lines derived from F_1 progeny of a cross between the Australian wheat cultivars Trident and Molineux (Ranjbar, 1997). Jayatilake (2014) selected these two lines based on their genotypes at markers linked with *Cre8* and two other CCN resistance loci that had been mapped using a Trident/Molineux population (Jayatilake, 2014; Williams *et al.*, 2003; Williams *et al.*, 2006). At the *Cre8* locus on chromosome 6B, TMDH6 carries the Molineux-derived resistance allele, while TMDH82 carries the Trident-derived susceptibility allele. Neither TMDH6 nor TMDH82 carry resistance alleles at the *QCre.srd-1B* locus on chromosome 1B or at the *Cre5* locus on chromosome 2A.

Jayatilake (2014) crossed TMDH6 and TMDH82 with each other and F_1 plants were grown and allowed to self-pollinate to provide F_2 seeds. Other members of the lab advanced these materials by self-pollination for two further generations and this provided the F_4 seeds for the research reported in this thesis. These seeds were dissected into embryo and endosperm sections. DNA was extracted from endosperm sections (protocol as described by Van Gansbeke *et al.* (2019)) and screened with *Cre8*-linked molecular markers reported by Jayatilake et al. (2015) and with additional markers that will be reported in Chapter 8 of this thesis. For seeds that were determined to be heterozygous in the *Cre8* region, the embryo-

containing portions were retrieved and sown. Plants grown from these seeds were allowed to self-pollinate and were grown to maturity, providing $F_{4:5}$ families. With marker screening of individual seeds within these families, it was possible to establish pairs of sister lines (with both members coming from the same F_4 plant), in which one member was homozygous for Molineux alleles in the *Cre8* region and the other was homozygous for Trident alleles in that region (Fig. 6-1). These pairs of lines were then tested using markers for polymorphisms at the *Rht-B1* and *Rht-D1* dwarfing alleles to select pairs in which both members exhibited the same 'semi-dwarf' genotypic combination: a 'wild type' genotype at one locus and 'dwarf' genotype at the other. Two pairs of lines (139-R and 139-S; 57-R and 57-S) matched all criteria.

In one experiment, the Australian cultivar Chara (AUS30031) was included. Chara has strong resistance against CCN (due to resistance at the *Cre1* locus) but is considered to be intolerant (Smiley *et al.*, 2013).

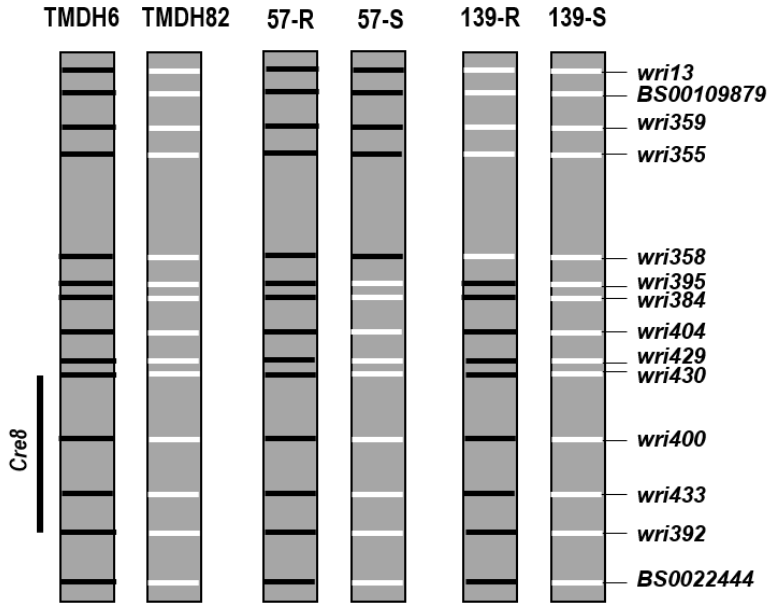

Figure 6-1: Graphical representation the *Cre8* region of 6BL in parental lines TMDH06 and TMDH82, sister lines 57-R and 57-S and sister lines 139-R and 139-S. Approximate marker positions shown as bars. Coloured differences indicate parental genotype: Molineux-like (black) and Trident-like (white). Mapped *Cre8* region annotated as vertical black line.

6.3.2 Nematode Inoculum

'Farms' of *H. avenae* pathotype Ha13 were prepared as described in Chapter 3 (3.3.1.2). Juvenile nematodes were collected by filtering the surrounding water through a 38 µm sieve. Water was added to provide inoculum with a concentration of approximately 100 nematodes/mL.

6.4 Experiment 1: Responses in parental lines, TMDH6 and TMDH82

To investigate whether the +*Cre8* line TMDH6 differs in early vigour from the -*Cre8* line TMDH82, an experiment was conducted in which plants of both lines were grown with and without inoculation with CCN. Shoot length was monitored, final plant biomass was measured and root systems were visually examined.

6.4.1 Methods

Fifty seeds of each of TMDH6, TMDH82 and Chara were placed on moist Whatman filter paper for 3 d at 15°C in darkness. After germination, seedlings were transferred to circular pots (8 cm tall × 5 cm diameter) filled with sandy loam, with one seedling per pot. Pots were arranged in a completely randomised layout, with 25 pots of each line randomly assigned to be inoculated with J2 nematodes and the other 25 pots to be mock inoculated with water. Inoculation was then conducted by pipetting 1 mL of inoculum (or water) onto the surface of the soil surface at each of five positions around the seedling (for a total of 5 mL of inoculum per inoculated pot). At 7, 14, 21, 28, 35, and 42 DAI, shoot length (from the base of the plant to the tip of the longest leaf) was measured. At 42 d, 10 plants of each line-treatment combination were sampled at random, removed from their pots and washed of all soil. The root systems of these plants were photographed, then the plants were dried at 50°C for 2 d and weighed.

6.4.2 Results

Shoot length differed significantly among lines at all sampling times (Table 6-1), with the susceptible line TMDH82 having longer shoots than TMDH6 or Chara (Fig. 6-2). TMDH82 also had the greatest plant biomass at the end of the experiment (Fig. 6-3).

In all three lines, inoculation with nematodes decreased shoot length and plant biomass (Table 6-1 and Figs. 6-2; 6-4). The root systems of inoculated plants contained swollen regions and had more lateral roots than control plants (Fig. 6-3). Proliferation of lateral roots was more extreme for the susceptible line TMDH82 than for TMDH6 or Chara.

Table 6-1: Analysis of variance for shoot length and plant biomass in Experiment 1. Degrees of freedom and F statistics from an analysis of variance for shoot length between 7 and 42 DAI with J2-stage cereal cyst nematodes (CCN, *Heterodera avenae*) and for plant biomass at 42 DAI.

		F						
		Shoot length						
Source of Variation	*Degrees of freedom*	*7 d*	*14 d*	*21 d*	*28 d*	*35 d*	*42 d*	*Plant biomass*
Line	2	37.7**	47.7**	99.6**	73.9**	77.7**	102.7**	11.79**
Treatment	1	117.0**	19.2*	59.6**	3.5	16.4**	19.9**	12.31**
Line × treatment	2	2.1	4.7*	2.5	0.9	0.4	1.9	0.02

*,** Significant at the 0.05 and 0.01 levels of probability, respectively.

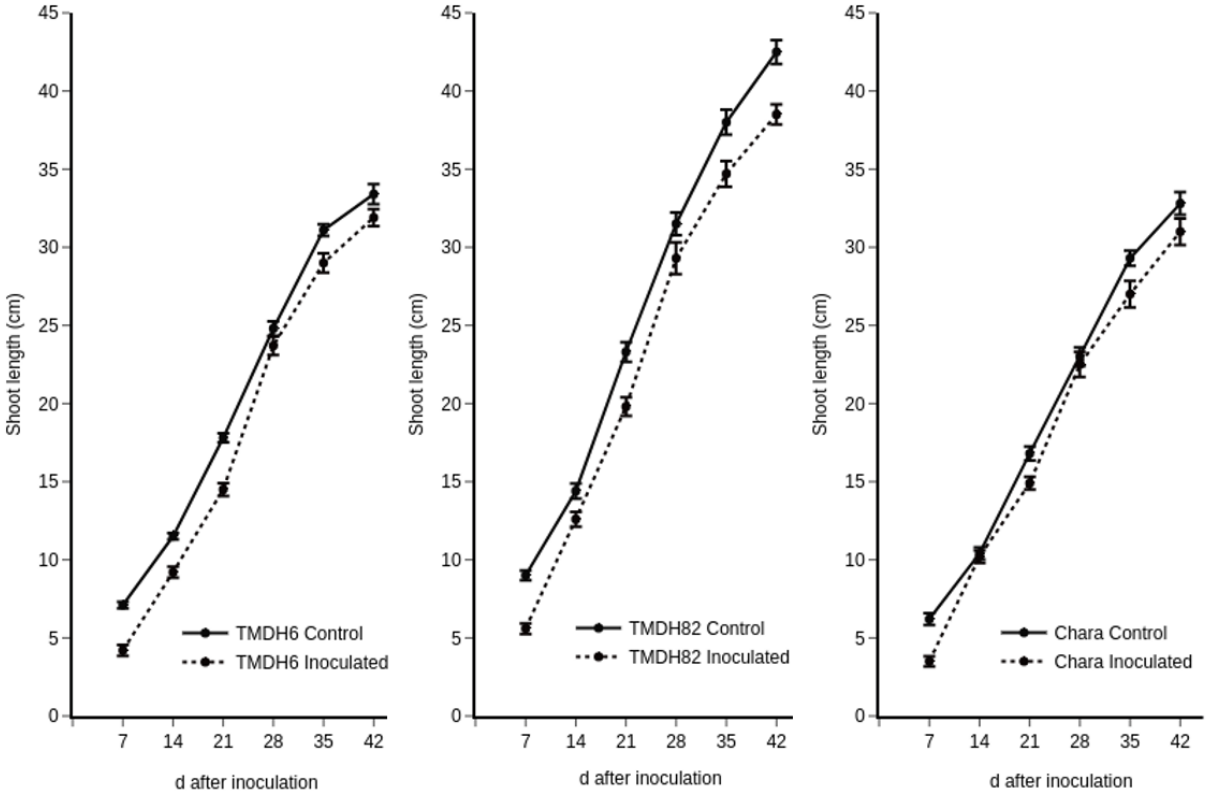

Figure 6-2: Shoot length in Experiment 1. Means and standard errors for the shoot length of TMDH6, TMDH82 and Chara from 7 to 42 DAI with J2-stage *H. avenae* or mock inoculated with water (control). Analysis of significance shown in Table 6-1.

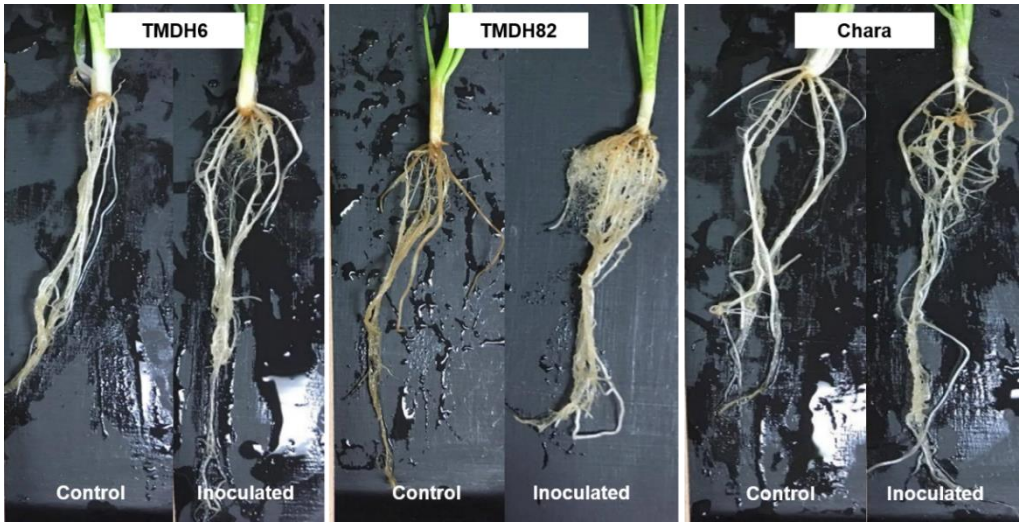

Figure 6-3: Root systems in Experiment 1. Root systems of plants of TMDH6, TMDH82 and Chara at 42 DAI with J2-stage *H. avenae* or mock inoculated with water (control).

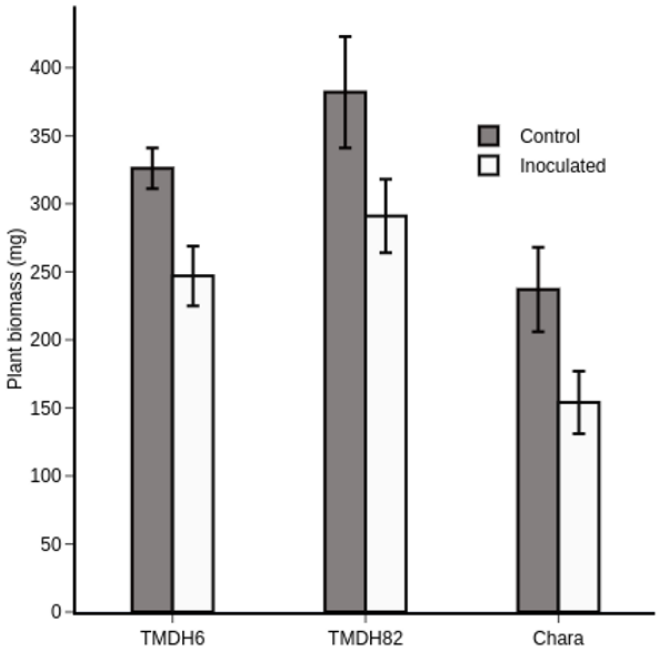

Figure 6-4: Plant biomass in Experiment 1. Means and standard errors for plant biomass of TMDH6, TMDH82 and Chara at 42 DAI with J2-stage *H. avenae* or mock inoculated with water (control). Analysis of significance shown in Table 6-1.

6.5 Experiment 2: Analysis of sister lines

After observing that even mock-inoculated control plants of TMDH6 and TMDH82 differed in both shoot length and plant biomass, the *Rht-B1* and *Rht-D1* genotypes were assessed, revealing that TMDH6 is a 'double dwarf' type and TMDH82 is a tall type. In light of this, new pairs of sister lines were selected in which both members would exhibit semi-dwarf phenotypes. Experiment 2 involved evaluation of two new pairs of sister lines in a tube test (O'Brien & Fisher, 1977).

6.5.1 Methods

The 'tube test' was set up as described by Van Gansbeke *et al.* (2019). Pre-germinated seeds of two pairs of sister lines (57-R and 57-S; 139-R and 139-S) and their parental lines TMDH6 and TMDH82 were sown in tubes (2.5 cm wide × 13 cm deep) filled with sandy loam soil (one seed per tube, 20 tubes per line) and kept in a controlled environment room (15°C with

12 h light/dark cycle). Each tube was inoculated five times (at 1, 4, 5, 11 and 14 d after sowing) by pipetting 1 mL of nematode inoculum onto the soil surface.

On each of four days (at 21, 28, 35 and 42 d after the first inoculation) three plants from each line were gently removed from their tubes. Their roots were washed and photographed. The number of 'knotted' points in each root system was counted. Roots were cut at their base, dried for 3 hours at 50°C and then weighed. The remaining eight plants of each line were kept in the tube test until 70 d after the first inoculation. These plants were removed from their tubes, soil was washed from their roots and the final number of adult white female nematodes was counted.

6.5.2 Results

Visual examination of the root systems of the plants that were removed during the tube test did not reveal any striking differences in root length or branching among the six lines (Fig. 6-5). Nevertheless, analysis of variance revealed significant variation among lines, among sampling dates and for the interaction between lines and sampling dates, for both the number of swollen regions and root biomass (Table 6-2).

The +*Cre8* line TMDH6 had fewer swollen regions than the -*Cre8* line TMDH82 (Fig. 6-6), but these two lines did not differ much in root biomass (Fig. 6-7). At most sampling times, and particularly at 35 and 42 DAI, the +*Cre8* lines 57-R and 139-R had fewer swollen regions (Fig. 6-6) and greater root biomass (Fig. 6-7) than their -*Cre8* sister lines 57-S and 139-S. Differences between 57-R and 57-S were greater than those between 139-R and 139-S.

At the end of the tube test, the number of white female nematodes was significantly lower ($p<0.001$) in the root systems of the +*Cre8* lines (TMDH6, 57-R, 139-R) than in those of the -*Cre8* lines (TMDH82, 57-S, 139-S) (Fig. 6-8). For +*Cre8* plants, this number was always below 30, with line means ranging from 18 to 24. For -*Cre8* plants, cyst counts ranged from 14 to 83, with line means ranging from 39 to 48.

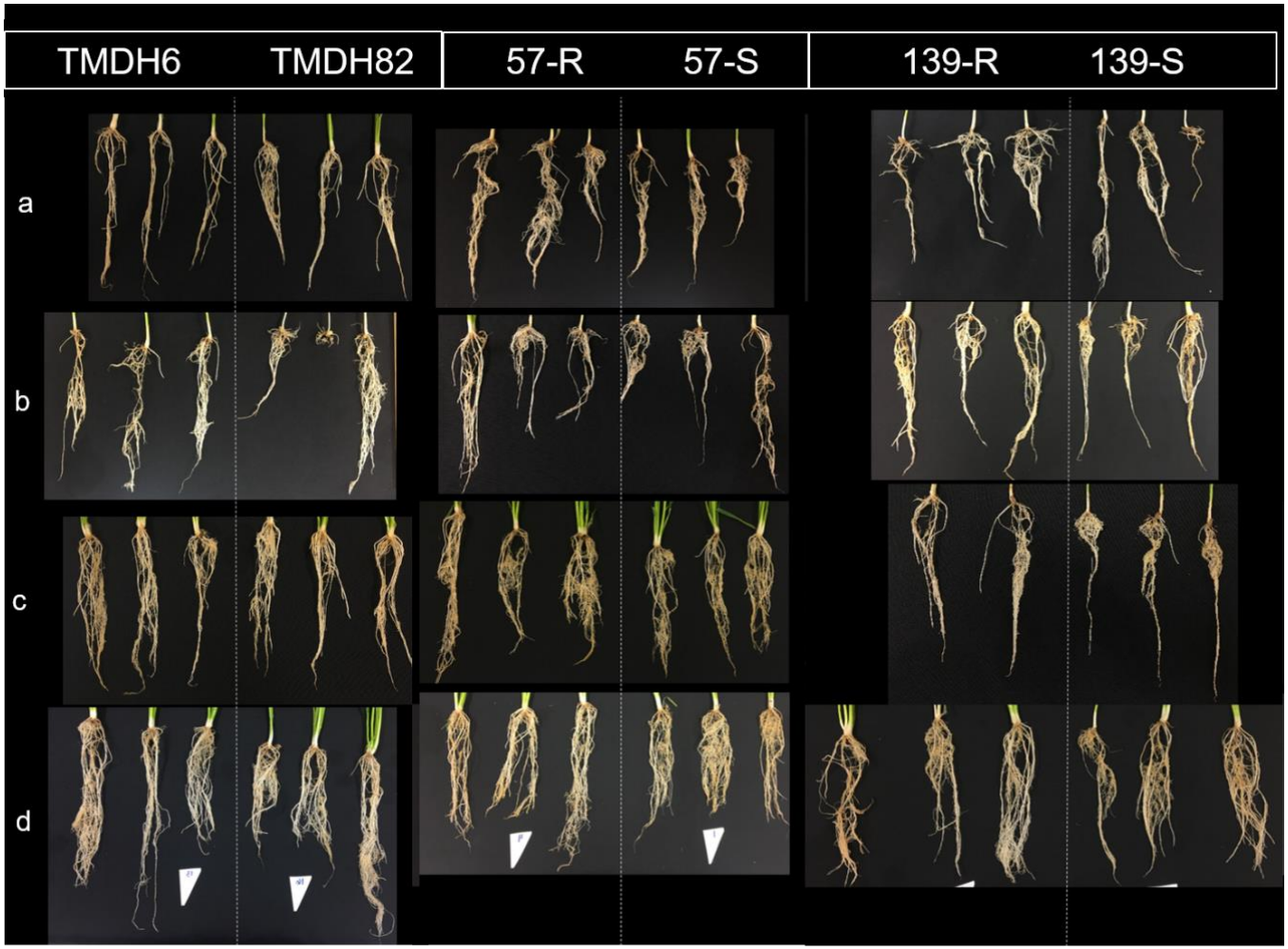

Figure 6-5: Roots systems in Experiment 2. Comparison of root systems of TMDH6 and TMDH82, 57-R and 57-S and 139-R and 139-S at (a) 21, (b) 28, (c) 35, and (d) 42 DAI with J2-stage *H. avenae*.

Table 6-2: Analysis of variance for number of swollen regions and root biomass in Experiment 2. Degrees of freedom and F statistics from an analysis of variance for number of swollen regions and root biomass of plants inoculated with J2-stage *H. avenae*.

Source of Variation	*Degrees of freedom*	F	
		Swollen regions	*Root biomass*
Line (TMDH6, TMDH82, 57-R, 57-S, 139-R, 139-S)	5	24.0**	20.7**
Sample date (21, 28, 35, 42 d)	3	17.6**	119.4**
Line × sample date	15	7.6**	6.8**

*,** Significant at the 0.05 and 0.01 levels of probability, respectively.

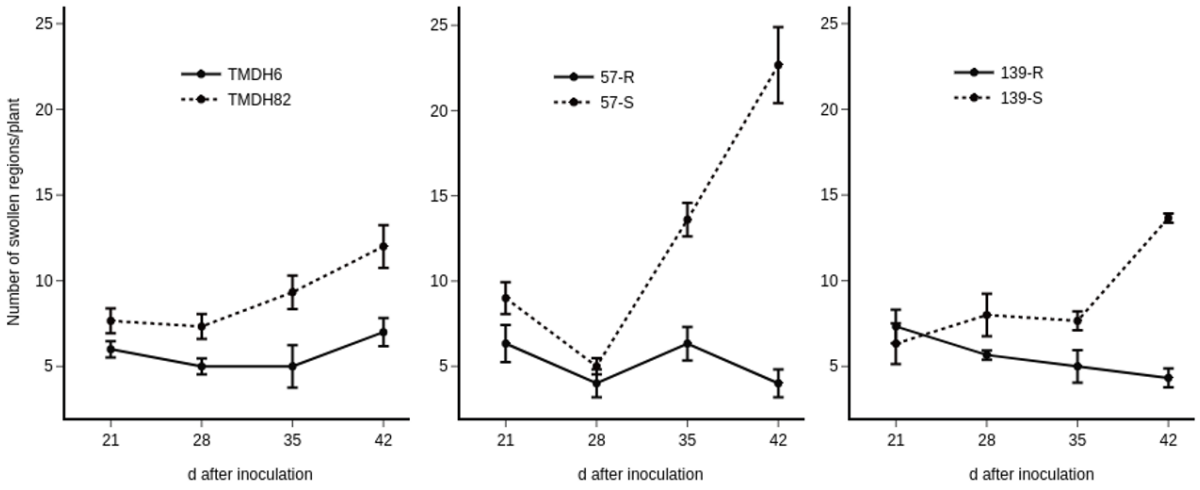

Figure 6-6: Number of swollen regions per plant in Experiment 2. Means and standard errors for number of swollen regions of 57-R, 57-S, 139-R, 139-S, TMDH6 and TMDH82 from 21 to 42 DAI with J2-stage *H. avenae*. Analysis of significance shown in Table 6-2.

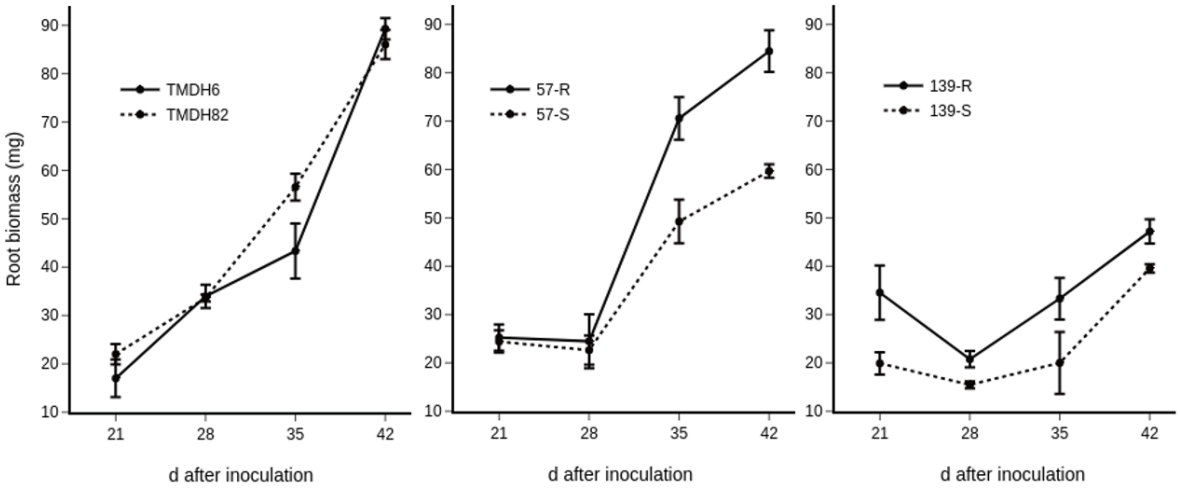

Figure 6-7: Root biomass in Experiment 2. Means and standard errors for root biomass of TMDH6 and TMDH82, 57-R and 57-S and 139-R and 139-S from 21 to 42 DAI with J2-stage *H. avenae*. Analysis of significance shown in Table 6-2.

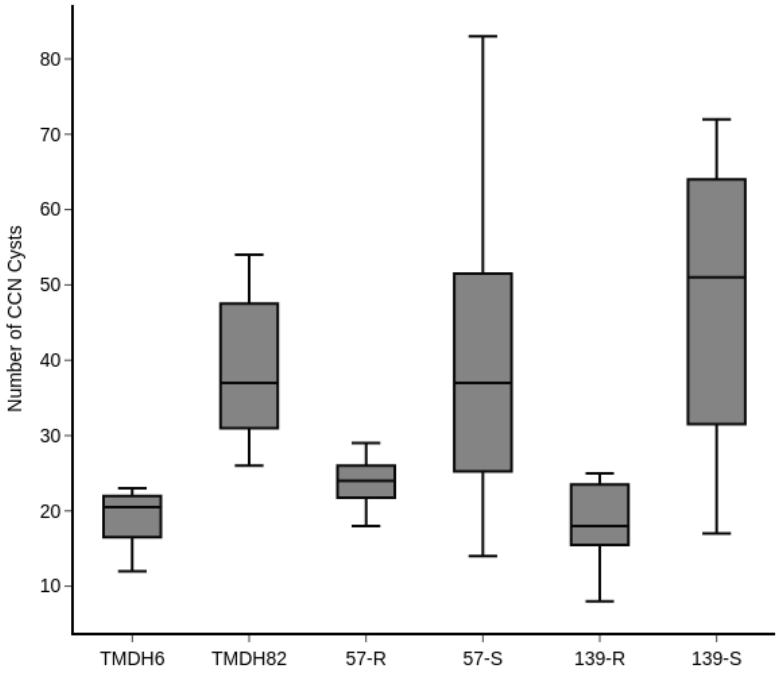

Figure 6-8: Tube test results of sister lines for Experiment 2. Analysis of parental lines and two sets of sister lines for comparing number of CCN cysts on +*Cre8* (TMDH6, 57-R, 139-R) and -*Cre8* (TMDH82, 57-S, 139-S) lines at 70 DAI with J2-stage *H. avenae*.

6.6 Experiment 3: Responses of sister lines

To investigate whether the +*Cre8* line 139-R differs in early vigour from its -*Cre8* sister line 139-S, an experiment was conducted in which plants of these lines were grown with and without inoculation with CCN. Shoot length was monitored and nematodes were counted within the root systems of inoculated plants.

6.6.1 Methods

The experimental setup was similar to that used for Experiment 1 described in 6.4.1, but with 50 seeds of each of 139-R and 139-S. At each of 14, 21 and 28 d after inoculation, the root systems of five inoculated plants from each line were washed of all soil and stained with acid fuchsin (protocol described in Chapter 3, section 3.4.1). Stained nematodes within roots were counted.

6.6.2 Results

In inoculated plants, the number of nematodes varied significantly between lines and among sampling dates, with significant interaction between lines and sampling dates (Table 5-3). At 14 d, the two lines had very similar numbers of nematodes, but at 21 and 28 d, the number of nematodes was much higher for 139-S than for 139-R (Fig. 6-9).

The two lines did not differ in shoot length at any of the sampling dates (Table 6-4). In both lines, shoot length was reduced by inoculation with nematodes (Table 6-4 and Fig. 6-10).

Table 6-3: Analysis of variance for number of CCN in Experiment 3. Degrees of freedom and F statistics from an analysis of variance for number of CCN from 14 to 28 DAI with J2-stage *H. avenae*.

Source of Variation	*Degrees of freedom*	*F* *Number of CCN*
Line (139-R, 139-S)	1	17.8**
Sampling date (14, 21, 28 d)	2	11.7**
Line × sampling date	1	5.2*

*,** Significant at the 0.05 and 0.01 levels of probability, respectively.

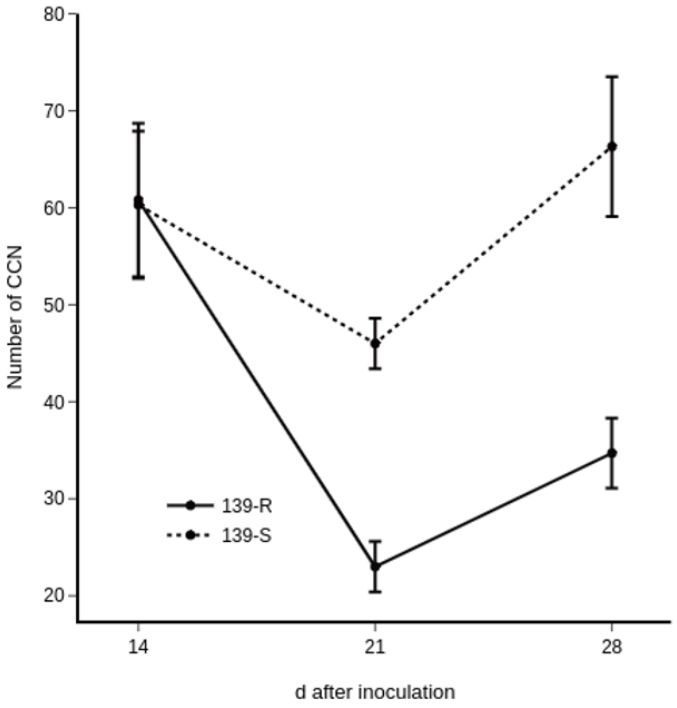

Figure 6-9: CCN count in Experiment 3. Mean and standard errors of number of *H. avenae* in sister lines, 139-R and 139-S, from 14 to 28 DAI with J2-stage CCN. Analysis of significance shown in Table 6-3.

Table 6-4: Analysis of variance for shoot length in Experiment 3. Degrees of freedom and F statistics from an analysis of variance for shoot length from 7 to 28 DAI with J2-stage *H. avenae* or mock-inoculation with water (control).

	Degrees of freedom	*F*			
		Shoot length			
Source of Variation		7 d	14 d	21 d	28 d
Line	1	0.258	0.003	0.570	1.390
Treatment	1	11.7**	6.7*	20.4**	25.3**
Line × treatment	1	0.84	0.05	1.01	0.56

*,** Significant at the 0.05 and 0.01 levels of probability, respectively.

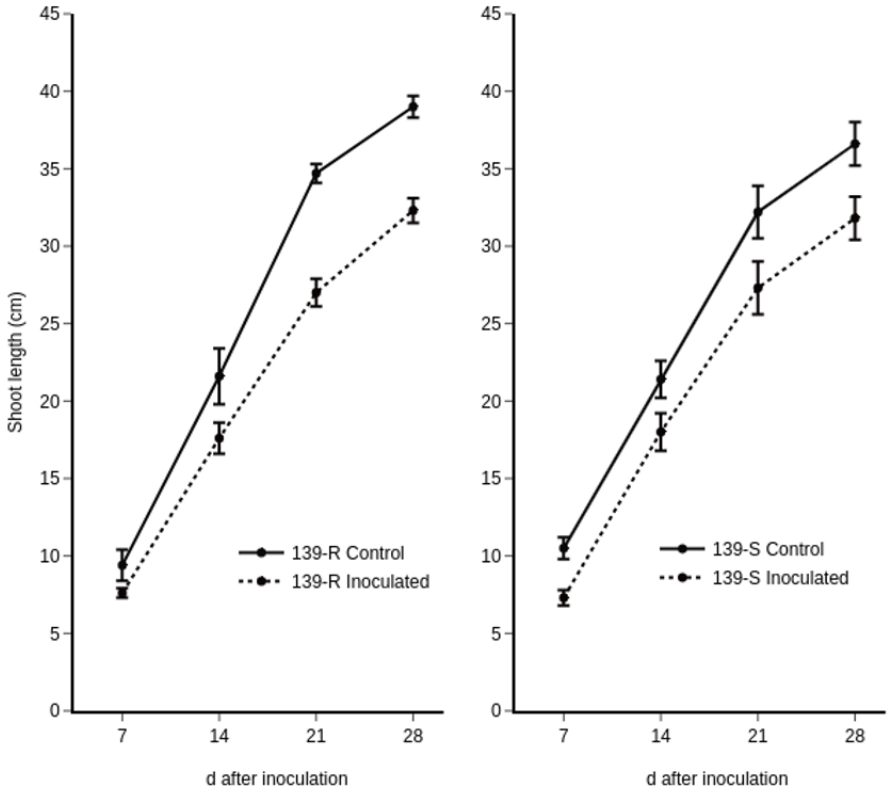

Figure 6-10: Shoot length in Experiment 3. Mean and standard errors of shoot length in sister lines, 139-R and 139-S, from 7 to 21 DAI with J2-stage *H. avenae*. Analysis of significance shown in Table 6-4.

6.7 Discussion

The overall aim of the research reported in this chapter was to investigate whether +*Cre8* and -*Cre8* materials differ in their root and shoot development, and specifically to see whether +*Cre8* materials are able to maintain plant vigour despite CCN infection. Another aim was to determine when antibiosis resistance could be detected.

Initially (in Experiment 1), Trident/Molineux DH lines TMDH6 and TMDH82 and the cultivar Chara were used. The results showed that CCN infection reduced shoot length and plant biomass. This was observed regardless of presence of resistance (*Cre8* in TMDH6 or *Cre1* in Chara) or known intolerance (Chara). In this experiment, all three lines seemed equally intolerant.

Despite a previous report of greater plant vigour being associated with *Cre8* resistance (Williams *et al.*, 2003), the +*Cre8* line TMDH6 exhibited less shoot growth than the -*Cre8* line TMDH82. This was probably due to their contrasting genotypes at *Rht1* dwarfing loci, which had not been considered when Jayatilake (2014) selected these lines for further investigation. Genotyping with *Rht1* marker assays revealed that TMDH6 has the 'double dwarf' allele combination while TMDH82 has the 'tall' allele combination. This could explain the observed difference in shoot growth between TMDH6 and TMDH82 and it meant that these lines were not ideally suited to this investigation.

Fortunately, TMDH6 and TMDH82 had already been crossed with each other and selfed progeny had been generated and genotyped. From among these progeny, two F_4 plants (57 and 139) were selected. Both of these were heterozygous in the *Cre8* region and each of them was homozygous for one of the two semi-dwarf allele combinations. With self-pollination and selection based on *Cre8*-linked markers, two pairs of sister lines (each consisting of one +*Cre8* line and one -*Cre8* line) were obtained. This allowed the *Cre8* effects to be investigated without confounding effects from the *Rht1* loci.

A tube test (Experiment 2), in which the number of swollen regions in root systems was monitored between 21 and 42 DAI and white female cysts were counted at 70 DAI, confirmed that the +*Cre8* lines TMDH6, 57-R and 139-R are all more resistant than their -*Cre8* counterparts TMDH82, 57-S and 139-S. Monitoring of root biomass in the same experiment revealed no obvious differences between the resistant (but double dwarf) line TMDH6 and the susceptible (but tall) line TMDH82. In contrast, inoculation with nematodes depressed root biomass to a greater extent in each semi-dwarf susceptible line compared to its semi-dwarf resistant counterpart, especially with increasing time after inoculation.

Comparisons of inoculated and non-inoculated plants of the +*Cre8* line 139-R and the -*Cre8* line 139-S (Experiment 3) showed that shoot growth was negatively affected by CCN infection but did not yield any evidence of differential effects between the two lines.

While none of the experiments reported in this chapter confirmed the previously reported effects of *Cre8* on plant vigour, it is important to note that these experiments were conducted in tube test experiments under controlled environment conditions. These conditions cannot be expected to adequately represent the full range of conditions that might be encountered in the field. Nevertheless, it seems safe to conclude that there is no obviously diagnostic 'vigour phenotype' that could replace nematode counting or marker genotyping for the resistance conferred by *Cre8*.

While the previous reported association of *Cre8* with plant vigour was not confirmed in the research conducted here, analyses of the number of nematodes and swollen regions within root systems confirmed that *Cre8* induces antibiosis resistance that can be readily detected at 21 d after the final inoculation, but not at 14 d or earlier. These results indicate that the *Cre8* resistance response acts quite late in feeding site development relative to what has been reported for *Cre3* resistance, which involves substantial reduction of the number of J2 nematodes within just 5 DAI (Cui *et al.*, 2017).

Based on the results reported in this chapter, it seemed that further investigation of the effects of *Cre8* resistance could benefit from microscopic analysis of infected roots of *+Cre8* and *-Cre8* plants. The results of that analysis will be presented in Chapter 7.

Chapter 7 : Cytological analysis of CCN feeding site development in +*Cre8* and -*Cre8* wheat lines

7.1 Summary

This chapter reports on the cytological differences in CCN-infected roots of -*Cre8* and +*Cre8* plants. Confocal microscopy was used to examine the structure and composition of nematode feeding sites. Transverse sections showed that feeding sites induced in -*Cre8* plants were adjacent to the cMX and contained many intricate 'web-like' cell walls, while feeding sites induced in roots of +*Cre8* plants varied in position relative to cMX and lacked inner cell wall structures. Longitudinal sections revealed that although xylem modification, discussed in Chapter 4, occurred in infected roots of both -*Cre8* and +*Cre8* plants, this modification was more extreme in -*Cre8* plants. Further investigations using cell-wall-specific antibodies and stains showed CCN-infected roots of +*Cre8* plants had more secondary thickening around xylem vessels and more (1,3;1,4)-β-glucan surrounding feeding sites than those of -*Cre8* plants. The results reported in this chapter provide a basis for consideration of how *Cre8* confers resistance against CCN.

7.2 Introduction

The microscopy techniques reported in Chapter 3 and 4 provided the ability to obtain quality images of depth and structure within wheat roots. This highlighted spatial arrangements between the feeding site and vascular tissue and revealed xylem modification in CCN-infected roots. The work reported in those chapters was conducted using a CCN-susceptible wheat line and does not show whether xylem modification occurs in CCN-resistant wheat. In the research reported in this chapter, similar microscopy techniques were applied to compare structural features (presence of xylem modification and incorporation of xylem in syncytia) and compositional features (composition of (1,3;1,4)-β-glucan, lignin and callose) between CCN-infected roots of +*Cre8* and -*Cre8* plants.

7.3 Materials and methods

7.3.1 Plant materials, inoculation and growth conditions

The doubled haploid lines TMDH6 (+*Cre8*) and TMDH82 (-*Cre8*) (described in Chapter 6) and the sister lines 139-R (+*Cre8*) and 139-S (-*Cre8*) (described in Chapter 5) were used. Seeds were germinated on sterile 2% agar plates and kept at 15°C for 3 d. Roots were inoculated at the root tip, left on agar for 24 h, then washed and transferred to a hydroponic tank as described in Chapter 3 (3.3.1.4.2). Plants were kept in a controlled environment growth chamber at 15°C for 12 h light and 12 h dark. For each experiment conducted, enough plants of each line (+*Cre8* or -*Cre8*) were inoculated and put into hydroponics, so that at least four plants (from each line) were collected for every time point.

7.3.2 Sample preparation, microscopy and imaging

Roots collected from inoculated plants of TMDH6 and TMDH82 at specific times between 7, and 21 DAI were either treated with acid fuchsin (as described in Chapter 3, (3.4.1)) or cleared with ClearSee for 30 d. At each time point, four to six roots containing swollen regions were collected from each line. Swollen regions (2-4 mm in length) were excised and embedded in 4% agarose and sectioned transversely (acid-fuchsin-stained samples) or longitudinally (cleared samples) at 150 µm intervals using a vibratome. Sections containing feeding sites were stained with calcofluor white and propidium iodide (as described in Chapter 3 (3.4.5.2)), mounted and imaged using a confocal microscope (as described in Chapter 3 (3.5.2.1)). To make 3D models, consecutive sections were imaged and resulting z-stack images were analysed using IMARIS (as described in Chapter 4 (4.3)).

For immunolabelling, inoculated 139-R and 139-S roots were collected at 6 DAI, four swollen regions (2-4 mm in length) from each line were excised and fixed in 4% paraformaldehyde (PFA) for 1 h under vacuum. Tissue was embedded into 4% agarose and sectioned at 100 µm intervals using a vibratome. Selected sections containing feeding sites were stained using a (1,3;1,4)-β-glucan-specific mouse primary antibody BG1 (Meikle *et al.*,

1994) or a callose-specific antibody (Meikle *et al.*, 1991) by following protocols described by Aditya *et al.* (2015). Secondary antibodies were conjugated to Alexafluor 555 (Life Technologies, Carlsbad, CA, USA). Sections were counterstained with 0.1% calcofluor white for 5 min then mounted in 50% glycerol and imaged as described above.

For histochemical staining of lignin, inoculated 139-R and 139-S roots were collected at 4, 6, and 8 DAI. At each collection date, three to four swollen regions from each line were excised and embedded into 4% agarose. Transverse sections were cut at 100 µm using a vibratome. Sections containing feeding seeds were stained in 0.2% basic fuchsin dissolved in ClearSee as described by Ursache *et al.* (2018) except that the incubation time was reduced to 20 min. Sections were then washed in 1× phosphate-buffered saline (PBS) for 1 min, washed in sterile water for 1 min, stained with 0.1% calcofluor white in 20% EtOH for 10 min, then washed in water again. Sections were mounted in 50% glycerol and imaged as described above.

7.4 Results

In transverse sections taken from CCN-infected regions of wheat roots, the cMX and CCN feeding sites were both clearly visible (Fig. 7-1). Feeding sites were irregular in shape and contained networks of partially degraded cell walls. In the *-Cre8* line TMDH82, feeding sites were consistently located directly adjacent to the cMX (Fig. 7-1a-e) and some even directly connected with it *via* openings through the outer walls of cMX vessel elements (Fig. 7-1a, b). In the *+Cre8* line TMDH6, some feeding sites were adjacent to the cMX (Fig. 7-1g, j) while others were separated from the cMX by one or more layers of cells (Fig. 7-1f, h). No direct connections were observed between feeding sites and the cMX of the *+Cre8* lines.

Examination of longitudinal sections showed that feeding sites in roots of the *-Cre8* line 139-S were adjacent to the cMX for much of their length (Fig. 7-2a-d). Some of these feeding sites were directly connected with the cMX (Fig. 7-2c, d; Fig. 7-3a). In contrast, not all feeding sites in roots of the *+Cre8* line 139-R were directly adjacent to the cMX; some were separated

from it by one or more layers of cells (Fig. 7-2 f-h,j; Fig. 7-3b) while some were adjacent to the cMX (Fig. 7-2i). No direct connections to the cMX were observed in samples from 139-R. Modification of xylem vessels near feeding sites was more pronounced in the cMX of the -*Cre8* line (Fig. 7-3a) than in the cMX of the +*Cre8* line (Fig. 7-3b). The internal cell walls within feeding sites differed between the -*Cre8* line 139-S and the +*Cre8* line 139-R. At 17 and 21 DAI, internal cell walls of feeding sites had a more intricate and 'web-like' structure in the -*Cre8* line (Fig. 7-2c, d; Fig. 7-4a) while feeding sites lacked internal cell walls in the +*Cre8* line (Fig. 7-2 h, i; Fig. 7-4b).

Examination of consecutive sections from infected root segments and generation of 3D models from each section clarified the spatial relationships among cMX vessels, nematodes and nematode feeding sites (Fig. 7-5). For example, in one longitudinal section from the -*Cre8* line 139-S, several cMX vessel elements were clearly visible (Fig. 7-5a). In the adjacent section, the most obvious feature was a nematode feeding site with a web-like network of internal cell walls (Fig. 7-5b). In a third section, the main features were the outer wall of the feeding site and the head of a nematode (Fig. 7-5c). Similarly, in a series of sections from the +*Cre8* line 139-R, the first section contained the outer walls of an intact cMX vessel (Fig. 7-5f), a second section contained a series of enlarged cMX vessel elements with apparently intact end walls between vessel elements (Fig. 7-5g) and a third section included both outer walls of the cMX vessels and a nearby feeding site (Fig. 7-5h). Three-dimensional modelling of the key features within each section and rotation of the resulting models clarified how features 'fit together' and how the overall structure differs between roots of -*Cre8* and +*Cre8* lines. In the roots of -*Cre8* plants, it was evident that the feeding site was directly connected to the cMX showing the 'web-like' walls of a feeding site adjacent to cMX vessels (Fig. 7-5d, e). In contrast, roots of +*Cre8* plants showed a completely intact cMX with model pieces fitting together (Fig. 7-5i, j).

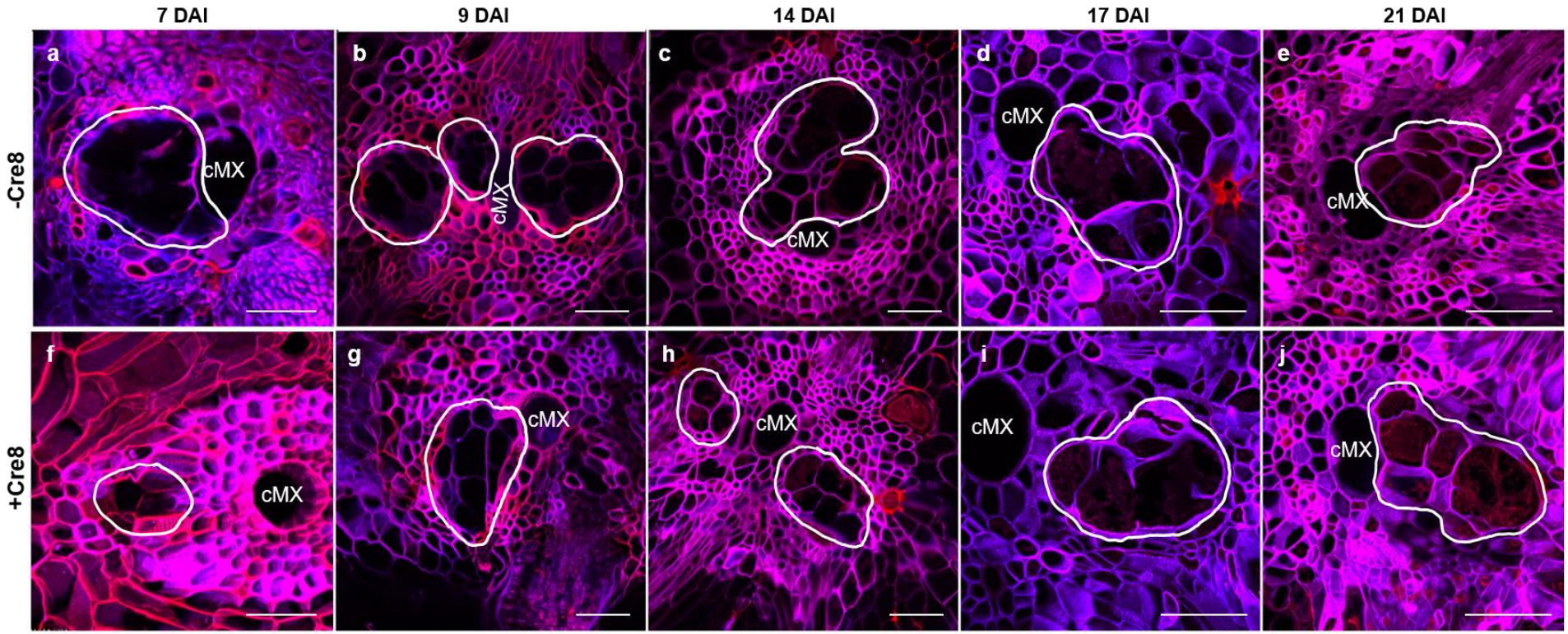

Figure 7-1: Transverse sections of CCN-infected roots in +*Cre8* and -*Cre8* plants. Transverse sections of (a-e) -*Cre8* and (f-j) +*Cre8* infected wheat roots with J2-stage *H. avenae* at 7, 9, 14, 17, and 21 DAI. (white outline) feeding sites, (cMX) central metaxylem. Scale bar: 100 µm.

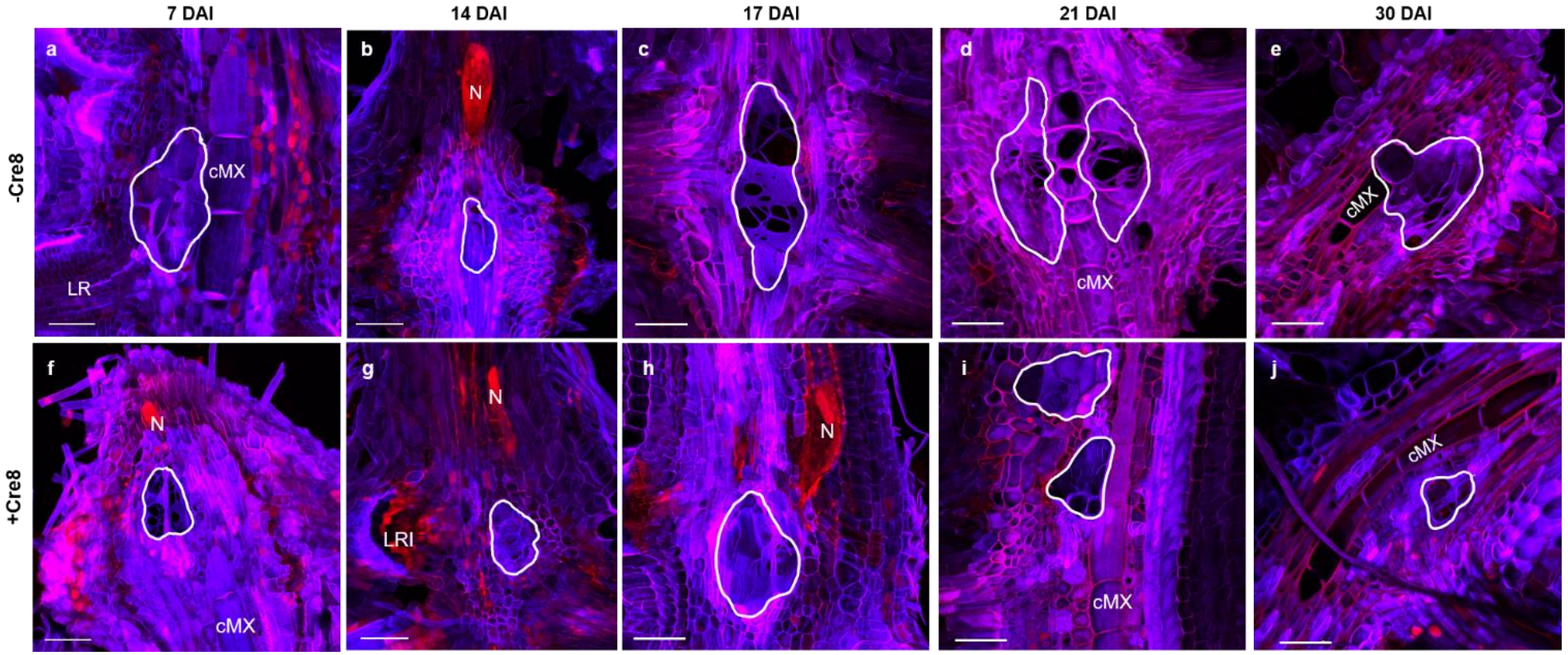

Figure 7-2: Longitudinal sections of CCN-infected roots in +*Cre8* and -*Cre8* plants. Maximum projected longitudinal sections of (a-e) roots of -*Cre8* plants and (f-j) roots of +*Cre8* plants inoculated with J2-stage *H. avenae* at 7, 14, 17, 21, and 30 DAI. (N) nematode, (cMX) central metaxylem, (LR) lateral root, (white outline) feeding site. Scale bar 100 µm.

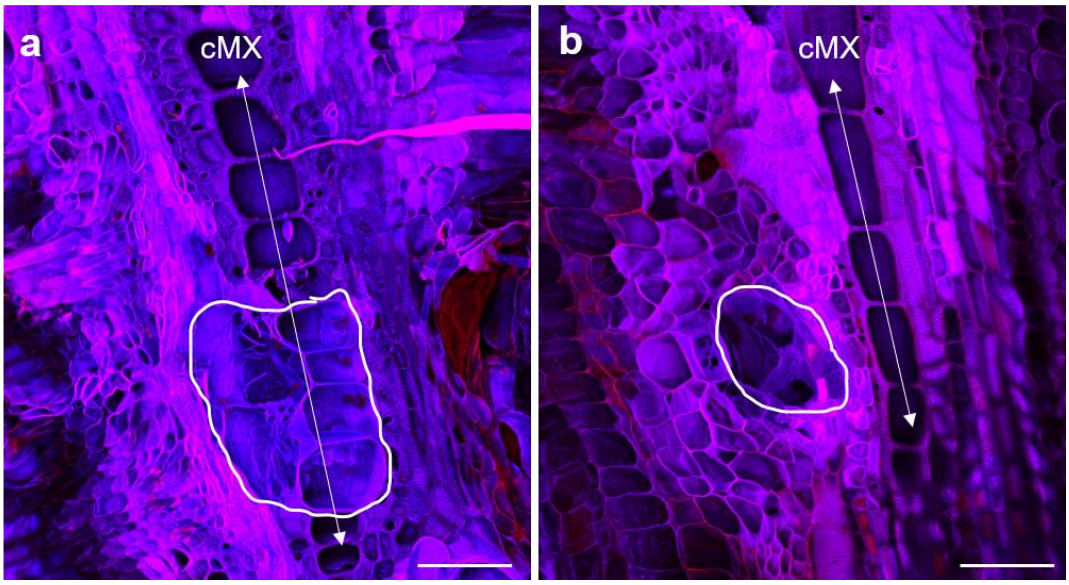

Figure 7-3: cMX structure in CCN-infected roots of -*Cre8* and +*Cre8* plants. Maximum projected longitudinal sections of (a) roots of -*Cre8* plants and (b) roots of +*Cre8* plants inoculated with J2-stage *H. avenae* at 21 DAI. (cMX) central metaxylem, arrow indicating cells within the cMX, (white outline) feeding site. Scale bar 100 µm.

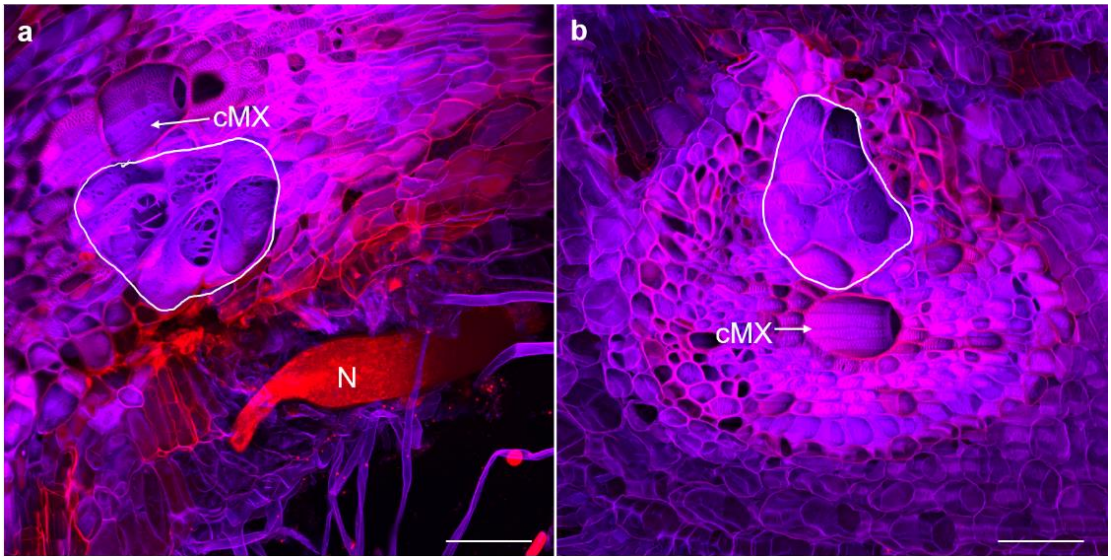

Figure 7-4: Feeding site structure in CCN-infected roots of -*Cre8* and +*Cre8* plants. Maximum projected angled sections of *H. avenae* infected root in a (a) -*Cre8* plant and (b) +*Cre8* plant at 21 DAI. (N) nematode, (cMX) central metaxylem, (white outline) feeding site. Scale bar 100 µm.

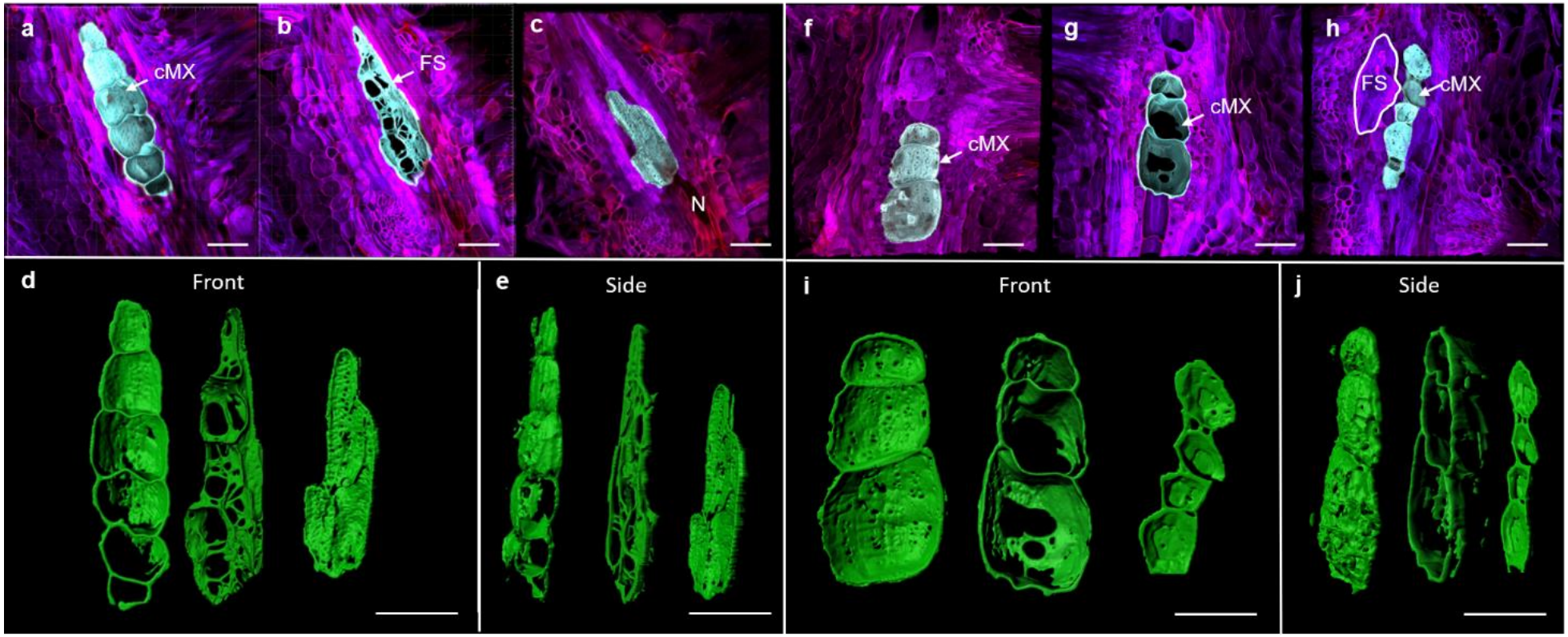

Figure 7-5: Three-dimensional reconstruction of cMX structure within CCN-infected -*Cre8* and +*Cre8* plants. Consecutive sections through the vascular cylinder of *H. avenae* inoculated roots in (a-e) -*Cre8* and (f-j) +*Cre8* at 21 DAI. For each series, three sections were taken for (a-c) -*Cre8* and (f-h) +*Cre8*, and the central metaxylem (cMX) or connected feeding site (FS) were highlighted in blue. From selections, (d-f) -*Cre8* and (i-j) +*Cre8* models (green) were made (Front). Models were rotated to show how they would fit together (Side). Scale bar 100 µm.

Immunolabelling with the antibody BG1 detected (1,3;1,4)-β-glucan in the internal cell walls of feeding sites in 139-S (Fig. 7-6a,b) but not in 139-R (Fig. 7-6c,d). Conversely, in the outer cell walls of feeding sites, more (1,3;1,4)-β-glucan was detected in 139-R than in 139-S. There was no (1,3;1,4)-β-glucan detected within the cMX. Immunolabelling with a callose-specific antibody did not detect callose in the cell walls of cMX or feeding sites in either 139-S (Fig. 7-6e) or 139-R (Fig. 7-6f).

With application of basic fuchsin, lignification of some cell walls was detected. In tissue sampled from inoculated plants of the susceptible line 139-S at 4 and 6 DAI, lignin was detected in the walls of protoxylem cells, peripheral metaxylem (pMX) cells and some additional cells near feeding sites (Fig. 7-7a, b). Further in 139-S at 8 DAI, there was very little lignification of the cMX and direct connections between the cMX and feeding sites in made it appear as though the cMX had been incorporated into the feeding site (Fig. 7-7c,d). In tissue sampled from inoculated plants of the resistant line 139-R at 4 and 6 DAI, lignin was also detected in the walls of protoxylem cells, pMX cells and some additional cells near feeding sites (Fig. 7-7e,f). However, at 8 DAI, extensive staining was observed in the walls of these cell types as well as those of phloem cells and the cMX (Fig. 7-7g,h). In both lines, remnants of internal cell walls were visible within feeding sites, but these seemed more robust in 139-S (e.g. Fig. 7-7c) than in 139-R (e.g. Fig. 7-7g).

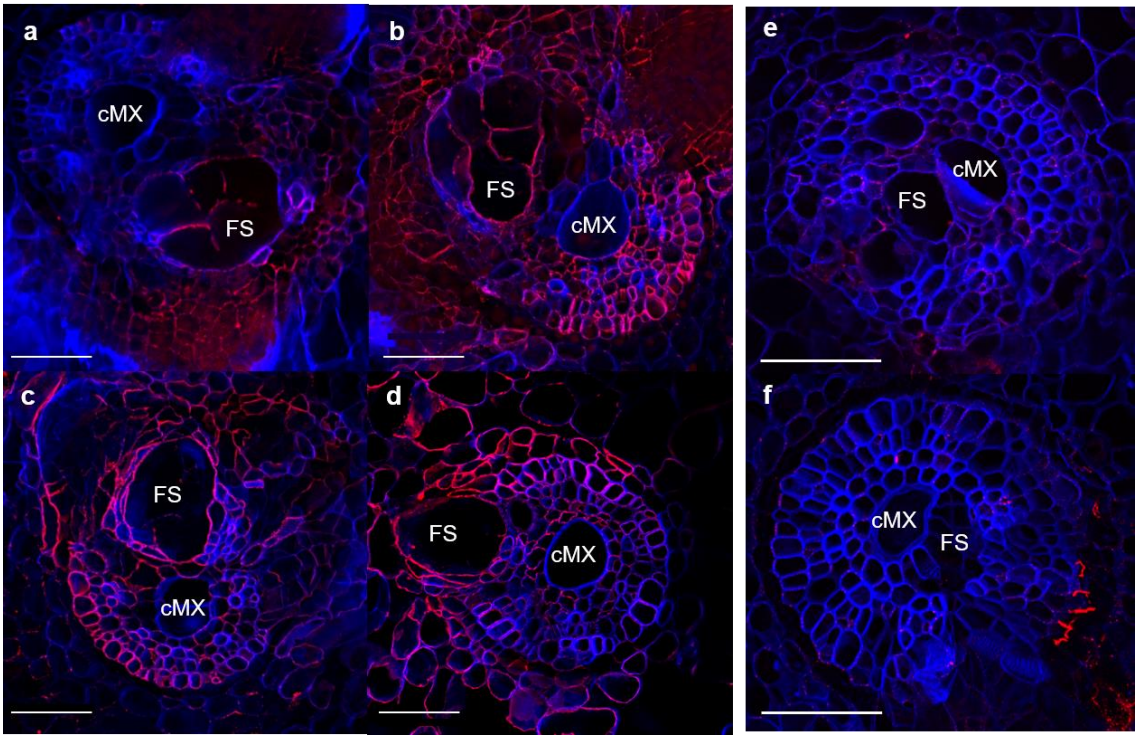

Figure 7-6: Immunohistological analysis of cell wall components at 6 DAI with *H. avenae*. (a-d) (1,3;1,4)-β-glucan and (e-f) callose. Transverse sections of (a-b) -*Cre8* 139-S roots and (c-d) +*Cre8* 139-R roots stained with BG1 antibody (red) and calcofluor white (blue). Transverse sections of (e) resistant +*Cre8* 139-R roots and (f) susceptible -*Cre8* 139-S roots stained with callose antibody (red) and calcofluor white (blue). Scale bar 100 µm.

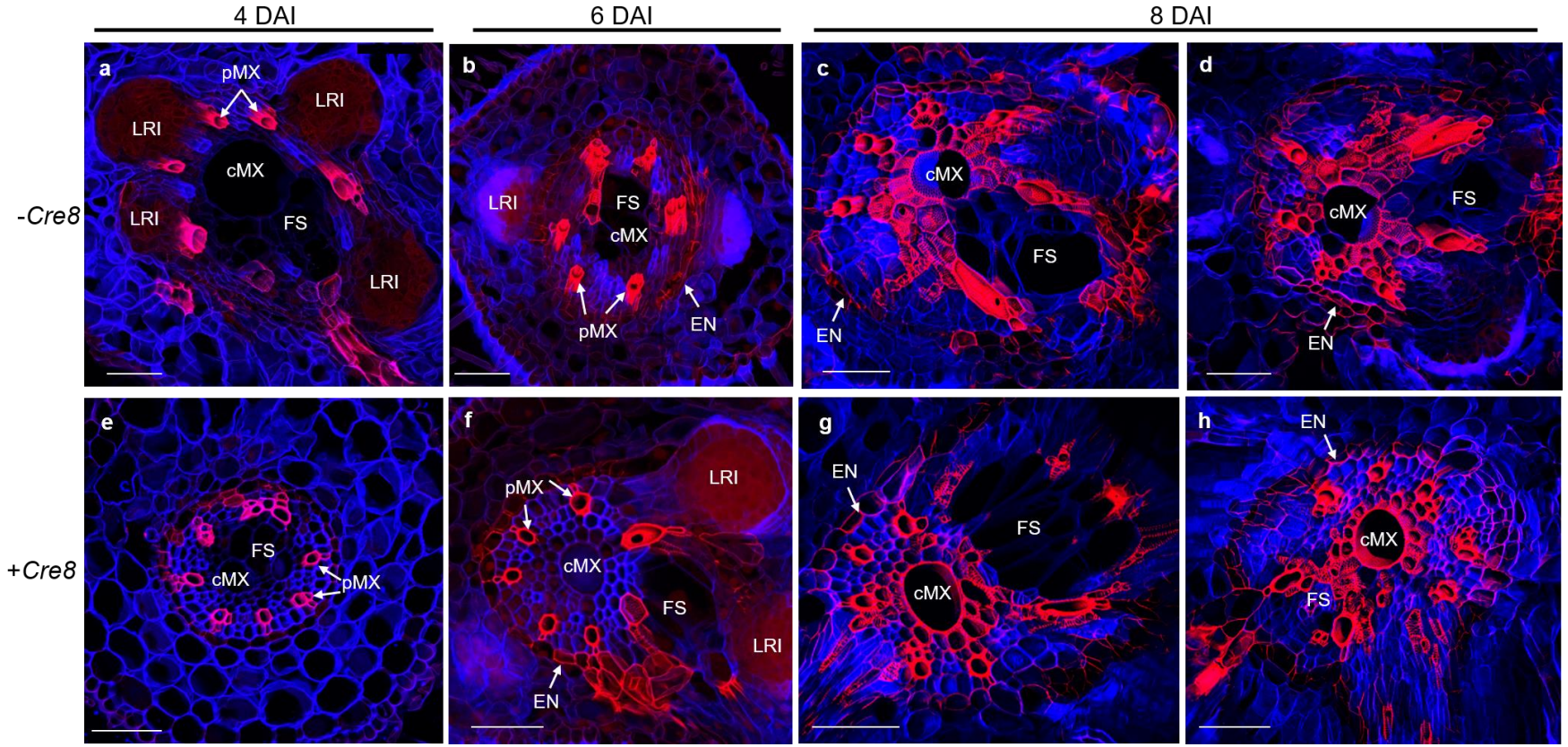

Figure 7-7: **Maximum projected confocal images of lignin staining in CCN-infected wheat roots.** (a-d) Susceptible -*Cre8* line 139-S and (e-h) resistant +*Cre8* line 139-R inoculated roots at 6 DAI with J2-stage *H. avenae*. Basic fuchsin (red), calcofluor white (blue). Central metaxylem (cMX), feeding site (FS), peripheral metaxylem (pMX), lateral root initial (LRI), endodermis (EN). Scale bar 100 µm.

7.5 Discussion

Previous investigations of CCN feeding sites using thin (< 3 µm) sections observed differences in susceptible and resistant plants containing *Cre1* and *Cre3* (Cui *et al.*, 2017; Seah *et al.*, 2000; Williams & Fisher, 1993). By 13 to 15 DAI, feeding sites in resistant plants were smaller than in susceptible plants and contained dense cytoplasm and condensed nuclei. Jayatilake (2014) attempted a similar approach but did not observe any clear differences between +*Cre8* and -*Cre8* materials. In the research reported here, a different approach was taken, using thick (150 µm) transverse and longitudinal sections and a 3D imaging technique. The images obtained in this way revealed differences in (**1**) the distance of feeding sites from the cMX, (**2**) incorporation of cMX cells into feeding sites and (**3**) cell wall structure within syncytia. Further comparisons of cell wall components in infected roots of +*Cre8* and -*Cre8* plants revealed differences in (1,3;1,4)-β-glucan and lignin composition.

The advantage of using thick sections and a clearing agent was an increase in the depth of image capture. This clarified the relative positions of feeding sites and the 3D structure of cell walls. It was revealed that feeding sites induced in roots of +*Cre8* plants developed at a distance from the cMX while feeding sites within roots of -*Cre8* plants developed directly adjacent to the cMX, eventually incorporating these cells. It therefore seems possible that the *Cre8* resistance mechanism involves preventing feeding sites from expanding further through phloem cells and connecting with the cMX. Xylem connections increase the symplast-apoplast interface, increasing water and solute supply for syncytia (Golinowski *et al.*, 1997; Heinrich *et al.*, 1998; Lilley *et al.*, 2005; Sobczak & Golinowski, 2009; Williams & Fisher, 1993). Further, if the feeding sites expand into cMX elements of –*Cre8* plants while those cells are still immature, then cMX cytoplasm may be incorporated into syncytial cytoplasm. This might benefit the parasite, supporting the maturation of more female nematodes in –*Cre8* plants compared to +*Cre8* plants.

It is unknown why syncytia in roots of *+Cre8* plants are unable to successfully form connections with cMX cells. One explanation could be programmed cell death. The *H1* gene in potato, which confers resistance against *G. rostochiensis*, was found to cause necrosis in cells surrounding the syncytia (Gebhardt *et al.*, 1993). It is possible *Cre8* induces a cell death response around the syncytia which stops it from reaching the cMX. This may explain why layers of small cells between the feeding site and cMX were sometimes observed in *+Cre8* host roots. The variability in the position of feeding sites within roots of resistant plants may clarify why some feeding sites are successful in *+Cre8* plants and therefore some cysts are observed on *Cre8*-containing plants in phenotype tests.

The CCN-induced xylem morphology reported in Chapter 4 was observed in both roots of *+Cre8* and *-Cre8* plants but appeared less severe in *+Cre8* plants. Perhaps the structural modification of cMX contributes in some way to successful parasitism. Alternatively, it may be that the extreme structural modification of cMX in susceptible plants is a consequence of the cMX elements becoming connected with feeding sites. It has been reported that there is immense pressure inside feeding sites (Böckenhoff & Grundler, 1994), which may contribute to the expansion of cMX cells in *-Cre8* plants.

The 'web-like' cell walls observed within feeding sites of susceptible plants were similar to the 'Parthenon pillar' cell walls induced by *H. glycines* reported by Ohtsu *et al.* (2017). These pillars, which were observed only in longitudinal sections, may contain more cellulose than normal cell walls and might reinforce the feeding site structure. Although the 'web-like' cell walls observed here are not as uniform as pillars, they may play a similar role.

In cMX model reconstructions, the web-like features were observed directly connected to the cMX in roots of *-Cre8* plants. In contrast, the dense cell walls found in feeding sites of *+Cre8* plants may reflect the inability to not only expand but also transfer nutrients. The lack of feeding site and cMX connection in *+Cre8* feeding sites may be the reason for unsuccessful

female development. It is possible that the inability of feeding sites to expand into cMX is not necessarily due to an impediment (such as cell death), but rather to its inability to break down the cell walls necessary for successful connection.

To better understand these differences, feeding sites were analysed at early stages and selected key cell wall components were examined including (1,3;1,4)-β-glucan, callose and lignin. Previous studies have examined cell wall composition in and around cyst nematode feeding sites (Zhang *et al.*, 2017) and have even identified differences in cell wall compositions between resistant and susceptible plants (Aditya *et al.*, 2015). In the research reported here, feeding sites induced in resistant plants contained (1,3;1,4)-β-glucan in their outer cell walls, but no epitope was detected within the feeding site. In contrast, feeding sites induced in susceptible plants showed some (1,3;1,4)-β-glucan in the outer cell walls of feeding sites and in cell walls within the feeding sites. Internal cell walls that are richer in (1,3;1,4)-β-glucan within susceptible feeding sites may reflect a more successful feeding site since reinforcement of these cell walls within syncytia help maintain structure with its immense turgor pressure (Böckenhoff & Grundler, 1994). However, it is not clear why these walls are absent within early development of feeding sites in resistant plants. One explanation could be that instead of deposition in internal cell walls, (1,3;1,4)-β-glucan is recruited into the outer cell walls of feeding sites, leading to the richer signal observed in these cell walls. Similar to conclusions made by Aditya *et al.* (2015) about CCN-infected barley, an abundance of (1,3;1,4)-β-glucan around cell walls of syncytia within resistant roots could impede nutrient flow into feeding sites.

Consistent with observations made by Sobczak and Golinowski (2009), lignin was not detected in the cell walls of feeding sites. However, lignin was observed in the cMX cell walls, particularly in resistant plants. It is possible that the thick layer of lignin around xylem vessels in roots of *+Cre8* plants acts as a physical barrier that prevents the nematode from accessing cMX cells. Lignin biosynthesis has previously been identified as an early resistance

response to nematode infection (Melillo *et al.*, 1992, 1993) and increased lignin deposition has been identified in CCN-infected wheat containing the resistance gene *Cre2* (Andres *et al.*, 2001). Additionally, the enzymes involved in the production of lignin, class III plant peroxidases, are also involved in synthesis of ROS which activate the hypersensitive response leading to plant cell death (Almagro *et al.*, 2008). Research on class III peroxidase expression in CCN-infected wheat showed certain classes of peroxidases were induced by nematode infection and were highly expressed in cells close to the vascular cylinder (Simonetti *et al.*, 2009). The presence of highly lignified cells within roots of +*Cre8* plants may also be an indication of subsequent cell necrosis.

7.6 Conclusion

Cytological analysis of CCN-infected roots revealed spatial, structural and compositional differences between feeding sites induced in the roots of -*Cre8* and +*Cre8* plants. Feeding sites induced in susceptible -*Cre8* plants were able to develop adjacent to the cMX and to incorporate cMX cells, while feeding sites in roots of +*Cre8* plants were able to develop near cMX but did not incorporate cMX cells. Feeding sites induced in resistant +*Cre8* plants showed clear deposition of (1,3;1,4)-β-glucan around feeding site cell walls, while feeding sites induced in -*Cre8* plants showed less deposition around the feeding site but abundant (1,3;1,4)-β-glucan epitopes in cell walls within the feeding site. Infected roots of +*Cre8* plants also showed more lignin around cMX vessels than in -*Cre8* plants. Although xylem modification occurred in both +*Cre8* and -*Cre8*, the perturbation of cMX was more severe in susceptible -*Cre8* plants.

The research reported in this chapter identifies new insights into possible antibiosis mechanisms by which *Cre8* may reduce feeding site development. This knowledge is useful for support in identification of candidate genes for the resistance against CCN.

Chapter 8 : Genetic analysis of the wheat *Cre8* locus

8.1 Summary

This chapter reports on research to genetically fine-map the region of wheat chromosome 6B that contains the *Cre8* locus. Through an iterative process of marker development, recombinant identification and resistance testing, *Cre8* was fine-mapped to a region of 0.22 cM. On the International Wheat Genome Sequencing Consortium RefSeq 2.0 assembly for chromosome 6B, that region consists of 334 kbp and contains 10 high-confidence gene models. Two of these represent genes that are known to be expressed in roots. One of these genes, TraesCS6B02G466600, which encodes a sucrose synthase (SuSy) was found to have non-synonymous polymorphisms between resistant and susceptible lines. Comparisons with SuSy sequences from other plant species classified the predicted product of this gene as a SUS III sucrose synthase. Initial investigations of protein modelling are described. The work reported in this chapter significantly narrows the candidate region for *Cre8* and identifies a likely candidate gene.

8.2 Introduction

Cre8 was originally mapped using progeny from a cross between the resistant wheat cultivar Molineux and the susceptible cultivar Trident (Williams *et al*., 2003, 2006). Using the same materials and additional molecular markers, Jayatilake *et al.* (2015) improved the linkage map and assigned *Cre8* to an interval of 8.1 cM between markers *wri16* and *BS00022444* . Kumsa (2015) mapped additional markers in this region including *BS00109879* and determined that *Cre8* mapped between *BS00109879* and *BS00022444*. These markers were assigned to the same genetic bin (‘6B 139.160 cM’) on the TGACv1 draft wheat genome assembly. There were 41 predicted genes in that bin. Hendrikse (2016) mapped 12 of these and excluded nine as being outside of the flanking markers. The research reported in this chapter was conducted to continue this work and to further refine estimates of the genetic and physical positions of the *Cre8* region.

Jayatilake *et al.* (2015) reported that none of the markers that were tested in the *Cre8* region detected polymorphisms between Chinese Spring and the resistant parent Molineux. Kumsa (2015) therefore investigated whether Chinese Spring might carry the resistance allele at *Cre8*. His results showed Chinese Spring to be more resistant than nullisomic-tetrasomic genetic stocks lacking chromosome 6B, more resistant than terminal deletion stocks lacking the terminal region of the 6BL chromosome arm and not as resistant as nullisomic-tetrasomic genetic stocks with four copies of chromosome 6B. Based on all of these results, it seems likely that Chinese Spring (the reference cultivar for wheat genome sequencing) carries the *Cre8* resistance allele.

During the course of this PhD research, the International Wheat Genome Sequencing Consortium (IWGSC) released genome assemblies RefSeq v1.0 (Appels *et al.*, 2018) and RefSeq v2.0 (https://urgi.versailles.inra.fr/download/iwgsc/IWGSC_RefSeq_Assemblies/v2.0/) for Chinese Spring wheat. These presented new opportunities for discovery of sequence polymorphisms and identification of candidate genes.

8.3 Materials and methods

8.3.1 Plant materials

The wheat materials used include: the susceptible cultivars Trident and Spear; the moderately resistant cultivars Molineux, Barunga, Buckley, Correll, Festiguay, Frame, Stylet and Yitpi, all of which carry the *Cre8* resistance allele; wheat materials derived from a cross between the Trident/Molineux DH lines TMDH6 and TMDH82; Chinese Spring and six nullisomic-tetrasomic genetic stocks derived from Chinese Spring (Sears et al., 1954). Each nullisomic-tetrasomic line is nullisomic for one group-6 chromosome and tetrasomic for another group-6 chromosome: nullisomic 6A tetrasomic 6D (N6AT6D), nullisomic 6D tetrasomic 6A (N6DT6A), nullisomic 6B tetrasomic 6A (N6BT6A), nullisomic 6B tetrasomic 6D

(N6BT6D), nullisomic 6D tetrasomic 6B (N6DT6B) and nullisomic 6A tetrasomic 6B (N6AT6B).

The DH lines, TMDH6 and TMDH82 were selected by Jayatilake (2014): TMDH6 as a resistant parent with Molineux alleles throughout chromosome 6B and TMDH82 as a susceptible parent, with Trident alleles throughout chromosome 6B. Neither TMDH6 nor TMDH82 carries resistance alleles at either of two other CCN resistance loci that had been mapped using the Trident/Molineux population (*QCre.srd-1B* on chromosome 1B and *Cre5* on chromosome 2A) (Williams *et al.*, 2006).

At the outset of this research, 768 TMDH6/TMDH82 F_4 seeds were available. These had been harvested from 122 F_3 plants that Hendrikse (2016) had confirmed to be heterozygous in the *Cre8* region. Each F_4 seed was manually dissected into two parts, with one part including the embryo and the other part consisting mostly of endosperm tissue. DNA was extracted from the endosperm portion according to protocols described by Van Gansbeke *et al.* (2019). The DNA samples were tested with Kompetitive Allele Specific PCR (KASP^{TM}) (LGC Genomics Limited, Hoddlesdon, UK) assays *wri16* and *BS0022444* (Jayatilake et al. 2015). Based on this genotyping, 208 F_4 heterozygous seeds were selected, and embryo portions of those seeds were germinated to provide heterozygous F_4 plants. Those plants were grown to maturity, providing 3,696 TMDH6/TMDH82 F_5 seeds.

Additionally, based on genotyping, homozygous recombinant F_4 seeds were identified and were used for evaluating resistance against CCN. These seeds were germinated and used in a 'tube test' (see section 8.2.5 below). To confirm the genotypes of plants tested, leaf tissue was sampled from TMDH82/TMDH6 F_4 plants and freeze-dried, then DNA was extracted using an SDS-based method according to protocols described by Van Gansbeke *et al.* (2019) and tested with the *wri15* KASP assay (Jayatilake et al. 2015).

A similar approach was used in subsequent generations, providing F_6 seeds from heterozygous F_5 plants and F_8 seeds from heterozygous F_7 plants. In each generation, progeny were genotyped at markers that flank *Cre8* (initially *wri16* and *BS0022444* from Jayatilake *et al.* (2015) but later at markers that were discovered during the research) to allow for identification of both heterozygotes and recombinants. This genotyping was conducted using DNA extracted from endosperm tissue and was confirmed using DNA extracted from leaf tissue.

8.3.2 Polymorphism discovery, marker assay development and marker genotyping

To identify an initial candidate region on chromosome 6B, previously mapped markers (Jayatilake *et al.*, 2015) were anchored to the International Wheat Genome Sequencing Consortium (IWGSC) RefSeq 1.0 gene assembly for Chinese Spring (https://wheat-urgi.versailles.inra.fr). To resolve discrepancies between the genetic order of polymorphic loci and the order of corresponding sequences in the IWGSC RefSeq V1.0 Chinese Spring reference genome assembly, additional sources of genomic sequence were considered. These included genome assemblies from the 10+Genome Project (http://www.10wheatgenomes.com) for nine wheat cultivars (Arina, Jagger, Julius, CDC Stanley, SY Mattis, Lancer, CDC Landmark, Mace, and Norin 61). Once the IWGSC RefSeq 2.0 gene assembly for Chinese Spring (https://wheat-urgi.versailles.inra.fr) became available, it was used as the reference assembly. All IWGSC high-confidence (HC) predicted genes (from all chromosomes) were used as queries in a BLASTn search (NCBI) against the candidate region. For each predicted gene for which the alignment match was ≥ 95%, homoeologues on chromosome 6A and 6D were identified and their sequences were aligned with the sequence of the predicted gene on chromosome 6B. Pairs of 6B-specific primers were designed using the software Geneious 10 (Biomatters Ltd., New Zealand) and used to amplify products from Chinese Spring, TMDH6, TMDH82, and the group-6 nullisomic-tetrasomic lines. PCR products were gel-extracted, Sanger-sequenced (performed by AGRF,

www.agrf.org.au), and aligned to identify 6B-specific single-nucleotide polymorphisms (SNPs) and insertion-deletion (INDEL) polymorphisms between TMDH6 and TMDH82.

In addition, DNA was extracted from leaf tissue sampled from plants of Molineux, Trident, Barunga, Buckley, Correll, Festiguay, Frame, Spear, Yitpi, TMDH006, TMDH082 and 43 F_5 TMDH6/TMDH82 lines using a phenol-chloroform method (Rogowsky et al. 1991), with modifications as described by Pallotta et al. (2000). These DNA samples were sent to Diversity Arrays Technology (Bruce, ACT, Australia) for analysis using its DArTseq GBS platform. All tag sequences reported by Diversity Arrays Technology as including SNPs were used in a BLASTn analysis (Altschul et al. 1990) against the 6B pseudomolecule of the wheat reference genome. Tags with a BLAST hit alignment (minimum e-value = 1e−5) were selected. Among these, tag pairs that differentiated CCN-resistant TMDH6/TMDH82 lines from CCN-susceptible TMDH6/TMDH82 lines were selected.

For selected polymorphisms that were discovered based on amplicon sequencing or on analysis of GBS data, primer sets for KASP assays were designed using Kraken™ software (LGC Genomics Limited, Hoddlesdon, UK). The KASP assays were applied to TMDH6/TMDH82 progeny and the SNPs and INDELs were genetically ordered and the genetic distances between adjacent markers were estimated based on observed recombination frequencies.

8.3.3 Inoculum preparation

Inoculum of cereal cyst nematode (*Heterodera avenae* Woll., pathotype Ha13) was prepared as described by Van Gansbeke *et al.* (2019). Cysts originated from infected soil collected at Winulta and South Kilkerran on the Yorke Peninsula in South Australia. A mixture of cysts and other organic matter was placed into synthetic silk bags and incubated in water at 5°C in darkness. One day prior to the collection of juvenile nematodes, the water was replaced, to remove nematodes that had already hatched. On the following day, freshly hatched J2

nematodes were harvested by passing the water through a 38 µm sieve. Inoculum was prepared by diluting juvenile nematodes to a concentration of 100 J2-stage nematodes/mL.

8.3.4 Evaluation of resistance against cereal cyst nematode

A 'tube test' method (O'Brien & Fisher, 1977) was used to evaluate resistance of wheat against CCN, following the protocol described by Van Gansbeke *et al.* (2019). In short, pre-germinated seeds were sown in a tube (2.5 cm wide x 13 cm deep) filled with sandy loam soil and kept in a controlled environment room (15°C with 12 h light/dark cycle). To inoculate, 1 mL of nematode inoculum was pipetted onto the soil surface at 1, 4, 7, 11, and 14 d after sowing. At 74 d after sowing, soil was washed off roots and *H. avenae* white cysts were counted.

8.3.5 Transcript analysis

Seeds of the sister lines 139R and 139S were surface sterilised then germinated on sterile 2% agar plates for 3 d in darkness at 15˚C in a controlled environment room. After 3 d, when roots were approximately 2-4 cm in length, root tips were inoculated with approximately 50 freshly hatched J2-stage nematodes. For control plants, root tips were mock-inoculated with water. Plants were kept on agar for 24 h then roots were washed with water and transplanted into a hydroponic system containing Johnson's modified nutrient solution as described by Melino *et al.* (2015). Plants were kept in a controlled environment room at 15°C with 12 h light/dark cycle.

Root tissue segments (2-4 mm in length) were collected at 2, 4, 6, and 8 DAI. These segments were taken from the visibly swollen regions of the roots of inoculated plants and from similar positions in the roots of control plants. At each time point, six plants were harvested for each treatment (control and inoculated) of each sister line (139-R and 139-S). Excised regions from three plants were pooled into one tube for a total of two tubes per treatment per line. RNA was extracted using a Sigma Total RNA Kit and cDNA was synthesised using a Sigma First

Strand cDNA Synthesis Kit. Q-PCR analysis and data normalisation were performed as described by Burton *et al*. (2008) using housekeeping genes TaCyclo, TaActin, and TaEFA.

8.3.6 Phylogenetic analysis, sequence comparison and protein modelling

Sequences for *T. aestivum* were taken from EnsemblPlants (https://plants.ensembl.org) by searching for all 'sucrose synthase' genes. Sequences for *Arabidopsis*, rice, barley and a gymnosperm outgroup sequence (PAB00010305) were obtained from supplementary materials of Stein and Granot (2019). A phylogenetic tree was generated using Geneious 10 using the Jukes-Cantor genetic distance model and the neighbour-joining method. To investigate conserved regions, all 138 sequences from Stein and Granot (2019) and 21 *T. aestivum* sequences were aligned using MUSCLE with default options and analysed in Geneious 10. To enable comparison of the predicted product of TraesCS6B02G466600 with the characterised crystalline structure of AtSUS1 (Zheng *et al.*, 2011), a consensus alignment was made using Geneious 10. Predicted protein models were made using SWISS-MODEL (https://swissmodel.expasy.org) (Waterhouse *et al.*, 2018).

8.4 Results

8.4.1 Fine mapping of *Cre8*

Primer design based on sequences of GBS tags and on sequences of amplicons from IWGSC-predicted genes led to the development of 85 KASP marker assays (Appendix 2) of which 18 were between the markers *wri16* and *BS0022444*. At all 85 of these, Molineux exhibited the same allele as Chinese Spring. Based on marker genotyping and recombination frequencies observed in self-pollinated progeny of confirmed heterozygous non-recombinant plants, a genetic map was established for 23 markers in a 2.99-cM region that contains *Cre8* (Fig. 8-1a).

Based on marker genotyping and resistance testing of 535 homozygous recombinant TMDH006/TMDH082 progeny plants (51 F_3, 105 F_4, 132 F_5, 96 F_6, 131 F_7, and 20 F_8), *Cre8*

was determined to co-segregate with markers *wri434*, *wri433*, *wri410* and *wri427* which map within a 0.22 cM interval between *wri392* and a cluster of four co-segregating markers (*wri414*, *wri400*, *wri438* and *wri412*) (Fig. 8-1b).

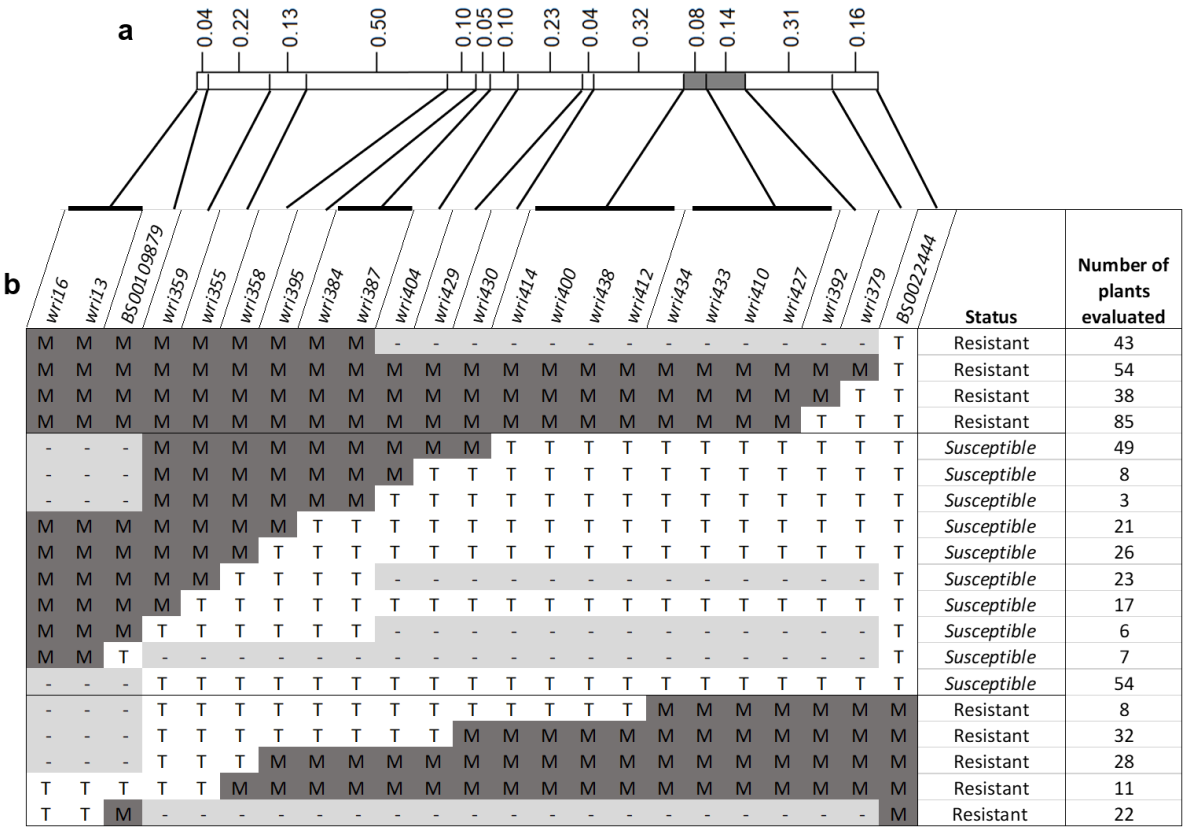

Figure 8-1: Fine-mapping of *Cre8*. (a) Genetic linkage map of a region of chromosome 6B, showing interval lengths (in cM) deduced from observed recombination frequencies among TMDH6/TMDH82 progeny plants. The region containing *Cre8* is shaded in grey. (b) Resistance status (resistant or susceptible) for each of 19 recombinant haplotypes involving marker alleles from Trident (T, susceptible) and Molineux (M, resistant), based on the results of tube tests (Appendix 3). Unknown marker genotypes are indicated by '-'.

8.4.2 Candidate gene investigation

The markers that flanked or co-segregated with *Cre8* were all anchored to one continuous 703,509 bp contig in the IWGSC V2.0 reference genome in the order *wri414-wri400-wri438-wri412-wri434-wri433-wri410-wri427-wri392*, defining the 334,253 bp region between *wri412* and *wri392* as the candidate region for *Cre8*. This region of the reference assembly

contained 10 IWGSC high-confidence (HC) predicted genes (Fig. 8-2). Two of these (TraesCSU01G071800 and TraesCS7B01G497000) appeared twice within the region of interest as direct sequence duplications at two different locations (Fig. 8-2). Each of the four markers that cosegregated with *Cre8* had been designed for a SNP within one of the 10 genes: *wri434* within TraesCSU01G071800, *wri433* within TraesCS7B01G497000, *wri427* within TraesCS6B02G466600, and *wri392* within TraesCS6B02G466700. According to information in the WheatExp database (Pearce *et al.*, 2015), two of the 10 predicted genes (TraesCS6B02G466400 and TraesCS6B02G466600) are expressed in root tissue at Zadoks stages Z10, Z13 and Z39 (Zadoks *et al.*, 1974). According to information in the BARLEX database (Colmsee *et al.*, 2015), the barley orthologues of these two genes (HORVU6Hr1G094910 and HORVU6Hr1G094880, respectively) are also expressed in root tissue.

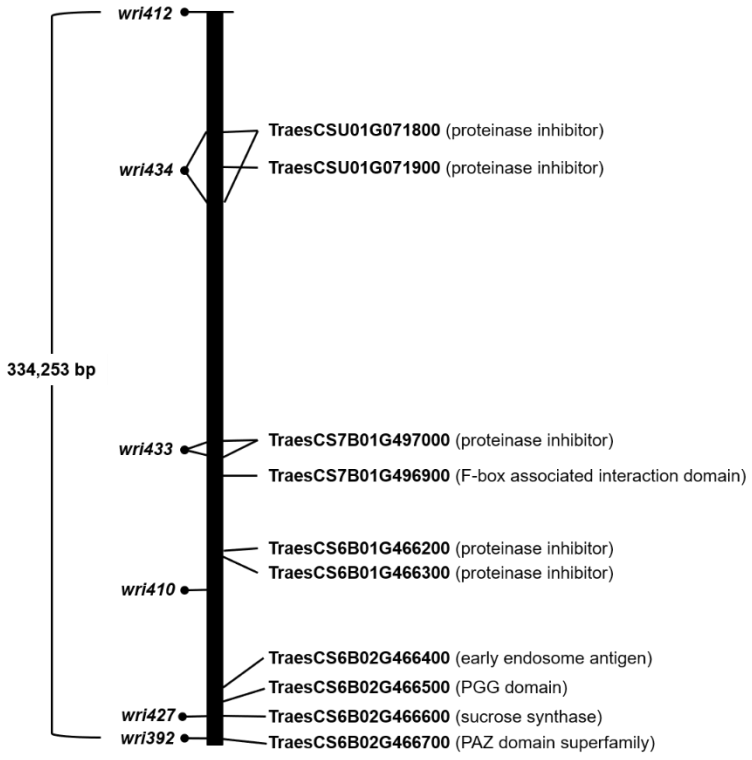

Figure 8-2: IWGSC high-confidence genes within a region of the IWGSC RefSeq v2.0 assembly that was identified as the candidate region for *Cre8*. Marker positions annotated on the left, gene names in bold on the right and annotations from EnsemblPlants in parentheses.

Sequencing of the TMDH6 and TMDH82 alleles of TraesCS6B02G466400 and TraesCS6B02G466600 revealed polymorphisms in TraesCS6B02G466600 but not in TraesCS6B02G466400. Five non-synonymous SNPs were detected in TraesCS6B02G466600 (sequences in Appendix 4). These would cause amino acid substitutions at positions 61, 66, 116, 247 and 511 of the predicted gene product (a sucrose synthase). At each of these positions, the amino acid residue predicted for the susceptible line TMDH82 was the same as that predicted for each of nine wheat cultivars for which TraesCS6B02G466600 was sequenced by the 10+Genome Project (Fig. 8-3), while the amino acid residue predicted for the resistant line TMDH6 was predicted only for TMDH6 and Chinese Spring.

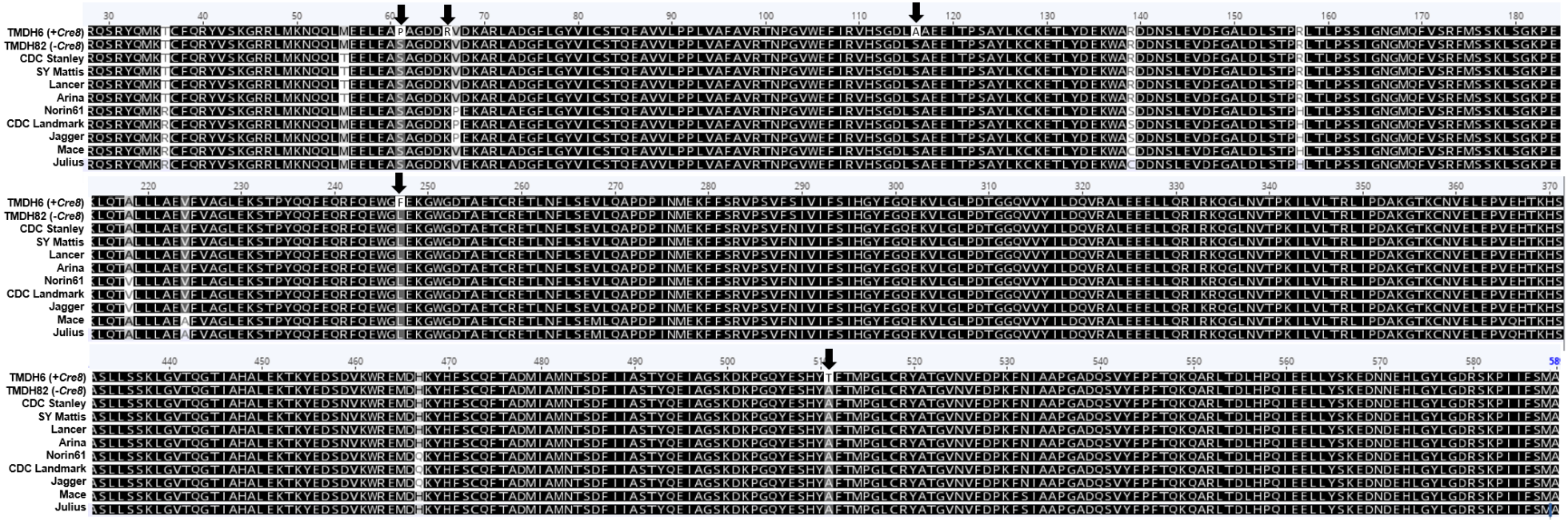

Figure 8-3: Amino acid alignment of SuSy in wheat. Partial alignment of TraesCS6B02G466600 from TMDH6 and TMDH82 and nine orthologues from the 10+Genome Project including CDC Stanley, SY Mattis, Lancer, Arina, Norin 61, CDC Landmark, Jagger, Mace and Julius. Black arrows highlight the five amino acid residues that differed between TMDH6 and TMDH82.

A phylogenetic tree of all 'sucrose synthase' annotated proteins in wheat and known SuSy in *Arabidopsis*, barley, *Brachypodium*, rice, sorghum and maize showed that there are wheat sucrose synthases within each of the three previously identified clades, SUS I, SUS II and SUS III (Stein and Granot (2019)) (Fig. 8-4). The predicted product of candidate gene TraesCS6B02G466600 is within the SUS III clade along with those of its two homoeologues (TraesCSU02G082000 and TraesCS6D02G403800) and those of two other homoeologous sets of three genes. The products of TraesCS6B02G466600 and its homoeologues clustered with rice (*Oryza sativa* L.) OsSUS6 (Fig. 8-4), while those of the other two sets of genes clustered with rice OsSUS5.

Investigation of the positions at which amino acid residues differ between *Cre8* and non-*Cre8* materials (positions 61, 66, 116, 247 and 511) indicated that the residues present in non-*Cre8* materials are largely conserved across other members of the SUS III clade. At these positions, the predicted products for Molineux, other *Cre8* materials and Chinese Spring have a unique series of residues (Pro-61, Arg-66, Ala-116, Phe-247, Thr-511) that was not found in the predicted product of any other gene or allele. The Thr-511 residue was particularly rare. It was present in only one of the other sequences examined (HbSUS6 from para rubber (*Hevea brasiliensis*), while Ala-511 was present in 127 of 133 sequences.

Alignment with AtSUS1 (Zheng *et al.*, 2011) showed that positions 61, 66, 247 and 511 in TraesCS6B02G466600 correspond with the positions of Leu-56, Arg-61, Val-108, Leu-238 and Arg-501 in AtSUS1. The first three of these residues are within the N-terminal regulatory domain of AtSUS1 (Fig. 8-5). The fourth residue is within the Endo40 peptide-binding domain (EPBD), and the fifth is within the GT-B-glycosyltransferase domain. Among these positions, there was only one at which the amino acid residue in the TraesCS6B02G466600 product (Arg-66) was the same as that in AtSUS1 (Arg-61) (Fig. 8-5).

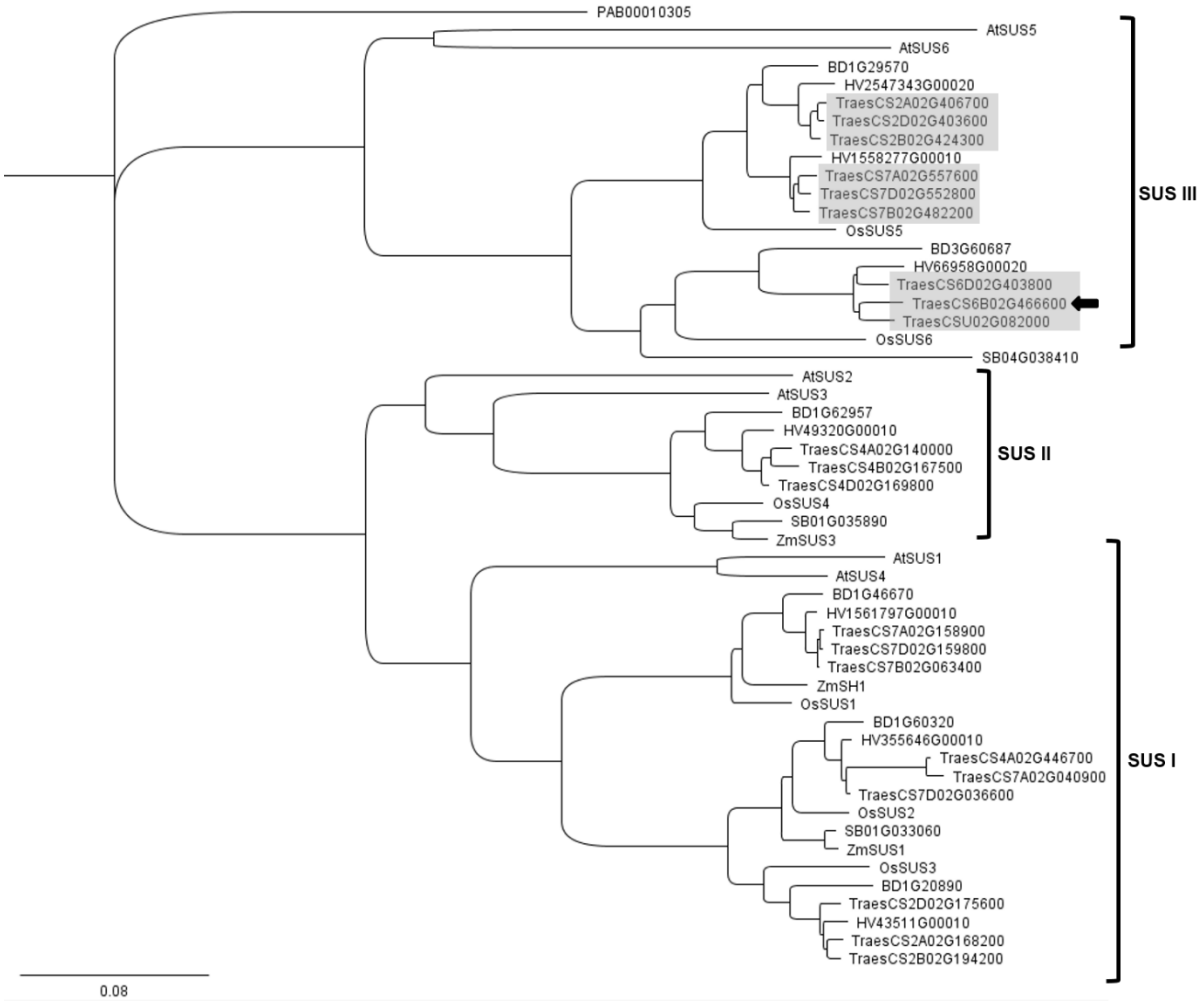

Figure 8-4: Phylogenetic comparison of selected sucrose synthases. Phylogenetic tree of SuSy amino acid sequences from wheat (*Triticum aestivum*, 'Traes'; EnsemblPlants), Arabidopsis (*Arabidopsis thaliana*), barley (*Hordeum vulgare*), *Brachypodium distachyon*, rice (*Oryza sativa*), *Sorghum bicolor*, maize (*Zea mays*). Wheat sequences were obtained from EnsemblPlants. Other sequences were obtained from Stein *et al*. (2019). A black arrow indicates the predicted product of the candidate gene, TraesCS6B02G466600. Grey boxes highlight nine predicted wheat SUS III proteins.

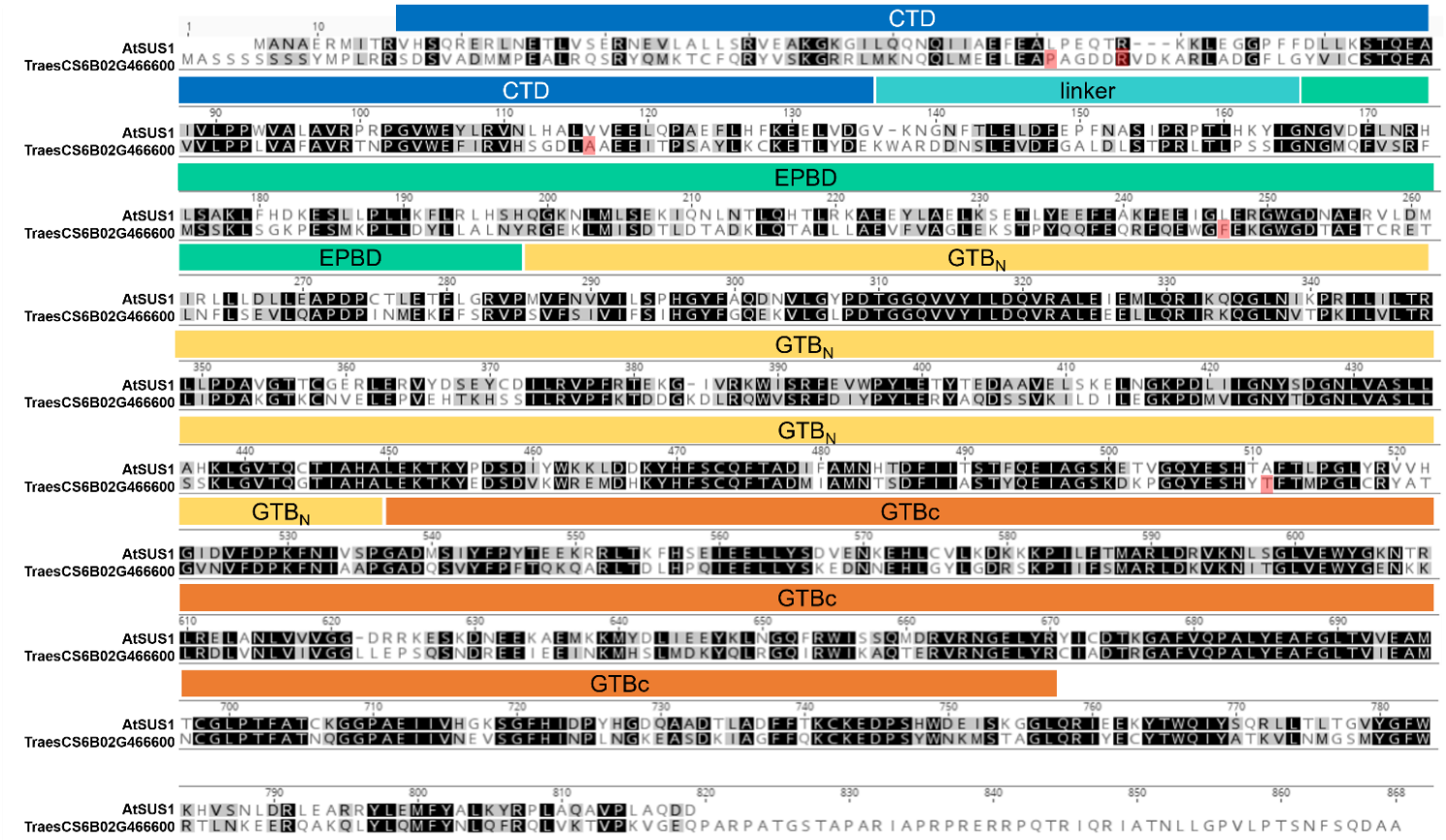

Figure 8-5: Alignment of a candidate wheat sucrose synthase with AtSUS1. Alignment of the TraesCS6B02G466600 protein sequence with the AtSUS1 sequence, annotated with AtSUS1 domains (Zheng et al 2011). Background shading indicates whether the two proteins have identical (black), similar (grey) or dissimilar (white) amino acid residues. Positions at which non-*Cre8* materials have amino acid substitutions are highlighted in red. (CTD) cellular targeting domain, (EPBD) Endo40 peptide-binding domain, (GTB_N) GT-B glycosyltransferase N-terminal, (GTB_C) GT-B glycosyltransferase C-terminal.

To investigate whether the amino acid substitutions are likely to affect SuSy protein structure or function, the AtSUS1 model (Fig. 8-6a) was used as a template in SWISS-MODEL to model the *Cre8* and non-*Cre8* TraesCS6B02G466600 proteins (Fig. 8-6b and c) and the *Arabidopsis* SUS III proteins AtSUS5 (AT5G37180) (Fig. 8-6d) and AtSUS6 (AT1G73370) (Fig. 8-6e). While no major differences were observed among the models (Fig. 8-6a-e), there is a minor difference between the *Cre8* and non-*Cre8* models in the region containing residue 66 (Fig. 8-6f). This part of the protein extends outward in the *Cre8* model but folds inwards the non-*Cre8* model. Comparisons at the other substitution positions (61, 116, 247 and 511) did not reveal any obvious structural differences (Fig. 8-6f).

Q-PCR analysis of root tissue sampled from CCN-inoculated and mock-inoculated wheat plants showed that the transcript levels for both TraesCS6B02G466400 and TraesCS6B02G466600 were much lower than those of the housekeeping gene *TaCyclo* (Fig. 8-7). At 2 DAI, TraesCS6B02G466400 transcripts were more abundant in 139-S than in 139-R (especially in CCN-inoculated plants), while TraesCS6B02G466600 transcripts were more abundant in mock-inoculated roots than in CCN-inoculated roots. At 4, 6 and 8 DAI, both TraesCS6B02G466400 and TraesCS6B02G466600 transcripts showed similar levels in control and inoculated roots (Fig. 8-7).

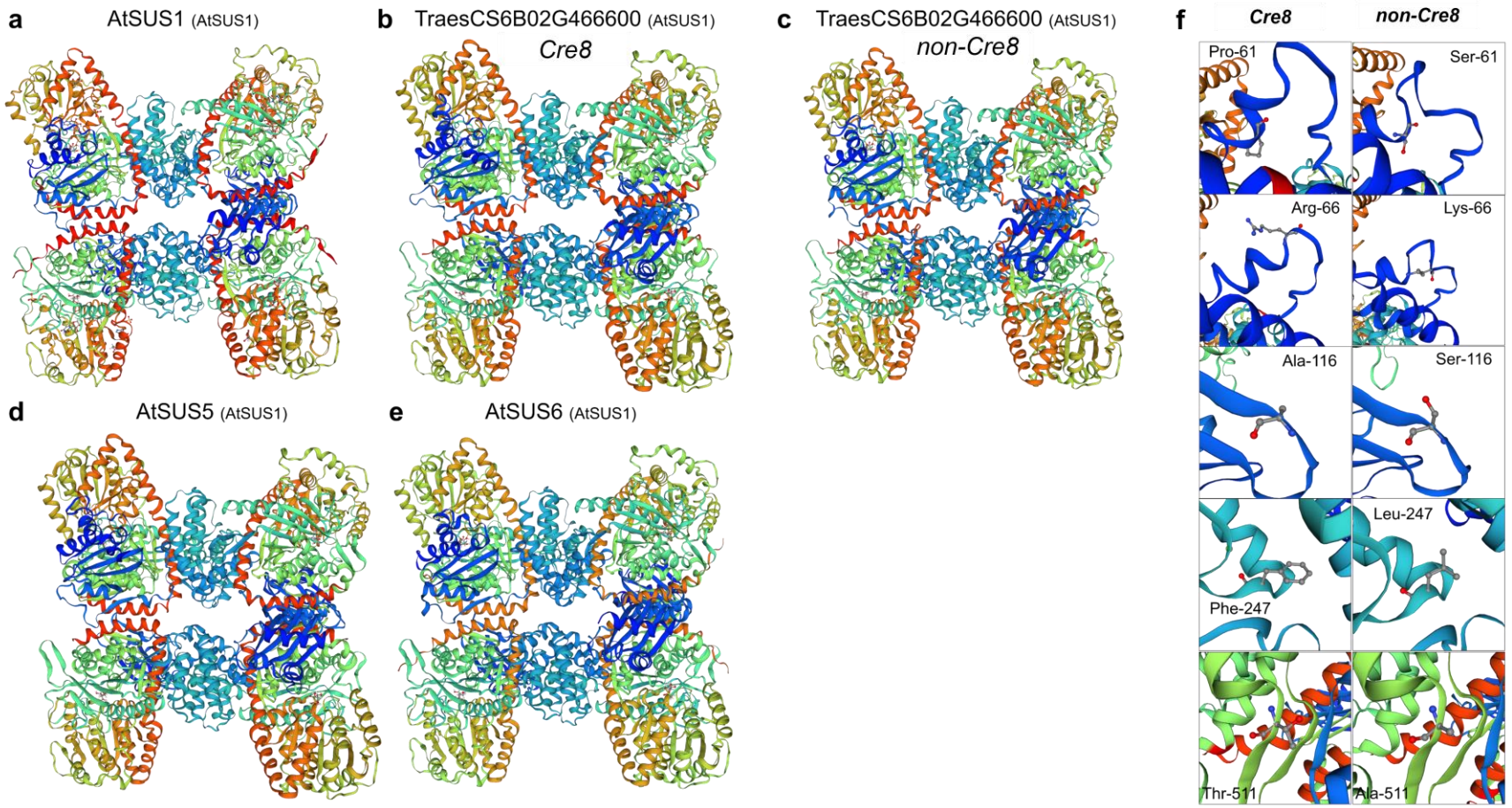

Figure 8-6: Protein models obtained using SWISS-MODEL with the AtSUS1 3s27 model as a template. a) AtSUS1 b) TraesCS6B02G466600 (Chinese Spring and *Cre8* materials) c) TraesCS6B02G466600 (non-*Cre8* materials) d) AtSUS5 and e) AtSUS6. f) Regions of TraesCS6B02G466600 proteins in the *Cre8* and non-*Cre8* proteins which differed in amino acid residues.

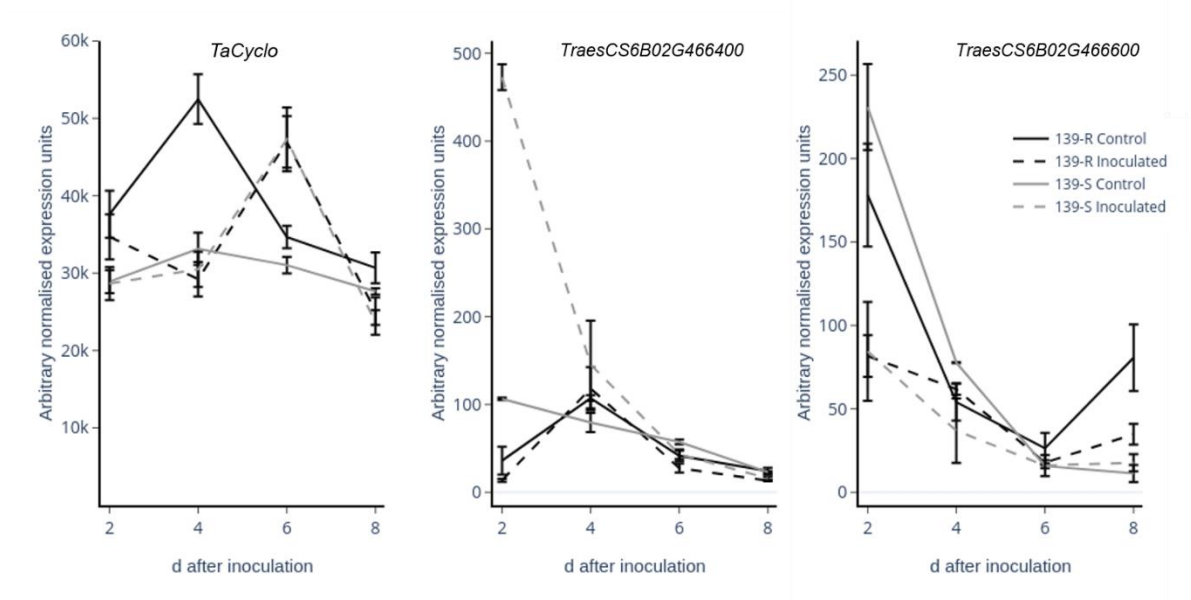

Figure 8-7: Transcript analysis of selected candidate genes. Gene expression in wheat roots from 2 to 8 DAI with *H. avenae* or water for mock-inoculation (control). Mean and standard error of relative quantity of transcript abundance of a housekeeping gene, TaCyclo, and selected candidate genes, TraesCS6B02G466400 and TraesCS6B02G466600.

8.5 Discussion

Fine-mapping of the *Cre8* locus for CCN resistance required identification of new progeny with recombinant haplotypes and phenotyping of those progeny for resistance. This work was facilitated using the Chinese Spring reference genome, which can be expected to include the *Cre8* resistance allele, to develop new molecular markers within the candidate region. As additional markers were developed, discrepancies were noticed between the genetic order of markers and the physical order of corresponding sequences in the IWGSC Ref Seq 1.0 reference genome. Once genome sequences became available for other cultivars of wheat, it was determined that some of these matched the predicted genetic order. With the release of IWGSC RefSeq 2.0 of Chinese Spring, the discrepancies were resolved. In that genome sequence assembly, all of the markers that were found to co-segregate with or flank *Cre8*

were located on one contig, with no discrepancies between genetic order and physical order. This narrowed the region of interest to 334 kbp between markers *wri412* and *wri392.* Ten high confidence genes were predicted within the region. Two of these, TraesCS6B02G466400 and TraesCS6B02G466600, had previously been shown to be expressed in roots. With Q-PCR, both of these genes were found to be expressed at low levels in root tissue of inoculated and control plants of *+Cre8* and *-Cre8* sister lines. Some differences in transcript abundance were observed between treatments, mainly at 2 DAI. While such early differences may reflect differential responses to infection, they are not likely to fully explain differences in resistance, given that CCN is able to form syncytia even in *+Cre8* plants. Another possibility is that the gene of interest is only induced during CCN infection and therefore the other candidate genes may be considered, however, since the gene must be present in root tissue, this research focuses only on genes known to be expressed in roots.

While TraesCS6B02G466400 has not been fully analysed, its predicted protein product has been assigned to 'early endosome antigen' subfamily PTHR35689:SF1 by PANTHER (www.pantherdb.org). None of the proteins in this subfamily have been analysed in any detail, but other early endosome antigens (EEAs) are known to function in the endocytic pathway, receiving material from the plasma membrane and either recycling the material or tagging it for degradation (Craddock & Yang, 2012; Geldner & Jurgens, 2006). If the product of TraesCS6B02G466400 has a similar function, perhaps it is involved in trafficking or processing molecules involved in plant-nematode interactions. Although TraesCS6B02G466400 cannot be excluded as a candidate gene for *Cre8*, it would be a difficult one to investigate given its low level of expression, the current lack of knowledge about its putative product and the lack of sequence polymorphisms between *Cre8* and non-*Cre8* alleles.

In contrast, TraesCS6B02G46660, which belongs to the well-known sucrose synthase gene family, exhibits non-synonymous polymorphisms between *Cre8* and non-*Cre8* materials.

Sucrose synthases catalyse the breakdown of sucrose into fructose and uridine diphosphate glucose (UDP-G) or adenosine diphosphate glucose (ADP-G). These products are key substrates for synthesis of polysaccharides, including cellulose, callose, lignin and starch. There are several SUS isoforms in plants which exhibit various spatial expression patterns and serve different roles in plant development (Angeles-Nunez & Tiessen, 2010). Changes in SUS expression or function can alter sugar processing and signalling (Bolouri Moghaddam & Van den Ende, 2012) and have been reported to affect cyst nematode development (Cabello *et al.*, 2014; Hofmann & Grundler, 2007). In some double mutants of Arabidopsis (*Atsus1*/*Atsus4* and *Atsus5*/*Atsus6*), infection by *H. schachtii* was enhanced relative to what was observed in wild-type plants with functional copies of these genes (Cabello *et al.*, 2014). Further, infection of Arabidopsis by *H. schactii* significantly affected expression levels of *AtSUS1*, *AtSUS4* and *AtSUS6* (Cabello et al. 2014).

In wheat, TaSus1 genes (*TaSus1-7A*, *TaSus1-7B*) and TaSus2 genes (*TaSus2-2A*, *TaSus2-2B*) are known to encode sucrose synthases that affect starch accumulation in developing grains (Hou *et al.*, 2014), but other members of the sucrose synthase gene family have not been studied in detail. Here, phylogenetic analysis indicated that the closest characterised orthologue of TraesCS6B02G466600 is the rice gene Os02g0831500 (known as OsSUS6), which encodes a SUS III sucrose synthase. The specific roles of SUS III enzymes are still not clear, but the *Arabidopsis* SUS III enzymes *AtSUS5* and *AtSUS6* have been reported to be phloem specific (Barratt *et al.*, 2009). Expression levels of TraesCS6B02G466600 did not differ significantly between inoculated and mock-inoculated (control) tissues, but this does not exclude the possibility of cell-specific or tissue-specific expression differences within specific parts of the sampled tissue. Five non-synonymous polymorphisms were identified between the TraesCS6B02G466600 alleles of the resistant (*Cre8*) and susceptible parents. At the positions affected by these differences, the amino acid residues predicted for the susceptible parent are conserved across the nine cultivars for which pangenome sequences are

available and across all other predicted SUS III proteins in wheat. It is not known whether any of these amino acid substitutions affect protein localisation or function.

Alignment with AtSUS1 showed that none of the substitution positions are within critical binding sites that have been identified in AtSUS1 (Zheng *et al.*, 2011). However, three of them are within the N-terminal regulatory domain, which influences cellular targeting. Protein modelling was performed for the predicted products of the TraesCS6B02G466600 alleles using AtSUS1 as a template. Since AtSUS1 is within the SUS I clade and TraesCS6B02G466600 is within the SUS III clade, models were also generated for *Arabidopsis* SUS III proteins AtSUS5 and AtSUS6. Despite differences in the lengths of these proteins (808 amino acids in AtSUS1 and between 837 and 942 amino acids in the SUS III proteins) the overall structure of each SUS III protein was quite similar, with sequence identities between 55-61%, to that of AtSUS1.

Comparison of the *Cre8* and non-*Cre8* TraesCS6B02G466600 models revealed a structural difference in the region containing residue 66, which extends outward in the *Cre8* model but folds inward in the non-*Cre8* model. Given that this region is on the surface of the protein and is within the N-terminal regulatory domain, it is possible that this change could affect localisation of the protein. Another factor that can affect the localisation of proteins is phosphorylation of serine residues in the N-terminal regulatory domains, and this has been reported for SUS1 proteins in maize (Ser-170, (Hardin *et al.*, 2004) and *Arabidopsis* (Ser-167, (Zheng *et al.*, 2011). This phosphorylation has been reported to enhance SUS turnover in maize (Hardin & Huber, 2004). If phosphorylation of the serines at residues 61 and 116 of the non-*Cre8* TraesCS6B02G466600 protein helps determine its cellular localisation, substitutions by proline (position 61) and alanine (position 116) in the *Cre8*-containing TraesCS6B02G466600 protein might alter its localisation. This might in turn affect protein function and/or the fate of reaction products.

At position 247, a conserved leucine is replaced by phenylalanine in *Cre8* lines. Although both amino acids are non-polar, phenylalanine has a large benzene ring. According to the modelling conducted here, this did not affect protein folding, but it might affect signalling. The residue Ala-511 is highly conserved (present in 127 of 133 SuSy sequences) relative to Thr-511, which was found only in the *Cre8* TraesCS6B02G466600 protein and in HbSUS6 of *Hevea brasiliensis* (para rubber tree), which is encoded by a gene for which only very low transcript levels have been detected (Xiao *et al.*, 2014). The polarity difference between alanine (non-polar) and threonine (polar) makes this substitution unusual, but there is no indication that it affects protein structure and it seems too far from the catalytic site to affect protein function.

Given that TraesCS6B02G466600 is just one of nine predicted SUS III genes in wheat, it seems likely that reduction in or loss of function of the TraesCS6B02G466600 SuSy would be compensated by the activity of other SUS III enzymes. Accordingly, if TraesCS6B02G466600 is the causal gene for *Cre8* resistance, the resistance allele likely encodes a product with an enhanced function. This would be consistent with results observed in *Arabidopsis*, in which loss of SUS III function increased the number of female nematodes (Cabello *et al.*, 2014). Potential resistance mechanisms will be discussed in Chapter 9.

The research reported here narrowed the candidate region for the *Cre8* resistance gene to a region of 334 kbp that contains two high-confidence predicted genes that are known to be expressed in roots. One of these genes, TraesCS6B02G466600, encodes a SUS III sucrose synthase and with non-synonymous polymorphisms. This work advanced knowledge about the genetics of resistance to cereal cyst nematode and led to identification of a possible candidate gene for the wheat *Cre8* resistance locus.

Chapter 9 : General Discussion

This thesis presents the work completed to (**1**) develop methods to visualise feeding sites within wheat root tissue; (**2**) identify phenotypic differences between susceptible and *Cre8*-containing CCN-resistant wheat; (**3**) fine map the CCN resistance locus *Cre8* and (**4**) identify possible candidate genes for *Cre8*. While working on developing microscopy methods reported in Chapter 3, I discovered a striking structural modification of cMX vessels. This led to the research reported in Chapter 4, in which I determined that these modifications can be detected as early as 2 d, and to questions about water transport that are addressed in Chapter 5. To answer questions about the resistance locus, *Cre8*, I first developed sister lines, reported in Chapter 6, to investigate whether any phenotypic differences existed in root and shoot growth. With no differences detected in plant vigour, I then applied microscopy techniques to analyse feeding site development within sister lines. This led to the results reported in Chapter 7 where I showed evidence of an antibiosis resistance mechanism. Finally, in Chapter 8, I presented my results of fine-mapping and identified a possible candidate gene for *Cre8*.

This chapter will provide a general discussion that (**a**) presents suggestions for future research on feeding site visualisation and nematode-induced cMX modification, (**b**) discusses possible connections between a sucrose synthase candidate gene and cytological differences between *+Cre8* and *-Cre8* materials and (**c**) considers possible resistance mechanisms for *Cre8* and ways in which these might be investigated in future.

9.1 Feeding site visualisation and cMX modification

The work reported in Chapter 3 showed that hydroponics was suitable for growing CCN-infected wheat for microscopy use. The work also established a systematic method of imaging thick sections to generate three-dimensional views of roots. This work underpinned the rest of the thesis research, making it possible to view and compare feeding site development and to discover CCN-induced cMX modification. While invasion of cMX cells by feeding sites has been reported previously (Grymaszewska & Golinowski, 1991), the discovery of xylem modification is novel and the detailed information of cyst nematode feeding sites and

surrounding tissues was revealed in remarkable clarity. Given the extent of previous cytological investigation of cyst nematode infection sites, it is striking that there are no previous reports of the xylem modification revealed here. A review on plant cellular responses to nematode infection (Dropkin, 1969) indicated that it would be "the last one to be written on the cellular effects of nematodes in plants that is based almost exclusively on observations made with the light microscope and classical histological procedures" and suggested electron microscopy, histochemistry and autoradiography as more advanced techniques. Subsequent research on CN pathosystems has indeed benefited from the use of scanning and electron microscopy (Jones, 1981; Jones & Dropkin, 1975; Jones & Northcote, 1972) and histochemistry (Aditya *et al.*, 2015; Zhang *et al.*, 2017) but has also continued use of light microscopy and classical histology (Cui *et al.*, 2017; Golinowski *et al.*, 1996; Golinowski *et al.*, 1997; Grymaszewska & Golinowski, 1991; Seah *et al.*, 2000; Williams & Fisher, 1993). Autoradiography has been applied for RKN pathosystems (Rohde & McClure, 1975) but not CN systems.

While the cMX modification reported in this thesis was discovered and investigated using technologies that were not even envisioned in 1969, including confocal microscopy and imaging software, it is worth noting that distorted cMX can be easily seen in thick longitudinal sections using a light microscope (as presented in Figure 3-14). Further, as discussed in Chapter 4, distorted cMX is visible in earlier published micrographs but was not labelled or discussed, probably because the classical use of very thin sections used made it difficult to fully understand the complex three-dimensional structure of infected regions.

As technology continues to advance, new insight will likely be gained about host-parasite relationships. The recent use of laser ablation tomography (LAT) is one example of this, revealing exact dimensions of nematode feeding sites in three dimensions (Strock *et al.*, 2019; Van Gansbeke, 2019). For future experiments, I suggest using LAT to quantitatively track the development of distorted cMX in both resistant and susceptible materials. Another tool is

light sheet microscopy (Huisken *et al.*, 2004), which has been used to investigate biological processes in plants (Berthet & Maizel, 2016) including live imaging of lateral root development (von Wangenheim *et al.*, 2017). This would be a tremendous tool to show the swelling that occurs around nematode feeding sites and where lateral roots develop. Using a conventional dissecting microscope, I was able to observe the internal vascular tissue within swollen (infected) regions of wheat roots. CMX elements were short and wide and there were lateral root initials just above feeding sites (Appendix 5). Repetition of this method over time could provide further detail about the proliferation of lateral roots in CCN-infected regions and development, leading to testable hypotheses about the importance and role(s) of lateral roots in CCN-infected roots. One theory is that the apoplastic/symplastic impediment leads to an accumulation of hormones which may induce lateral root growth. Previous reports have indicated that CN-induced lateral root proliferation directly supports syncytium development (Hewezi *et al.*, 2015; Lee *et al.*, 2011b). This might involve by-pass flow of additional water and nutrients into the plant vascular system and then into feeding sites and nematodes. This could be tested using the protocol described by Krishnamurthy *et al.* (2011). Another possibility is that lateral root proliferation supports the host plant by establishing pathways that supply water and nutrients to tissues above feeding sites.

In another preliminary experiment, I recorded a time-lapse video of a wheat root after nematode inoculation. This revealed rapid root hair growth very early (within 5 h) after inoculation (Appendix 6). With time-lapse videos recorded over a longer period, it might be possible to determine exactly when root swelling becomes visible. This time-lapse approach, however, does have some limitations since roots needs to be illuminated for the entirety of the video (which could affect nematode infection). Improved understanding of these early responses to infection (and perhaps even nematode presence) might contribute to understanding of nematode-induced cMX modification.

It would also be interesting to test known nematode signalling hormones or proteins in isolation to determine if any single component induces distorted cMX cells. For example the cyst nematode protein 10A06 has been reported to elevate expression of the Arabidopsis gene SPD2, which encodes a spermidine synthase (Hewezi *et al.*, 2010). Given that spermidine is a known inhibitor of root cell elongation (Tisi *et al.*, 2011) it might affect elongation of cMX vessels. While no morphological effects were seen in Arabidopsis (Tisi *et al.*, 2011), it is possible that the prominent cMX in the roots of wheat and other cereals could provide a better model for investigation of the effects of spermidine or other molecular signals.

Future work on structural modification of the cMX could also include investigation of whether and how cMX development is affected by plant growth conditions (e.g. hydroponics vs. soil). Although most of the microscopy work reported in this thesis was done using tissue from plants grown in hydroponics, some work did use soil-grown infected plants. In soil-grown plants, structural modification of CCN-infected plants appeared even more extreme in susceptible lines compared to resistant lines. More research is needed to determine whether growth conditions affect cMX distortion. It is possible that nematode signals are more concentrated in plants grown in soil (where the nematodes can persist in the growth medium) than in plants grown in the hydroponic system used here. Using hydroponics, most nematodes are washed prior to transfer to hydroponics and any remaining nematodes would be dispersed in the initial nutrient solution and removed when it is replaced.

9.2 Investigation of water transport

The discovery of distorted cMX led to the research reported in Chapter 5, which showed that water transport is hindered in nematode-infected roots. Given that the discovery of distorted cMX occurred quite late in my PhD research program, it was not feasible to complete a full investigation. Nevertheless, some preliminary tracer-dye experiments were conducted (Chapter 5) and the findings from those experiments provide a basis for future research to investigate how and why cMX disruptions occur. This research might involve:

1. Repetition of the HPTS-acetate experiment using the apoplastic form of HPTS. Results from such research could replace the preliminary experiments that were conducted here using blue food colouring of unknown chemical constitution.
2. Development and application of improved methods for visualising and recording the transport of tracer dyes. Due to its yellow colour, HPTS can be detected visually, but it can be difficult to assess exactly how far it has been transported based on external observations of plant roots. Given that HPTS can be more readily detected based on UV-induced fluorescence (Barrash-Shiftan *et al.*, 1998), it might be possible to track HPTS in a gel documentation system to track dye uptake. Development of protocols for this would require consideration of a setup that allows roots to uptake dye in the dark but keeps the shoots illuminated. The clarity of image using this system should also be considered. If reliable protocols can be established, this might allow investigation of whether water taken up by lateral roots ends up entering nematode feeding sites or the cMX above feeding sites.

9.3 The *Cre8* candidate gene and proposed resistance mechanisms

A main objective of this thesis research was to determine phenotypic differences between *+Cre8* and *-Cre8* plants to help uncover a resistance mechanism and inform the identification of a candidate gene. This was done by developing sister lines (one resistant and one susceptible), comparing their plant growth (Chapter 6) and using microscopy to observe feeding sites develop within their roots (Chapter 7).

While plant growth studies did not detect any differences in plant vigour between *+Cre8* and *-Cre8* plants, they did show that by 21 DAI, the numbers of nematodes in the root systems of susceptible plants exceeded those in resistant plants. This helped establish the time frame within which more detailed experiments were conducted. Cytological analysis of feeding sites in susceptible plants showed that they were close to the cMX, often incorporated cMX vessels and contained 'web-like' networks of MLG-rich internal cell walls. These networks likely consisted of cell wall remnants from successfully invaded host cells. In contrast, feeding sites within resistant plants were often a few cells away from the cMX, were not directly connected with cMX vessels and lacked 'web-like' structures. Further, the walls of cMX vessels were thicker and richer in lignin in infected *+Cre8* plants than in infected *-Cre8* plants. This might cause a physical barrier that stops feeding sites in *+Cre8* plants from expanding.

Another key objective of this thesis research was to fine-map the *Cre8* region to identify candidate genes. Fine-mapping can be slow, considering that each cycle requires several months to obtain viable wheat seeds, several weeks to screen for recombinants, several more months to obtain homozygous recombinant progeny and twelve weeks to phenotype resistance against CCN. This is challenging within the time constraints allowed for PhD research. This meant that my final phenotyping results became available only six months before thesis submission, limiting the prospects for thorough investigation of candidate genes that remained in the region. Furthermore, the gene order in the IWGSC RefSeq v1.0 sequence assembly for Chinese Spring differed from that of my genetic map. I was able to address this

by using other sequence assemblies, but this effort became redundant once the RefSeq v2.0 assembly became available in July 2019, resolving all of the discrepancies. While a rapid succession of exciting progress during the final year of experimental work was paramount to the outcomes of the research, it left limited time to completely investigate all potential candidate genes. Nevertheless, a promising a candidate gene was identified and considered. This gene, which is predicted to encode a SUS III sucrose synthase, is known to be expressed in roots and has non-synonymous SNPs between the alleles of *Cre8* and non-*Cre8* plants.

Sucrose synthases are glycosyl transferase enzymes that can catalyse production of fructose and uridine diphosphate glucose (UDP-G) or adenosine diphosphate glucose (ADP-G), which are used as substrates for synthesis of polysaccharides. Conversely, SuSy can catalyse the reverse reaction, synthesising sucrose. Since feeding sites receive sucrose from the phloem, the role of SuSy in the cellular context of feeding sites is likely one that breaks down sucrose. Thus, if differences in CCN resistance are due to polymorphisms in a sucrose synthase gene, the resistance mechanism may involve the supply of substrates for synthesis of polysaccharides including cellulose, starch and callose. Any of these could potentially affect the development of feeding sites and the success of the parasite. Cellulose has been detected in syncytial cell walls (Davies *et al.*, 2012; Sobczak, 1996; Zhang *et al.*, 2017) and has been suggested to provide structural support to withstand the high turgor pressure within feeding sites (Böckenhoff & Grundler, 1994; Zhang *et al.*, 2017). Starch has been reported in nematode feeding sites (Hofmann & Grundler, 2007) and acts as a temporary sink for carbohydrates between cycles of intermittent feeding by nematodes (Hofmann *et al.*, 2008). Callose has been associated with plant defence against nematodes and has been detected in the walls of feeding sites within resistant hosts (Sobczak & Golinowski, 2009). Therefore, differences in which polysaccharides are synthesised from the products of SuSy activity might support (with cellulose or starch) or harm (due to callose) nematode feeding site development.

While the role of sucrose synthases in plant-nematode interactions is not completely understood, research on infection of *Arabidopsis* by *H. schachtii* revealed several potential roles of SuSy (Cabello *et al.*, 2014). Due to the number of homoeologues in wheat, it seems likely that the resistance allele confers enhanced function of its product. Based on the literature and the results obtained from this research, there are several possible mechanisms by which polymorphism in a sucrose synthase gene could affect nematode resistance:

(1)- Enhanced function of a SUS III SuSy increases callose deposition:

An enhanced function of the *Cre8*-associated SuSy may increase substrates used for polysaccharides that are subsequently harmful for nematode development including callose. Studies on the *Arabidopsis* SUS IIIs AtSUS5 and AtSUS6 showed these proteins are localised in the phloem and play a role in callose synthesis (Barratt *et al.*, 2009).

Investigations using immunolabeling of callose with the (1,3)-β-glucan-specific antibody did not reveal callose deposition. However, that analysis was done using only transverse sections, which depending on the section taken, may not show the location of callose plugs. Therefore, further investigation of callose may be interesting.

(2) Localisation change of SuSy diminishes starch reservoirs and increases cellulose

The subcellular localisation of SuSy determines where its products are released, and therefore which polysaccharides are likely to be synthesised. For example, if the change of products impaired starch synthesis, it could reduce the energy supply that the nematodes need to support their intermittent feeding patterns. Alternatively, if the change of products impaired cellulose synthesis, it could reduce the structural support needed for nematode feeding sites.

Although plastids (where starch is synthesised) normally rely on the activity of cytosolic SuSy, a SuSy that is re-localised to the cell wall would provide UDP-G for the immediate substrate for cellulose (or callose) (Amor *et al.*, 1995; Doblin *et al.*, 2002; Ruan, 2007).

One of the non-synonymous SNPs between alleles of the SuSy candidate gene leads to an amino acid substitution in the cellular targeting (Ser-116 in susceptible plants vs. Arg-116 in resistant plants). Other SUS III enzymes had serine residues at this position, while SUS I enzymes had arginine. If this difference helps determine subcellular localisation, this could cause a shift from one product to another. For example, the resistance-associated allele could result in a decrease in starch, which may explain why the nematode is less successful, and increase in cellulose, which may explain why an increase of (1,3;1,4)-β-glucan is seen around feeding sites.

(3) Enhanced SuSy leads to enhanced plant defence signals

Another potential role of the SuSy candidate gene may be to enhance a plant defence signalling pathway. Sugars including sucrose, glucose and fructose can act as signalling molecules which regulate developmental and stress responses (Eveland & Jackson, 2011; Sheen *et al.*, 1999). Transgenic tomatoes with RNAi suppression of SUS1, SUS3 and SUS4 showed increased auxin signalling (Goren *et al.*, 2017). Studies have shown that auxin stimulates cell elongation (Chapman *et al.*, 2012; Gendreau *et al.*, 1997) and upregulates cellulose synthase genes (Cosgrove, 1999; Majda & Robert, 2018). Additional studies on nematode infection found that initiation of feeding sites depends on auxin (Goverse *et al.*, 2000; Grunewald *et al.*, 2009; Karczmarek *et al.*, 2004). Specifically, research on *H. schachtii* in *Arabidopsis* showed that inhibition of auxin transport could impede the expansion of feeding sites toward the vascular cylinder (Goverse *et al.*, 2000). Thus, it could be hypothesised that an enhanced SuSy in *Cre8* resistant plants may inhibit auxin which explains the lack of feeding site development close to cMX vessels.

Although host-parasite interactions may differ between CN and RKN pathosystems, there may be some common elements in plant defence mechanisms. In a model for how gene regulation affects RKN resistance in soybeans, Beneventi *et al.* (2013) included roles for key

genes encoding glycosyltransferases, peroxidases and auxin-responsive proteins. The proposed model, based on transcription data, shows ROS signalling causing increased levels of Ca^{2+} leading to increased callose deposition and sugar accumulation (Beneventi *et al.*, 2013). However, it is possible that in the CCN-wheat resistance pathway, this is reversed: increased sugar accumulation (due to enhanced SuSy activity) increases callose deposition and ultimately leads to increased ROS signalling. Increased synthesis of ROS, caused by class III plant peroxidases, may then also lead to increased production of lignin (Almagro *et al.*, 2008).

The cytological analysis in this research showed that *Cre8* plants had a thicker lignified cMX than non-*Cre8* plants. Although not directly linked with SuSy activity, lignin is associated with plant defence against nematode infection (Andres *et al.*, 2001; Kumari *et al.*, 2016; Melillo *et al.*, 1993) and with plant cell death, interrupting feeding site expansion (Andres *et al.*, 2001; Melillo *et al.*, 1992). Previous studies in wheat roots have shown that SuSy activity increased under stress and was correlated with thickened cell walls (Albrecht & Mustroph, 2003). Similarly, thickened cell walls have also been reported in overexpression of a SUS I in a poplar hybrid (Coleman *et al.*, 2009; Wei *et al.*, 2015). An increase in lignin deposition may be a downstream effect from sugar signalling and may prevent feeding site expansion toward the cMX.

9.4 Future *Cre8* work

In order to investigate the validity of TraesCS6B02G466400 as a candidate for resistance against *H. avenae*, more research is needed. The following outlines some suggested future work:

1. Fine-mapping of the remaining plant material to search for more recombinants. Material that is still heterozygous in the candidate region could be selfed and progeny screened for recombination. However, based on the current estimate of the recombination distance between flanking markers, recombinant haplotypes would be rare.
2. *In situ* hybridisation (ISH) of genes of interest to determine localisation within infected roots. Preliminary ISH work did not show any gene expression in CCN-infected tissue for selected candidate genes TraesCS6B02G466400 and TraesCS6B02G466600 (Appendix 7). However, even the housekeeping gene TaCyclo was detected only in lateral root initials and not the feeding site. A lack of signal within feeding sites may be due to inadequate fixation deep within the tissue. A longer fixation period (> 2 hr) may help fix the innermost tissues.
3. Investigation of callose differences either through an optimised immunolabelling protocol or another method such as aniline blue staining described by Schenk and Schikora (2015).
4. Investigation of SuSy function using wheat genetic transformation. Alternatively, heterologous expression of the predicted products of the alternate alleles of TraesCS6B02G466600 followed by purification of these proteins and subsequent experiments could help assess their function (protocol described by Fedosejevs *et al.* (2014)). This will determine whether both enzymes perform the same function at the same rate.

9.5 Closing remarks

Cereal cyst nematode was once a major economic threat to cereal crops before the use of resistant cultivars. The resistance locus, *Cre8,* was introduced to Australian wheat breeding *via* the cultivar, Festiguay, which was said to "sweeten the soil" since use of the cultivar decreased CCN numbers in soil for the following season. This resistance gene has been deployed in wheat to confer tolerance and resistance against CCN. The research reported in this thesis found that although *Cre8* may not confer early plant vigour, it does confer resistance against CCN and likely in a way that is unlike any other CCN resistance gene. The suggested candidate gene, sucrose synthase, may even literally "sweeten the soil" by providing sugar molecules that act to trigger plant defence signals or to alter structural or storage polysaccharides in ways that hinder nematode development.

The research presented in this thesis provides insight into the host-parasite relationship, by presenting new views of feeding sites, and identifies a potential candidate gene and possible resistance mechanisms for a CCN-resistance locus in wheat. These discoveries improve our understanding of CCN and may help scientists and breeders to respond when problems arise in the future.

References

Aditya, J., Lewis, J., Shirley, N. J., Tan, H. T., Henderson, M., Fincher, G. B., Burton, R. A., Mather, D. E., & Tucker, M. R. (2015). The dynamics of cereal cyst nematode infection differ between susceptible and resistant barley cultivars and lead to changes in (1,3;1,4)-beta-glucan levels and *HvCslF* gene transcript abundance. *New Phytologist, 207*, 135-147.

Alaux, M., Rogers, J., Letellier, T., Flores, R., Alfama, F., Pommier, C., Mohellibi, N., Durand, S., Kimmel, E., Michotey, C., Guerche, C., Loaec, M., Lainé, M., Steinbach, D., Choulet, F., Rimbert, H., Leroy, P., Guilhot, N., Salse, J., Feuillet, C., Paux, E., Eversole, K., Adam-Blondon, A.-F., & Quesneville, H. (2018). Linking the International Wheat Genome Sequencing Consortium bread wheat reference genome sequence to wheat genetic and phenomic data. *bioRxiv*, 363259.

Albani, J. R., & Plancke, Y. D. (1998). Interaction between calcofluor white and carbohydrates of alpha 1-acid glycoprotein. *Carbohydrate Research, 314*(3-4), 169-175.

Albrecht, G., & Mustroph, A. (2003). Localization of sucrose synthase in wheat roots: increased *in situ* activity of sucrose synthase correlates with cell wall thickening by cellulose deposition under hypoxia. *Planta, 217*(2), 252-260.

Ali, M., Anjam, M., Nawaz, M., Lam, H.-M., & Chung, G. (2018). Signal Transduction in Plant–Nematode Interactions. *International Journal of Molecular Sciences, 19*, 1648.

Almagro, L., Gómez Ros, L. V., Belchi-Navarro, S., Bru, R., Ros Barceló, A., & Pedreño, M. A. (2008). Class III peroxidases in plant defence reactions. *Journal of Experimental Botany, 60*(2), 377-390.

Amor, Y., Haigler, C. H., Johnson, S., Wainscott, M., & Delmer, D. P. (1995). A membrane-associated form of sucrose synthase and its potential role in synthesis of cellulose and callose in plants. *Proceedings of the National Academy of Sciences of the United States of America, 92*(20), 9353-9357.

Andersen, K., & Andersen, S. (1968). Inheritance of resistance to *Heterodera avenae* in barley. *Nematologica, 14*, 128-130.

Andersen, S., & Andersen, K. (1973). Linkage between marker genes on barley chromosome 2 and a gene for resistance to *Heterodera avenae*. *Hereditas, 73*, 271-276.

Andersen, S., & Andersen, K. (1982). Suggestions for determination and terminology of pathotypes and genes for resistance in cyst-forming nematodes, especially *Heterodera avenae*. *EPPO Bulletin, 12*(4), 379-386.

Andres, M. F., Melillo, M. T., Delibes, A., Romero, M. D., & Bleve-Zacheo, T. (2001). Changes in wheat root enzymes correlated with resistance to cereal cyst nematodes. *New Phytologist, 152*(2), 343-354.

Angeles-Nunez, J. G., & Tiessen, A. (2010). *Arabidopsis* sucrose synthase 2 and 3 modulate metabolic homeostasis and direct carbon towards starch synthesis in developing seeds. *Planta, 232*(3), 701-718.

Antonino de Souza Junior, J. D., Pierre, O., Coelho, R. R., Grossi-de-Sa, M. F., Engler, G., & de Almeida Engler, J. (2017). Application of nuclear volume measurements to comprehend the cell cycle in root-knot nematode-induced giant cells. *Frontiers in Plant Science, 8*, 961.

Appels, R., Eversole, K., Stein, N., Feuillet, C., Keller, B., Rogers, J., Pozniak, C. J., Choulet, F., Distelfeld, A., Poland, J., Ronen, G., Sharpe, A. G., Barad, O., Baruch, K., Keeble-Gagnère, G., Mascher, M., Ben-Zvi, G., Josselin, A.-A., Himmelbach, A., Balfourier, F., Gutierrez-Gonzalez, J., Hayden, M., Koh, C., Muehlbauer, G., Pasam, R. K., Paux, E., Rigault, P., Tibbits, J., Tiwari, V., Spannagl, M., Lang, D., Gundlach, H., Haberer, G., Mayer, K. F. X., Ormanbekova, D., Prade, V., Šimková, H., Wicker, T., Swarbreck, D., Rimbert, H., Felder, M., Guilhot, N., Kaithakottil, G., Keilwagen, J., Leroy, P., Lux, T., Twardziok, S., Venturini, L., Juhász, A., Abrouk, M., Fischer, I., Uauy, C., Borrill, P., Ramirez-Gonzalez, R. H., Arnaud, D., Chalabi, S., Chalhoub, B., Cory, A., Datla, R., Davey, M. W., Jacobs, J., Robinson, S. J., Steuernagel, B., van Ex, F., Wulff, B. B. H., Benhamed, M., Bendahmane, A., Concia, L., Latrasse, D., Bartoš, J., Bellec, A., Berges, H., Doležel, J., Frenkel, Z., Gill, B., Korol, A., Letellier, T., Olsen, O.-A., Singh, K., Valárik, M., van der Vossen, E., Vautrin, S., Weining, S., Fahima, T., Glikson, V., Raats, D., Číhalíková, J., Toegelová, H., Vrána, J., Sourdille, P., Darrier, B., Barabaschi, D., Cattivelli, L., Hernandez, P., Galvez, S., Budak, H., Jones, J. D. G., Witek, K., Yu, G., Small, I., Melonek, J., Zhou, R., Belova, T., Kanyuka, K., King, R., Nilsen, K., Walkowiak, S., Cuthbert, R., Knox, R., Wiebe, K., Xiang, D., Rohde, A., Golds, T., Čížková, J., Akpinar, B. A., Biyiklioglu, S., Gao, L., N'Daiye, A., Kubaláková, M., Šafář, J., Alfama, F., Adam-Blondon, A.-F., Flores, R., Guerche, C., Loaec, M., Quesneville, H., Condie, J., Ens, J., Maclachlan, R., Tan, Y., Alberti, A., Aury, J.-M., Barbe, V., Couloux, A., Cruaud, C., Labadie, K., Mangenot, S., Wincker, P., Kaur, G., Luo, M., Sehgal, S., Chhuneja, P., Gupta, O. P., Jindal, S., Kaur, P., Malik, P., Sharma, P., Yadav, B., Singh, N. K., Khurana, J. P., Chaudhary, C., Khurana, P., Kumar, V., Mahato, A., Mathur, S., Sevanthi, A., Sharma, N., Tomar, R. S., Holušová, K., Plíhal, O., Clark, M. D., Heavens, D., Kettleborough, G., Wright, J., Balcárková, B., Hu, Y., Salina, E., Ravin, N., Skryabin, K., Beletsky, A., Kadnikov, V., Mardanov, A., Nesterov, M., Rakitin, A., Sergeeva, E., Handa, H., Kanamori, H., Katagiri, S., Kobayashi, F., Nasuda, S., Tanaka, T., Wu, J., Cattonaro, F., Jiumeng, M., Kugler, K., Pfeifer, M., Sandve, S., Xun, X., Zhan, B., Batley, J., Bayer, P. E., Edwards, D., Hayashi, S., Tulpová, Z., Visendi, P., Cui, L., Du, X., Feng, K., Nie, X., Tong, W., & Wang, L. (2018). Shifting the limits in wheat research and breeding using a fully annotated reference genome. *Science, 361*(6403), eaar7191.

Bailey-Serres, J., & Mittler, R. (2006). The roles of reactive oxygen species in plant cells. *Plant Physiology, 141*(2), 311.

Bari, R., & Jones, J. D. (2009). Role of plant hormones in plant defence responses. *Plant Molecular Biology, 69*(4), 473-488.

Barloy, D., Lemoine, J., Abelard, P., Tanguy, A., Rivoal, R., & Jahier, J. (2007). Marker-assisted pyramiding of two cereal cyst nematode resistance genes from *Aegilops variabilis* in wheat. *Molecular Breeding, 20*, 31-40.

Barr, A., Chalmers, K., Karakousis, A., Kretschmer, J., Manning, S., Lance, R., Lewis, J., Jeffries, S., & Langridge, P. (1998). RFLP mapping of a new cereal cyst nematode resistance locus in barley. *Plant Breeding, 117*, 185-187.

Barrash-Shiftan, N., Brauer, B., & Pines, E. (1998). Solvent dependence of pyranine fluorescence and UV-visible absorption spectra. *Journal of Physical Organic Chemistry, 11*(10), 743-750.

Barratt, D. H. P., Derbyshire, P., Findlay, K., Pike, M., Wellner, N., Lunn, J., Feil, R., Simpson, C., Maule, A. J., & Smith, A. M. (2009). Normal growth of *Arabidopsis* requires cytosolic invertase but not sucrose synthase. *Proceedings of the National Academy of Sciences, 106*(31), 13124.

Bartlem, D. G., Jones, M. G. K., & Hammes, U. Z. (2014). Vascularization and nutrient delivery at root-knot nematode feeding sites in host roots. *Journal of Experimental Botany, 65*, 1789-1798.

Beneventi, M. A., da Silva, O. B., de Sá, M. E. L., Firmino, A. A. P., de Amorim, R. M. S., Albuquerque, É. V. S., da Silva, M. C. M., da Silva, J. P., Campos, M. d. A., Lopes, M. J. C., Togawa, R. C., Pappas, G. J., & Grossi–de–Sa, M. F. Transcription profile of soybean-root-knot nematode interaction reveals a key role of phythormones in the resistance reaction. *BMC Genomics, 14*(1), 322

Berthet, B., & Maizel, A. (2016). Light sheet microscopy and live imaging of plants. *Journal of Microscopy, 263*(2), 158-164.

Bird, D. M. (1996). Manipulation of host gene expression by root-knot nematodes. *The Journal of Parasitology, 82*, 881-888.

Bird, D. M., & Wilson, M. A. (1994). Molecular and cellular dissection of giant cell formation. In F. Lamberti, C. De Giorgi, & D. M. Bird (Eds.), *Advances in Molecular Plant Nematology* (pp. 181-195). New York: Plenum Press.

Böckenhoff, A., & Grundler, F. (1994). Studies on the nutrient uptake by the beet cyst nematode *Heterodera schachtii* by *in situ* microinjection of fluorescent probes into the feeding structures in *Arabidopsis thaliana*. *Parasitology, 109*, 249-255.

Böckenhoff, A., Prior, D. A. M., Grundler, F. M. W., & Oparka, K. J. (1996). Induction of phloem unloading in *Arabidopsis thaliana* roots by the parasitic nematode *Heterodera schachtii*. *Plant Physiology, 112*, 1421-1427.

Bohlmann, H., & Sobczak, M. (2014). The plant cell wall in the feeding sites of cyst nematodes. *Frontiers in Plant Science, 5*, 89-89.

Bohlmann, H., & Wieczorek, K. (2015). Infection assay of cyst nematodes on *Arabidopsis* roots. *Bio-protocol, 5*(18), e1596.

Bolouri Moghaddam, M. R., & Van den Ende, W. (2012). Sugars and plant innate immunity. *Journal of Experimental Botany, 63*(11), 3989-3998.

Bowden, P., Edwards, J., Ferguson, N., McNee, T., Manning, B., Roberts, K., Schipp, A., Schulze, K., & Wilkins, J. (2007). *Wheat growth and development*. New South Whales: NSW Department of Primary Industries

Brundrett, M. C., Enstone, D. E., & Peterson, C. A. (1988). A berberine-analine blue fluorescent staining procedure for suberin, lignin, and callose in plant tissue. *Protoplasma, 146*, 133-142.

Bybd, D. W., Kirkpatrick, T., & Barker, K. R. (1983). An improved technique for clearing and staining plant tissues for detection of nematodes. *Journal of Nematology, 15*(1), 142.

Cabello, S., Lorenz, C., Crespo, S., Cabrera, J., Ludwig, R., Escobar, C., & Hofmann, J. (2014). Altered sucrose synthase and invertase expression affects the local and systemic sugar metabolism of nematode-infected *Arabidopsis thaliana* plants. *Journal of Experimental Botany, 65*(1), 201-212.

Cai, D., Kleine, M., Kifle, S., Harloff, H. J., Sandal, N. N., Marcker, K. A., Klein-Lankhorst, R. M., Salentijn, E. M., Lange, W., Stiekema, W. J., Wyss, U., Grundler, F. M., & Jung, C. (1997). Positional cloning of a gene for nematode resistance in sugar beet. *Science (New York, N.Y.), 275*(5301), 832-834.

Caño-Delgado, A., Lee, J-Y., & Demura, T. (2010). Regulatory mechanisms for specification and patterning of plant vascular tissues. *Annual Review of Cell and Developmental Biology, 26*, 605-637.

Carlsbecker, A., Lee, J.-Y., Roberts, C. J., Dettmer, J., Lehesranta, S., Zhou, J., Lindgren, O., Moreno-Risueno, M. A., Vatén, A., Thitamadee, S., Campilho, A., Sebastian, J., Bowman, J. L., Helariutta, Y., & Benfey, P. N. (2010). Cell signalling by microRNA165/6 directs gene dose-dependent root cell fate. *Nature, 465*(7296), 316-321.

Chapman, E. J., Greenham, K., Castillejo, C., Sartor, R., Bialy, A., Sun, T. P., & Estelle, M. (2012). Hypocotyl transcriptome reveals auxin regulation of growth-promoting genes through GA-dependent and -independent pathways. *PLoS One, 7*(5), e36210.

Coleman, H. D., Yan, J., & Mansfield, S. D. (2009). Sucrose synthase affects carbon partitioning to increase cellulose production and altered cell wall ultrastructure. *Proceedings of the National Academy of Sciences, 106*(31), 13118.

Colmsee, C., Beier, S., Himmelbach, A., Schmutzer, T., Stein, N., Scholz, U., & Mascher, M. (2015). BARLEX - the Barley Draft Genome Explorer. *Molecular Plant, 8*(6), 964-966.

Cosgrove, D. J. (1999). Enzymes and other agents that enhance cell wall extensibility. *Annual Review of Plant Physiology and Plant Molecular Biology, 50*, 391-417.

Cotten, J., & Hayes, J. (1969). Genetic resistance to the cereal cyst nematode (*Heterodera avenae*). . *Heredity, 24*, 593-600.

Craddock, C., & Yang, Z. (2012). Endocytic signaling in leaves and roots: same rules different players. *Frontiers in Plant Science, 3*, 219-219.

Cui, H., Tsuda, K., & Parker, J. E. (2015). Effector-triggered immunity: from pathogen perception to robust defense. *Annual Review of Plant Biology, 66*(1), 487-511.

Cui, J., Peng, H., Huang, W., Liu, S., Wu, D., Kong, L., He, W., & Peng, D. (2017). Phenotype and cellular response of wheat lines carrying *Cre* genes to *Heterodera avenae* pathotype Ha91. *Plant Disease, 101*(11), 1885-1894.

Dangl, J. L., Horvath, D. M., & Staskawicz, B. J. (2013). Pivoting the plant immune system from dissection to deployment. *Science, 341*(6147), 746-751.

Davies, L. J., Lilley, C. J., Paul Knox, J., & Urwin, P. E. (2012). Syncytia formed by adult female *Heterodera schachtii* in *Arabidopsis thaliana* roots have a distinct cell wall molecular architecture. *New Phytology, 196*(1), 238-246.

Davis, E. L., Hussey, R. S., Mitchum, M. G., & Baum, T. J. (2008). Parasitism proteins in nematode-plant interactions. *Current Opinion in Plant Biology, 11*(4), 360-366.

de Majnik, J., Ogbonnaya, F. C., Moullet, O., & Lagudah, E. S. (2003). The *Cre1* and *Cre3* nematode resistance genes are located at homeologous loci in the wheat genome. *Molecular Plant Microbe Interactions, 16*(12), 1129-1134.

Denancé, N., Sánchez-Vallet, A., Goffner, D., & Molina, A. (2013). Disease resistance or growth: the role of plant hormones in balancing immune responses and fitness costs. *Frontiers in Plant Science, 4*, 155-155.

Dickson, J. G. (1956). *Diseases of field crops* (2nd ed.). New York: McGraw-Hill.

Doblin, M. S., Kurek, I., Jacob-Wilk, D., & Delmer, D. P. (2002). Cellulose biosynthesis in plants: From genes to rosettes. *Plant and Cell Physiology, 43*(12), 1407-1420.

Dropkin, V. H. (1969). Cellular responses of plants to nematode infections. *Annual Review of Phytopathology, 7*, 101-122.

Ellenby, C., & Perry, R. (1976). The influence of the hatching factor on the water uptake of the second stage larva of the potato cyst nematode *Heterodera rostochiensis*. *Journal of Experimental Botany, 64*, 141-147.

Ernst, K., Kumar, A., Kriseleit, D., Kloos, D.-U., Phillips, M. S., & Ganal, M. W. (2002). The broad-spectrum potato cyst nematode resistance gene (*Hero*) from tomato is the only member of a large gene family of NBS-LRR genes with an unusual amino acid repeat in the LRR region. *The Plant Journal, 31*(2), 127-136.

Esau, K. (1965). *Vascular differentiation in plants*. New York: Holt, Rinehart and Winston.

Escamez, S., Bollhoner, B., & Tuominen, H. (2017). Quick histochemical staining methods to detect cell death in xylem elements of plant tissues. *Methods in Molecular Biology, 1544*, 27-36.

Eveland, A. L., & Jackson, D. P. (2011). Sugars, signalling, and plant development. *Journal of Experimental Botany, 63*(9), 3367-3377.

Fatemy, F., & Evans, K. (1986). Growth, water uptake and calcium content of potato cultivars in relation to tolerance of cyst nematodes. *Revue de Nematologie, 9*(2), 171-179.

Fedosejevs, E., Ying, S., Park, J., Anderson, E., Mullen, R., She, Y.-M., & Plaxton, W. (2014). Biochemical and molecular characterization of RcSUS1, a cytosolic sucrose synthase phosphorylated *in vivo* at serine 11 in developing castor oil seeds. *Journal of Biological Chemistry, 289*, 33412–33424

Fisher, J. M., Rathjen, A. J., & Dube, A. J. (1981). Tolerance of commercial cultivars and breeders lines to *Heterodera avenae* Woll. *Australian Journal of Agricultural Research, 32*, 545–552.

Friebe, B., Jiang, J., Raupp, W. J., McIntosh, R. A., & Gill, B. S. (1996). Characterization of wheat-alien translocations conferring resistance to diseases and pests: current status. *Euphytica*, 91(1), 59-87.

Gebhardt, C., Mugniery, D., Ritter, E., Salamini, F., & Bonnel, E. (1993). Identification of RFLP markers closely linked to the *HI* gene conferring resistance to *Globodera rostochiensis* in potato. *Theoretical and Applied Genetics*, *85*, 541-544.

Geldner, N., & Jurgens, G. (2006). Endocytosis in signalling and development. *Current Opinion in Plant Biology, 9*(6), 589-594.

Gendreau, E., Traas, J., Desnos, T., Grandjean, O., Caboche, M., & Hofte, H. (1997). Cellular basis of hypocotyl growth in *Arabidopsis thaliana*. *Plant Physiology, 114*(1), 295-305.

Golinowski, W., Grundler, F. M. W., & Sobczak, M. (1996). Changes in the structure of *Arabidopsis thaliana* during female development of the plant-parasitic nematode *Heterodera schachtii*. *Protoplasma, 194*, 103-116.

Golinowski, W., Sobczak, M., Kurek, W., & Grymaszewska, G. (1997). The structure of syncytia. In C. Fenoll, F. M. W. Grundler, & S. A. Ohl (Eds.), *Cellular and Molecular Aspects of Plant–Nematode Interactions in Plant Pathology* (Vol. 10, pp. 80-97). Dordrecht, Netherlands: Kluwer.

Goren, S., Lugassi, N., Stein, O., Yeselson, Y., Schaffer, A. A., David-Schwartz, R., & Granot, D. (2017). Suppression of sucrose synthase affects auxin signaling and leaf morphology in tomato. *PLoS ONE, 12*(8), e0182334.

Goverse, A., Overmars, H., Engelbertink, J., Schots, A., Bakker, J., & Helder, J. (2000). Both induction and morphogenesis of cyst nematode feeding cells are mediated by auxin. *Molecular Plant-Microbe Interactions, 13*(10), 1121-1129.

Grundler, F. M. W., Böckenhoff, A., Schmidt, K.-P., Sobczak, M., Golinowski, W., & Wyss, U. (1994). *Arabidopsis thaliana* and *Heterodera schachtii*: A versatile model to characterize the interaction between host plants and cyst nematodes. In F. Lamberti, C. d. Giorgi, & D. M. Bird (Eds.), *Advances in Molecular Plant Nematology* (Vol. 268, pp. 171-180). Boston, MA: Springer US.

Grundler, F. M. W., Sobczak, M., & Golinowski, W. (1998). Formation of wall openings in root cells of *Arabidopsis thaliana* following infection by the plant-parasitic nematode *Heterodera schachtii*. *European Journal of Plant Pathology, 104*, 545-551.

Grunewald, W., van Noorden, G., Van Isterdael, G., Beeckman, T., Gheysen, G., & Mathesius, U. (2009). Manipulation of auxin transport in plant roots during Rhizobium symbiosis and nematode parasitism. *Plant Cell, 21*(9), 2553-2562.

Grymaszewska, G., & Golinowski, W. (1991). Structure of syncytia induced by *Heterodera avenae* Woll. in roots of susceptible and resistant wheat (*Triticum aestivum L.*). *Journal of Phytopathology, 133*, 307-319.

Guo, Y., Fitz, J., Schneeberger, K., Ossowski, S., Cao, J., & Weigel, D. (2011). Genome-wide comparison of nucleotide-binding site-leucine-rich repeat-encoding genes in *Arabidopsis*. *Plant Physiology, 157*, 757–769.

Hamamouch, N., Li, C., Hewezi, T., Baum, T. J., Mitchum, M. G., Hussey, R. S., Vodkin, L. O., & Davis, E. L. (2012). The interaction of the novel 30C02 cyst nematode effector protein with a plant beta-1,3-endoglucanase may suppress host defence to promote parasitism. *Journal of Experimental Botany, 63*(10), 3683-3695.

Hardin, S. C., & Huber, S. C. (2004). Proteasome activity and the post-translational control of sucrose synthase stability in maize leaves. *Plant Physiology and Biochemistry, 42*(3), 197-208.

Hardin, S. C., Winter, H., & Huber, S. C. (2004). Phosphorylation of the amino terminus of maize sucrose synthase in relation to membrane association and enzyme activity. *Plant Physiology, 134*(4), 1427-1438.

Hasegawa, J., Sakamoto, Y., Nakagami, S., Aida, M., Sawa, S., & Matsunaga, S. (2016). Three-dimensional imaging of plant organs using a simple and rapid transparency technique. *Plant and Cell Physiology, 57*, 462-472.

Heath, M. (2000). Hypersensitive response-related death. *Plant Molecular Biology, 69*(4), 473-488.

Heinrich, T., Bartlem, D., & Jones, M. (1998). Molecular aspects of plant-nematode interactions and their exploitation for resistance strategies. *Australasian Plant Pathology, 27*, 59-72.

Hendrikse, Y. (2016). *Analysis of the Cre8 nematode resistance locus in wheat (Triticum aestivum)*. (Scholars), The University of Adelaide, Adelaide, Australia.

Hewezi, T., & Baum, T. J. (2013). Manipulation of plant cells by cyst and root-knot nematode effectors. *Molecular Plant-Microbe Interactions, 26*(1), 9-16.

Hewezi, T., & Baum, T. J. (2017). Communication of sedentary plant-parasitic nematodes with their host plants. In G. Becard (Ed.), *Advances in Botanical Research* (Vol. 82, pp. 305-324): Academic Press.

Hewezi, T., Howe, P., Maier, T. R., Hussey, R. S., Mitchum, M. G., Davis, E. L., & Baum, T. J. (2008). Cellulose binding protein from the parasitic nematode *Heterodera schachtii* interacts with *Arabidopsis* pectin methylesterase: cooperative cell wall modification during parasitism. *Plant Cell, 20*(11), 3080-3093.

Hewezi, T., Howe, P. J., Maier, T. R., Hussey, R. S., Mitchum, M. G., Davis, E. L., & Baum, T. J. (2010). *Arabidopsis* spermidine synthase is targeted by an effector protein of the cyst nematode *Heterodera schachtii*. *Plant Physiology, 152*(2), 968-984.

Hewezi, T., Juvale, P. S., Piya, S., Maier, T. R., Rambani, A., Rice, J. H., Mitchum, M. G., Davis, E. L., Hussey, R. S., & Baum, T. J. (2015). The cyst nematode effector protein 10A07 targets and recruits host posttranslational machinery to mediate its nuclear trafficking and to promote parasitism in *Arabidopsis*. *Plant Cell, 27*(3), 891-907.

Hofmann, J., & Grundler, F. M. W. (2007). How do nematodes get their sweets? Solute supply to sedentary plant-parasitic nematodes. *Nematology, 9*, 451-458.

Hofmann, J., Szakasits, D., Blöchl, A., Sobczak, M., Daxböck-Horvath, S., Golinowski, W., Bohlmann, H., & Grundler, F. M. W. (2008). Starch serves as carbohydrate storage in nematode-induced syncytia. *Plant Physiology, 146*(1), 228-235.

Hofmann, J., Wieczorek, K., Blochl, A., & Grundler, F. M. (2007). Sucrose supply to nematode-induced syncytia depends on the apoplasmic and symplasmic pathways. *Journal of Experimental Botany, 58*, 1591-1601.

Hou, J., Jiang, Q., Hao, C., Wang, Y., Zhang, H., & Zhang, X. (2014). Global selection on sucrose synthase haplotypes during a century of wheat breeding. *Plant Physiology, 164*(4), 1918-1929.

Huisken, J., Swoger, J., Del Bene, F., Wittbrodt, J., & Stelzer, E. H. (2004). Optical sectioning deep inside live embryos by selective plane illumination microscopy. *Science, 305*(5686), 1007-1009.

Hussey, R. S. (1989). Disease-inducing secretions of plant-parasitic nematodes. *Annual Review of Phytopathology, 27*(1), 123-141.

Jacob, F., Vernaldi, S., & Maekawa, T. (2013). Evolution and conservation of plant NLR functions. *Frontiers in Immunology, 4*, 297.

Jahier, J., Abelardbelard, P., Anguy, M. T., Dedryveredryve, F., Rivoalivoa, R., Khatkar, S., & Bariana, H. S. (2001). The *Aegilops ventricosa* segment on chromosome 2AS of the wheat cultivar `VPM1' carries the cereal cyst nematode resistance gene *Cre5*. *Plant Breeding*. *120*(2), 125-128.

Jahier, J., Rivoal, R., Yu, M. Q., Abelard, P., Tanguy, A. M., & Barloy, D. (1998). Transfer of genes for resistance to cereal cyst nematode from *Aegilops variabilis* Eig to wheat. *Journal of Genetics and Breeding, 52*, 253-257.

Jayatilake, D. V. (2014). *Fine mapping of nematode resistance genes Rlnn1 and Cre8 in wheat (Triticum aestivum).* (PhD) The University of Adelaide, Adelaide, Australia.

Jayatilake, D. V., Tucker, E. J., Brueggemann, J., Lewis, J., Garcia, M., Dreisigacker, S., Hayden, M. J., Chalmers, K. J., & Mather, D. E. (2015). Genetic mapping of the *Cre8* locus for resistance against cereal cyst nematode (*Heterodera avenae* Woll.) in wheat. *Molecular Breeding*. *35*(66).

Johnson, C. M., Stout, P. R., Broyer, T. C., & Carlton, A. B. (1957). Comparative chlorine requirements of different plant species. *Plant and Soil, 8*, 337-353.

Jones, J. D. G., & Dangl, J. L. (2006). The plant immune system. *Nature, 444*(7117), 323-329.

Jones, K. H., & Senft, J. A. (1985). An improved method to determine cell viability by simultaneous staining with fluorescein diacetate-propidium iodide. *Journal of Histochemistry & Cytochemistry, 33*(1), 77-79.

Jones, M. G. K. (1981). Host cell responses to endoparasitic nematode attack: structure and function of giant cells and syncytia. *Annals of Applied Biology, 97*, 353-372.

Jones, M. G. K., & Dropkin, V. H. (1975). Scanning electron microscopy of syncytical transfer cells induced in roots by cyst-nematodes. . *Physiological Plant Pathology I,*, 259-263.

Jones, M. G. K., & Northcote, D. H. (1972). Nematode-induced syncytium: a multinucleate transfer cell. *Journal of Cell Science, 10*, 789-809.

Karasov, T., Horton, M., & Bergelson, J. (2014). Genomic variability as a driver of plant-pathogen coevolution? *Current Opinion in Plant Biology, 18*, 24–30.

Karczmarek, A., Overmars, H., Helder, J., & Goverse, A. (2004). Feeding cell development by cyst and root-knot nematodes involves a similar early, local and transient activation of a specific auxin-inducible promoter element. *Molecular Plant Pathology, 5*(4), 343-346.

Kim, Y. H., Riggs, R. D., & Kim, K. S. (1987). Structural changes associated with resistance of soybean to *Heterodera glycines*. *Journal of Nematology, 19*(2), 177-187.

Kretschmer, J., Chalmers, K., Manning, S., Karakousis, A., Barr, A., Islam, A., Logue, S., Choe, Y., Barker, S., Lance, R., & Langridge, P. (1997). RFLP mapping of the *Ha2* cereal cyst nematode resistance gene in barley. *Theoretical and Applied Genetics, 94*, 1060-1064.

Krishnamurthy, P., Ranathunge, K., Nayak, S., Schreiber, L., & Mathew, M. (2011). Root apoplastic barriers block Na^+ transport to shoots in rice (*Oryza sativa* L.). *Journal of Experimental Botany, 62*, 4215-4228.

Kumari, C., Dutta, T. K., Banakar, P., & Rao, U. (2016). Comparing the defence-related gene expression changes upon root-knot nematode attack in susceptible versus resistant cultivars of rice. *Scientific Reports, 6*(1), 22846.

Kumsa, N. B. (2015). *Analysis of the Cre8 region of wheat chromosome 6B reveals a callose synthase gene as a candidate for resistance against cereal cyst nematode.* (Masters), The University of Adelaide, Adelaide, Australia.

Kurihara, D., Mizuta, Y., Sato, Y., & Higashiyama, T. (2015). ClearSee: a rapid optical clearing reagent for whole-plant fluorescence imaging. *Development, 142*, 4168-4179.

Kyndt, T., Vieira, P., Gheysen, G., & de Almeida-Engler, J. (2013). Nematode feeding sites: unique organs in plant roots. *Planta, 238*, 807-818.

Lee, C., Chronis, D., Kenning, C., Peret, B., Hewezi, T., Davis, E. L., Baum, T. J., Hussey, R., Bennett, M., & Mitchum, M. G. (2011a). The novel cyst nematode effector protein 19C07 interacts with the *Arabidopsis* auxin influx transporter LAX3 to control feeding site development. *Plant Physiol, 155*(2), 866-880.

Lee, C., Chronis, D., Kenning, C., Peret, B., Hewezi, T., Davis, E. L., Baum, T. J., Hussey, R., Bennett, M., & Mitchum, M. G. (2011b). Novel cyst nematode effector protein 19C07 interacts with the *Arabidopsis* auxin influx transporter LAX3 to control feeding site development. *Plant Physiology, 155*(2), 866-880.

Lilley, C. J., Atkinson, H. J., & Urwin, P. E. (2005). Molecular aspects of cyst nematodes. *Molecular Plant Pathology, 6*, 577-588.

Luxová, M. (1986). The hydraulic safety zone at the base of barley roots. *Planta, 169*, 465-470.

Maeda, H., & Ishida, N. (1967). Specificity of binding of hexopyranosyl polysaccharides with fluorescent brightener. *Journal of Biochemistry, 62*(2), 276-278.

Majda, M., & Robert, S. (2018). The role of auxin in cell wall expansion. *International Journal of Molecular Sciences, 19*(4), 951.

Martin, J. T. (1964). Role of cuticle in the defense against plant disease. *Annual Review of Phytopathology, 2*(1), 81-100.

Mason, A. S. (2017). *Polyploidy and hybridization for crop improvement*. Boca Raton, FL: CRC Press.

McBeth, C. W., Taylor, A., & Smith, A. (1941). Note on staining nematodes in root tissues. *Proceedings of the Helminthological Society of Washington, 8*, 26.

Meikle, P., Bonig, I., Hoogenraad, N., Clarke, A., & Stone, B. (1991). The location of (1→3)-β-glucans in the walls of pollen tubes of *Nicotiana alata* using a (1→3)-β-glucan-specific monoclonal antibody. *An International Journal of Plant Biology, 185*(1), 1-8.

Meikle, P. J., Hoogenraad, N. J., Bonig, I., Clarke, A. E., & Stone, B. A. (1994). A (1→3,1→4)-β-glucan-specific monoclonal antibody and its use in the quantitation and immunocytochemical location of (1→3,1→4)-β-glucans. *The Plant Journal, 5*(1), 1-9.

Melillo, M. T., Bleve-Zacheo, T., & Zacheo, G. (1992). Role of peroxidase and esterase isoenzymes in pea roots infected with *Heterodera goettingiana*. *Nematoligua Mediterranea, 20*, 171-179.

Melillo, M. T., Bleve-Zacheo, T., & Zacheo, G. (1993). Rapid lignin biosynthesis in pea roots infected with *Heterodera goettingiana*. *Giom. Bot. Ital. , 127*, 1202-1204.

Melino, V. J., Fiene, G., Enju, A., Cai, J., Buchner, P., & Heuer, S. (2015). Genetic diversity for root plasticity and nitrogen uptake in wheat seedlings. *Functional Plant Biology, 42*, 942-956.

Meon, S. (1978). *The physiology of tomato plants infected with root-knot nematode, Meloidogyne javanica.* (Doctor of Philosophy PhD thesis), The University of Adelaide, South Australia, Waite Agricultural Research Institute.

Milligan, S. B., Bodeau, J., Yaghoobi, J., Kaloshian, I., Zabel, P., & Williamson, V. M. (1998). The root knot nematode resistance gene Mi from tomato is a member of the leucine zipper, nucleotide binding, leucine-rich repeat family of plant genes. *Plant Cell, 10*(8), 1307-1319.

Müller, Rembock, & Wyss, U. (1981). Growth of *Heterodera schachtii* with remarks on amounts of food consumed. *Revue de Nematologie, 4*, 227-234.

Murray, G., & Brennan, J. (2009). The current and potential costs from diseases of wheat in Australia. In G. R. A. D. Corporation (Ed.). Australia.

Nicol, J. M., Turner, S. J., Coyne, D. L., Nijs, L. d., Hockland, S., & Maafi, Z. T. (2011). Current nematode threats to world agriculture. In: Jones J., Gheysen G., Fenoll C. (Eds) *Genomics and Molecular Genetics of Plant-Nematode Interactions*. (pp. 21-43) Springer, Dordrecht.

Nurnberger, T., Brunner, F., Kemmerling, B., & Piater, L. (2004). Innate immunity in plants and animals: striking similarities and obvious differences. *Immunological Reviews, 198*, 249-266.

O'Brien, P. C., & Fisher, J. M. (1977). Development of *Heterodera avenae* on resistant wheat and barley cultivars. *Nematologica.*

Ogbonnaya, F. C., Seah, S., Delibes, A., Jahier, J., López-Braña, I., Eastwood, R. F., & Lagudah, E. S. (2000). Molecular-genetic characterisation of a new nematode resistance gene in wheat. *Theoretical and Applied Genetics*. *102*, 623-629

Ohtsu, M., Sato, Y., Kurihara, D., Suzaki, T., Kawaguchi, M., Maruyama, D., & Higashiyama, T. (2017). Spatiotemporal deep imaging of syncytium induced by the soybean cyst nematode *Heterodera glycines*. *Protoplasma, 254*, 2107-2115.

Paal, J., Henselewski, H., Muth, J., Meksem, K., Menendez, C., Salamini, F., Ballvora, A., & Gebhardt, C. (2004). Molecular cloning of the potato *Gro1-4* gene conferring resistance to pathotype *Ro1* of the root cyst nematode *Globodera rostochiensis*, based on a candidate gene approach. . *The Plant Journal, 38*, 285-297.

Painter, R. H. (1951). Insect resistance in crop plants. *Soil Science, 72*(6), 481.

Patel, N., Hamamouch, N., Li, C., Hewezi, T., Hussey, R. S., Baum, T. J., Mitchum, M. G., & Davis, E. L. (2010). A nematode effector protein similar to annexins in host plants. *Journal of Experimental Botany, 61*(1), 235-248.

Paull, J. G., Chalmers, K. J., Karakousis, A., Kretschmer, J. M., Manning, S., & Langridge, P. (1998). Genetic diversity in Australian wheat varieties and breeding material based on RFLP data. *Theoretical and Applied Genetics, 96*, 435-446.

Pearce, S., Vazquez-Gross, H., Herin, S., Hane, D., Wang, Y., Gu, Y., & Dubcovsky, J. (2015). WheatExp: an RNA-seq expression database for polyploid wheat. *BMC Plant Biology, 15*, 299.

Perry, R. (1996). Chemoreception in plant parasitic nematodes. *Annual Review of Phytopathology, 34*(1), 181-199.

Perry, R., & Moens, M. (2011). Survival of parasitic nematodes outside the host. In R. Perry & D. Wharton (Eds.), *Molecular and Physiological Basis of Nematode Survival*. Wallingford, UK: CABI.

Pieterse, C. M., Van der Does, D., Zamioudis, C., Leon-Reyes, A., & Van Wees, S. C. (2012). Hormonal modulation of plant immunity. *Annual Review of Cell and Developmental Biology*, 28, 489-521.

Popeijus, H., Overmars, H., Jones, J., Blok, V., Goverse, A., Helder, J., Schots, A., Bakker, J., & Smant, G. (2000). Degradation of plant cell walls by a nematode. *Nature, 406*(6791) 36-37.

Ranjbar, G. (1997). *Production and utilization of doubled haploid lines in wheat breeding programs* (PhD) The University of Adelaide, Adelaide, Australia.

Rathjen, A. J., Eastwood, R. E., Lewis, J. G., & Dube, A. J. (1998). Breeding wheat for resistance to *Heterodera avenae* in southeastern Australia. *Euphytica, 100*, 55–62.

Riccardi, C., & Nicoletti, I. (2006). Analysis of apoptosis by propidium iodide staining and flow cytometry. *Nature Protocols, 1*(3), 1458-1461.

Rohde, R. A., & McClure, M. A. (1975). Autoradiography of developing syncytia in cotton roots infected with *Meloidogyne incognita*. *Journal of Nematology, 7*(1), 64-68.

Romero, M. D., Montes, M. J., Sin, E., Lopez-Brana, I., Duce, A., Martin-Sanchez, J. A., & Delibes, A. (1998). A cereal cyst nematode (*Heterodera avenae* Woll.) resistance gene transferred from *Aegilops triuncialis* to hexaploid wheat. *Theoretical and Applied Genetics, 96*, 1135-1140.

Ruan, Y.-L. (2007). Rapid cell expansion and cellulose synthesis regulated by plasmodesmata and sugar: insights from the single-celled cotton fibre. *Functional Plant Biology, 34*(1), 1-10.

Růžička, K., Ursache, R., Hejátko, J., & Helariutta, Y. (2015). Xylem development – from the cradle to the grave. *New Phytologist, 207*, 519-535.

Safari, E., Gororo, N. N., Eastwood, R. F., Lewis, J., Eagles, H. A., & Ogbonnaya, F. C. (2005). Impact of *Cre1, Cre8* and *Cre3* genes on cereal cyst nematode resistance in wheat. *Theoretical and Applied Genetics, 110*(3), 567-572.

Schenk, S., & Schikora, A. (2015). Staining of callose depositions in root and leaf tissues. *Bio-protocol 5*(6), e1429.

Seah, S., Miller, C., Sivasithamparam, K., & Lagudah, E. S. (2000). Root responses to cereal cyst nematode (*Heterodera avenae*) in hosts with different resistance genes. *New Phytologist, 146*, 527-533.

Sears, E. R. (1939). Cytogenetic studies with polyploid species of wheat. I. Chromosomal aberrations in the progeny of a haploid of *Triticum vulgare*. *Genetics*, 24(4), 509-523.

Sears, E. R. (1976). Genetic control of chromosome pairing in wheat. *Annual Review of Genetics* (10), 31-51.

Sears, E. R. (1981). Transfer of alien genetic material to wheat. In L. T. Evans & W. J. Peacock (Eds.), *Wheat science-today and tomorrow* (pp. 75–89.). Cambridge: Cambridge University Press.

Sears, E. R., & Miller, T. E. (1985). The history of Chinese Spring wheat. *Cereal Research Communications*, 13(2/3), 261-263

Sekhwal, M. K., Li, P., Lam, I., Wang, X., Cloutier, S., & You, F. M. (2015). Disease resistance gene analogs (RGAs) in plants. *International Journal of Molecular Sciences, 16*(8), 19248-19290.

Sheen, J., Zhou, L., & Jang, J-C. (1999). Sugars as signaling molecules. *Current Opinion in Plant Biology, 2*(5), 410-418.

Shirasu, K., Lahaye, T., Tan, M.-W., Zhou, F., Azevedo, C., & Schulze-Lefert, P. (1999). A novel class of eukaryotic zinc-binding proteins is required for disease resistance signaling in barley and development in *C. elegans. Cell, 99*, 355–366.

Sijmons, P. C., Grundler, F. M. W., von Mende, N., Burrows, P. R., & Wyss, U. (1991). *Arabidopsis thaliana* as a new model host for plant-parasitic nematodes. *The Plant Journal, 1*, 245-254.

Simonetti, E., Veronico, P., Melillo, M. T., Delibes, Á., Andrés, M. F., & López-Braña, I. (2009). Analysis of Class III peroxidase genes expressed in roots of resistant and susceptible wheat lines infected by *Heterodera avenae*. *Molecular Plant-Microbe Interactions, 22*(9), 1081-1092.

Smant, G., Stokkermans, J., Yan, Y., de Boer, J., Baum, T., Wang, X., Hussey, R., Gommers, F., Henrissat, B., Davis, E., Helder, J., Schots, A., & Bakker, J. (1998). Endogenous cellulases in animals: isolation of β-1, 4-endoglucanase genes from two species of plant-parasitic cyst nematodes. *Proceedings of the National Academy of Sciences of the United States of America, 95*, 4906-4911.

Smiley, R., Marshall, Gourlie, J., Paulitz, Kandel, S., Pumphrey, M., Garland-Campbell, K., Yan, Anderson, Flowers, & Jackson, C. (2013). Spring wheat tolerance and resistance to *Heterodera avenae* in the Pacific Northwest. *Plant Disease, 97*, 590-600.

Smiley, R. W., & Marshall, J. M. (2016). Detection of dual *Heterodera avenae* resistance plus tolerance traits in spring wheat. *Plant Disease, 100*(8), 1677-1685.

Sobczak, M. (1996). *Investigations on the structure of syncytia in roots of Arabidopsis thaliana induced by the beet cyst nematode Heterodera schachtii and its relevance to the sex of the nematode.* (PhD), University of Kiel, Kiel, Germany.

Sobczak, M., & Golinowski, W. (2009). Structure of cyst nematode feeding sites. In R. H. Berg & C. G. Taylor (Eds.), *Cell Biology of Plant Nematode Parasitism* (pp. 153-187). Berlin, Heidelberg: Springer Berlin Heidelberg.

Stein, O., & Granot, D. (2019). An overview of sucrose synthases in plants. *Frontiers in Plant Science, 10*, 95.

Stirling, G. R., & Stanton, J. (1997). Nematode diseases and their control. In J. F. Brown & H. J. Ogle (Eds.), *Plant Pathogens and Plant Diseases* (pp. 505-517). Armidale, NSW, Australia: Botany Department. University of New England.

Strock, C. F., Schneider, H. M., Galindo-Castaneda, T., Hall, B. T., Van Gansbeke, B., Mather, D. E., Roth, M. G., Chilvers, M. I., Guo, X., Brown, K., & Lynch, J. P. (2019). Laser ablation tomography for visualization of root colonization by edaphic organisms. *Journal of Experimental Botany*. *70*(19), 5327-5342.

Subbotin, S., Sturhan, D., Rumpenhorst, H., & Moens, M. (2002). Description of Australian cereal cyst nematode *Heterodera australis* sp. n. (Tylenchida: Heteroderidae). *Russian Journal of Nematology, 10*, 139-148.

Subbotin, S., Sturhan, D., Rumpenhorst, H., & Moens, M. (2003). Molecular and morphological characterisation of the *Heterodera avenae* species complex (Tylenchida: Heteroderidae). *Nematology, 5*, 515-538.

Taylor, C., Shepherd, K. W., & Langridge, P. (1998). A molecular genetic map of the long arm of chromosome 6R of rye incorporating the cereal cyst nematode resistance gene, *CreR*. *Theoretical and Applied Genetics, 97*(5), 1000-1012.

Tisi, A., Angelini, R., & Cona, A. (2011). Does polyamine catabolism influence root development and xylem differentiation under stress conditions? *Plant Signaling and Behavior, 6*(11), 1844-1847.

Trudgill, D. L. (1967). The effect of environment on sex determination in *Heterodera rostochiensis*. *13*(2), 263.

Trudgill, D. L. (1986). Concepts of resistance, tolerance and susceptibility in relation to cyst nematodes. In F. Lamberti & C. E. Taylor (Eds.), *Cyst Nematodes* (pp. 179-189). Boston, MA: Springer US.

Trudgill, D. L. (1991). Resistance to and tolerance of plant parasitic nematodes in plants. *Annual Review of Phytopathology, 29*, 167-192.

Ursache, R., Andersen, T. G., Marhavý, P., & Geldner, N. (2018). A protocol for combining fluorescent proteins with histological stains for diverse cell wall components. *The Plant Journal, 93*, 399-412.

Ursache, R., Miyashima, S., Chen, Q., Vaten, A., Nakajima, K., Carlsbecker, A., Zhao, Y., Helariutta, Y., & Dettmer, J. (2014). Tryptophan-dependent auxin biosynthesis is required for HD-ZIP III-mediated xylem patterning. *Development, 141*(6), 1250-1259.

van der Vossen, E., van der Voort, J., Kanyuka, K., Bendahmane, A., Sandbrink, H., Baulcombe, D., Bakker, J., Stiekema, W., & Klein-Lankhorst, R. (2000). Homologues of a single resistance-gene cluster in potato confer resistance to distinct pathogens: a virus and a nematode. . *The Plant Journal, 23*, 567-576.

Van Gansbeke, B. (2019). *Analysis of the barley cereal cyst nematode resistance locus Rha2.* (PhD), The University of Adelaide, Adelaide, Australia.

Van Gansbeke, B., Khoo, K. H. P., Lewis, J. G., Chalmers, K. J., & Mather, D. E. (2019). Fine mapping of *Rha2* in barley reveals candidate genes for resistance against cereal cyst nematode. *Theoretical and Applied Genetics*. *132*(5), 1309-1320.

Vanholme, B., De Meutter, J., Tytgat, T., Van Montagu, M., Coomans, A., & Gheysen, G. (2004). Secretions of plant-parasitic nematodes: a molecular update. *Gene, 332*, 13-27.

Verhertbruggen, Y., Walker, J. L., Guillon, F., & Scheller, H. V. (2017). A comparative study of sample preparation for staining and immunodetection of plant cell walls by light microscopy. *Frontiers in Plant Science, 8*(1505).

von Wangenheim, D., Hauschild, R., & Friml, J. (2017). Light sheet fluorescence microscopy of plant roots growing on the surface of a gel. *Journal of Visualized Experiments*(119), 55044.

Wang, D. Y-C., Kumar, S., & Hedges, B. S. (1999). Divergence time estimates for the early history of animal phyla and the origin of plants, animals and fungi. *Proceedings of the Royal Society of London, 266*, 163-171.

Wang, N., & Fisher, D. B. (1994). The use of fluorescent tracers to characterize the post-phloem transport pathway in maternal tissues of developing wheat grains. *Plant Physiology, 104*(1), 17.

Waterhouse, A., Bertoni, M., Bienert, S., Studer, G., Tauriello, G., Gumienny, R., Heer, F. T., de Beer, T. A P., Rempfer, C., Bordoli, L., Lepore, R., & Schwede, T. (2018). SWISS-MODEL: homology modelling of protein structures and complexes. *Nucleic Acids Research, 46*(W1), W296-W303.

Weaver, J. E. (1926). *Root development of field crops*. New York: McGraw-Hill Book Co. Inc.

Wei, Z., Qu, Z., Zhang, L., Zhao, S., Bi, Z., Ji, X., Wang, X., & Wei, H. (2015). Overexpression of poplar xylem sucrose synthase in tobacco leads to a thickened cell wall and increased height. *PLoS ONE, 10*(3), 1-20.

Williams, K. J., & Fisher, J. M. (1993). Development of *Heterodera avenae* Woll. and host cellular responses in susceptible and resistant wheat. *Fundamental and Applied Nematology, 16*, 417-423.

Williams, K. J., Lewis, J. G., Bogacki, P., Pallotta, M. A., Willsmore, K. L., Kuchel, H., & Wallwork, H. (2003). Mapping of a QTL contributing to cereal cyst nematode tolerance and resistance in wheat. *Australian Journal of Agricultural Research*. 54, 731-737.

Williams, K. J., Willsmore, K. L., Olson, S., Matic, M., & Kuchel, H. (2006). Mapping of a novel QTL for resistance to cereal cyst nematode in wheat. *Theoretical and Applied Genetics, 112*(8), 1480-1486.

Wright, K., & Oparka, K. J. (1996). The fluorescent probe HPTS as a phloem-mobile, symplastic tracer: an evaluation using confocal laser scanning microscopy. *Journal of Experimental Botany, 47*, 439-445.

Wyss, U., & Grundler, F. M. W. (1992). Feeding behavior of sedentary plant parasitic nematodes. *Netherlands Journal of Plant Pathology, 98*(2), 165-173.

Wyss, U., Stender, C., & Lehmann, H. (1984). Ultrastructure of feeding sites of the cyst nematode *Heterodera schachtii* Schmidt in roots of susceptible and resistant *Raphanus sativus* L. var. oleiformis Pers. cultivars. *Physiological Plant Pathology, 25*(1), 21-37.

Xiao, X., Tang, C., Fang, Y., Yang, M., Zhou, B., Qi, J., & Zhang, Y. (2014). Structure and expression profile of the sucrose synthase gene family in the rubber tree: indicative of roles in stress response and sucrose utilization in the laticifers. *FEBS Journal, 281*(1), 291-305.

Yue, J., Meyers, B., Chen, J., Tian, D., & Yang, S. (2012). Tracing the origin and evolutionary history of plant nucleotide-binding site-leucine-rich repeat (NBS-LRR) genes. *New Phytologist, 193*, 1049–1063.

Zadoks, J. C., Chang, T. T., & Konzak, C. F. (1974). A decimal code for the growth stages of cereals. *Weed Research, 14*(6), 415-421.

Zhang, L., Lilley, C. J., Imren, M., Knox, J. P., & Urwin, P. E. (2017). The complex cell wall composition of syncytia induced by plant parasitic cyst nematodes reflects both function and host plant. *Frontiers in Plant Science, 8*, 1087.

Zheng, Y., Anderson, S., Zhang, Y., & Garavito, R. M. (2011). The structure of sucrose synthase-1 from Arabidopsis thaliana and its functional implications. *The Journal of Biological Chemistry*, 286(41), 36108-36118.

Appendices

Appendix 1: Wheat hydroponic nutrient solution. Outline of the six stock solutions made in preparation for hydroponic tank and amounts of each stock solution to make final concentrations for a 10L tank.

Stock Solutions	Chemical	Molecular Weight (MW)	Stock [M]	g / L stock	mls stock/ 1.0 L growth soln.	Soln. Vol. (L)	mls stock to add for 10L hydroponics	Final Soln. [mM]
1	**$MgSO_4.7H2O$**	246.47	1.0	246.5	0.50	10	**5**	0.5
2	**KH_2PO_4**	136.09	1.0	136.1	0.50	10	**5**	0.5
3	**Trace Elements**							
	H_3BO_3	61.83	0.025	1.546	1.0	10	**10**	0.025
	$MnSO_4.H2O$	169.00	0.002	0.338	1.0	10		0.002
	$ZnSO_4.7H2O$	287.54	0.002	0.575	1.0	10		0.002
	$CuSO_4.5H2O$	249.68	0.0005	0.125	1.0	10		0.001
	$Na_2MoO_4.2H2O$	241.95	0.0005	0.121	1.0	10		0.001
	KCl	74.55	0.05	3.728	1.0	10		0.05
4	**Fe-EDTA**	367.10	0.1	36.71	0.50	10	**5.0**	0.05
5	**$Ca(NO_3)_2.4H2O$**	236.15	1.0	236.2	0.25	10	**2.5**	0.25
6	**KNO_3**	101.10	1.0	101.1	0.50	10	**5.0**	0.5

Appendix 2: Designed KASP™ primer sequences for Cre8 fine-mapping.

wri no.	SNP assay name	Allele-specific primer 1	Allele-specific primer 2	Common primer
wri355	Gene4_SNP1	GAAGGTGACCAAGTTCATGCTCATCAGTTAGCTAAAATTTGATAGTACTGA	GAAGGTCGGAGTCAACGGATTATCAGTTAGCTAAAATTTGATAGTACTGG	AGCTTACCATTGCCCAATCCACATTTAAA
wri356	Gene5_SNP1	GAAGGTGACCAAGTTCATGCTTTCATATCAATCATATTCATGTCTAACATTTT	GAAGGTCGGAGTCAACGGATTTCATATCAATCATATTCATGTCTAACATTTG	TAAGAGAGCATGTATCAGAGCTCACAA
wri357	Gene6_SNP1	GAAGGTGACCAAGTTCATGCTGCAAATTTTCACGGAAGTCCTCG	GAAGGTCGGAGTCAACGGATTAGGCAAATTTTCACGGAAGTCCTCA	GCTTTGATTCTCCTTGCTGAAATTGCTTA
wri358	Gene15_SNP1	GAAGGTGACCAAGTTCATGCTCAATGCAGCACATGTCCAATCCATTT	GAAGGTCGGAGTCAACGGATTAATGCAGCACATGTCCAATCCATTC	TTGAGGTCAACGATGTCTCAAGAAAGATT
wri359	Gene20_SNP1	GAAGGTGACCAAGTTCATGCTGTAAGCTAGGCACCCAGAATCTC	GAAGGTCGGAGTCAACGGATTGTAAGCTAGGCACCCAGAATCTT	CGTGTAAGAGGCTACTCCCTTTATAAATA
wri360	Gene23_SNP1	GAAGGTGACCAAGTTCATGCTGAGCAGCAAATACTTTAATCCATTTGCTT	GAAGGTCGGAGTCAACGGATTGCAGCAAATACTTTAATCCATTTGCTG	CTGAAAATATGATACTAGAAATCAGGGGTA
wri361	Gene23_SNP5	GAAGGTGACCAAGTTCATGCTGACGATCAGGTAGAAATCGTACG	GAAGGTCGGAGTCAACGGATTCGACGATCAGGTAGAAATCGTACA	GAAGCCGTGCTAGTTTTGAACAGGAT
wri362	Gene25_SNP1	GAAGGTGACCAAGTTCATGCTCCCATCTCTACTACTCTTCTTTGG	GAAGGTCGGAGTCAACGGATTAATCCCATCTCTACTACTCTTCTTTGA	AAATCGCTACCACGCCGGGCAA
wri363	Gene25_SNP11	GAAGGTGACCAAGTTCATGCTAGCCATCTGGCTTTTCATCTTTGTC	GAAGGTCGGAGTCAACGGATTAAGCCATCTGGCTTTTCATCTTTGTT	GATGCCATCGACGACTTCATGCAAA
wri364	Gene29_SNP1	GAAGGTGACCAAGTTCATGCTGTGCATGAGGAATCTGCAAAAGAGAT	GAAGGTCGGAGTCAACGGATTGCATGAGGAATCTGCAAAAGAGAC	GGACGATGATGATTTTTACTGTCTTGGTA
wri365	Gene32_SNP1	GAAGGTGACCAAGTTCATGCTCCCAATTAGACAAACTTTCATAGCTTAC	GAAGGTCGGAGTCAACGGATTAACCCAATTAGACAAACTTTCATAGCTTAT	CAGTTTAGTGCTTCAGTTAAACAGAGCAA
wri366	Gene32_SNP5	GAAGGTGACCAAGTTCATGCTCGGAGCATCGGCGACTCT	GAAGGTCGGAGTCAACGGATTCGGAGCATCGGCGACTCC	GAACCTGCGGCGCAGGTTGTT
wri367	Gene36_SNP1	GAAGGTGACCAAGTTCATGCTAGGACGAGGATCCTGATGTGG	GAAGGTCGGAGTCAACGGATTAGGACGAGGATCCTGATGTGC	CTCTCGCACCTCATTCATCCAAACTT
wri368	Gene40_SNP1	GAAGGTGACCAAGTTCATGCTAGATGTCAGAGGAGGAGGAACC	GAAGGTCGGAGTCAACGGATTAAGATGTCAGAGGAGGAGGAACA	CTCATTCATCCAAACTTTATCYTGCACAT
wri369	Gene40_SNP7	GAAGGTGACCAAGTTCATGCTCATCGATGACTTCATGAAACATGTTGAT	GAAGGTCGGAGTCAACGGATTATCGATGACTTCATGAAACATGTTGAC	GCCTTCATCTTCCCTAGCRAGCT
wri370	Gene41_SNP1	GAAGGTGACCAAGTTCATGCTCGGTGACAAGTACAAGCGTTTCAAT	GAAGGTCGGAGTCAACGGATTCGGTGACAAGTACAAGCGTTTCAAA	GTCGGTGAGGGACTTGRTATCCTT
wri371	Gene41_SNP4	GAAGGTGACCAAGTTCATGCTCGACGACTTCATGTTGTGTGTCG	GAAGGTCGGAGTCAACGGATTATCGACGACTTCATGTTGTGTGTCA	ATGCCATCTGGCTTAGTGTCTTTATCAT
wri372	Gene27_SNP4	GAAGGTGACCAAGTTCATGCTCGACGGCCGAGACCCTGC	GAAGGTCGGAGTCAACGGATTCGACGGCCGAGACCCTGT	GTATAATGGTTGGAAATTCATGGGTGCAA
wri373	Gene27_SNP1	GAAGGTGACCAAGTTCATGCTGTTGCACACAGAGTGGTCATTTTG	GAAGGTCGGAGTCAACGGATTGTTGCACACAGAGTGGTCATTTTA	CACGTTGTGGTGGCAACAGTTACTA
wri374	Gene43_SNP1	GAAGGTGACCAAGTTCATGCTCACTTTGCGTTTGCACTTCTGTTGT	GAAGGTCGGAGTCAACGGATTACTTTGCGTTTGCACTTCTGTTGC	CAACACCTCTGCGTTCTCAATCCTA
wri375	Gene45_INDEL1	GAAGGTGACCAAGTTCATGCTGTCGAGATCCTGGGTATATATATATAG	GAAGGTCGGAGTCAACGGATTAAGTCGAGATCCTGGGTATATATATATAT	GCTGCTGCTGCTGTATTAATTAATCCTTA
wri376	Gene45_SNP1	GAAGGTGACCAAGTTCATGCTATGTCTAGTTAGCTCACTCACTGC	GAAGGTCGGAGTCAACGGATTATGTCTAGTTAGCTCACTCACTGG	GTGATGGACGGAGCATAAATAAACATGAT
wri377	Gene7_INDEL1	GAAGGTGACCAAGTTCATGCTCGATGCTAAATTCTCATGCAAATACGA	GAAGGTCGGAGTCAACGGATTCGATGCTAAATTCTCATGCAAATACGT	CAATCGAAAGAGAAGCAGCAGACCAT
wri378	Gene47_SNP1	GAAGGTGACCAAGTTCATGCTAAACAGGTTCGGTATAAACCAGAATG	GAAGGTCGGAGTCAACGGATTCATAAACAGGTTCGGTATAAACCAGAATA	GCAGTTCATGTATTTGAGCTGTCACATTA
wri379	Gene48_SNP1	GAAGGTGACCAAGTTCATGCTATATTAAGTGCACACAGAGGCTACG	GAAGGTCGGAGTCAACGGATTATATTAAGTGCACACAGAGGCTACC	ATTTTGCTGCTGAGGTAAAACAAATGACTA
wri380	CS455800_SNP1	GAAGGTGACCAAGTTCATGCTGTCGCCCTCGCCGGCTC	GAAGGTCGGAGTCAACGGATTGTCGCCCTCGCCGGCTT	CTCAAACAGTCCTCCGGTGGTGAT
wri381	CS467800_SNP1	GAAGGTGACCAAGTTCATGCTGCCTGGCGGACCTGGC	GAAGGTCGGAGTCAACGGATTCTGCCTGGCGGACCTGGT	AGTGGCCGCACCGCGGCA

wri382	CS467800_SNP2	GAAGGTGACCAAGTTCATGCTGCCACCATCATCGACTCGTCAA	GAAGGTCGGAGTCAACGGATTCCACCATCATCGACTCGTCAG	TGGCGCCGGCGGCGAGCA
wri383	CS470600_SNP1	GAAGGTGACCAAGTTCATGCTCACCAAGACATCAAGCCCGGT	GAAGGTCGGAGTCAACGGATTCACCAAGACATCAAGCCCGGC	GCGCCGCCAAGGAGGACGTT
wri384	Gene23_SNP3	GAAGGTGACCAAGTTCATGCTGGATCACTCTTCAGATCTGTGCTT	GAAGGTCGGAGTCAACGGATTGATCACTCTTCAGATCTGTGCTC	CCACCTCTTCTATCAAGTATGGTATACAT
wri385	Gene23_SNP4	GAAGGTGACCAAGTTCATGCTGACTGAGATTATACCTCAACATGTAACA	GAAGGTCGGAGTCAACGGATTACTGAGATTATACCTCAACATGTAACG	CTTCTTCACGGACAACAGGGTCAAT
wri386	Gene32_SNP2	GAAGGTGACCAAGTTCATGCTCAGGCATTCGAGTAAATGGGTGG	GAAGGTCGGAGTCAACGGATTCAGGCATTCGAGTAAATGGGTGA	GCAACAGTTGCTCTGCACAAAACCAT
wri387	Gene32_SNP3	GAAGGTGACCAAGTTCATGCTCCATTTACTCGAATGCCTGAGCA	GAAGGTCGGAGTCAACGGATTCCATTTACTCGAATGCCTGAGCG	GCGGCTGAAAAGAAAGTACACTCATTAAT
wri389	CS456200_SNP3	GAAGGTGACCAAGTTCATGCTGACGGAGGCCTCACGGTG	GAAGGTCGGAGTCAACGGATTGGACGGAGGCCTCACGGTT	GAGCATGTTGAGCGCCATGAAACAT
wri390	CS472000_SNP1	GAAGGTGACCAAGTTCATGCTGAGTCCTTCCTGCTTGATCTGCT	GAAGGTCGGAGTCAACGGATTAGTCCTTCCTGCTTGATCTGCG	AGTTCGGACCAAGAGTCGTTTCCAA
wri391	CS445700_INDEL1	GAAGGTGACCAAGTTCATGCTATAGACCATGCAGAGCTTTCCATC	GAAGGTCGGAGTCAACGGATTCATAGACCATGCAGAGCTTTCCATT	GCAACAGACGGTGTTTCCATGGTT
wri392	CS466700_INDEL1	GAAGGTGACCAAGTTCATGCTCGCGGCGCGCGGGGC	GAAGGTCGGAGTCAACGGATTCGCGGCGCGCGGGGG	CCCAACGGCCCTGCGGCTA
wri393	CS466700_SNP1	GAAGGTGACCAAGTTCATGCTCTTCCATTGCTTGGCGCAGG	GAAGGTCGGAGTCAACGGATTCTTCCATTGCTTGGCGCAGC	GCCGCAGGGCCGTTGGGC
wri394	Gene28_INDEL1	GAAGGTGACCAAGTTCATGCTGGCGGGAGGCAGAAAGCCTA	GAAGGTCGGAGTCAACGGATTGCGGGAGGCAGAAAGCCTC	CTAGCCGCCGCCTCCTCCTT
wri395	Gene37_SNP1	GAAGGTGACCAAGTTCATGCTCCTCATCCAGCCCCATATTCGT	GAAGGTCGGAGTCAACGGATTCTCATCCAGCCCCATATTCGG	CTGGTACAAGGAAGAAGAGGACCTT
wri396	CS471000_SNP3	GAAGGTGACCAAGTTCATGCTCGCCACGACAGGGCTCTGT	GAAGGTCGGAGTCAACGGATTGCCACGACAGGGCTCTGC	TAGGAACCAAAGAAGAGCATGATGAAGAA
wri397	CS471000_SNP4	GAAGGTGACCAAGTTCATGCTTTGGAGAACAAGGAACTGTCACCA	GAAGGTCGGAGTCAACGGATTGGAGAACAAGGAACTGTCACCG	CAATTTCAAGGACGAGAGCAGCCTT
wri398	CS471000_SNP5	GAAGGTGACCAAGTTCATGCTGCGAATGTTGTCAAAGGAAGCTCT	GAAGGTCGGAGTCAACGGATTCGAATGTTGTCAAAGGAAGCTCG	TATGTGGAGAGAGCAGTTGCGCTA
wri399	CS288600_SNP1	GAAGGTGACCAAGTTCATGCTCCTCCACGTCCTCCGGC	GAAGGTCGGAGTCAACGGATTCCTCCACGTCCTCCGGG	TCGCCTTCGCCTGCAAGTCCAT
wri400	CS471100_SNP2	GAAGGTGACCAAGTTCATGCTATAACTCATAAAATTGGACAAGGTGGC	GAAGGTCGGAGTCAACGGATTCATAACTCATAAAATTGGACAAGGTGGT	ACAAGCTCAGCATAATAAACAGCACCAAA
wri401	CS471600_SNP1	GAAGGTGACCAAGTTCATGCTCAACCGAGAGCGTGAGAGGC	GAAGGTCGGAGTCAACGGATTGCAACCGAGAGCGTGAGAGGA	AGGAGAAGAGCGAGCTGCCCAT
wri402	CS471600_2_SNP1	GAAGGTGACCAAGTTCATGCTTTGCCTGCATCGCCTGCC	GAAGGTCGGAGTCAACGGATTCTTTGCCTGCATCGCCTGCA	ATGGCCTTTCTCCTGCTGATGACAA
wri403	CS471600_SNP2	GAAGGTGACCAAGTTCATGCTCACCAACCTGTCGGATGAGCTTT	GAAGGTCGGAGTCAACGGATTACCAACCTGTCGGATGAGCTTC	GCAAGCACATGGTGGCTATGAACTA
wri404	Gene2_INDEL1	GAAGGTGACCAAGTTCATGCTGGTGGAACTCTTCTTCTTCTTCTTCA	GAAGGTCGGAGTCAACGGATTGGTGGAACTCTTCTTCTTCTTCTCT	GTCGAGGCAAACACCGAGGACAT
wri405	Gene2_SNP1	GAAGGTGACCAAGTTCATGCTTTGCCTGCATCGCCTGCC	GAAGGTCGGAGTCAACGGATTCTTTGCCTGCATCGCCTGCA	ATGGCCTTTCTCCTGCTGATGACAA
wri406	CS466700_INDEL2	GAAGGTGACCAAGTTCATGCTGCCGTGCTGCACGTGGCA	GAAGGTCGGAGTCAACGGATTGCCGTGCTGCACGTGGCG	CCCAACGGCCCTGCGGCTA
wri407	CS471100_SNP3	GAAGGTGACCAAGTTCATGCTTATGTTGAAGCCTTCTGTAGCATTG	GAAGGTCGGAGTCAACGGATTGTTATGTTGAAGCCTTCTGTAGCATTA	ACAGTTGACAAATCAGTCGAGTTCACATA
wri408	CS471100_SNP4	GAAGGTGACCAAGTTCATGCTCAGCACCAAAACCACCTTGTCCT	GAAGGTCGGAGTCAACGGATTCAGCACCAAAACCACCTTGTCCA	CTTTTCAATGCTACAGAAGGCTTCAACAT
wri409	CS471100_SNP5	GAAGGTGACCAAGTTCATGCTGACAAGGTGGCTTTGGTGCTGTT	GAAGGTCGGAGTCAACGGATTACAAGGTGGCTTTGGTGCTGTC	ATTTTTTGAACTAACCTCGCCTACAAGCT
wri410	TM1023227_SNP1	GAAGGTGACCAAGTTCATGCTTAAAGATGGTGATAGAAACACCAAT	GAAGGTCGGAGTCAACGGATTGCTTAAAGATGGTGATAGAAACACCAAA	GCCAAACCGCCTTCCGATGGAA
wri411	TM4002555_SNP1	GAAGGTGACCAAGTTCATGCTGGCCTGCGGCTCCTCCG	GAAGGTCGGAGTCAACGGATTGGCCTGCGGCTCCTCCA	AACACGAGCAGCTGCAGCTGCA
wri412	TM4989718_SNP1	GAAGGTGACCAAGTTCATGCTGAACATCGGCCTGTGCTCC	GAAGGTCGGAGTCAACGGATTCTGAACATCGGCCTGTGCTCT	GCAACAGATGCACCAGGACGAGAA

wri413	TM4990960_SNP1	GAAGGTGACCAAGTTCATGCTGCAGCGTGGGCTGCGAC	GAAGGTCGGAGTCAACGGATTCTGCAGCGTGGGCTGCGAT	TCGTGTCCTTGGGGGCGTAGTA
wri414	Gene28_SNP1	GAAGGTGACCAAGTTCATGCTCTTTGCTTGGCAAGATTAATGTT	GAAGGTCGGAGTCAACGGATTGCTCTTTGCTTGGCAAGATTAATGTG	ACACCTAAAATCTCACCAGGCATCATTTT
wri415	Gene28_SNP2	GAAGGTGACCAAGTTCATGCTGGAATAATGTTAATACAGTTTGCTCTTTGT	GAAGGTCGGAGTCAACGGATTGAATAATGTTAATACAGTTTGCTCTTTGC	GTAACATGCAGTGGAGTAACCAATCTATA
wri416	PGene815_2_4_SNP1	GAAGGTGACCAAGTTCATGCTAGGCGCAAGAAACAGATCGATCAA	GAAGGTCGGAGTCAACGGATTGGCGCAAGAAACAGATCGATCAG	CCTCCTATTTAAATTAATCCAGCCATTGAA
wri417	CS471300_SNP1	GAAGGTGACCAAGTTCATGCTTGCCTACGCGCCGCTT	GAAGGTCGGAGTCAACGGATTCTTGCCTACGCGCCGCTG	CGTCGATGATCCGGACACCGAT
wri418	CS445700_SNP1	GAAGGTGACCAAGTTCATGCTGACCATGCAGAGCTTTCCATCC	GAAGGTCGGAGTCAACGGATTATAGACCATGCAGAGCTTTCCATCT	GCAACAGACGGTGTTTCCATGGTT
wri419	TM1091698_SNP1	GAAGGTGACCAAGTTCATGCTAAACAGAATCGTAACGGCACGAC	GAAGGTCGGAGTCAACGGATTAAACAGAATCGTAACGGCACGAG	TGCAGCCTGCGCCGCGATTTTT
wri420	TM1116764_SNP1	GAAGGTGACCAAGTTCATGCTACATGCTACTGCATGCCACCG	GAAGGTCGGAGTCAACGGATTGTACATGCTACTGCATGCCACCA	CCGGCCCGGTCATCGTCGT
wri421	TM3942671_SNP1	GAAGGTGACCAAGTTCATGCTCCGACGCCTGCGACGCG	GAAGGTCGGAGTCAACGGATTGCCGACGCCTGCGACGCA	CCGGCCTGGAGGTGCACGTA
wri422	CS298900_SNP1	GAAGGTGACCAAGTTCATGCTGATGAGGATGGTCAAATTGGAAGTG	GAAGGTCGGAGTCAACGGATTGATGAGGATGGTCAAATTGGAAGTT	CCCTCTTCCACCTCTACATCTTCTT
wri423	CS298900_SNP2	GAAGGTGACCAAGTTCATGCTCAACTTCAGTGTCACCCTCAC	GAAGGTCGGAGTCAACGGATTCTCAACTTCAGTGTCACCCTCAT	CAGATGATGATCAATCAGAAGAGGAAGAA
wri424	CS439600_SNP1	GAAGGTGACCAAGTTCATGCTGGCCTCACCAACTGCGCC	GAAGGTCGGAGTCAACGGATTCGGCCTCACCAACTGCGCT	TGGCAGCCGCGGAGGGCAT
wri425	CS446200_SNP1	GAAGGTGACCAAGTTCATGCTAGAAGACAGTCCACATCTTAGCG	GAAGGTCGGAGTCAACGGATTCTAGAAGACAGTCCACATCTTAGCA	GTGCCCAATTGTATGTAAAAACATCGCTA
wri426	CS450400_SNP1	GAAGGTGACCAAGTTCATGCTCCTTGGCGAAGAGCTCCATTAC	GAAGGTCGGAGTCAACGGATTCCTTGGCGAAGAGCTCCATTAT	CAATGGTGTTCTTCGACGTGACCAT
wri427	CS466600_SNP1	GAAGGTGACCAAGTTCATGCTCCTTGTCAACCTGGTCATCGTC	GAAGGTCGGAGTCAACGGATTACCTTGTCAACCTGGTCATCGTT	CTCCTCGATCTCTTCTCTGTCGTTT
wri428	CS466600_SNP2	GAAGGTGACCAAGTTCATGCTCCTGAGCTGGTACTTGTCCATC	GAAGGTCGGAGTCAACGGATTCCCTGAGCTGGTACTTGTCCATT	GAGGAGATCAACAAGATGCACAGCTT
wri429	CS471400_SNP1	GAAGGTGACCAAGTTCATGCTGCATCTTTGCAAACACGTGTTGTTC	GAAGGTCGGAGTCAACGGATTGCATCTTTGCAAACACGTGTTGTTG	TCCGGAGGCATGTAACCGAATGTA
wri430	CS471400_SNP2	GAAGGTGACCAAGTTCATGCTGAATCTAGCGCAATCCGAACA	GAAGGTCGGAGTCAACGGATTCTGAATCTAGCGCAATCCGAACT	GTTATGAGCCTCTTTCTTGGGCTGAA
wri431	CS496900_SNP1	GAAGGTGACCAAGTTCATGCTGCACATGCGCTCTCCGATTGT	GAAGGTCGGAGTCAACGGATTGCACATGCGCTCTCCGATTGA	GGCCAAGCAAGTCATCCATCTCAAA
wri432	CS496900_SNP2	GAAGGTGACCAAGTTCATGCTGGAACAATCGGAGAGCGCATG	GAAGGTCGGAGTCAACGGATTGGAACAATCGGAGAGCGCATC	GGGCACAAAGCGACTGATAATGGTA
wri433	CS7B497000_SNP1	GAAGGTGACCAAGTTCATGCTGCATTCAGTTCAGTACCAATCAA	GAAGGTCGGAGTCAACGGATTCTGCATTCAGTTCAGTACCAATCAG	ATGCCTGGTCCGGTGCCTGAAT
wri434	CSU071900_SNP1	GAAGGTGACCAAGTTCATGCTACCACAAGACCAAGTACGCGTC	GAAGGTCGGAGTCAACGGATTCACCACAAGACCAAGTACGCGTT	CCGGGCCGACACCGTTGTAAAT
wri435	CSU072000_SNP1	GAAGGTGACCAAGTTCATGCTCGTGTCGCTCCCGGTGTAC	GAAGGTCGGAGTCAACGGATTCGTGTCGCTCCCGGTGTAG	GGACGGCACCGGGGAGGAA
wri436	CSU072000_SNP2	GAAGGTGACCAAGTTCATGCTGCGACCTTCTCATATACCGTGC	GAAGGTCGGAGTCAACGGATTGGCGACCTTCTCATATACCGTGT	CAGGCTCAAGAACACGGCAGCT
wri437	CSU072000_SNP3	GAAGGTGACCAAGTTCATGCTGGCGAGCAAGGCGCAGC	GAAGGTCGGAGTCAACGGATTGGCGAGCAAGGCGCAGG	GCTGGAGTCGTCCTGCGCGTT
wri438	CSU072000_SNP4	GAAGGTGACCAAGTTCATGCTACGTACACCGACATGATCAAGTCT	GAAGGTCGGAGTCAACGGATTCGTACACCGACATGATCAAGTCC	TGCTCGCCAGCTTCTTGCCGTA
wri439	CS471400_SNP3	GAAGGTGACCAAGTTCATGCTCAGGTTAATTTGCCGTTTCAATGTTC	GAAGGTCGGAGTCAACGGATTCAGGTTAATTTGCCGTTTCAATGTTG	CAATAACCAATCAAGCGCACCTGCAT

Appendix 3: Tube Test Results. Marker genotype as Molineux (M, resistant), Trident (T, susceptible), heterozygous (H), or no result (-) for each TMDH06/TMDH82 plant from generations F3 to F9 and the number of CCN females as assessed using a CCN tube test. For each test date, a series of control plants were tested and are listed at the end of each test date.

Test Date	Generation	Plant	wri16	wri13	BS00109879	Gene20	Gene4	Gene15	Gene37	Gene23	Gene32	Gene2	CS471400_SNP1	CS471400_SNP2	Gene28	CS471100_SNP2	CSU072000_SNP4	TM4989718_SNP1	CS78497000_SNP1	CSU071900_SNP1	TM1023227_SNP1	CS466700_INDEL1	Gene48	BS0022444	CCN female count
March 2016	F3	TM10-311-S1	M	M	M						T													T	44
March 2016	F3	TM22-789-S2	M	M	M						T													T	50
March 2016	F3	TM44-1669-S1	M	M	M						T													T	57
March 2016	F3	TM44-1669-S3	M	M	M						T													T	54
March 2016	F3	TM52-2014-S4	M	M	M						T													T	57
March 2016	F3	TM54-2100-S1	M	M	M						T													T	48
March 2016	F3	TM54-2100-S2	M	M	M						T													T	61
March 2016	F3	TM27-996-S4	M	M	M						T													T	54
March 2016	F3	TM37-1397-S2	M	M	M						T													T	62
March 2016	F3	TM44-1620-S1	M	M	M						T													T	59
March 2016	F3	TM14-538-S2	M	M	M						M_													T	14
March 2016	F3	TM14-538-S3	M	M	M						M_													T	15
March 2016	F3	TM14-538-S4	M	M	M						M_													T	20
March 2016	F3	TM48-1872-S2	M	M	M						M_													T	15
March 2016	F3	TM53-2049-S2	M	M	M						M_													T	22
March 2016	F3	TM54-2107-S1	M	M	M						M_													T	24
March 2016	F3	TM70-2718-S1	M	M	M						M_													T	20
March 2016	F3	TM13-444-S3	M	M	M						M_													T	42
March 2016	F3	TM20-708-S4	M	M	M						M_													T	44
March 2016		TMDH06	M	M	M						M													M	4
March 2016		TMDH06	M	M	M						M													M	9
March 2016		TMDH06	M	M	M						M													M	13
March 2016		TMDH06	M	M	M						M													M	16
March 2016		TMDH06	M	M	M						M													M	19
March 2016		TMDH06	M	M	M						M													M	22
March 2016		TMDH06	M	M	M						M													M	23
March 2016		TMDH06	M	M	M						M													M	24
March 2016		TMDH06	M	M	M						M													M	27
March 2016		TMDH06	M	M	M						M													M	30

March 2016		TMDH82	T	T	T					T	T	33
March 2016		TMDH82	T	T	T					T	T	50
March 2016		TMDH82	T	T	T					T	T	54
March 2016		TMDH82	T	T	T					T	T	55
March 2016		TMDH82	T	T	T					T	T	58
March 2016		TMDH82	T	T	T					T	T	64
March 2016		TMDH82	T	T	T					T	T	65
Dec. 2016	F4	TM22-790-S3-S13	M	M	M	M	M	M	M	M	M	T	0
Dec. 2016	F4	TM22-790-S3-S2	M	M	M	M	M	M	M	M	M	T	1
Dec. 2016	F4	TM14-538-S1-S10	M	M	M	M	M	M	M	M	M	T	2
Dec. 2016	F4	TM13-444-S2-S12	M	M	M	M	M	M	M	M	M	T	4
Dec. 2016	F4	TM14-538-S1-S8	M	M	M	M	M	M	M	M	M	T	4
Dec. 2016	F4	TM20-708-S3-S12	M	M	M	M	M	M	M	M	M	T	4
Dec. 2016	F4	TM22-790-S3-S15	M	M	M	M	M	M	M	M	M	T	4
Dec. 2016	F4	TM22-790-S2-S6	M	M	M	M	M	M	M	M	M	T	5
Dec. 2016	F4	TM53-2049-S3-S4	M	M	M	M	M	M	M	M	M	T	5
Dec. 2016	F4	TM13-444-S1-S4	M	M	M	M	M	M	M	M	M	T	6
Dec. 2016	F4	TM14-538-S1-S14	M	M	M	M	M	M	M	M	M	T	6
Dec. 2016	F4	TM14-538-S1-S15	M	M	M	M	M	M	M	M	M	T	6
Dec. 2016	F4	TM22-790-S1-S4	M	M	M	M	M	M	M	M	M	T	6
Dec. 2016	F4	TM13-444-S2-S3	M	M	M	M	M	M	M	M	M	T	7
Dec. 2016	F4	TM20-708-S2-S8	M	M	M	M	M	M	M	M	M	T	7
Dec. 2016	F4	TM22-790-S1-S5	M	M	M	M	M	M	M	M	M	T	7
Dec. 2016	F4	TM70-2718-S3-S10	M	M	M	M	M	M	M	M	M	T	7
Dec. 2016	F4	TM13-444-S2-S6	M	M	M	M	M	M	M	M	M	T	8
Dec. 2016	F4	TM22-790-S1-S2	M	M	M	M	M	M	M	M	M	T	8
Dec. 2016	F4	TM22-790-S1-S6	M	M	M	M	M	M	M	M	M	T	8
Dec. 2016	F4	TM22-790-S3-S3	M	M	M	M	M	M	M	M	M	T	8
Dec. 2016	F4	TM13-444-S2-S9	M	M	M	M	M	M	M	M	M	T	9
Dec. 2016	F4	TM22-790-S1-S12	M	M	M	M	M	M	M	M	M	T	9
Dec. 2016	F4	TM70-2718-S3-S11	M	M	M	M	M	M	M	M	M	T	9
Dec. 2016	F4	TM14-538-S1-S9	M	M	M	M	M	M	M	M	M	T	10
Dec. 2016	F4	TM22-790-S1-S7	M	M	M	M	M	M	M	M	M	T	10
Dec. 2016	F4	TM13-444-S2-S13	M	M	M	M	M	M	M	M	M	T	11
Dec. 2016	F4	TM20-708-S3-S10	M	M	M	M	M	M	M	M	M	T	11
Dec. 2016	F4	TM22-790-S2-S14	M	M	M	M	M	M	M	M	M	T	11
Dec. 2016	F4	TM20-708-S3-S2	M	M	M	M	M	M	M	M	M	T	12
Dec. 2016	F4	TM20-708-S3-S3	M	M	M	M	M	M	M	M	M	T	12
Dec. 2016	F4	TM48-1872-S3-S8	M	M	M	M	M	M	M	M	M	T	12
Dec. 2016	F4	TM20-708-S3-S13	M	M	M	M	M	M	M	M	M	T	13
Dec. 2016	F4	TM22-790-S1-S11	M	M	M	M	M	M	M	M	M	T	13
Dec. 2016	F4	TM22-790-S3-S1	M	M	M	M	M	M	M	M	M	T	13

Dec. 2016	F4	TM22-790-S2-S13	M	M	M	M	M	M	M	M	M	T	14
Dec. 2016	F4	TM22-790-S3-S12	M	M	M	M	M	M	M	M	M	T	14
Dec. 2016	F4	TM13-444-S1-S13	M	M	M	M	M	M	M	M	M	T	16
Dec. 2016	F4	TM22-790-S3-S4	M	M	M	M	M	M	M	M	M	T	16
Dec. 2016	F4	TM70-2718-S3-S14	M	M	M	M	M	M	M	M	M	T	16
Dec. 2016	F4	TM20-708-S2-S11	M	M	M	M	M	M	M	M	M	T	18
Dec. 2016	F4	TM70-2718-S3-S3	M	M	M	M	M	M	M	M	M	T	19
Dec. 2016	F4	TM20-708-S3-S8	M	M	M	M	M	M	M	M	M	T	20
Dec. 2016	F4	TM22-789-S4-S7	M	M	M	M	M	M	T	T	T	T	12
Dec. 2016	F4	TM22-789-S4-S6	M	M	M	M	M	M	T	T	T	T	16
Dec. 2016	F4	TM22-789-S4-S1	M	M	M	M	M	M	T	T	T	T	21
Dec. 2016	F4	TM22-789-S3-S4	M	M	M	M	M	M	T	T	T	T	26
Dec. 2016	F4	TM22-789-S4-S14	M	M	M	M	M	M	T	T	T	T	31
Dec. 2016	F4	TM22-789-S4-S11	M	M	M	M	M	M	T	T	T	T	32
Dec. 2016	F4	TM22-789-S4-S2	M	M	M	M	M	M	T	T	T	T	32
Dec. 2016	F4	TM22-789-S4-S4	M	M	M	M	M	M	T	T	T	T	32
Dec. 2016	F4	TM22-789-S4-S12	M	M	M	M	M	M	T	T	T	T	36
Dec. 2016	F4	TM22-789-S4-S3	M	M	M	M	M	M	T	T	T	T	39
Dec. 2016	F4	TM22-789-S4-S8	M	M	M	M	M	M	T	T	T	T	39
Dec. 2016	F4	TM22-789-S1-S1	M	M	M	M	M	M	T	T	T	T	40
Dec. 2016	F4	TM22-789-S4-S10	M	M	M	M	M	M	T	T	T	T	40
Dec. 2016	F4	TM22-789-S4-S9	M	M	M	M	-	M	T	T	T	T	42
Dec. 2016	F4	TM22-789-S1-S13	M	M	M	M	M	M	T	T	T	T	43
Dec. 2016	F4	TM22-789-S4-S15	M	M	M	M	M	M	T	T	T	T	43
Dec. 2016	F4	TM22-789-S4-S13	M	M	M	M	M	M	T	T	T	T	45
Dec. 2016	F4	TM22-789-S1-S14	M	M	M	M	M	M	T	M	T	T	51
Dec. 2016	F4	TM73-2850-S3-S11	M	M	M	M	M	T	T	T	T	T	3
Dec. 2016	F4	TM73-2850-S4-S13	M	M	M	M	M	T	T	T	T	T	5
Dec. 2016	F4	TM73-2850-S3-S6	M	M	M	M	M	T	T	T	T	T	12
Dec. 2016	F4	TM10-311-S2-S5	M	M	M	M	M	T	T	T	T	T	20
Dec. 2016	F4	TM73-2850-S4-S6	M	M	M	M	M	T	T	T	T	T	22
Dec. 2016	F4	TM54-2100-S3-S5	M	M	M	M	M	T	T	T	T	T	25
Dec. 2016	F4	TM10-311-S2-S1	M	M	M	M	M	T	T	T	T	T	26
Dec. 2016	F4	TM73-2850-S2-S1	M	M	M	M	M	T	T	T	T	T	26
Dec. 2016	F4	TM54-2100-S3-S10	M	M	M	M	M	T	T	T	T	T	28
Dec. 2016	F4	TM73-2850-S4-S4	M	M	M	M	M	T	T	T	T	T	29
Dec. 2016	F4	TM73-2850-S2-S6	M	M	M	M	M	T	T	T	T	T	30
Dec. 2016	F4	TM54-2100-S3-S7	M	M	M	M	M	T	T	T	T	T	36
Dec. 2016	F4	TM54-2100-S3-S14	M	M	M	M	M	T	T	T	T	T	37
Dec. 2016	F4	TM10-311-S2-S9	M	M	M	M	M	T	T	T	T	T	38
Dec. 2016	F4	TM73-2850-S4-S1	M	M	M	M	M	T	T	T	T	T	39
Dec. 2016	F4	TM71-2754-S3-S8	M	M	M	M	M	T	T	T	T	T	40

Dec. 2016	F4	TM10-311-S2-S8	M	M	M	M	M	T	T	T	T	T	42
Dec. 2016	F4	TM71-2754-S3-S3	M	M	M	M	M	T	T	T	T	T	44
Dec. 2016	F4	TM71-2754-S1-S11	M	M	M	M	M	T	T	T	T	T	47
Dec. 2016	F4	TM73-2850-S2-S9	M	M	M	M	M	T	T	T	T	T	48
Dec. 2016	F4	TM73-2850-S3-S3	M	M	M	M	M	T	T	T	T	T	50
Dec. 2016	F4	TM20-724-S1-S9	M	M	M	M	T	T	T	T	T	T	11
Dec. 2016	F4	TM20-724-S1-S12	M	M	M	M	T	T	T	T	T	T	14
Dec. 2016	F4	TM20-724-S4-S8	M	M	M	M	T	T	T	T	T	T	21
Dec. 2016	F4	TM20-724-S4-S14	M	M	M	M	T	T	T	T	T	T	23
Dec. 2016	F4	TM20-724-S1-S14	M	M	M	M	T	T	T	T	T	T	25
Dec. 2016	F4	TM20-724-S4-S2	M	M	M	M	T	T	T	T	T	T	26
Dec. 2016	F4	TM20-724-S4-S1	M	M	M	M	T	T	T	T	T	T	30
Dec. 2016	F4	TM20-724-S4-S4	M	M	M	M	T	T	T	T	T	T	41
Dec. 2016	F4	TM20-724-S4-S3	M	M	M	M	T	T	T	T	T	T	42
Dec. 2016	F4	TM19-699-S4-S6	M	M	M	T	T	T	T	T	T	T	5
Dec. 2016	F4	TM27-996-S1-S10	M	M	M	T	T	T	T	T	T	T	18
Dec. 2016	F4	TM27-996-S1-S5	M	M	M	T	T	T	T	T	T	T	24
Dec. 2016	F4	TM27-996-S1-S6	M	M	M	T	T	T	T	T	T	T	33
Dec. 2016	F4	TM19-699-S2-S14	M	M	M	T	T	T	T	T	T	T	36
Dec. 2016	F4	TM19-699-S1-S8	M	M	M	T	T	T	T	M	T	T	39
Dec. 2016	F4	TM43-1593-S1-S14	T	T	T	T	T	T	T	T	T	M	10
Dec. 2016	F4	TM43-1593-S1-S6	T	T	T	T	T	T	T	T	T	M	14
Dec. 2016	F4	TM48-1853-S1-S4	T	T	T	T	T	M	M	M	M	M	8
Dec. 2016	F4	TM48-1853-S1-S9	T	T	T	T	T	M	M	M	M	M	13
Dec. 2016	F4	TM48-1853-S1-S15	T	T	T	T	T	M	M	M	M	M	15
Dec. 2016	F4	TM48-1853-S1-S13	T	T	T	T	T	M	M	M	M	M	19
Dec. 2016		Molineux	M	M	M	M	M	M	M	M	M	M	0
Dec. 2016		Molineux	M	M	M	M	M	M	M	M	M	M	0
Dec. 2016		Molineux	M	M	M	M	M	M	M	M	M	M	8
Dec. 2016		Molineux	M	M	M	M	M	M	M	M	M	M	14
Dec. 2016		Molineux	M	M	M	M	M	M	M	M	M	M	16
Dec. 2016		Molineux	M	M	M	M	M	M	M	M	M	M	18
Dec. 2016		Molineux	M	M	M	M	M	M	M	M	M	M	18
Dec. 2016		Molineux	M	M	M	M	M	M	M	M	M	M	20
Dec. 2016		Molineux	M	M	M	M	M	M	M	M	M	M	22
Dec. 2016		Molineux	M	M	M	M	M	M	M	M	M	M	26
Dec. 2016		Janz	T	T	T	T	T	T	T	T	T	T	27
Dec. 2016		Janz	T	T	T	T	T	T	T	T	T	T	27
Dec. 2016		Janz	T	T	T	T	T	T	T	T	T	T	28
Dec. 2016		Janz	T	T	T	T	T	T	T	T	T	T	28
Dec. 2016		Janz	T	T	T	T	T	T	T	T	T	T	42
Dec. 2016		Janz	T	T	T	T	T	T	T	T	T	T	45

Dec. 2016		Janz	T	T	T	T	T	T	T	T	T													T	49
Dec. 2016		Janz	T	T	T	T	T	T	T	T	T													T	50
Dec. 2016		Janz	T	T	T	T	T	T	T	T	T													T	50
Dec. 2016		Janz	T	T	T	T	T	T	T	T	T													T	67
May 2017.	F5	KL1.9-1	M	M	M	M	M	M	M	M	M	M	M	M	M	M	M	M	M	M	M	M	M	T	8
May 2017.	F5	KL1.9-10	M	M	M	M	M	M	M	M	M	M	M	M	M	M	M	M	M	M	M	M	M	T	18
May 2017.	F5	KL1.9-2	M	M	M	M	M	M	M	H	M	M	M	M	M	M	M	M	M	M	M	M	M	T	5
May 2017.	F5	KL1.9-3	M	M	M	M	M	M	M	M	M	M	M	M	M	M	M	M	M	M	M	M	M	T	10
May 2017.	F5	KL1.9-4	M	M	M	M	M	M	M	M	M	M	M	M	M	M	M	M	M	M	M	M	M	T	4
May 2017.	F5	KL1.9-6	M	M	M	M	M	M	M	M	M	M	M	M	M	M	M	M	M	M	M	M	M	T	1
May 2017.	F5	KL1.9-7	M	M	M	M	M	M	M	M	M	M	M	M	M	M	M	M	M	M	M	M	M	T	8
May 2017.	F5	KL1.9-8	M	M	M	M	M	M	M	M	M	M	M	M	M	M	M	M	M	M	M	M	M	T	8
May 2017.	F5	KL1.9-9	M	M	M	M	M	M	M	M	M	M	M	M	M	M	M	M	M	M	M	M	M	T	10
May 2017.	F5	KL1.3-1	M	M	M	M	M	M	H	H	H	H	H	H	H	H	H	H	H	H	M	T	T		11
May 2017.	F5	KL1.5-1	M	M	M	M	M	M	M	M	M	M	M	M	M	M	M	M	M	M	M	T	T		4
May 2017.	F5	KL1.5-10	M	M	M	M	M	M	M	M	M	M	M	M	M	M	M	M	M	M	M	T	T		15
May 2017.	F5	KL1.5-2	M	M	M	M	M	M	M	M	M	M	M	M	M	M	M	M	M	M	M	T	T		15
May 2017.	F5	KL1.5-3	M	M	M	M	M	M	M	M	M	M	M	M	M	M	M	M	M	M	M	T	T		9
May 2017.	F5	KL1.5-4	M	M	M	M	M	M	M	M	M	M	M	M	M	M	M	M	M	M	M	T	T		8
May 2017.	F5	KL1.5-5	M	M	M	M	M	M	M	M	M	M	M	M	M	M	M	M	M	M	M	T	T		10
May 2017.	F5	KL1.5-6	M	M	M	M	M	M	M	M	M	M	M	M	M	M	M	M	M	M	M	T	T		7
May 2017.	F5	KL1.5-7	M	M	M	M	M	M	M	M	M	M	M	M	M	M	M	M	M	M	M	T	T		13
May 2017.	F5	KL1.5-8	M	M	M	M	M	M	M	M	M	M	M	M	M	M	M	M	M	M	M	T	T		15
May 2017.	F5	KL1.5-9	M	M	M	M	M	M	M	M	M	M	M	M	M	M	M	M	M	M	M	T	T		15
May 2017.	F5	KL1.8-1	M	M	M	M	M	M	M	M	M	M	M	M	M	M	M	M	M	M	M	T	T		7
May 2017.	F5	KL1.8-10	M	M	M	M	M	M	M	M	M	M	M	M	M	M	M	M	M	M	M	T	T		5
May 2017.	F5	KL1.8-3	M	M	M	M	M	M	M	M	M	M	M	M	M	M	M	M	M	M	M	T	T		6
May 2017.	F5	KL1.8-4	M	M	M	M	M	M	M	M	M	M	M	M	M	M	M	M	M	M	M	T	T		9
May 2017.	F5	KL1.8-5	M	M	M	M	M	M	M	M	M	M	M	M	M	M	M	M	M	M	M	T	T		2
May 2017.	F5	KL1.8-6	M	M	M	M	M	M	M	M	M	M	M	M	M	M	M	M	M	M	M	T	T		4
May 2017.	F5	KL1.8-7	M	M	M	M	M	M	M	M	M	M	M	M	M	M	M	M	M	M	M	T	T		7
May 2017.	F5	KL1.8-8	M	M	M	M	M	M	M	M	M	M	M	M	M	M	M	M	M	M	M	T	T		2
May 2017.	F5	KL1.8-9	M	M	M	M	M	M	M	M	M	M	M	M	M	M	M	M	M	M	M	T	T		5
May 2017.	F5	KL1.1-1	M	M	M	M	M	M	M	M	M	M	M	M	M	M	M	M	M	M	M	T	T		7
May 2017.	F5	KL1.1-10	M	M	M	M	M	M	M	M	M	M	M	M	M	M	M	M	M	M	M	T	T		9
May 2017.	F5	KL1.1-2	M	M	M	M	M	M	M	M	M	M	M	M	M	M	M	M	M	M	M	T	T		7
May 2017.	F5	KL1.1-3	M	M	M	M	M	M	M	M	M	M	M	M	M	M	M	M	M	M	M	T	T		10
May 2017.	F5	KL1.1-4	M	M	M	M	M	M	M	M	M	M	M	M	M	M	M	M	M	M	M	T	T		16
May 2017.	F5	KL1.1-5	M	M	M	M	M	M	M	M	M	M	M	M	M	M	M	M	M	M	M	T	T		10
May 2017.	F5	KL1.1-7	M	M	M	M	M	M	M	M	M	M	M	M	M	M	M	M	M	M	M	T	T		18
May 2017.	F5	KL1.1-8	M	M	M	M	M	M	M	M	M	M	M	M	M	M	M	M	M	M	M	T	T		11
May 2017.	F5	KL1.1-9	M	M	M	M	M	M	M	M	M	M	M	M	M	M	M	M	M	M	M	T	T		14

May 2017.	F5	KL5.130-10	M	M	M	M	M	M	M	M	M	M	M	M	M	M	M	M	M	M	M	M	T	T	4
May 2017.	F5	KL5.61-12	M	M	M	M	M	M	M	M	M	M	M	M	M	M	M	M	M	M	M	M	T	T	3
May 2017.	F5	KL5.61-14	M	M	M	M	M	M	M	M	M	M	M	M	M	M	M	M	M	M	M	M	T	T	4
May 2017.	F5	KL5.61-3	M	M	M	M	M	M	M	M	M	M	M	M	M	M	M	M	M	M	M	M	T	T	5
May 2017.	F5	KL5.61-5	M	M	M	M	M	M	M	M	M	M	M	M	M	M	M	M	M	M	M	M	T	T	10
May 2017.	F5	KL5.66-14	M	M	M	M	M	M	M	M	M	M	M	M	M	M	M	M	M	M	M	M	T	T	9
May 2017.	F5	KL5.66-17	M	M	M	M	M	M	M	M	M	M	M	M	M	M	M	M	M	M	M	M	T	T	1
May 2017.	F5	KL5.66-6	M	M	M	M	M	M	M	M	M	M	M	M	M	M	M	M	M	M	M	M	T	T	9
May 2017.	F5	KL5.68-4	M	M	M	M	M	M	M	M	M	M	M	M	M	M	M	M	M	M	M	M	T	T	6
May 2017.	F5	KL5.121-1	M	M	M	M	M	M	M	M	M	M	M	M	M	M	M	M	M	M	M	T	T	T	2
May 2017.	F5	KL5.121-10	M	M	M	M	M	M	M	M	M	M	M	M	M	M	M	M	M	M	M	T	T	T	14
May 2017.	F5	KL5.121-21	M	M	M	M	M	M	M	M	M	M	M	M	M	M	M	M	M	M	M	T	T	T	12
May 2017.	F5	KL5.128-12	H	H	H	H	H	M	M	M	M	M	M	M	M	M	M	M	M	M	M	T	T	T	5
May 2017.	F5	KL5.121-3	M	M	M	M	M	M	M	M	M	M	M	M	M	M	M	M	M	M	M	T	T	T	24
May 2017.	F5	KL5.121-31	M	M	M	M	M	M	M	M	M	M	M	M	M	M	M	M	M	M	M	T	T	T	22
May 2017.	F5	KL5.121-33	M	M	M	M	M	M	M	M	M	M	M	M	M	M	M	M	M	M	M	T	T	T	10
May 2017.	F5	KL5.121-35	M	M	M	M	M	M	M	M	M	M	M	M	M	M	M	M	M	M	M	T	T	T	4
May 2017.	F5	KL5.121-43	M	M	M	M	M	M	M	M	M	M	M	M	M	M	M	M	M	M	M	T	T	T	18
May 2017.	F5	KL5.121-44	M	M	M	M	M	M	M	M	M	M	M	M	M	M	M	M	M	M	M	T	T	T	10
May 2017.	F5	KL5.121-45	M	M	M	M	M	M	M	M	M	M	M	M	M	M	M	M	M	M	M	T	T	T	21
May 2017.	F5	KL5.121-9	M	M	M	M	M	M	M	-	-	-	M	M	M	M	M	-	M	M	M	T	T	T	16
May 2017.	F5	KL5.122-5	M	M	M	M	M	M	M	M	M	M	M	M	M	M	M	M	M	M	M	T	T	T	4
May 2017.	F5	KL5.124-10	M	M	M	M	M	M	M	M	M	M	M	M	M	M	M	M	M	M	M	T	T	T	2
May 2017.	F5	KL5.124-14	M	M	M	M	M	M	M	M	M	M	M	M	M	M	M	M	M	M	M	T	T	T	4
May 2017.	F5	KL5.124-5	M	M	M	M	M	M	M	M	M	M	M	M	M	M	M	M	M	M	M	T	T	T	14
May 2017.	F5	KL5.128-14	M	M	M	M	M	M	M	M	M	M	M	M	M	M	M	M	M	M	M	T	T	T	16
May 2017.	F5	KL5.128-15	M	M	M	M	M	M	M	M	M	M	M	M	M	M	M	M	M	M	M	T	T	T	10
May 2017.	F5	KL5.128-16	M	M	M	M	M	M	M	M	M	M	M	M	M	M	M	M	M	M	M	T	T	T	13
May 2017.	F5	KL5.129-16	M	M	M	M	M	M	M	M	M	M	M	M	M	M	M	M	M	M	M	T	T	T	9
May 2017.	F5	KL5.128-4	M	M	M	M	M	M	M	M	M	M	M	M	M	M	M	M	M	M	M	T	T	T	7
May 2017.	F5	KL5.128-8	M	M	M	M	M	M	M	M	M	M	M	M	M	M	M	M	M	M	M	T	T	T	9
May 2017.	F5	KL5.129-15	M	M	M	M	M	M	M	M	M	M	M	M	M	M	M	M	M	M	M	T	T	T	3
May 2017.	F5	KL5.129-25	M	M	M	M	M	M	M	M	M	M	M	M	M	M	M	M	M	M	M	T	T	T	16
May 2017.	F5	KL5.129-26	M	M	M	M	M	M	M	M	M	-	M	M	M	M	M	M	M	M	M	T	T	T	6
May 2017.	F5	KL5.129-34	M	M	M	M	M	M	M	M	M	M	M	M	M	M	M	M	M	M	M	T	T	T	6
May 2017.	F5	KL5.129-4	M	M	M	M	M	M	M	M	M	M	M	M	M	M	M	M	M	M	M	T	T	T	10
May 2017.	F5	KL5.129-43	M	M	M	M	M	M	M	M	M	M	M	M	M	M	M	M	M	M	M	T	T	T	5
May 2017.	F5	KL5.129-46	M	M	M	M	M	M	M	M	M	M	M	M	M	M	M	M	M	M	M	T	T	T	14
May 2017.	F5	KL5.129-51	M	M	M	M	M	M	M	M	M	M	M	M	M	M	M	M	M	M	M	T	T	T	20
May 2017.	F5	KL5.129-54	M	M	M	M	M	M	M	M	M	M	M	M	M	M	M	M	M	M	M	T	T	T	7
May 2017.	F5	KL5.130-15	M	M	M	M	M	M	M	M	M	M	M	M	M	M	M	M	M	M	M	T	T	T	3
May 2017.	F5	KL5.130-16	M	M	M	M	M	M	M	M	M	M	M	M	M	M	M	M	M	M	M	T	T	T	15

May 2017.	F5	KL5.130-2	M	M	M	M	M	M	M	M	M	M	M	M	M	M	M	M	M	M	M	T	T	T	13
May 2017.	F5	KL5.130-23	M	M	M	M	M	M	M	M	M	M	M	M	M	M	M	M	M	M	M	T	T	T	1
May 2017.	F5	KL5.130-3	M	M	M	M	M	M	M	M	M	M	M	M	M	M	M	M	M	M	M	T	T	T	9
May 2017.	F5	KL5.130-4	M	M	M	M	M	M	M	M	M	M	M	M	M	M	M	M	M	M	M	T	T	T	7
May 2017.	F5	KL5.61-8	M	M	M	M	M	M	M	M	M	M	M	M	M	M	M	M	M	M	M	T	T	T	7
May 2017.	F5	KL1.10-1	M	M	M	M	M	M	M	M	M	M	M	M	M	M	M	M	M	M	M	T	T	T	3
May 2017.	F5	KL1.10-10	M	M	M	M	M	M	M	M	M	M	M	M	M	M	M	M	M	M	M	T	T	T	9
May 2017.	F5	KL1.10-2	M	M	M	M	M	M	M	M	M	M	M	M	M	M	M	M	M	M	M	T	T	T	2
May 2017.	F5	KL1.10-4	M	M	M	M	M	M	M	M	M	M	M	M	M	M	M	M	M	M	M	T	T	T	1
May 2017.	F5	KL1.10-5	M	M	M	M	M	M	M	M	M	M	M	M	M	M	M	M	M	M	M	T	T	T	6
May 2017.	F5	KL1.10-6	M	M	M	M	M	M	M	M	M	M	M	M	M	M	M	M	M	M	M	T	T	T	21
May 2017.	F5	KL1.10-7	M	M	M	M	M	M	M	M	M	M	M	M	M	M	M	M	M	M	M	T	T	T	9
May 2017.	F5	KL1.10-8	M	M	M	M	M	M	M	M	M	M	M	M	M	M	M	M	M	M	M	T	T	T	9
May 2017.	F5	KL1.10-9	M	M	M	M	M	M	M	M	M	M	M	M	M	M	M	M	M	M	M	T	T	T	13
May 2017.	F5	KL1.11-1	M	M	M	M	M	M	M	T	T	T	T	T	T	T	T	T	T	T	T	T	T	T	34
May 2017.	F5	KL1.11-2	M	M	M	M	M	M	M	T	T	T	T	T	T	T	T	T	T	T	T	T	T	T	14
May 2017.	F5	KL1.11-3	M	M	M	M	M	M	M	T	T	T	T	T	T	T	T	T	T	T	T	T	T	T	50
May 2017.	F5	KL1.11-4	M	M	M	M	M	M	M	T	T	T	T	T	T	T	T	T	T	T	T	T	T	T	37
May 2017.	F5	KL1.11-5	M	M	M	M	M	M	M	T	T	T	T	T	T	T	T	T	T	T	T	T	T	T	36
May 2017.	F5	KL1.11-6	M	M	M	M	M	M	M	T	T	T	T	T	T	T	T	T	T	T	T	T	T	T	51
May 2017.	F5	KL1.11-7	M	M	M	M	M	M	M	T	T	T	T	T	T	T	T	T	T	T	T	T	T	T	58
May 2017.	F5	KL1.11-8	M	M	M	M	M	M	M	T	T	T	T	T	T	T	T	T	T	T	H	T	T	T	19
May 2017.	F5	KL1.12-2	M	M	M	M	M	M	M	T	T	T	T	T	T	T	T	T	T	T	T	T	T	T	42
May 2017.	F5	KL1.12-3	M	M	M	M	M	M	M	T	T	T	T	T	T	T	T	T	T	T	T	T	T	T	46
May 2017.	F5	KL1.12-4	M	M	M	M	M	M	M	T	T	T	T	T	T	T	T	T	T	T	T	T	T	T	48
May 2017.	F5	KL1.12-5	M	M	M	M	M	M	M	T	T	T	T	T	T	T	T	T	T	T	T	T	T	T	42
May 2017.	F5	KL1.12-6	M	M	M	M	M	M	M	T	T	T	T	T	T	T	T	T	T	T	T	T	T	T	33
May 2017.	F5	KL1.12-7	M	M	M	M	M	M	-	T	T	T	T	T	T	T	T	T	T	T	T	T	T	T	29
May 2017.	F5	KL1.12-8	M	M	M	M	M	M	M	T	T	T	T	T	T	T	T	T	T	T	T	T	T	T	32
May 2017.	F5	KL1.3-10	M	M	M	M	M	M	T	T	T	T	T	T	T	T	T	T	T	T	T	T	T	T	34
May 2017.	F5	KL1.3-2	M	M	M	M	M	M	T	T	T	T	T	T	T	T	T	T	T	T	T	T	T	T	10
May 2017.	F5	KL1.3-3	M	M	M	M	M	M	T	T	T	T	T	T	T	T	T	T	T	T	T	T	T	T	14
May 2017.	F5	KL1.3-4	M	M	M	M	M	M	T	T	T	T	T	T	T	T	T	T	T	T	H	T	T	T	18
May 2017.	F5	KL1.3-5	M	M	M	M	M	M	T	T	T	T	T	T	T	T	T	T	H	T	T	T	T	T	14
May 2017.	F5	KL1.3-6	M	M	M	M	M	M	T	T	T	T	T	T	T	T	T	T	H	T	T	T	T	T	28
May 2017.	F5	KL1.3-7	M	M	M	M	M	M	T	T	T	T	T	T	T	T	T	T	T	T	T	T	T	T	36
May 2017.	F5	KL1.3-8	M	M	M	M	M	M	T	T	T	T	T	T	T	T	T	T	H	T	T	T	T	T	20
May 2017.	F5	KL1.13-1	T	T	T	T	T	T	T	T	T	T	T	T	T	T	T	T	T	T	T	T	T	T	49
May 2017.	F5	KL1.13-2	T	T	T	T	T	T	T	T	T	T	T	T	T	T	T	T	T	T	T	T	T	T	33
May 2017.	F5	KL1.13-3	T	T	T	T	T	T	T	T	T	T	T	T	T	T	T	T	T	T	T	T	T	T	20
May 2017.	F5	KL1.13-4	T	T	T	T	T	T	T	T	T	T	T	T	T	T	T	T	T	T	T	T	T	T	39
May 2017.	F5	KL1.13-5	T	T	T	T	T	T	T	T	T	T	T	T	T	T	T	T	T	T	T	T	T	T	51

May 2017.	F5	KL1.13-6	T	T	T	T	T	T	T	T	T	T	T	T	T	T	T	T	T	T	T	T	T	T	54
May 2017.	F5	KL1.13-7	T	T	T	T	T	T	T	T	T	T	T	T	T	T	T	T	T	T	T	T	T	T	53
May 2017.	F5	KL1.13-8	T	T	T	T	T	T	T	T	T	T	T	T	T	T	T	T	T	T	T	T	T	T	41
May 2017.	F5	KL1.14-2	T	T	T	T	T	M	M	M	M	M	M	M	M	M	M	M	M	M	M	M	M	M	20
May 2017.	F5	KL1.14-3	T	T	T	T	T	M	M	M	M	M	M	M	M	M	M	M	M	M	M	M	M	M	14
May 2017.	F5	KL1.14-4	T	T	T	T	T	M	M	M	M	M	M	M	M	M	M	M	M	M	M	M	M	M	21
May 2017.	F5	KL1.14-5	T	T	T	T	T	M	M	M	M	M	M	M	M	M	M	M	M	M	M	M	M	M	16
May 2017.	F5	KL1.14-6	T	T	T	T	T	M	M	M	M	M	M	M	M	M	M	M	M	M	M	M	M	M	9
May 2017.	F5	KL1.14-7	T	T	T	T	T	M	M	M	M	M	M	M	M	M	M	M	M	M	M	M	M	M	6
May 2017.	F5	KL1.14-8	T	T	T	T	T	M	M	M	M	M	M	M	M	M	M	M	M	M	M	M	M	M	6
May 2017.		TMDH06	M	M	M	M	M	M	M	M	M	M	M	M	M	M	M	M	M	M	M	M	M	M	19
May 2017.		TMDH06	M	M	M	M	M	M	M	M	M	M	M	M	M	M	M	M	M	M	M	M	M	M	18
May 2017.		TMDH06	M	M	M	M	M	M	M	M	M	M	M	M	M	M	M	M	M	M	M	M	M	M	23
May 2017.		TMDH06	M	M	M	M	M	M	M	M	M	M	M	M	M	M	M	M	M	M	M	M	M	M	12
May 2017.		TMDH06	M	M	M	M	M	M	M	M	M	M	M	M	M	M	M	M	M	M	M	M	M	M	23
May 2017.		TMDH06	M	M	M	M	M	M	M	M	M	M	M	M	M	M	M	M	M	M	M	M	M	M	15
May 2017.		TMDH06	M	M	M	M	M	M	M	M	M	M	M	M	M	M	M	M	M	M	M	M	M	M	22
May 2017.		TMDH06	M	M	M	M	M	M	M	M	M	M	M	M	M	M	M	M	M	M	M	M	M	M	22
May 2017.		TMDH06	M	M	M	M	M	M	M	M	M	M	M	M	M	M	M	M	M	M	M	M	M	M	22
May 2017.		TMDH06	M	M	M	M	M	M	M	M	M	M	M	M	M	M	M	M	M	M	M	M	M	M	31
May 2017.		TMDH82	T	T	T	T	T	T	T	T	T	T	T	T	T	T	T	T	T	T	T	T	T	T	48
May 2017.		TMDH82	T	T	T	T	T	T	T	T	T	T	T	T	T	T	T	T	T	T	T	T	T	T	31
May 2017.		TMDH82	T	T	T	T	T	T	T	T	T	T	T	T	T	T	T	T	T	T	T	T	T	T	26
May 2017.		TMDH82	T	T	T	T	T	T	T	T	T	T	T	T	T	T	T	T	T	T	T	T	T	T	31
May 2017.		TMDH82	T	T	T	T	T	T	T	T	T	T	T	T	T	T	T	T	T	T	T	T	T	T	20
May 2017.		TMDH82	T	T	T	T	T	T	T	T	T	T	T	T	T	T	T	T	T	T	T	T	T	T	37
May 2017.		TMDH82	T	T	T	T	T	T	T	T	T	T	T	T	T	T	T	T	T	T	T	T	T	T	46
May 2017.		TMDH82	T	T	T	T	T	T	T	T	T	T	T	T	T	T	T	T	T	T	T	T	T	T	54
Feb. 2018	F6	F6.105.26.1	M	M	M	M	M	M	M	M	M	M	M	M	M	M	M	M	M	M	M	M	M	M	12
Feb. 2018	F6	KL.R1.1	M	M	M	M	M	M	M	M	M	M	M	M	M	M	M	M	M	M	M	M	M	M	26
Feb. 2018	F6	KL.R1.2	M	M	M	M	M	M	M	M	M	M	M	M	M	M	M	M	M	M	M	M	M	M	7
Feb. 2018	F6	KL.R1.3	M	M	M	M	M	M	M	M	M	M	M	M	M	M	M	M	M	M	M	M	M	M	16
Feb. 2018	F6	KLR2.1	M	M	M	M	M	M	M	M	M	M	M	M	M	M	M	M	M	M	M	M	M	M	11
Feb. 2018	F6	KL.R2.2	M	M	M	M	M	M	M	M	M	M	M	M	M	M	M	M	M	M	M	M	M	M	9
Feb. 2018	F6	KL.R2.4	M	M	M	M	M	M	M	M	M	M	M	M	M	M	M	M	M	M	M	M	M	M	3
Feb. 2018	F6	KL.R3.2	M	M	M	M	M	M	M	M	M	M	M	M	M	M	M	M	M	M	M	M	M	M	36
Feb. 2018	F6	KL.R3.3	M	M	M	M	M	M	M	M	M	M	M	M	M	M	M	M	M	M	M	M	M	M	16
Feb. 2018	F6	KL.R3.4	M	M	M	M	M	M	M	M	M	M	M	M	M	M	M	M	M	M	M	M	M	M	6
Feb. 2018	F6	KL.R3.5	M	M	M	M	M	M	M	M	M	M	M	M	M	M	M	M	M	M	M	M	M	M	37
Feb. 2018	F6	KL.R3.6	M	M	M	M	M	M	M	M	M	M	M	M	M	M	M	M	M	M	M	M	M	M	2
Feb. 2018	F6	KL.R4.1	M	M	M	M	M	M	M	M	M	M	M	M	M	M	M	M	M	M	M	M	M	M	17
Feb. 2018	F6	KL.R4.2	M	M	M	M	M	M	M	M	M	M	M	M	M	M	M	M	M	M	M	M	M	M	19

Feb. 2018	F6	KL.R4.3	M	M	M	M	M	M	M	M	M	M	M	M	M	M	M	M	M	M	M	M	M	35
Feb. 2018	F6	KL.R4.4	M	M	M	M	M	M	M	M	M	M	M	M	M	M	M	M	M	M	M	M	M	25
Feb. 2018	F6	KL.R4.5	M	M	M	M	M	M	M	M	M	M	M	M	M	M	M	M	M	M	M	M	M	29
Feb. 2018	F6	KL.R4.6	M	M	M	M	M	M	M	M	M	M	M	M	M	M	M	M	M	M	M	M	M	27
Feb. 2018	F6	KL.R6.6	M	M	M	M	M	M	M	M	M	M	M	M	M	M	M	M	M	M	M	M	M	17
Feb. 2018	F6	KL.R7.2	M	M	M	M	M	M	M	M	M	M	M	M	M	M	M	M	M	M	M	M	M	23
Feb. 2018	F6	KL.R7.3	M	M	M	M	M	M	M	M	M	M	M	M	M	M	M	M	M	M	M	M	M	29
Feb. 2018	F6	KL.R7.4	M	M	M	M	M	M	M	M	M	M	M	M	M	M	M	M	M	M	M	M	M	18
Feb. 2018	F6	KL.R7.6	M	M	M	M	M	M	M	M	M	M	M	M	M	M	M	M	M	M	M	M	M	25
Feb. 2018	F6	F6.5.6.9	T	T	T	T	T	T	T	T	T	T	M	M	M	M	M	M	M	M	M	M	M	1
Feb. 2018	F6	F6.5.6.1	T	T	T	T	T	T	T	T	T	T	M	M	M	M	M	M	M	M	M	M	M	12
Feb. 2018	F6	F6.5.6.20	T	T	T	T	T	T	T	T	T	T	M	M	M	M	M	M	M	M	M	M	M	23
Feb. 2018	F6	F6.5.6.21	T	T	T	T	T	T	T	T	T	T	M	M	M	M	M	M	M	M	M	M	M	30
Feb. 2018	F6	F6.5.6.29	T	T	T	T	T	T	T	T	T	T	M	M	M	M	M	M	M	M	M	M	M	29
Feb. 2018	F6	F6.5.6.30	T	T	T	T	T	T	T	T	T	T	M	M	M	M	M	M	M	M	M	M	M	28
Feb. 2018	F6	F6.5.6.24	T	T	T	T	T	T	T	T	T	T	M	M	M	M	M	M	M	M	M	M	M	25
Feb. 2018	F6	F6.D16.5	M	M	M	M	M	M	M	M	M	M	M	M	M	M	M	M	M	M	M	T	T	37
Feb. 2018	F6	D16.12	M	M	M	M	M	M	M	M	M	M	M	M	M	M	M	M	M	M	M	T	T	17
Feb. 2018	F6	D16.20	M	M	M	M	M	M	M	M	M	M	M	M	M	M	M	M	M	M	M	T	T	4
Feb. 2018	F6	F6.D16.13	M	M	M	M	M	M	M	M	M	M	M	M	M	M	M	M	M	M	M	T	T	28
Feb. 2018	F6	F6.D16.15	M	M	M	M	M	M	M	M	M	M	M	M	M	M	M	M	M	M	M	T	T	25
Feb. 2018	F6	F6.D16.16	M	M	M	M	M	M	M	M	M	M	M	M	M	M	M	M	M	M	M	T	T	15
Feb. 2018	F6	F6.D18.3	M	M	M	M	M	M	M	M	M	M	M	M	M	M	M	M	M	M	M	T	T	29
Feb. 2018	F6	F6.D18.8	M	M	M	M	M	M	M	M	M	M	M	M	M	M	M	M	M	M	M	T	T	17
Feb. 2018	F6	F6.D18.11	M	M	M	M	M	M	M	M	M	M	M	M	M	M	M	M	M	M	M	T	T	5
Feb. 2018	F6	F6.D18.12	M	M	M	M	M	M	M	M	M	M	M	M	M	M	M	M	M	M	M	T	T	27
Feb. 2018	F6	F6.D18.18	M	M	M	M	M	M	M	M	M	M	M	M	M	M	M	M	M	M	M	T	T	27
Feb. 2018	F6	D18.20	M	M	M	M	M	M	M	M	M	M	M	M	M	M	M	M	M	M	M	T	T	9
Feb. 2018	F6	F6.D21.2	M	M	M	M	M	M	M	M	M	M	M	M	M	M	M	M	M	M	M	T	T	11
Feb. 2018	F6	F6.D21.5	M	M	M	M	M	M	M	M	M	M	M	M	M	M	M	M	M	M	M	T	T	17
Feb. 2018	F6	F6.D21.15	M	M	M	M	M	M	M	M	M	M	M	M	M	M	M	M	M	M	M	T	T	23
Feb. 2018	F6	KL.R5.3	M	M	M	M	M	M	M	M	M	M	M	M	M	M	M	M	M	M	M	T	T	23
Feb. 2018	F6	KL.R5.1	M	M	M	M	M	M	M	M	M	M	M	M	M	M	M	M	M	M	M	T	T	25
Feb. 2018	F6	KL.R5.2	M	M	M	M	M	M	M	M	M	M	M	M	M	M	M	M	M	M	M	T	T	8
Feb. 2018	F6	KL.R5.4	M	M	M	M	M	M	M	M	M	M	M	M	M	M	M	M	M	M	M	T	T	18
Feb. 2018	F6	KL.R5.5	M	M	M	M	M	M	M	M	M	M	M	M	M	M	M	M	M	M	M	T	T	18
Feb. 2018	F6	F6.50.4.6	M	M	M	M	M	M	M	M	M	M	T	T	T	T	T	T	T	T	T	T	T	46
Feb. 2018	F6	F6.50.4.11	M	M	M	M	M	M	M	M	M	M	T	T	T	T	T	T	T	T	T	T	T	47
Feb. 2018	F6	F6.50.4.21	M	M	M	M	M	M	M	M	M	M	T	T	T	T	T	T	T	T	T	T	T	27
Feb. 2018	F6	KL.S2.1	M	M	M	M	M	M	M	T	T	T	T	T	T	T	T	T	T	T	T	T	T	49
Feb. 2018	F6	KL.S2.5	M	M	M	M	M	M	M	T	T	T	T	T	T	T	T	T	T	T	T	T	T	54
Feb. 2018	F6	KL.S3.1	M	M	M	M	M	M	M	T	T	T	T	T	T	T	T	T	T	T	T	T	T	68

Feb. 2018	F6	KL.S3.2	M	M	M	M	M	M	M	T	T	T	T	T	T	T	T	T	T	T	T	T	T	T	80
Feb. 2018	F6	KL.S3.3	M	M	M	M	M	M	M	T	T	T	T	T	T	T	T	T	T	T	T	T	T	T	50
Feb. 2018	F6	KL.S3.4	M	M	M	M	M	M	M	T	T	T	T	T	T	T	T	T	T	T	T	T	T	T	64
Feb. 2018	F6	F6.105.26.2	T	T	T	T	T	T	T	T	T	T	T	T	T	T	T	H	T	T	T	T	T	T	31
Feb. 2018	F6	F6.50.4.4	T	T	T	T	T	T	T	T	T	T	T	T	T	T	T	T	T	T	T	T	T	T	24
Feb. 2018	F6	F6.50.4.13	T	T	T	T	T	T	T	T	T	T	T	T	T	T	T	H	T	T	T	T	T	T	30
Feb. 2018	F6	F6.D16.6	T	T	T	T	T	T	T	T	T	T	T	T	T	T	T	T	T	T	T	T	T	T	49
Feb. 2018	F6	F6.D16.8	T	T	T	T	T	T	T	T	T	T	T	T	T	T	T	T	T	T	T	T	T	T	56
Feb. 2018	F6	F6.D16.17	T	T	T	T	T	T	T	T	T	T	T	T	T	T	T	T	T	T	T	T	T	T	33
Feb. 2018	F6	F6.D18.4	T	T	T	T	T	T	T	T	T	T	T	T	T	T	T	T	T	T	T	T	T	T	61
Feb. 2018	F6	F6.D18.21	T	T	T	T	T	T	T	T	T	T	T	T	T	T	T	H	T	T	T	T	T	T	51
Feb. 2018	F6	F6.D18.26	T	T	T	T	T	T	T	T	T	T	T	T	T	T	T	T	T	T	T	T	T	T	56
Feb. 2018	F6	F6.D21.7	T	T	T	T	T	T	T	T	T	T	T	T	T	T	T	T	T	T	T	T	T	T	51
Feb. 2018	F6	F6.D21.12	T	T	T	T	T	T	T	T	T	T	T	T	T	T	T	T	T	T	T	T	T	T	54
Feb. 2018	F6	F6.D21.16	T	T	T	T	T	T	T	T	T	T	T	T	T	T	T	T	T	T	T	T	T	T	36
Feb. 2018	F6	F6.D21.17	T	T	T	T	T	T	T	T	T	T	T	T	T	T	T	T	T	T	T	T	T	T	67
Feb. 2018	F6	KL.S1.1	T	T	T	T	T	T	T	T	T	T	T	T	T	T	T	T	T	T	T	T	T	T	48
Feb. 2018	F6	KL.S1.2	T	T	T	T	T	T	T	T	T	T	T	T	T	T	T	T	T	T	T	T	T	T	23
Feb. 2018	F6	KL.S1.3	T	T	T	T	T	T	T	T	T	T	T	T	T	T	T	T	T	T	T	T	T	T	39
Feb. 2018	F6	KL.S1.4	T	T	T	T	T	T	T	T	T	T	T	T	T	T	T	T	T	T	T	T	T	T	14
Feb. 2018	F6	KL.S1.5	T	T	T	T	T	T	T	T	T	T	T	T	T	T	T	T	T	T	T	T	T	T	17
Feb. 2018	F6	KL.S1.6	T	T	T	T	T	T	T	T	T	T	T	T	T	T	T	T	T	T	T	T	T	T	13
Feb. 2018	F6	KL.S2.2	T	T	T	T	T	T	T	T	T	T	T	T	T	T	T	T	T	T	T	T	T	T	42
Feb. 2018	F6	KL.S2.4	T	T	T	T	T	T	T	T	T	T	T	T	T	T	T	T	T	T	T	T	T	T	49
Feb. 2018	F6	KLS2.5	T	T	T	T	T	T	T	T	T	T	T	T	T	T	T	T	T	T	T	T	T	T	38
Feb. 2018	F6	KL.S4.2	T	T	T	T	T	T	T	T	T	T	T	T	T	T	T	T	T	T	T	T	T	T	72
Feb. 2018	F6	KL.S4.3	T	T	T	T	T	T	T	T	T	T	T	T	T	T	T	T	T	T	T	T	T	T	30
Feb. 2018	F6	KL.S4.5	T	T	T	T	T	T	T	T	T	T	T	T	T	T	T	H	T	T	T	T	T	T	36
Feb. 2018	F6	KL.S4.6	T	T	T	T	T	T	T	T	T	T	T	T	T	T	T	T	T	T	T	T	T	T	14
Feb. 2018	F6	KL.S5.1	T	T	T	T	T	T	T	T	T	T	T	T	T	T	T	T	T	T	T	T	T	T	46
Feb. 2018	F6	KL.S5.2	T	T	T	T	T	T	T	T	T	T	T	T	T	T	T	T	T	T	T	T	T	T	72
Feb. 2018	F6	KL.S5.3	T	T	T	T	T	T	T	T	T	T	T	T	T	T	T	T	T	T	T	T	T	T	56
Feb. 2018	F6	KL.S5.5	T	T	T	T	T	T	T	T	T	T	T	T	T	T	T	T	T	T	T	T	T	T	17
Feb. 2018	F6	KL.S6.1	T	T	T	T	T	T	T	T	T	T	T	T	T	T	T	T	T	T	T	T	T	T	17
Feb. 2018	F6	KLS6.5	T	T	T	T	T	T	T	T	T	T	T	T	T	T	T	T	T	T	T	T	T	T	36
Feb. 2018	F6	KL.S6.6	T	T	T	T	T	T	T	T	T	T	T	T	T	T	T	T	T	T	T	T	T	T	26
Feb. 2018	F6	KL.S7.1	T	T	T	T	T	T	T	T	T	T	T	T	T	T	T	T	T	T	T	T	T	T	83
Feb. 2018	F6	KL.S7.5	T	T	T	T	T	T	T	T	T	T	T	T	T	T	T	T	T	T	T	T	T	T	29
Feb. 2018	F6	S7.4	T	T	T	T	T	T	T	T	T	T	T	T	T	T	T	T	T	T	T	T	T	T	14
Feb. 2018	F6	KL.S7.6	T	T	T	T	T	T	T	T	T	T	T	T	T	T	T	T	T	T	T	T	T	T	37
Feb. 2018		TMDH82	T	T	T	T	T	T	T	T	T	T	T	T	T	T	T	T	T	T	T	T	T	T	56
Feb. 2018		TMDH82	T	T	T	T	T	T	T	T	T	T	T	T	T	T	T	T	T	T	T	T	T	T	64

Feb. 2018		TMDH6	M	M	M	M	M	M	M	M	M	M	M	M	M	M	M	M	M	M	M	M	M	M	29
Feb. 2018		TMDH6	M	M	M	M	M	M	M	M	M	M	M	M	M	M	M	M	M	M	M	M	M	M	10
Feb. 2018		TMDH6	M	M	M	M	M	M	M	M	M	M	M	M	M	M	M	M	M	M	M	M	M	M	20
Feb. 2018		TMDH6	M	M	M	M	M	M	M	M	M	M	M	M	M	M	M	M	M	M	M	M	M	M	27
Feb. 2018		TMDH6	M	M	M	M	M	M	M	M	M	M	M	M	M	M	M	M	M	M	M	M	M	M	34
Feb. 2019	F7	F7.94.3.149.3				M	M	M	M	M	M	M	M	M	M	M	M	M	M	M	M	M	T	T	T	13
Feb. 2019	F7	F7.94.3.149.11				M	M	M	M	M	M	M	M	M	M	M	M	M	M	M	M	M	T	T	T	12
Feb. 2019	F7	F7.129.23.1.1				M	M	M	M	M	M	M	M	M	M	M	M	M	M	M	M	M	T	T	T	9
Feb. 2019	F7	F7.129.23.1.36				M	M	M	M	M	M	M	M	M	M	M	M	M	M	M	M	M	T	T	T	9
Feb. 2019	F7	F7.129.44.32.24				M	M	M	M	M	M	M	T	M	M	M	M	M	M	M	M	M	T	T	T	8
Feb. 2019	F7	F7.129.23.1.10				M	M	M	M	M	M	M	M	M	T	T	M	M	M	M	M	M	T	T	T	6
Feb. 2019	F7	F7.129.23.1.44				M	M	M	M	M	M	M	M	M	M	M	M	M	M	M	M	M	T	T	T	6
Feb. 2019	F7	F7.129.23.1.48				M	M	M	M	M	M	M	M	M	M	M	M	M	M	M	M	M	T	T	T	6
Feb. 2019	F7	F7.94.3.149.66				M	M	M	M	M	M	M	M	M	M	M	M	M	M	M	M	M	T	T	T	6
Feb. 2019	F7	F7.129.23.1.90				M	M	M	M	M	M	M	M	M	M	M	M	M	M	M	M	M	T	T	T	4
Feb. 2019	F7	F7.129.23.1.11				M	M	M	M	M	M	M	M	M	M	M	M	M	M	M	M	M	T	T	T	3
Feb. 2019	F7	F7.129.23.1.28				M	M	M	M	M	M	M	M	M	M	M	M	M	M	M	M	M	T	T	T	2
Feb. 2019	F7	F7.129.23.1.18				M	M	M	M	M	M	M	M	M	M	M	M	M	M	M	M	M	T	T	T	2
Feb. 2019	F7	F7.94.3.149.12				M	M	M	M	M	M	M	M	M	M	M	M	M	M	M	M	M	T	T	T	2
Feb. 2019	F7	F7.129.44.32.20				M	M	M	M	M	M	M	M	M	M	M	M	M	M	M	M	M	T	T	T	1
Feb. 2019	F7	F7.129.44.32.10				M	M	M	M	M	M	M	M	M	M	M	M	M	M	M	M	M	T	T	T	0
Feb. 2019	F7	F7.129.44.32.25				M	M	M	M	M	M	M	M	M	M	M	M	M	M	M	M	M	T	T	T	0
Feb. 2019	F7	F7.94.3.149.14				M	M	M	M	M	M	M	M	M	M	M	M	M	M	M	M	M	T	T	T	0
Feb. 2019	F7	F7.142.17.2.10				M	M	M	M	M	M	M	M	M	T	T	T	T	T	T	T	T	T	T	T	53
Feb. 2019	F7	F7.129.23.1.6				M	M	M	M	M	M	M	M	M	T	T	T	T	T	T	T	T	T	T	T	29
Feb. 2019	F7	F7.142.17.2.73				M	M	M	M	M	M	M	M	M	T	T	T	T	T	T	T	T	T	T	T	27
Feb. 2019	F7	F7.129.23.1.72				M	M	M	M	M	M	M	M	M	T	T	T	T	T	T	T	T	T	T	T	21
Feb. 2019	F7	F7.142.17.2.8				M	M	M	M	M	M	M	M	M	T	T	T	T	T	T	T	T	T	T	T	21
Feb. 2019	F7	F7.142.17.2.87				M	M	M	M	M	M	M	M	M	T	T	T	T	T	T	T	T	T	T	T	20
Feb. 2019	F7	F7.142.17.2.33				M	M	M	M	M	M	M	M	M	T	T	T	T	T	T	T	T	T	T	T	18
Feb. 2019	F7	F7.142.17.2.50				M	M	M	M	M	M	M	M	M	T	T	T	T	T	T	T	T	T	T	T	18
Feb. 2019	F7	F7.142.17.2.14				M	M	M	M	M	M	M	M	M	T	T	T	T	T	T	T	T	T	T	T	16
Feb. 2019	F7	F7.129.23.1.46				M	M	M	M	M	M	M	M	M	T	T	T	T	T	T	T	T	T	T	T	14
Feb. 2019	F7	F7.129.23.1.56				M	M	M	M	M	M	M	M	M	T	T	T	T	T	T	T	T	T	T	T	14
Feb. 2019	F7	F7.142.17.2.5				M	M	M	M	M	M	M	M	M	T	T	T	T	T	T	T	T	T	T	T	13
Feb. 2019	F7	F7.129.23.1.9				M	M	M	M	M	M	M	M	M	T	T	T	T	T	T	T	T	T	T	T	12
Feb. 2019	F7	F7.129.23.1.38				M	M	M	M	M	M	M	M	M	T	T	T	T	T	M	T	T	T	T	T	12
Feb. 2019	F7	F7.129.23.1.31				M	M	M	M	M	M	M	M	M	T	T	T	T	T	T	T	T	T	T	T	10
Feb. 2019	F7	F7.129.23.1.62				M	M	M	M	M	M	M	M	M	T	T	T	T	T	T	T	T	T	T	T	9
Feb. 2019	F7	F7.129.23.1.77				M	M	M	M	M	M	M	M	M	T	T	T	T	T	T	T	T	T	T	T	8
Feb. 2019	F7	F7.142.17.2.1				M	M	M	M	M	M	M	M	M	T	T	T	T	T	T	T	T	T	T	T	8
Feb. 2019	F7	F7.142.17.2.66				M	M	M	M	M	M	M	M	M	T	T	T	T	T	T	T	T	T	T	T	8

Feb. 2019	F7	F7.129.23.1.82	M	M	M	M	M	M	M	M	M	T	T	T	T	T	T	T	T	T	T	T	6
Feb. 2019	F7	F7.129.23.1.80	M	M	M	M	M	M	M	M	M	T	T	T	T	T	M	T	T	T	T	T	4
Feb. 2019	F7	F7.129.23.1.5	M	M	M	M	M	M	M	T	M	T	T	T	T	T	T	T	T	T	T	T	4
Feb. 2019	F7	F7.142.17.2.20	M	M	M	M	M	M	M	M	M	T	T	T	T	T	T	T	T	T	T	T	3
Feb. 2019	F7	F7.142.17.2.22	M	M	M	M	M	M	M	M	M	T	T	T	T	T	T	T	T	T	T	T	3
Feb. 2019	F7	F7.142.17.2.31	M	M	M	M	M	M	M	M	M	T	T	T	T	T	T	T	T	T	T	T	3
Feb. 2019	F7	F7.142.17.2.86	M	M	M	M	M	M	M	M	M	T	T	T	T	T	T	T	T	T	T	T	3
Feb. 2019	F7	F7.129.23.1.65	M	M	M	M	M	M	M	M	M	T	T	T	T	T	T	T	T	T	T	T	2
Feb. 2019	F7	F7.142.17.2.15	M	M	M	M	M	M	M	M	M	T	T	T	T	T	T	T	T	T	T	T	2
Feb. 2019	F7	F7.142.17.2.42	M	M	M	M	M	M	M	M	M	T	T	T	T	T	T	T	T	T	T	T	2
Feb. 2019	F7	F7.142.17.2.52	M	M	M	M	M	M	M	M	M	T	T	T	T	T	T	T	T	T	T	T	2
Feb. 2019	F7	F7.142.17.2.80	M	M	M	M	M	M	M	M	M	T	T	T	T	T	T	T	T	T	T	T	2
Feb. 2019	F7	F7.129.44.32.11	M	M	M	M	M	M	M	T	T	T	T	T	T	T	T	T	T	T	M	T	27
Feb. 2019	F7	F7.129.44.32.7	M	M	M	M	M	M	M	T	T	T	T	T	T	T	T	T	T	T	T	T	16
Feb. 2019	F7	F7.129.44.32.8	M	M	M	M	M	M	M	T	T	T	T	T	T	T	T	T	T	T	T	T	13
Feb. 2019	F7	F7.129.44.32.6	M	M	M	M	M	M	M	T	T	T	T	T	T	T	T	T	T	T	T	T	2
Feb. 2019	F7	F7.129.44.32.29	M	M	M	M	M	M	M	T	T	T	T	T	T	T	T	T	T	T	T	T	2
Feb. 2019	F7	F7.129.44.32.32	M	M	M	M	M	M	T	T	T	T	T	T	T	T	T	T	T	T	T	T	22
Feb. 2019	F7	F7.129.44.32.44	M	M	M	M	M	M	T	T	T	T	T	T	T	T	T	T	T	T	T	T	21
Feb. 2019	F7	F7.129.44.32.1	M	M	M	M	M	M	T	T	T	T	T	T	T	T	T	T	T	T	T	T	6
Feb. 2019	F7	F7.140.8.10.26	T	T	T	T	T	T	T	T	T	T	T	T	T	T	T	T	T	T	T	T	34
Feb. 2019	F7	F7.140.8.10.31	T	T	T	T	T	T	T	T	T	T	T	T	T	T	T	T	T	T	T	T	29
Feb. 2019	F7	F7.140.8.10.1	T	T	T	T	T	T	T	T	T	T	T	T	T	T	T	T	T	T	T	T	15
Feb. 2019	F7	F7.140.8.10.5	T	T	T	T	T	T	T	T	T	T	T	T	T	T	T	T	T	T	T	T	15
Feb. 2019	F7	F7.140.8.10.72	T	T	T	T	T	T	T	T	T	T	T	T	T	T	T	T	T	T	T	T	15
Feb. 2019	F7	F7.105.26.6.47	T	T	T	T	T	T	T	T	T	T	T	T	T	T	T	T	T	T	T	T	11
Feb. 2019	F7	F7.140.8.10.4	T	T	T	T	T	T	T	T	T	T	T	T	T	T	T	T	T	T	T	T	7
Feb. 2019	F7	F7.140.8.10.27	T	T	T	T	T	T	T	T	T	T	T	T	T	T	T	T	T	T	T	T	5
Feb. 2019	F7	F7.140.8.10.9	T	T	T	T	T	T	T	T	T	T	T	T	T	T	T	T	T	T	T	T	4
Feb. 2019	F7	F7.105.26.6.51	T	T	T	T	T	T	T	T	T	T	T	T	T	T	T	T	T	T	T	T	3
Feb. 2019	F7	F7.140.8.10.66	T	T	T	T	T	T	T	T	T	T	T	T	T	T	T	T	T	T	T	T	3
Feb. 2019	F7	F7.140.8.10.13	T	T	T	T	T	T	T	T	T	T	T	T	T	T	T	T	T	T	T	T	2
Feb. 2019	F7	F7.140.8.10.8	T	T	T	T	T	T	T	T	T	T	T	T	T	T	M	M	M	M	M	M	4
Feb. 2019	F7	F7.5.6.2.52	T	T	T	T	T	T	T	T	M	M	M	M	M	M	M	M	M	M	M	M	22
Feb. 2019	F7	F7.5.6.2.49	T	T	T	T	T	T	T	T	M	M	M	M	M	M	M	M	M	M	M	M	20
Feb. 2019	F7	F7.5.6.2.66	T	T	T	T	T	T	T	T	M	M	M	M	M	M	M	M	M	M	M	M	16
Feb. 2019	F7	F7.5.6.2.29	T	T	T	T	T	T	T	T	M	M	M	M	M	M	M	M	M	M	M	M	15
Feb. 2019	F7	F7.5.6.2.1	T	T	T	T	T	T	T	T	M	M	M	M	M	M	M	M	M	M	M	M	13
Feb. 2019	F7	F7.5.6.2.57	T	T	T	T	T	T	T	T	M	M	M	M	M	M	M	M	M	M	M	M	11
Feb. 2019	F7	F7.5.6.2.10	T	T	T	T	T	T	T	T	M	M	M	M	M	M	M	M	M	M	M	M	9
Feb. 2019	F7	F7.5.6.2.85	T	T	T	T	T	T	T	T	M	M	M	M	M	M	M	M	M	M	M	M	8
Feb. 2019	F7	F7.5.6.2.14	T	T	T	T	T	T	T	T	M	M	M	M	M	M	M	M	M	M	M	M	6

Feb. 2019	F7	F7.5.6.2.37	T	T	T	T	T	T	T	T	M	M	M	M	M	M	M	M	M	M	M	6
Feb. 2019	F7	F7.5.6.2.53	T	T	T	T	T	T	T	T	M	M	M	M	M	M	M	M	M	M	M	6
Feb. 2019	F7	F7.5.6.2.13	T	T	T	T	T	T	T	T	M	M	M	M	M	M	M	M	M	M	M	5
Feb. 2019	F7	F7.5.6.2.24	T	T	T	T	T	T	T	T	M	M	M	M	M	M	M	M	M	M	M	3
Feb. 2019	F7	F7.5.6.2.76	T	T	T	T	T	T	T	T	M	M	M	M	M	M	M	M	M	M	M	2
Feb. 2019	F7	F7.5.6.2.15	T	T	T	T	T	T	T	T	M	M	M	M	M	M	M	M	M	M	M	1
Feb. 2019	F7	F7.5.6.2.3	T	T	T	T	T	T	T	T	M	M	M	M	M	M	M	M	M	M	M	0
Feb. 2019	F7	F7.141.1.1.20	M	M	M	M	M	M	M	M	M	M	M	M	M	M	M	M	M	M	M	22
Feb. 2019	F7	F7.140.8.10.15	M	M	M	M	M	M	M	M	M	M	M	M	M	M	M	M	M	M	M	20
Feb. 2019	F7	F7.5.6.2.12	M	M	M	M	M	M	M	M	M	M	M	M	M	M	M	M	M	M	M	16
Feb. 2019	F7	F7.141.1.1.4	M	M	M	M	M	M	M	M	M	M	M	M	M	M	M	M	M	M	M	13
Feb. 2019	F7	F7.142.17.2.39	M	M	M	M	M	M	M	M	M	M	M	M	M	M	M	M	M	M	M	12
Feb. 2019	F7	F7.140.8.10.39	M	M	M	M	M	M	M	M	M	M	M	M	M	M	M	M	M	M	M	9
Feb. 2019	F7	F7.5.6.2.34	M	M	M	M	M	M	M	M	M	M	M	M	M	M	M	M	M	M	M	8
Feb. 2019	F7	F7.105.26.6.61	M	M	M	M	M	M	M	M	M	M	M	M	M	M	M	M	M	M	M	7
Feb. 2019	F7	F7.141.1.1.21	M	M	M	M	M	M	M	M	M	M	M	M	M	M	M	M	M	M	M	5
Feb. 2019	F7	F7.141.1.1.3	M	M	M	M	M	M	M	M	M	M	M	M	M	M	M	M	M	M	M	4
Feb. 2019	F7	F7.141.1.1.31	M	M	M	M	M	M	M	M	M	M	M	M	M	M	M	M	M	M	M	4
Feb. 2019	F7	F7.105.26.6.42	M	M	M	M	M	M	M	M	M	M	M	M	M	M	M	M	M	M	M	3
Feb. 2019	F7	F7.140.8.10.54	M	M	M	M	M	M	M	M	M	M	M	M	M	M	M	M	M	M	M	3
Feb. 2019	F7	F7.142.17.2.34	M	M	M	M	M	M	M	M	M	M	M	M	M	M	M	M	M	M	M	3
Feb. 2019	F7	F7.142.17.2.7	M	M	M	M	M	M	M	M	M	M	M	M	M	M	M	M	M	M	M	3
Feb. 2019	F7	F7.5.6.2.24	M	M	M	M	M	M	M	M	M	M	M	M	M	M	M	M	M	M	M	3
Feb. 2019	F7	F7.141.1.1.14	M	M	M	M	M	M	M	M	M	M	M	M	M	M	M	M	M	M	M	2
Feb. 2019	F7	F7.141.1.1.7	M	M	M	M	M	M	M	M	M	M	M	M	M	M	M	M	M	M	M	2
Feb. 2019	F7	F7.142.17.2.3	M	M	M	M	M	M	M	M	M	M	M	M	M	M	M	M	M	M	M	2
Feb. 2019	F7	F7.5.6.2.19	M	M	M	M	M	M	M	M	M	M	M	M	M	M	M	M	M	M	M	2
Feb. 2019	F7	F7.5.6.2.20	M	M	M	M	M	M	M	M	M	M	M	M	M	M	M	M	M	M	M	2
Feb. 2019	F7	F7.105.26.6.55	M	M	M	M	M	M	M	M	M	M	M	M	M	M	M	M	M	M	M	1
Feb. 2019	F7	F7.105.26.6.68	M	M	M	M	M	M	M	M	M	M	M	M	M	M	M	M	M	M	M	1
Feb. 2019	F7	F7.140.8.10.3	M	M	M	M	M	M	M	M	M	M	M	M	M	M	M	M	M	M	M	1
Feb. 2019	F7	F7.140.8.10.11	M	M	M	M	M	M	M	M	M	M	M	M	M	M	M	M	M	M	M	0
Feb. 2019	F7	F7.140.8.10.43	M	M	M	M	M	M	M	M	M	M	M	M	M	M	M	M	M	M	M	0
Feb. 2019	F7	F7.5.6.2.27	M	M	M	M	M	M	M	M	M	M	M	M	M	M	M	M	M	M	M	0
Feb. 2019		NILR	M	M	M	M	M	M	M	M	M	M	M	M	M	M	M	M	M	M	M	15
Feb. 2019		NILR	M	M	M	M	M	M	M	M	M	M	M	M	M	M	M	M	M	M	M	12
Feb. 2019		NILR	M	M	M	M	M	M	M	M	M	M	M	M	M	M	M	M	M	M	M	9
Feb. 2019		NILR	M	M	M	M	M	M	M	M	M	M	M	M	M	M	M	M	M	M	M	8
Feb. 2019		NILR	M	M	M	M	M	M	M	M	M	M	M	M	M	M	M	M	M	M	M	6
Feb. 2019		NILR	M	M	M	M	M	M	M	M	M	M	M	M	M	M	M	M	M	M	M	6
Feb. 2019		NILR	M	M	M	M	M	M	M	M	M	M	M	M	M	M	M	M	M	M	M	4
Feb. 2019		NILR	M	M	M	M	M	M	M	M	M	M	M	M	M	M	M	M	M	M	M	3

Feb. 2019		NILR	M	M	M	M	M	M	M	M	M	M	M	M	M	M	M	M	M	M	M	M	1
Feb. 2019		NILS	T	T	T	T	T	T	T	T	T	T	T	T	T	T	T	T	T	T	T	T	68
Feb. 2019		NILS	T	T	T	T	T	T	T	T	T	T	T	T	T	T	T	T	T	T	T	T	45
Feb. 2019		NILS	T	T	T	T	T	T	T	T	T	T	T	T	T	T	T	T	T	T	T	T	31
Feb. 2019		NILS	T	T	T	T	T	T	T	T	T	T	T	T	T	T	T	T	T	T	T	T	23
Feb. 2019		NILS	T	T	T	T	T	T	T	T	T	T	T	T	T	T	T	T	T	T	T	T	22
Feb. 2019		NILS	T	T	T	T	T	T	T	T	T	T	T	T	T	T	T	T	T	T	T	T	10
Feb. 2019		NILS	T	T	T	T	T	T	T	T	T	T	T	T	T	T	T	T	T	T	T	T	8
Feb. 2019		NILS	T	T	T	T	T	T	T	T	T	T	T	T	T	T	T	T	T	T	T	T	4
Feb. 2019		NILS	T	T	T	T	T	T	T	T	T	T	T	T	T	T	T	T	T	T	T	T	3
Feb. 2019		NILS	T	T	T	T	T	T	T	T	T	T	T	T	T	T	T	T	T	T	T	T	2
Nov. 2019	F8	F7.5.6.2.3	T	T	T	T	T	T	T	T	M	M	M	M	M	M	M	M	M	M	M	M	22
Nov. 2019	F8	F7.5.6.2.3	T	T	T	T	T	T	T	T	M	M	M	M	M	M	M	M	M	M	M	M	29
Nov. 2019	F8	F7.5.6.2.3	T	T	T	T	T	T	T	T	M	M	M	M	M	M	M	M	M	M	M	M	32
Nov. 2019	F8	F7.5.6.2.3	T	T	T	T	T	T	T	T	M	M	M	M	M	M	M	M	M	M	M	M	33
Nov. 2019	F8	F7.5.6.2.3	T	T	T	T	T	T	T	T	M	M	M	M	M	M	M	M	M	M	M	M	33
Nov. 2019	F8	F7.5.6.2.3	T	T	T	T	T	T	T	T	M	M	M	M	M	M	M	M	M	M	M	M	34
Nov. 2019	F8	F7.140.8.10.8	T	T	T	T	T	T	T	T	T	T	T	T	T	M	M	M	M	M	M	M	11
Nov. 2019	F8	F7.140.8.10.8	T	T	T	T	T	T	T	T	T	T	T	T	T	M	M	M	M	M	M	M	12
Nov. 2019	F8	F7.140.8.10.8	T	T	T	T	T	T	T	T	T	T	T	T	T	M	M	M	M	M	M	M	12
Nov. 2019	F8	F7.140.8.10.8	T	T	T	T	T	T	T	T	T	T	T	T	T	M	M	M	M	M	M	M	18
Nov. 2019	F8	F7.140.8.10.8	T	T	T	T	T	T	T	T	T	T	T	T	T	M	M	M	M	M	M	M	27
Nov. 2019	F8	F7.140.8.10.8	T	T	T	T	T	T	T	T	T	T	T	T	T	M	M	M	M	M	M	M	27
Nov. 2019	F8	F7.140.8.10.8	T	T	T	T	T	T	T	T	T	T	T	T	T	M	M	M	M	M	M	M	31
Nov. 2019	F8	F7.142.17.2.8	M	M	M	M	M	M	M	M	M	T	T	T	T	T	T	T	T	T	T	T	24
Nov. 2019	F8	F7.142.17.2.8	M	M	M	M	M	M	M	M	M	T	T	T	T	T	T	T	T	T	T	T	26
Nov. 2019	F8	F7.142.17.2.8	M	M	M	M	M	M	M	M	M	T	T	T	T	T	T	T	T	T	T	T	28
Nov. 2019	F8	F7.142.17.2.8	M	M	M	M	M	M	M	M	M	T	T	T	T	T	T	T	T	T	T	T	32
Nov. 2019	F8	F7.142.17.2.8	M	M	M	M	M	M	M	M	M	T	T	T	T	T	T	T	T	T	T	T	38
Nov. 2019	F8	F7.142.17.2.8	M	M	M	M	M	M	M	M	M	T	T	T	T	T	T	T	T	T	T	T	38
Nov. 2019	F8	F7.142.17.2.8	M	M	M	M	M	M	M	M	M	T	T	T	T	T	T	T	T	T	T	T	47
Nov. 2019		NILR-10	M	M	M	M	M	M	M	M	M	M	M	M	M	M	M	M	M	M	M	M	18
Nov. 2019		NILR-10	M	M	M	M	M	M	M	M	M	M	M	M	M	M	M	M	M	M	M	M	20
Nov. 2019		NILR-10	M	M	M	M	M	M	M	M	M	M	M	M	M	M	M	M	M	M	M	M	22
Nov. 2019		NILR-10	M	M	M	M	M	M	M	M	M	M	M	M	M	M	M	M	M	M	M	M	25
Nov. 2019		NILR-10	M	M	M	M	M	M	M	M	M	M	M	M	M	M	M	M	M	M	M	M	25
Nov. 2019		NILR-10	M	M	M	M	M	M	M	M	M	M	M	M	M	M	M	M	M	M	M	M	33
Nov. 2019		NILS-2	T	T	T	T	T	T	T	T	T	T	T	T	T	T	T	T	T	T	T	T	20
Nov. 2019		NILS-2	T	T	T	T	T	T	T	T	T	T	T	T	T	T	T	T	T	T	T	T	20
Nov. 2019		NILS-2	T	T	T	T	T	T	T	T	T	T	T	T	T	T	T	T	T	T	T	T	24
Nov. 2019		NILS-2	T	T	T	T	T	T	T	T	T	T	T	T	T	T	T	T	T	T	T	T	27
Nov. 2019		NILS-2	T	T	T	T	T	T	T	T	T	T	T	T	T	T	T	T	T	T	T	T	38

Nov. 2019		NILS-2		T T T T T T T T T T T T T T T T T T T	47

Appendix 4: Amino acid sequences of the predicted products of the resistance-associated and susceptibility-associated alleles for TraesCS6B02G466600

>TraesCS6B02G466600 protein sequence

MASSSSSSSYMPLRRSDSVADMMPEALRQSRYQMKTCFQRYVSKGRRLMKNQQLMEELEAP
AGDDRVDKARLADGFLGYVICSTQEAVVLPPLVAFAVRTNPGVWEFIRVHSGDLAAEEITPS
AYLKCKETLYDEKWARDDNSLEVDFGALDLSTPRLTLPSSIGNGMQFVSRFMSSKLSGKPES
MKPLLDYLLALNYRGEKLMISDTLDTADKLQTALLLAEVFVAGLEKSTPYQQFEQRFQEWGF
EKGWGDTAETCRETLNFLSEVLQAPDPINMEKFFSRVPSVFSIVIFSIHGYFGQEKVLGLPDTG
GQVVYILDQVRALEEELLQRIRKQGLNVTPKILVLTRLIPDAKGTKCNVELEPVEHTKHSSILR
VPFKTDDGKDLRQWVSRFDIYPYLERYAQDSSVKILDILEGKPDMVIGNYTDGNLVASLLSSK
LGVTQGTIAHALEKTKYEDSDVKWREMDHKYHFSCQFTADMIAMNTSDFIIASTYQEIAGSK
DKPGQYESHYTFTMPGLCRYATGVNVFDPKFNIAAPGADQSVYFPFTQKQARLTDLHPQIEEL
LYSKEDNNEHLGYLGDRSKPIIFSMARLDKVKNITGLVEWYGENKKLRDLVNLVIVGGLLEPS
QSNDREEIEEINKMHSLMDKYQLRGQIRWIKAQTERVRNGELYRCIADTRGAFVQPALYEAF
GLTVIEAMNCGLPTFATNQGGPAEIIVNEVSGFHINPLNGKEASDKIAGFFQKCKEDPSYWNK
MSTAGLQRIYECYTWQIYATKVLNMGSMYGFWRTLNKEERQAKQLYLQMFYNLQFRQLVK
TVPKVGEQPARPATGSTAPARIAPRPRERRPQTRIQRIATNLLGPVLPTSNFSQDAA

>TraesCS6B02G466600 susceptible predicted protein sequence

MASSSSSSSYMPLRRSDSVADMMPEALRQSRYQMKTCFQRYVSKGRRLMKNQQLMEELEAS
AGDDKVDKARLADGFLGYVICSTQEAVVLPPLVAFAVRTNPGVWEFIRVHSGDLSAEEITPSA
YLKCKETLYDEKWARDDNSLEVDFGALDLSTPRLTLPSSIGNGMQFVSRFMSSKLSGKPESM
KPLLDYLLALNYRGEKLMISDTLDTADKLQTALLLAEVFVAGLEKSTPYQQFEQRFQEWGLE
KGWGDTAETCRETLNFLSEVLQAPDPINMEKFFSRVPSVFSIVIFSIHGYFGQEKVLGLPDTGG
QVVYILDQVRALEEELLQRIRKQGLNVTPKILVLTRLIPDAKGTKCNVELEPVEHTKHSSILRV
PFKTDDGKDLRQWVSRFDIYPYLERYAQDSSVKILDILEGKPDMVIGNYTDGNLVASLLSSKL
GVTQGTIAHALEKTKYEDSDVKWREMDHKYHFSCQFTADMIAMNTSDFIIASTYQEIAGSKD
KPGQYESHYAFTMPGLCRYATGVNVFDPKFNIAAPGADQSVYFPFTQKQARLTDLHPQIEELL
YSKEDNNEHLGYLGDRSKPIIFSMARLDKVKNITGLVEWYGENKKLRDLVNLVIVGGLLEPS
QSNDREEIEEINKMHSLMDKYQLRGQIRWIKAQTERVRNGELYRCIADTRGAFVQPALYEAF
GLTVIEAMNCGLPTFATNQGGPAEIIVNEVSGFHINPLNGKEASDKIAGFFQKCKEDPSYWNK
MSTAGLQRIYECYTWQIYATKVLNMGSMYGFWRTLNKEERQAKQLYLQMFYNLQFRQLVK
TVPKVGEQPARPATGSTAPARIAPRPRERRPQTRIQRIATNLLGPVLPTSNFSQDAA

Appendix 5: Dissection of CCN-infected root for cMX investigation.

Investigation using stereomicroscope revealed the anatomy of the cMX in relation to the swollen region and feeding site placement. The cMX appeared ‘normal’ below the swollen region, however, within the swollen region (boxed in Fig. 4-6A) cMX cells were slightly wider. Starting from the base of the swollen region, individual cMX cells also appeared shorter than cells outside the swollen region (Fig. 4-6B). The feeding site was identified by a region of ‘empty cells’ directly connected to the cMX (Fig. 4-6B) and was located near the top of the swollen region. In all swollen regions analysed, lateral root initials were located near feeding sites.

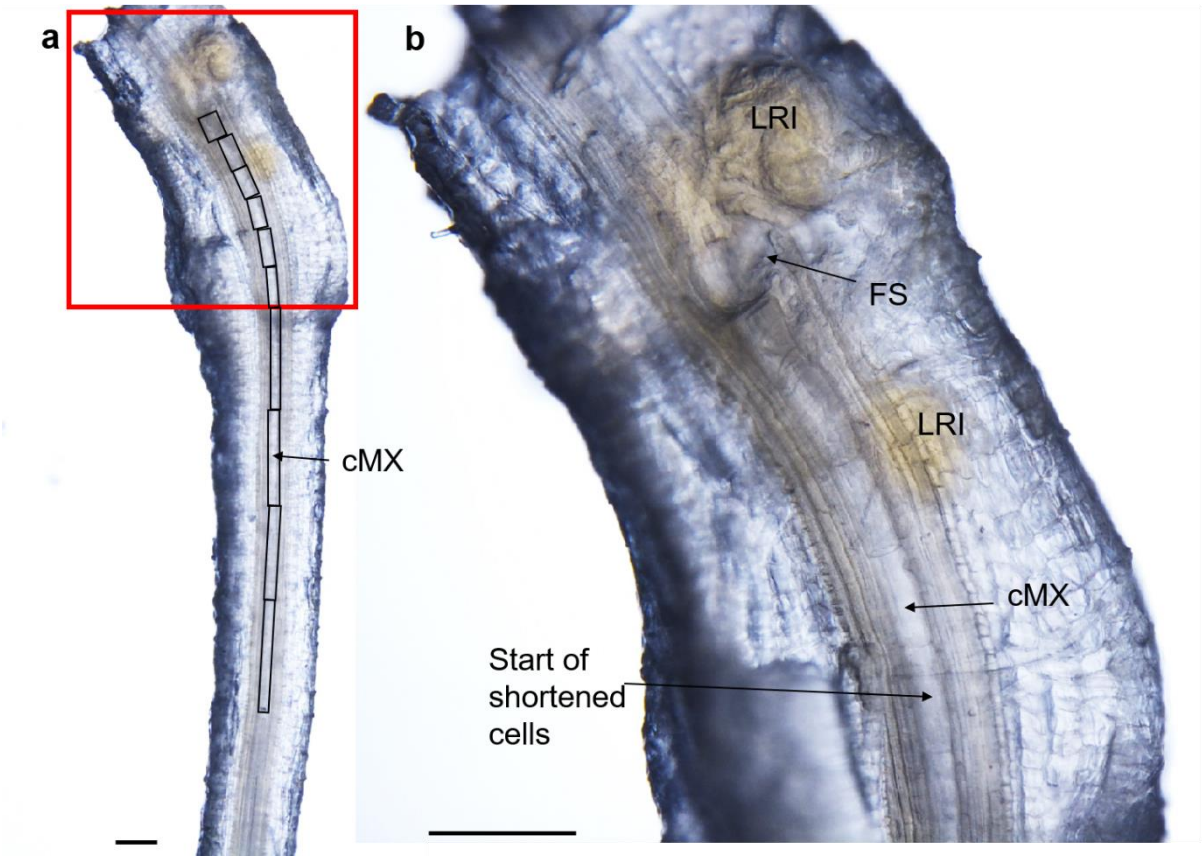

Figure: Stereomicroscope image of a cleared CCN-infected root sliced in half at 7 DAI. a) Red boxed area indicates swollen region. Black boxes indicate individual cMX cells. b) Close up on swollen region. central metaxylem (cMX); lateral root initial (LRI); feeding site (FS). Scale bar 200 µm.

Appendix 6: Time lapse images of a CCN-inoculated root

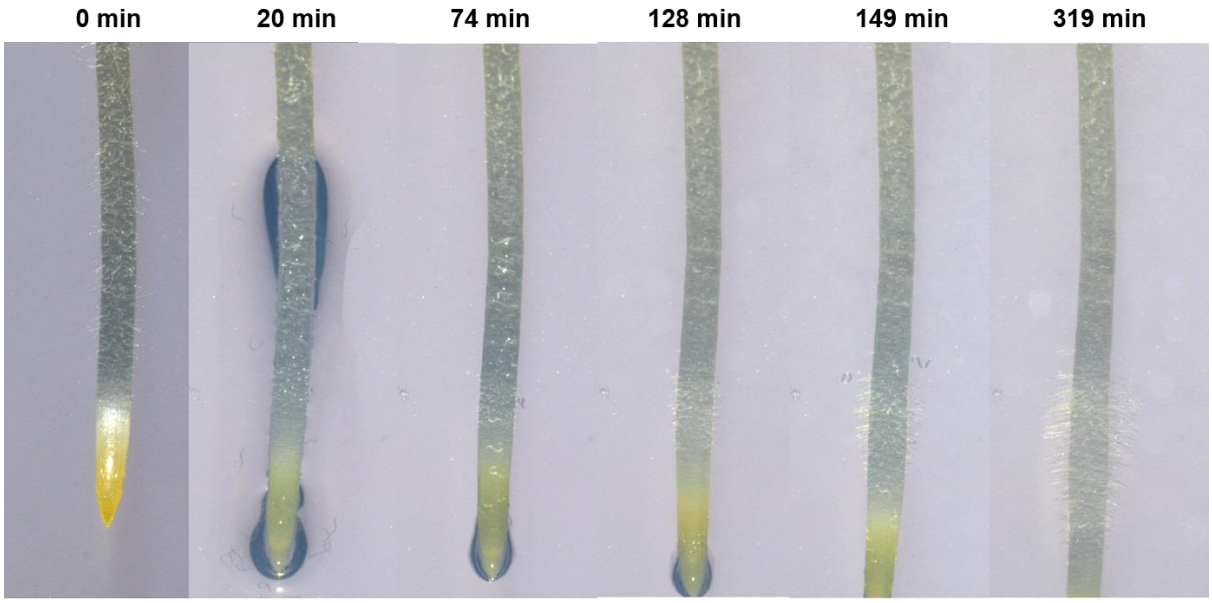

Figure: A wheat seedling (3 d after germination) root prior to inoculation (0 min), and the time after inoculation with approximately 20 J2 *Heterodera avenae* (20 min) and at 74, 128, 149 and 319 min. At 74 min, nematodes can be seen in contact with root. At 128 min, root hairs can be seen emerging. By 149 min, root hairs have elongated. By 319 min, the root tip has grown outside of view and root hairs are fully elongated.

Video: CCN_Infection on Wheat Root (1 min = 1 hr)

Available on FigShare: https://figshare.com/s/cee95212999fb9cba5bd

Appendix 7: *in situ* hybridisation analysis

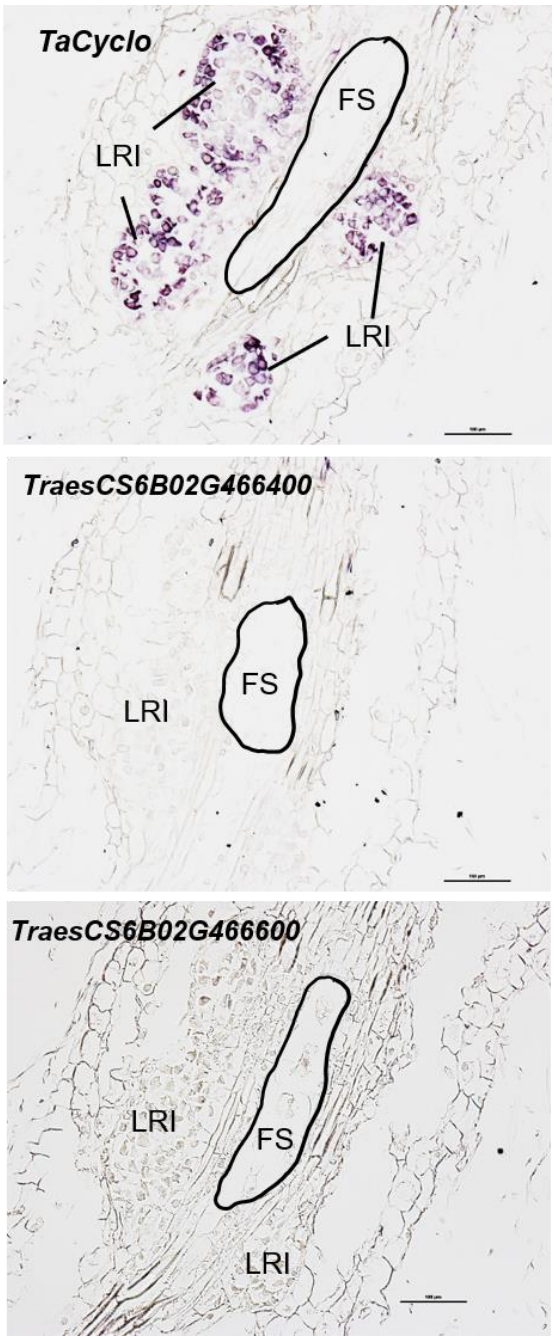

Figure: *in situ* hybridisation of wheat roots from 6 DAI with *Heterodera avenae*. Probes specific for housekeeping gene, TaCyclo, and selected candidate genes, TraesCS6B02G466400 and TraesCS6B02G466600. (LRI) lateral root initials, (FS) feeding site. Scale bar 100 µm.